HIGHWAY RESEARCH RECORD

Number 466

Pavement Systems Analyses

13 reports
prepared for the
52nd Annual Meeting

Subject Areas

25 Pavement Design
26 Pavement Performance
62 Foundations (Soils)
63 Mechanics (Earth Mass)

HIGHWAY RESEARCH BOARD
DIVISION OF ENGINEERING NATIONAL RESEARCH COUNCIL
NATIONAL ACADEMY OF SCIENCES—NATIONAL ACADEMY OF ENGINEERING
Washington, D.C. 1973

NOTICE

These papers report research work of the authors that was done at institutions named by the authors. The papers were offered to the Highway Research Board of the National Research Council for publication and are published here in the interest of the dissemination of information from research, one of the major functions of the Highway Research Board.

Before publication, each paper was reviewed by members of the HRB committee named as its sponsor and accepted as objective, useful, and suitable for publication by the National Research Council. The members of the review committee were chosen for recognized scholarly competence and with due consideration for the balance of disciplines appropriate to the subject concerned.

Responsibility for the publication of these reports rests with the sponsoring committee. However, the opinions and conclusions expressed in the reports are those of the individual authors and not necessarily those of the sponsoring committee, the Highway Research Board, or the National Research Council.

Each report is reviewed and processed according to the procedures established and monitored by the Report Review Committee of the National Academy of Sciences. Distribution of the report is approved by the President of the Academy upon satisfactory completion of the review process.

ISBN 0-309-02250-9
Library of Congress Catalog Card No. 73-21057
Price: $5.80

CONTENTS

FOREWORD

This RECORD contains 13 research papers that address several topics related to the analysis and performance of pavement systems. They will be of interest to both researchers and practicing engineers.

Friberg and Pasko report on observations and measurements made during and after construction of a 3,200-ft post-tensioned prestressed concrete highway pavement. Measurements included concrete strength, temperature profiles, surface profiles, strand elongation during stressing, and movements in the slabs and at the joints. In addition, deflections and strains were determined from selectively placed static loads.

The objective of the study by Kher and Darter was to make design processes sensitive to variabilities and uncertainties associated with design, construction, and performance of rigid pavements. Probabilistic concepts were applied to modify the AASHO interim guides to make it possible to design for any specified level of reliability. Variance models for the performance equation of the AASHO Guide are presented along with a revised nomograph that includes reliability and variance scales.

The paper by Abou-Ayyash and Hudson describes a sensitivity analysis performed to establish the relative importance of structural variables on the performance of continuously reinforced concrete pavements. The discrete-element method of slab analysis was used, and, for the range of variables studied, the analysis of variance showed that the most significant variables are slab bending and modulus of subgrade reaction.

A finite-element method programmed for high-speed computer was developed by Huang and Wang for determining the stresses in concrete slabs with load transfer at the transverse joints. Numerical results are presented to illustrate the effect of loading position, load transfer, and loss of subgrade contact on critical stresses in rigid pavements. An analysis of the data indicated that, when load transfer is provided at transverse joints, the most critical stresses occur when the load is near the edge and far from the joint. The authors suggest that edge stress, instead of stress at the joint, be used for the design of highway pavements.

The purpose of the study by Hopkins and Deen was to provide a basis for comparing flexible pavement designs from the AASHO Road Test with those based on Kentucky design criteria. Correlations were developed between the hypothetical AASHO soil support values and Kentucky strength values. Comparisons were also made between California bearing ratio values determined at the Road Test with those determined by ASTM and Kentucky methods on several soils including AASHO embankment soil.

The Virginia Department of Highways recognized a need for a method to quickly and economically estimate equivalent 18-kip axle loads from routinely available records and thus eliminate the need for on-location truck-axle weight studies. The paper by Vaswani and Thacker presents a three-equation method using yearly reports on average daily traffic volumes and truck weight studies. The researchers conclude that the method can be used to develop traffic projections in cases where load meter studies are not feasible.

Shahin and McCullough present a system for predicting the stiffness history of an asphalt concrete pavement in-service layer throughout its design analysis period. The system makes use of standard material properties and environmental inputs to predict the daily changes in stiffness due to temperature variations and also long-term changes in stiffness due to hardening of the asphalt cement binder.

Computer programs were used by Kamel et al. to calculate pavement structural response to stresses, strains, and deflections of the Brampton Test Road sections. Basic properties of the materials under consideration were determined from laboratory tests in the original materials. Calculated structural responses were correlated to observed pavement behavior and performance measurements, and the relations derived were

demonstrated by layered-analysis techniques to be applicable for use in designing flexible pavements and in determining equivalence of various types of base material.

Salam and Monismith present analyses of fracture occurring in asphalt pavement structures due to excessive wheel loads and to braking tractions applied at the pavement surface. Specific solutions are presented for three conditions of cracking in pavement layers, and, although the analyses presented are relatively crude, the authors conclude that critical areas can be defined in pavement structure in such a manner as to provide insight to techniques to minimize load-associated fracture.

The paper by Smith and Nair presents the concepts and a procedure for conducting a deterministic sensitivity analysis to determine the relative influence of materials characterization on the prediction of asphalt concrete pavement performance. Materials were characterized by linear-isotropic elasticity, and the effects on fatigue performance prediction are compared to effects associated with construction, environment, and fatigue criteria variability.

Ahlvin, Chou, and Hutchinson found that the principle of superposition was approximately valid in the analysis of instrumentation data taken from homogeneous soil test sections under plate loads and from flexible pavement test sections under single- and multiple-wheel loads. Based on the results, the authors conclude that linear-elastic theory is not unreasonable in application to pavement analysis even though laboratory tests have definitely proved pavement materials behave nonlinearly under loads.

The paper by Saxena presents a method for the solution of engineering problems involving slabs resting on an elastic foundation. The slab is represented by a physical model, and the subgrade is treated as an elastic solid. A matrix-analysis computer program has been developed to analyze reactive subgrade pressures and compute stresses and bending moments in the slab.

Systematic data collection from in-service pavement performance is recognized by Strom, Hudson, and Wu as an essential source of information to supplement road test data and mechanistic analysis in the design of new and reconstructed pavements. The authors present a case study example of a feedback data system in which the selected performance factors are basically the inputs to the computer-based pavement design system used by the state of Texas.

PRESTRESSED CONCRETE HIGHWAY PAVEMENT AT DULLES INTERNATIONAL AIRPORT

Bengt F. Friberg, Consultant, St. Louis; and
Thomas J. Pasko, Jr., Federal Highway Administration

A prestressed concrete highway pavement was constructed in late 1971 at the Dulles International Airport near Washington, D.C. The pavement is 3,200 ft long and consists of six slabs ranging in length from 400 to 760 ft. The concrete is 6 in. thick and 24 ft wide. Measurements made during construction, and for 3½ months thereafter, included concrete strengths, strand elongations during stressing, concrete temperatures and gradients, slab movements, and profile changes. In addition, prior to opening to traffic, the pavement was subjected to controlled tests with axle loadings of 20 and 33 kip at joints and edges while deflections and strains were measured. The prestressing tendons are ½-in. diameter 7-wire strands spaced at 24 in. and tensioned to 29 kip by jacking at both ends of each slab. In order from the west end, three slabs 400, 500, and 600 ft long were prestressed with the strand in smooth-wall steel tubing that was grouted after stressing, and three slabs 760, 500, and 400 ft long were prestressed with polypropylene-encased, greased strands. Friction in the encasements produced average strand effectiveness of 90 percent for the strand in steel tubing and 80 percent for the plastic-encased strand. The strands placed at ½ in. below middepth produce a favorable stress distribution and keep the slab ends from warping upward. The double layer of polyethylene over the cement-treated subbase allows daily slab end movements from 0.2 to 0.4 in., indicating a maximum diurnal friction coefficient of less than 0.5.

•ORDINARILY, pavement slabs dry at the top surface, whereas the bottom surface, which is in contact with the subbase, remains nearly saturated. This moisture differential, with drying and shrinkage at the surface, produces upward warping at the pavement edges and ends.

Longitudinal stresses from restrained warping of a long slab keep the slab flat on the subbase except at the ends. The longitudinal compressive stress at the bottom of the slab is a natural stress condition except within a few feet of the ends (6). This residual compressive stress is available to counter the high tension stresses at the bottom surface caused by axle loads in the longitudinal direction.

Longitudinal prestress can preserve the favorable natural stresses in the pavement away from the ends. Magnitude of the prestress at the ends is selected to induce some compressive stress in the top surface to counter corner load stresses and yet hold the ends down with much higher compressive prestress at the bottom.

It is desirable to aim for optimum dimensions of monolithic prestress pavement slabs by finding the practical maximum distance between transverse joints in normal construction practices, and by early application of prestress, before the developing tension stresses in the drying slab reach critical values.

Publication of this paper sponsored by Committee on Rigid Pavement Design.

Some reduction from normal pavement thickness is indicated for prestressed pavements because of the prestress and the favorable stress conditions in long monolithic slabs. At the transverse joints of this thinner pavement, adequate strength can be secured by joint-edge reinforcements and effective joint load transfer. Repeated, excessive yielding of a foundation, however, leads to deterioration of the support and failure of the system even if the thinner pavement itself can flex initially without failure. Permissible pavement deflections, rather than stresses, place a lower limit on prestressed concrete pavement thicknesses over normal road foundations.

PAVEMENT DESIGN

Project Site

The prestressed highway pavement project is located at Dulles International Airport in northern Virginia and consists of 3,200 ft of prestressed slabs 6 in. thick.

The soil in the area is a silty clay classified as an AASHO A-6(12). At a 2- to 4-ft depth, the project was underlain by a rippable shale. At about midlength of the project, the roadway crosses twin 7-ft diameter concrete culverts approximately 3 ft below the bottom of the pavement.

As given in Table 1, various vertical and horizontal alignments are incorporated in the demonstration project. The slab lengths are given in the table in the order in which they were built, from west to east. The first three slabs were grouted construction and the latter three ungrouted. Cross slopes in general are 2 percent toward the north shoulder on tangents, but on superelevated curves the slope ranges to 6 percent. The north and south edges are bounded with 2-ft deep drainage ditches (4, 7, 9). Figure 1 shows some of the distinguishing features of the project.

Structural Analysis

Preliminary structural analysis indicated that the design could consist of a 6-in. slab laid over a 6-in. cement-treated subbase having a modulus of subgrade reaction of 400 lb/in.^{3}. Slab ends contain 1¼-in. diameter dowels 12 in. on center that span a 3-in. wide joint and have a dowel looseness of less than 0.005 in. Traffic loading for design analysis was a 20-kip axle load for a single axle and two 20-kip axles spaced at 50 in. for tandem loading.

Sector analysis (8) was used to determine the stresses caused by the design axle loadings. Results compared favorably with values measured in the slab. Calculated deflections under loads were tolerable.

Details of Materials

The subbase is a crushed-stone material 6 in. deep and stabilized with 4 percent cement by weight. It is 28 ft wide and cured with a sprayed asphalt membrane.

A double layer of 4-mil thick high-slip polyethylene sheeting was placed as a bond breaker for the slabs.

The steel was preset over the polyethylene prior to concreting. It consists of the bulkhead I-beams at the ends of each slab and transverse reinforcing bars number 3 or 4, 30 in. on center, that support the 12 longitudinal tendons. Number 4 tie bars 36 in. long and 30 in. on center were used across the longitudinal joint.

The post-tensioned tendons are ½-in. nominal diameter 7-wire strands spaced 24 in. on center and ½ in. below middepth. The strand conforms to ASTM A 416, grade 270, with a minimum breaking strength of 41,300 lb. The tendons were supported and tied on the transverse reinforcing bars. Bare strands, enclosed in thin-wall smooth steel tubing, having a 0.68-in. inside diameter and a 0.035-in. wall thickness, were used in the three slabs in the west part of the project. The continuity of the tubing was interrupted every 100 ft with a 4-in. expansion space and a grout inlet that projected to the pavement surface. The butting tube ends and the expansion space were covered with close-fitting outer sleeves. The three slabs on the east end contained strand that is greased and encased in tight-fitting extruded polypropylene coating 0.02 in. thick.

The concrete was made with 1-in. maximum-sized crushed trap rock and type II cement. The air content was about 6 percent. The specified compressive strength of 4,000 psi at 28 days was easily met.

The ends of the prestressed slabs are 6-in., 17.25-lb/ft steel I-beams with holes $2\frac{1}{2}$ in. above the bottom flange for the prestressing strands. The $1\frac{1}{4}$-in. diameter sleeves are 4 in. long and 12 in. on center and were carefully aligned and welded in place for the joint dowels. The two 12-ft I-beams are hinged at the center joint. They serve to reinforce the transverse joint edge, distribute the concentrated strand forces, position the strands and dowels, confine the joint filler, and permit accurate squaring of the joints.

Steel I-beams, matching those at the prestressed slab ends, were slipped over the projecting dowels, shimmed to grade and to a position that provided an expansion joint at each end of the prestressed slab. The joint was dimensioned to close at 110 F. These 6-in. I-beams are integrated with the joint slab and reinforce the joint edges. Figure 2 shows the 8-ft space between the slabs with the beams in place, ready for the double layer of reinforcement and concrete.

At both ends of each joint, sliding steel end plates were installed to prevent infiltration of debris between the joint I-beams. A galvanized sheet-metal drain box was installed at the low end of each joint, through which water can drain from the bottom of the joint to the side under the shoulder through a $2\frac{1}{2}$-in. PVC pipe.

CONSTRUCTION

Paving

The cement-treated subbase was constructed during the last of September 1971. The concrete was placed November 30 through December 4, starting at the west end. The rate of paving was 400 ft on the first day and 900 ft on the last day because of the slow methods used to transfer concrete from the ready-mix trucks to the single Maxon spreader and the CMI slip-form paver.

Ready-mixed concrete was delivered at 65 to 70 F, whereas air temperatures ranged from 15 to 48 F. The burlap-polyethylene-straw curing kept the internal temperatures from dropping below 47 F. Subsequently a warming trend brought air temperatures above 50 F on December 7 and higher on the following days. Air and concrete temperatures are shown in Figure 3.

Post-Tensioning

Three steps were specified for stressing the strands to full tension of 29 kip per strand. The first step (to 10 kip per strand) was applied at 2 days of age when the concrete had a strength of more than 1,000 psi, the second step (to 20 kip) took place at 3 days and a concrete strength of 2,000 psi, and the third step (to full strand tension) was achieved when the concrete strength was a minimum of 3,000 psi. The corresponding concrete prestress at the slab end was 70, 140, and 200 psi respectively. The concrete placing and prestressing records are shown in Figure 3; full prestress was applied at a 7-day maximum to 4-day minimum age. In contrast, on a 300-ft slab placed during July in the state of Delaware (5), full prestress was applied on the day following construction.

Post-tensioning was done with two portable hydraulic jacks, one at each slab end. The strands were jacked against both slab ends in a specified sequence to produce a uniform stress distribution across the 24-ft width.

In the first two stressing steps, to 10 and 20 kip, the west ends of the strand were tensioned first, prior to the east end being jacked to the same specified tension. In the third step, the east end was stressed before the west end of the strand.

Strand elongations at each end were measured for each step of prestressing from the slab end to a mark on the strand. The slab shortening during stressing was not measured directly because the elastic deformations, which did not exceed 0.1 in. at the end, were masked by thermal movements. Typical force-elongation diagrams for the 600- and 760-ft slabs are shown in Figure 4 and are discussed later.

Table 1. Site features of the prestressed pavement.

Slab Length (ft)	Strand Encasement	Approximate Vertical Alignment: Grade (percent)	Approximate Vertical Alignment: Curve Length (ft)	Approximate Horizontal Alignment: Degree of Curve	Approximate Horizontal Alignment: Curve Length (ft)	Cuts and Fills (ft)
400	Steel tube	-1.4	0	0	0	0 to 3 C
500	Steel tube	-1.4 to -0.1	400	4	306	0 to 4 F
600	Steel tube	-0.1	0	6½	615	4 F to 10 F
760	Plastic	-0.1 to +3.5	600	3	533	4 F to 0
500	Plastic	+3.5 to -2.0	600	0	0	0 to 3 C
400	Plastic	-2.0	0	0	0	3 C to 0

Figure 1. Plastic-coated tendons and bulkhead beam with dowels in place.

Figure 2. Supplemental I-beams shimmed to proper opening and elevation just prior to concreting.

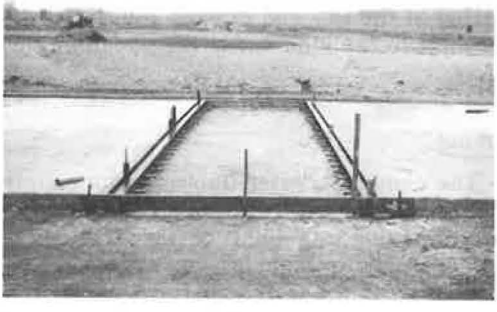

Figure 3. Air and concrete temperature.

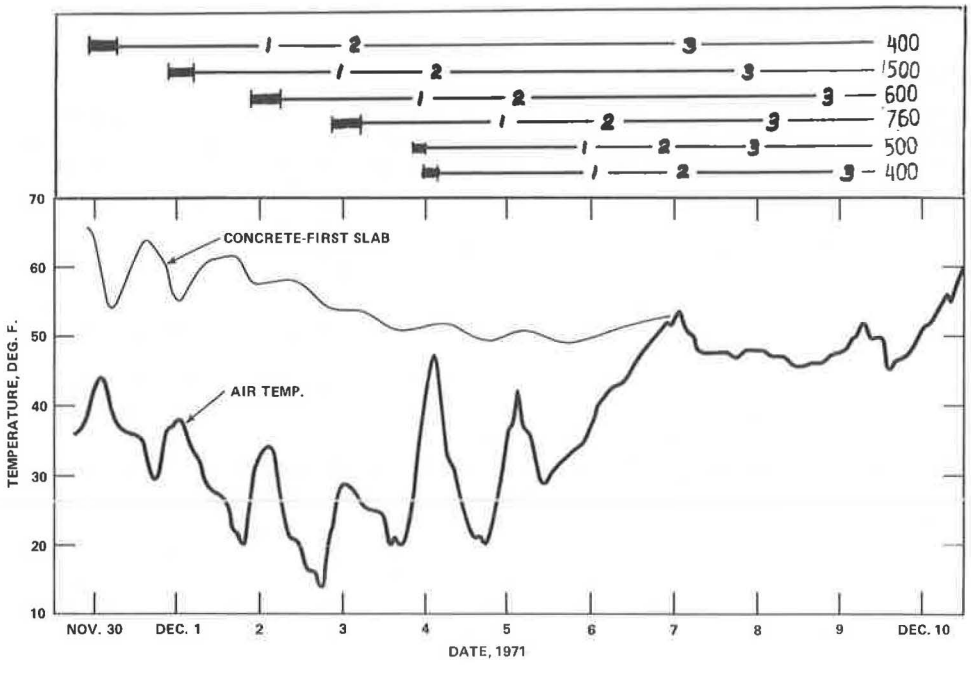

The total measured elongation is compared with the elongation that would take place if there were no friction of the strand in its enclosure; the ratio shows the average strand effectiveness from end to end of the slab. The minimum strand force, and the corresponding minimum section prestress, occurs near midlength.

The effectiveness of the initial stressing for all the slabs is given in Table 2. The zero-friction elongation was calculated using a modulus of elasticity of 28×10^6 psi and an area of steel equal to 0.153 in.^{2}.

The relatively low effectiveness for the 10-kip loading on the 400-ft slab with strand in steel tubing probably resulted from bends and mortar in the tubing. Although the resistance for the steel-tube tendons decreased with load, the resistance was high in the plastic-coated tendons at all levels of loading. It is possible that excessive wobble, plastic helical deformation around the individual strand wires, and high-viscosity grease could have caused the high resistance in the plastic-coated tendons.

Each strand was checked and adjusted to 30 kip prior to grouting on December 14 and 15. Because $\frac{1}{8}$ and $\frac{1}{4}$ in. of the elongation is lost in seating the strand chucks, the final strand force is estimated to be about 29.5 kip, or 205 psi on the concrete. The additional elongation of the strand during adjustment ranged up to a total of 3 in. depending on the slab length.

Following final stressing, the strand ends were cut with a Carborundum saw close to the strand chucks. The ends were sealed with 2-in. pipe caps, which were threaded into half couplings welded to the webs of the I-beams. The cap end was sealed with a standard pipe plug after it was grouted.

Grouting

Standard pipe tee fittings with extensions were attached to the tubing for injecting grout. The inlets were covered with metal caps that had short lengths of spring wire projecting upward from them to mark their locations in the concrete.

The grout mixture was made with both types III and I cement mixed with approximately 5 gal of water per sack to produce a flow cone viscosity of 11 sec.

The tubing was blown with air at 250 psi. The grout injection hose, coupled to the $\frac{1}{2}$-in. pipe fittings with quick-closing shutoff valves, was used to grout the tubing progressively, advancing in 100-ft increments.

Joint Slabs

The joint slabs were constructed about a month after the main slabs. The joint slab I-beams were carefully leveled and spaced adjacent to the heavier prestressed slab end beams. At the time of construction of these joint slabs, all prestressed slabs had shortened $\frac{3}{8}$ to $\frac{1}{2}$ in. independently of temperature.

Joint Filler

Polyurethane was formed in place to about 10 lb/ft^3 between the two I-beams at all joints. Four batches per joint were poured and foamed against temporary vertical bulkheads in the joint. The fillers were placed on January 12 and 13, when the air temperatures were 40 to 50 F, and it was necessary to heat the steel surfaces in the joints to obtain a foaming reaction.

Shoulders

The aggregate shoulders were roller-compacted to 3 in. below finished grade from January 10 to 12. The 3-in. bituminous surface was placed 10 ft wide on the north side on January 20 and 21 and 4 ft wide on the south side on February 1. The road was opened to traffic March 6 and was immediately put into use by heavy construction traffic.

Difficulties

Several minor problems that occurred are listed here so that they might be avoided on future projects:

1. Wind damage resulted from lifting of the polyethylene;
2. Use of excessively stiff concrete at the start made spreading difficult, caused excessive thickness at the first joint, and made visible the steel because of inadequate expansion space in the tubing;
3. The I-beams were difficult for the paver to traverse;
4. Grouting and fittings were inadequate;
5. One strand anchor split under 29 kip when 3 jaws were placed in a 2-jaw anchor body;
6. Dowel sleeves had to be reamed by hand to install dowels; and
7. The joint beams were difficult to align.

ANALYSIS

Strand Friction

Figure 4 shows the strand forces and the measured average strand elongation during each step of jacking. The incremental trapezoidal and triangular areas in the figure are dimensioned to represent the strand elongation, based on the steel stress imposed at the end and the assumption of a linear decrease in stress away from the end. The intersecting sloping lines show the elongation increments when the west ends were tensioned first, to 10 and 20 kip, and when the east ends were tensioned first, from 20 to 29 kip.

In the 600-ft slab, for a 29-kip strand force at the ends, the total measured strand elongation was 44.1 in.—compared to a 48.7-in. zero-friction elongation, an average efficiency of 91 percent, and about 82 percent minimum strand tension near midlength or 24 kip, which is equal to 165-psi minimum effective prestress. The sloping lines from the ends for 10-, 20-, and 29-kip strand force are nearly parallel, indicating a strand friction of the bare strand in the smooth steel tubing of less than 15 lb/ft relatively independent of force.

In the 760-ft slab, the total measured strand elongation for a 29-kip force was 43.4 in.—compared to a 61.7-in. zero-friction elongation, an average efficiency of 70 percent, and minimum strand force near 40 percent of 29 kip, about 12 kip near midlength, which is equal to about 85-psi minimum effective prestress. The greater slopes of the lines from the ends with increasing strand forces indicate that strand friction increases with force as well as distance in the plastic-encased tendons.

The term "wobble friction" is used to define the "friction caused by the unintended deviation of the prestressing steel from its specified profile" (2). It is often designated as the coefficient K per foot of strand length. In structural work its value is normally assumed from 0.0005 to 0.002 for 7-wire strand in metal sheathing and from 0.0003 to 0.002 for greased strand. For a rigid conduit with adequate clearance between the strand and the conduit, K is normally considered as zero.

"Curvature friction" is defined as "friction resulting from bends or curves in the specified prestressing cable profile." It is often designated as the coefficient U per radian of angular change. Its value normally is assumed from 0.05 to 0.15 for greased strand and from 0.15 to 0.25 for strand in metal sheathing.

The tensile force (T_x) in the strand at a distance x-feet from the end is computed by the exponential equation

$$T_x = T_o \times e^{-(Kx + U\alpha)}$$

where T_o is the jacking load; α is the curvature, in radians; and K, U, T_x, and x are the symbols defined previously.

The maximum curvature on the Dulles roadway is a $6\frac{1}{2}$-deg curve, or 0.0011 rad per ft, causing the curvature friction to be insignificant compared to the wobble friction.

For a constant K and equal loads at each end of a strand, the decrease in tension from each end should be equal and, hence, symmetrical about midlength. Because each end was tensioned separately, some shifting of the point of minimum load occurred as shown in Figure 4.

The incremental strand elongation, $d\epsilon$, in a length dx is

$$d\epsilon = \frac{T_x\, dx}{a_s E_s}$$

where a_s is the strand cross section. Integration produces the total elongation of

$$\epsilon = \frac{1}{a_s E_s} \int_0^x T_x\, dx$$

The integral is the area under the curve of force along the strand length. Figure 5 shows the variation in strand force away from the end for increasing values of Kx; also, the corresponding area, equal to the average strand force, is shown in units of T_o.

The total elongation, as measured, is proportional to the average force that acts over each half-slab. Knowing the distance x, K may be computed. Straight-line and exponential strand force variations are compared in Figure 5 where a_s and E_s are assumed as unity to simplify the discussion. It shows that, for the assumed conditions and Kx = 1, the strand stress at midlength is approximately 0.1 T_o higher for an exponential distribution of friction forces than with a linear distribution in this example.

The wobble friction coefficients K, which in this analysis include some curvature friction, were evaluated from the measured elongations and efficiency values given in Table 2. They are 0.0018, 0.0005, and 0.0006 for strands in tubing in the 400-, 500-, and 600-ft long slabs respectively. For the plastic-coated strand, the values are 0.0020, 0.0017, and 0.0020 for the 760-, 500-, and 400-ft long slabs respectively at full initial strand force.

The final calculated average minimum strand loads near the midlengths of the slabs for 29-kip strand force at the ends were 20.3, 25.8, 24.1, 13.3, 19.4, and 19.7 kip for the slabs from west to east respectively, assuming exponential, rather than linear, decrease in strand force.

Continued observations of the transverse crack at the midlength of the 760-ft long slab have not indicated any readjustment of prestress to an age of 100 days.

Slab Friction

Effective prestress counteracts the frictional tension stresses in contracting long slabs. The effective prestress, 200 psi at the slab ends in all slabs and from 135 to 180 psi near midlength in the 400-, 500-, and 600-ft slabs, has been sufficient to prevent transverse cracking of those slabs to date.

By frequent joint measurements, a complete record of principal slab end movements and slab temperatures was obtained for a 3-day period and is shown in Figure 6 for the 600-ft long slab. The figure shows the average joint opening at the two ends in relation to average slab temperature, from 58 F maximum to 34 F minimum. The solid lines are for sustained temperature drop and rise as indicated; the transition between the two lines occurred over several degrees change in temperature, as indicated above the low temperature for the period. The average 24-hour temperature cycle was about 20 F with significant contraction during 15 hours and expansion for 6 hours.

Short-period measurements of length changes were made with a 50-in. long gauge in the transverse and longitudinal directions near the relatively unrestrained ends of the slabs to determine the thermal coefficient of expansion for the trap rock concrete. Its average value was approximately 5.5×10^{-6} per deg F.

The typical slab end movements, as shown in Figure 6 for temperature changes in excess of a few degrees, were similar in all the slabs, with quantitative differences. The contraction and expansion movements occurred at rates linearly related to temperature change, less than the thermal coefficient. The apparent coefficients were 5.1, 4.8, 4.7, and 4.6 millionths per deg F for the half-lengths of the 400-, 500-, 600-, and 760-ft slabs respectively. The measured joint widths were wider during rising

Figure 4. Loading sequence and strand elongations for the 600-ft long slab with strand in tubing and the 760-ft slab with plastic-coated tendons.

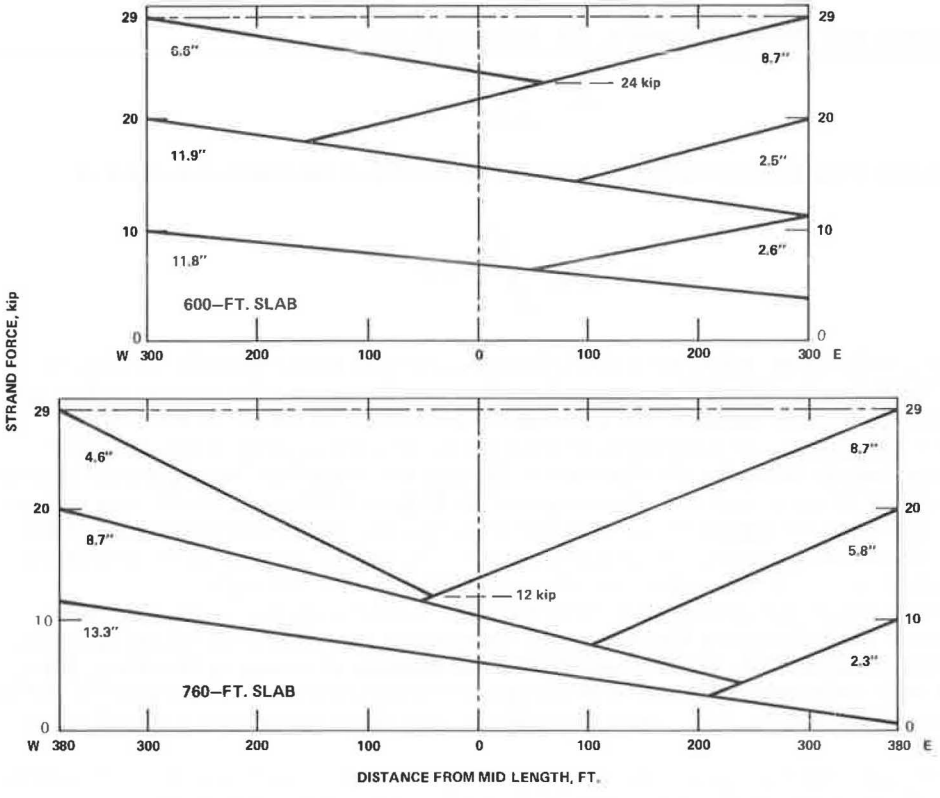

Table 2. Effectiveness of stressing at various loading steps.

Strand Load (kips)	Steel Tubing Slab			Plastic Slab		
	400-Ft	500-Ft	600-Ft	760-Ft	500-Ft	400-Ft
10	67	85	80	68	80	89
20	80	94	86	71	81	85
29	84	94	91	71	82	83

Note: Effectiveness = $\frac{\text{actual elongation}}{\text{theoretical elongation}}$ x 100 percent.

Figure 5. Comparison of linear friction distribution with exponental distribution for equal effectivensess.

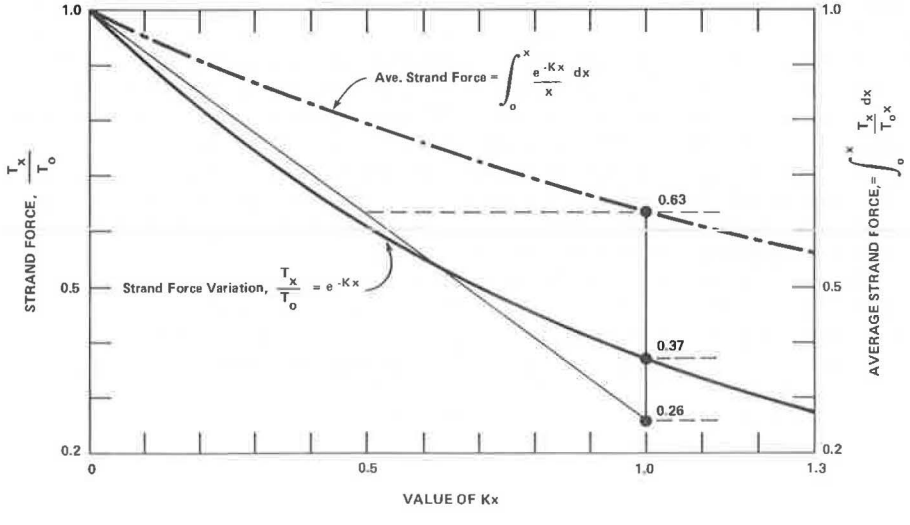

temperatures by 0.03 in. at the 400 ft to 0.06 in. at the 760-ft slab ends. Lines have been drawn in Figure 6 to indicate the contraction and expansion movements that would have taken place at the ends without frictional restraints for contraction from 58 F and expansion from 34 F.

The maximum frictional restraints were obviously present at the minimum and maximum temperatures of the sustained temperature change, tension, and compression. The changes in joint widths immediately following temperature reversal involve deformations in reversal from maximum frictional stress in one direction to some smaller friction stress in the opposite direction throughout the slab length. The visible end movements were small because of the large compensatory strain changes in the slabs, continuing for a few degrees. Thereafter, end movements took place at the greater rates corresponding to the apparent thermal coefficients with relatively small increase in the frictional restraints for the remainder of the sustained temperature change. Figure 6 shows the complex relations between slab movements and frictional restraints in long slabs, with movements continually changing from zero at a point of equilibrium near midlength, and friction stresses increasing from zero at the freely moving ends to a maximum at the point of equilibrium, with time-dependent strains acting to restrain the movements along the slab. If we assume that the tension stresses at minimum temperature and the compression stresses at maximum temperature are equal, the average friction stress at the extreme cyclic temperature can be estimated, provided stress-deformation relations in the concrete for the short times of stress duration are known.

The modulus of elasticity of the concrete was determined in the laboratory by short-time creep tests on 90-day old field-cured cylinders. The gauged cylinders were sealed and subjected to constant stresses that ranged from 90 to more than 200 psi for up to 60 hours, and the companion unstressed cylinder was used as control. The data are shown in Figure 7, along with creep data for longer periods from the literature and middepth deformation data from a 50-in. gauge line at one end of the pavement slab where the prestress could be assumed to be constant at 200 psi. The modulus of elasticity for the cylinders was approximately 5×10^6 psi immediately on load applications and decreased to 4.3×10^6 for 1 hour of load, 3.5×10^6 psi for 6 hours, and 3.0×10^6 for 15 hours of constant stress. The pavement observations indicate slightly higher modulus values, probably because of the higher moisture content in the pavement. No tests were conducted under tensile loadings.

The frictional restraint for the temperature cycle from 34 to 58 F in the 600-ft long slab can be computed as follows:

1. Theoretical unrestrained end movement for 24 F of the 3,600-in. half-length—$24 \times 5.5 \times 10^{-6} \times 3{,}600 = 0.48$ in.;
2. Observed end movement from Figure 6—0.36 in.;
3. Movement restraint, difference between 0.48 and 0.36 in.—0.12 in.;
4. Average change in friction strain—$0.12/3{,}600 = 33 \times 10^{-6}$; and
5. Average change in friction stress (using $E = 3.5 \times 10^6$ for 6-hour duration)—115 psi.

The computed change in friction stress is from maximum average tension to maximum average compression.

The maximum friction stress at midlength can be computed if the friction coefficient is assumed to be constant, with friction stress increasing linearly from zero at the ends to midlength.

The maximum restraint force is equal to the weight of the slab half (at 144 lb/ft^3) times the constant friction factor. The maximum restraint stress change is then twice the average, or 230 psi at midlength, or from 115-psi tension to 115-psi compression. The analysis yields a friction factor of $115/300 = 0.38$. Similar analyses of the other slabs produced friction factors of 0.44 and 0.46 for the 400- and 500-ft long slabs respectively. These coefficients are in good agreement with laboratory tests (3).

The actual friction coefficient would be higher near the slab ends and lower near midlength; however, for conservative use in design, the assumption of a constant friction coefficient produces the highest estimate of friction stress at midlength.

The most unfavorable average stress condition in the prestressed slabs exists at minimum temperature near midlength. Computed for the minimum prestress corresponding to the strand forces at midlength, and for 0.5 friction coefficient, a minimum compression stress of 10 to 54 psi exists in the 400- to 600-ft prestressed slabs; however, at midlength in the 760-ft slab, there would be present an average tension stress of about 100 psi for a normal temperature drop.

Transverse Cracking

From January 14 to 16, after rains on January 13, and with strong northerly winds on January 15, the air temperature at the project dropped from 68 to 3 F and the average concrete temperature from 58 to 16 F. The negative temperature gradient was 2 F per in. or more during the nights of January 15 and 16. Subfreezing temperatures at the subgrade lasted from late evening January 15 to 2 p.m. on January 17 and again from that evening to noon January 18. A transverse crack was discovered on January 17 at 8 a.m. 368 ft from the west end of the 760-ft slab. It probably had occurred a few hours previously. At its discovery, the crack measured about 0.17 in. in width with an average concrete temperature of 18 F. At 5 p.m. that day, the crack was closed at a concrete temperature of 42 F.

The stress conditions at the time of cracking can be estimated by using three major components. Restrained frictional movements for the sustained concrete temperature drop of 42 F produced maximum tensile stresses of about 230 psi, but the stress may have been more than 400 psi if the slab adhered to the frozen subbase. The fully restrained curling for the exceptionally high 2 F per in. negative thermal gradient could have produced a surface tensile stress of about 130 [(3 in. × 2 F/in.) × (5.5×10^{-6}/F) × (4×10^{6} psi)], added to the naturally existing warping restraint stress of 100-psi tension at the surface (6).

The tensile stresses are countered by the prestress. As previously determined, the effective minimum prestress near midlength of the 760-ft slab was about 13.3 kip per strand, which produces an average of 95-psi compressive stress on the cross section.

Summarizing the preceding estimates gives top tension stress from (230 + 130 + 100 - 95) 365 to (400 + 130 + 100 - 95) 535 psi, however, the top tension stress may have been even higher because of rapid drying of the wet concrete in the high wind after the rains on January 13, resulting in increased warping restraint stress at the surface.

The crack was carefully observed from March 7 to 10 when the slab end movements were measured for analysis on slab friction. On March 8, the maximum average concrete temperature was 58 F. The crack remained closed on decreasing temperature to 52 F and then widened at an even rate to 0.14 in. at 8 a.m. the next morning at 34 F minimum temperature. On increasing temperature the crack closed to 0.01 in. at 40 F. Figure 8 shows the measured average joint widths at each slab end, 3.01 in. at 58 F when expanding and 3.38 in. at 34 F when contracting, and the total length change, including the change in crack width, for the half-slab.

The friction restraint stresses can be computed, keeping in mind that the frictional tension stress at the crack must equal the strand tension across an open crack and that a contraction of 0.07 in. took place at the crack in each half-slab with a slight increase in tension from the crack to the equivalent 700-in. distance [(0.07)/(52 - 34)] 5.5×10^{-6} and with an equal, slight decrease to 1,400 in. from the crack and to zero at the slab end. Assuming a 4×10^{6} psi sustained modulus in the cracked slab, the following calculations can be made:

1. Unrestrained length change for 24 F at 380 ft (4,560 in.)—0.60 in.;
2. Observed length change, 0.37 + 0.07 in.—0.44 in.;
3. Total restraint from maximum expansion to contraction—0.16 in.;
4. Restraint in tension for 13½-kip strand force, maximum of 95 psi, (95/4,000,000) × 1,400 + [(95/2) × 4,000,000] × (4,560 - 1,400)—0.071 in.;
5. Restraint in compression during expansion (0.16 - 0.071)—0.089 in.; and
6. Maximum frictional stress change in compression, assuming linear change from zero at the ends to twice the average at midlength, 2(0.089/4,560) × 4,000,000—156 psi.

Figure 6. Slab end movements versus the concrete temperature for the 600-ft slab.

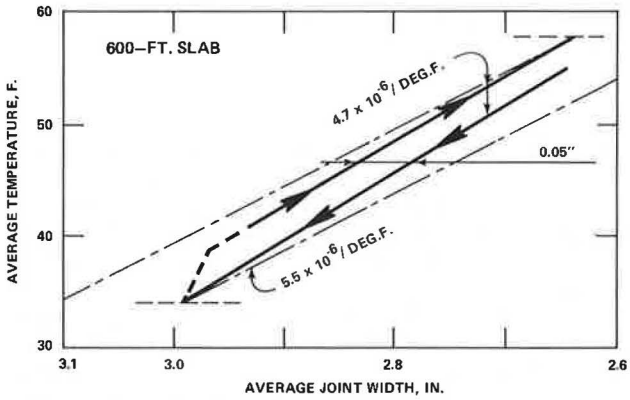

Figure 7. Effect of sustained loading on the modulus of elasticity.

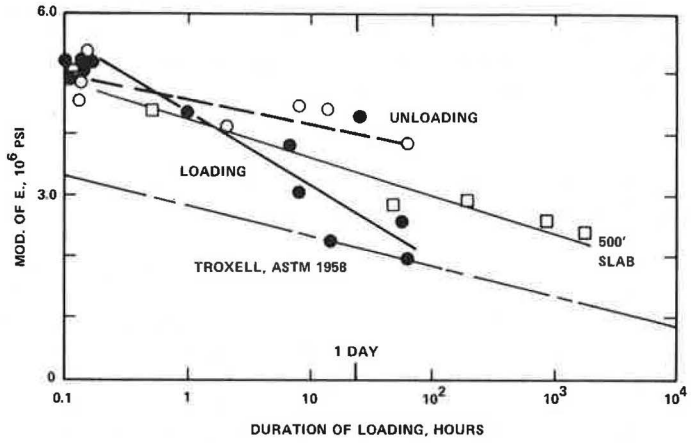

Figure 8. Slab end movements versus the concrete temperature for the cracked 760-ft slab.

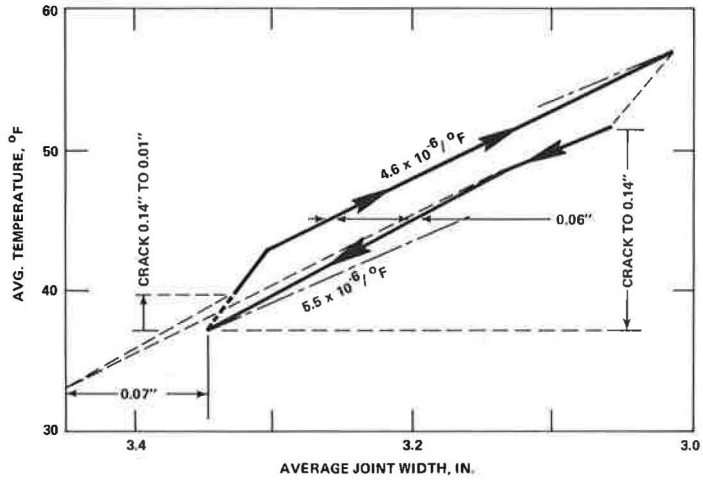

The corresponding average friction coefficient would be 156/380, or 0.41. This value compares with 0.38, 0.44, and 0.46 computed for the other slabs in the project. The observations and computations support use of 0.5 friction coefficient for frictional maximum stresses at normal temperature cycles in the long, uncracked, prestressed slabs.

Progressive Slab Length Changes

Monuments placed along both edges of the embankment were used in conjunction with measurements across the joints to determine long-time longitudinal movements of the pavement slabs beginning shortly after concrete placement (Fig. 9). The shortening of the slabs is the result of elastic and inelastic shortening during stressing, shrinkage, and creep. At 100 days, the progressive length changes varied from less than $\frac{3}{4}$ in. in the 400-ft slab to 1 in. in the 760-ft slab.

The information shown in Figure 9 is replotted in Figure 10 as the unit length change versus time for the slabs. It also shows the unit length changes at middepth, as projected from measurements with the 50-in. long gauge near the ends. The longitudinal measurements include deformations for the longitudinal prestress, and the transverse measurements are for zero prestress. The transverse measurements indicate a maximum shrinkage of about 70×10^{-6} at 40 days with some subsequent unit expansion of about 10×10^{-6}. These transverse shrinkage values may be slightly low because they include a transverse expansion of about 10×10^{6}, which is caused by Poisson's ratio effect of the 200-psi prestress at the ends in the longitudinal direction. These values are in agreement with previous studies (6). The longitudinal deformations probably also were affected by the expansion that occurred after 40 days.

Elevations

Profile measurements over 140-in. lengths showed that the slab ends curled up and down in response to the negative and positive temperature gradients. Full restraint, however, was reached at 50 to 100 in. from the slab ends.

The changes in curvature for overnight curling at the joints and at midlength of the 500-ft slab with plastic-coated tendons are shown in Figure 11. The profile line at the west joint was 2 ft from the edge, whereas that at the east joint was 6 ft from the edge. Although the profiler was supported on two points 100 in. apart, which fluctuated in elevations, the approximate deflections can be determined by projecting the slope changes at the support 120 in. from the joint. This assumes that no change in elevation occurred at that distance from the joint. The figure shows only differences and not the actual profile, but it does indicate that the ends are moving up and down daily, whereas the midlength of the slab remains flat and completely restrained.

The slab elevations near the joints at 3 months of age were derived from 20-in. clinometer slope measurements made about 24, 74, and 124 in. from the end (Fig. 12). Initial measurements were made while the slab was being cured. The data indicate that the slab ends have moved downward 0.02 to 0.03 in. at the joints.

Because the prestress was applied $\frac{1}{2}$ in. below middepth at the ends, it produced section compressive stresses of 100 psi at the top and 300 psi at the bottom.

Plain slabs or slabs with prestress at middepth would be expected to warp upward about 0.1 in. over this same period (6). Application of the prestress below middepth appears to have preserved subgrade support near the slab ends and prevented uplift and voids under the joints.

PRETRAFFIC LOAD TESTS

Static Loads

Controlled axle-load tests were made on the two 500-ft slabs on January 25 and 26 after the roadway was essentially completed but before it was subjected to any vehicle loadings. Testing was conducted with both $19\frac{1}{2}$- and 33-kip single-axle loads on the rear of the trailer with tire pressures of approximately 92 psi. The axle could come to about 3 in. of the slab end before the tires received support from the contiguous

Figure 9. Total early age shortening of the slabs, independent of temperature.

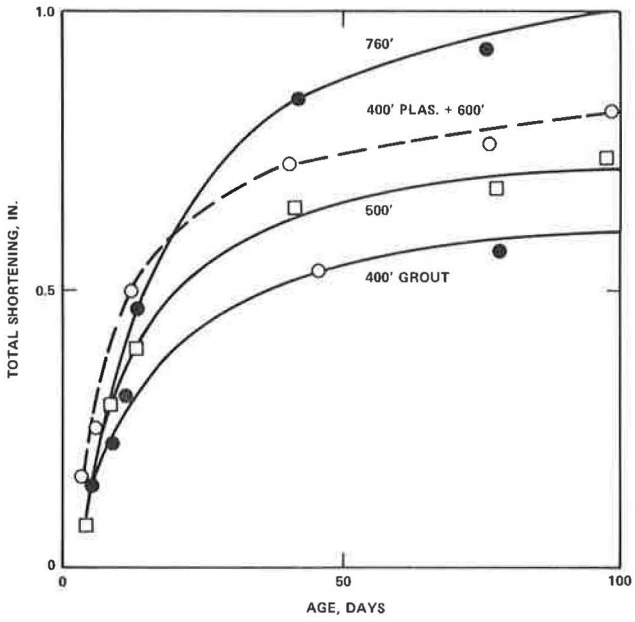

Figure 10. Unit shortening of main slabs compared to end and transverse length changes, independent of temperature.

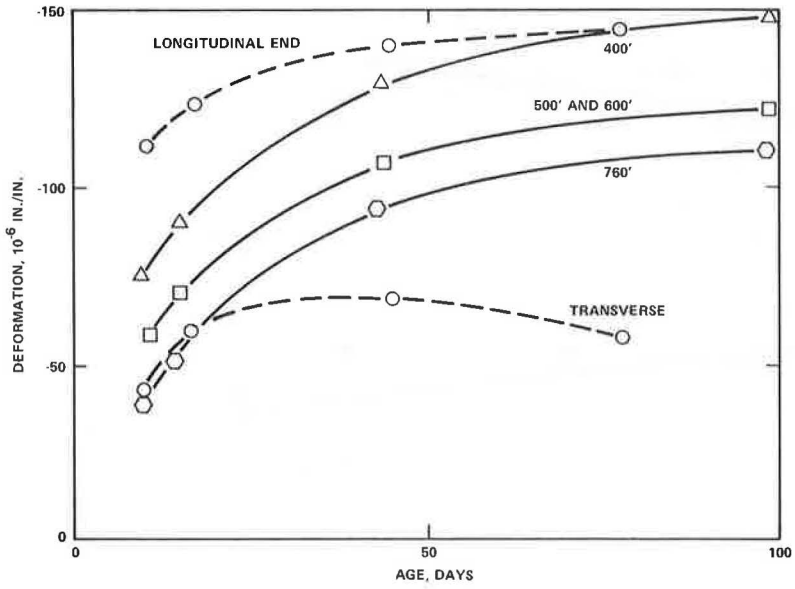

Figure 11. Relative movements for the ends and midlength of the 500-ft slab containing plastic-coated tendons.

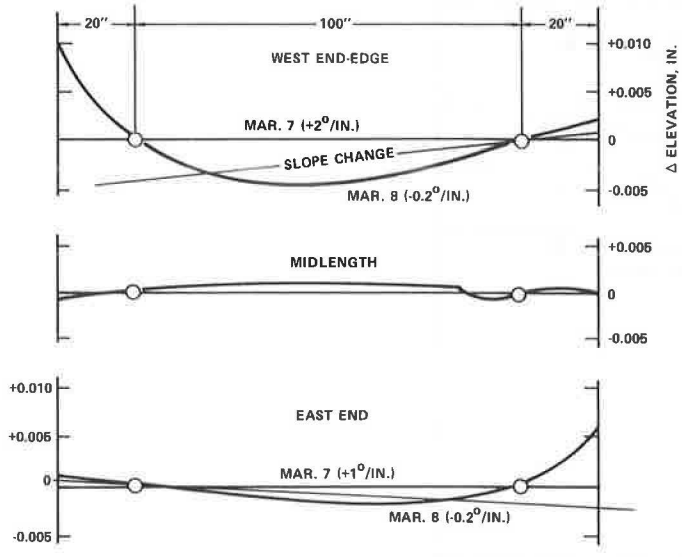

Figure 12. Permanent downward deformation of slab ends caused by prestress below middepth.

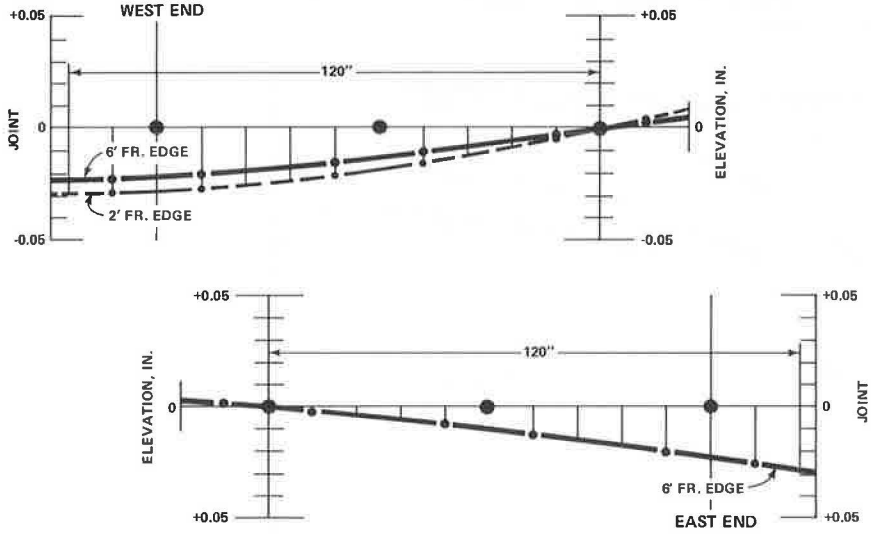

slab, and the center of the wheel could come to within 10 in. of the edge before the outside tire would receive support from the shoulder.

The east end of the 500-ft long slab prestressed with strand in steel tubing was tested by backing the loaded axle toward the transverse joint with the truck centered in the north lane (Fig. 13). The axle was positioned and left for 10 min at distances of 100, 40, 20, and 6 in. from the end while measurements were made. Strain gauges were mounted along the center of the I-beam flange as shown in the figure. The five Benkelman beams were supported on the shoulders and the adjacent slab, essentially outside the basin of influence.

The maximum measured strains and deflections obtained under first the 19.5-kip axle and later the 33-kip axle loadings when they were placed 6 in. from the slab end are shown in Figure 13. Maximum compressive strain occurred directly under the wheel and was about 50×10^{-6} for the 19.5-kip axle and about 70×10^{-6} for the 33-kip axle.

Deflections were a maximum between the wheels. For the axles at 6 in. from the joint, the deflections were about 0.04 in. under both axle loadings. The rebound deflection from axle loading at the joint was 0.02 in. for the 19.5-kip axle and 0.035 in. for the 33-kip axle.

A second series of 19.5-kip axle load tests was conducted with the center of the nearest wheel 16 in. from the shoulder edge of the pavement. The various positions are shown in Figure 14 along with the measured strains and deflections. With the axle stationary 6 in. from the joint, the maximum flexural strain along the joint was about 30×10^{-6}. Tension occurred at the surface between the wheels. Surface compressive strains of almost equal magnitude occurred under each wheel. Maximum deflection at the corner for this loading was about 0.045 in., and the rebound deflection was 0.038 in.

Five-in. long electric resistance strain gauges were mounted on the concrete along the outside edge of the pavement 20, 40, and 100 in. from the joint. They were used to measure surface edge strains for the 19.5-kip axle. Figure 15 shows the locations of the tires with the outside wheel 16 in. from the edge and the measured strains. When the axle was 6 in. from the joint, the surface tension strain was greatest at about 30 in. from the joint and was about 50×10^{-6}, which decreased to less than 30×10^{-6} at 40 in. from the joint.

With the axle in positions 100, 40, and 20 in. from the joint, surface tension was not critical, but bottom tensile edge strains at the wheel were 65×10^{-6} for the axle when it was 100 and 40 in. from the joint and 50×10^{-6} when it was 20 in. from the joint.

By extrapolating the preceding information, it is apparent that substantial top tension strains along the transverse joint occur only for the wheel loads near the corner, about 50×10^{-6} maximum for a 20-kip axle within 6 in. of the joint and the outside wheel 10 in. from the edge. Somewhat higher flexural strains along the joint can apparently occur under the wheels of a 20-kip axle tracking normally when crossing the joint, maximum 60×10^{-6} tension at the bottom. Along the pavement edge, for a 10-kip corner wheel, the top tension strain can possibly approach a value of 70×10^{-6} but is less than 30×10^{-6} for an axle 15 in. or more from the joint. The flexural strain along the edge reaches its maximum value of about 70×10^{-6} bottom tension at edge wheels more than 20 in. from the joint.

Applying the modulus of elasticity of 5×10^{6} psi for concrete (from laboratory tests) and 30×10^{6} psi for steel to these load tests, the maximum flexural stresses along the joint, under wheels 3 in. from the joint, are ±300 psi in the 6-in. concrete and ±1,800 psi in the 6-in. steel I-beam. Along the edge, the maximum computed flexural stress is ±350 psi. The longitudinal flexural stresses combine with the prestress of -100 psi at the top and -300 psi at the bottom in the 6-in. pavement near the joints; the resulting maximum combined tension stresses at the edge are +250 psi top tension for a wheel at the corner and +50 psi bottom tension for axles more than 20 in. from the joint.

Moving Loads

Deflections were measured at the west end outside corner of the 500-ft slab (grouted tendons) under the 33-kip axle load moving at creep speed. These were the first heavy

Figure 13. Joint edge strains and deflections under 19.5- and 33-kip axle loads.

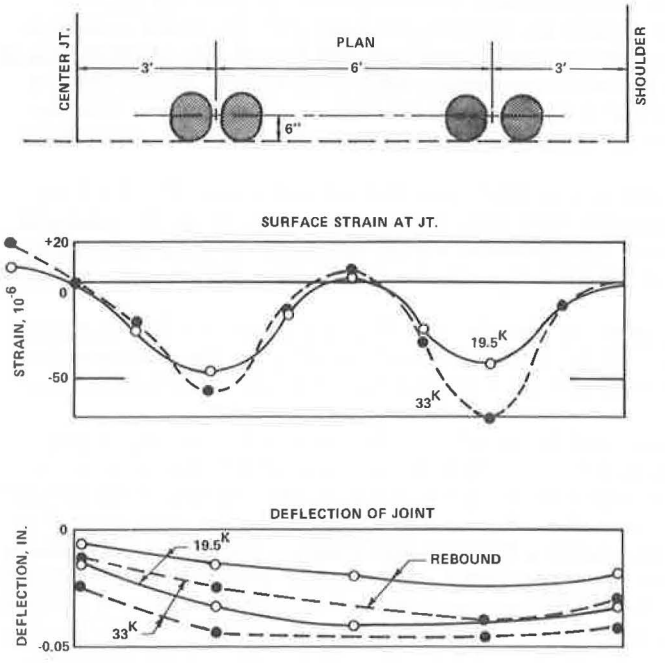

Figure 14. Strains and deflections at the joint under a 19.5-kip axle edge load placed at the joint and at 20 and 40 in. from the joint.

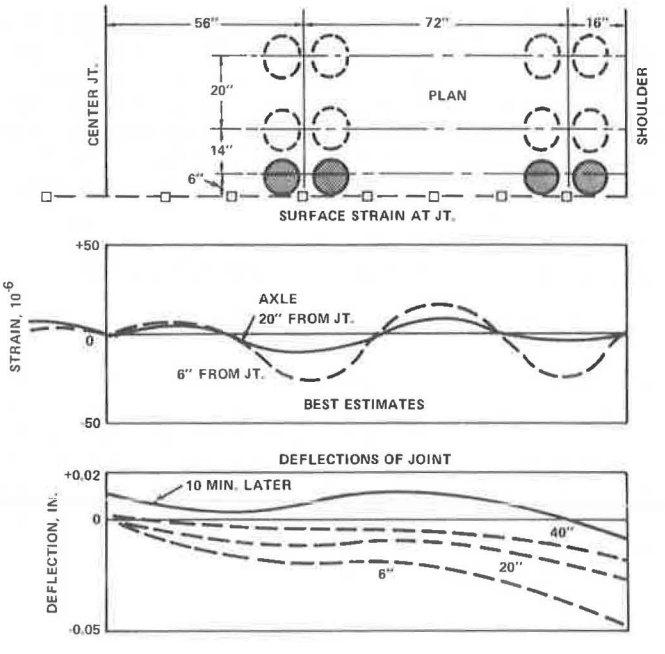

Figure 15. Strain distribution along the shoulder edge of the slab for axles placed from 6 to 100 in. from the joint.

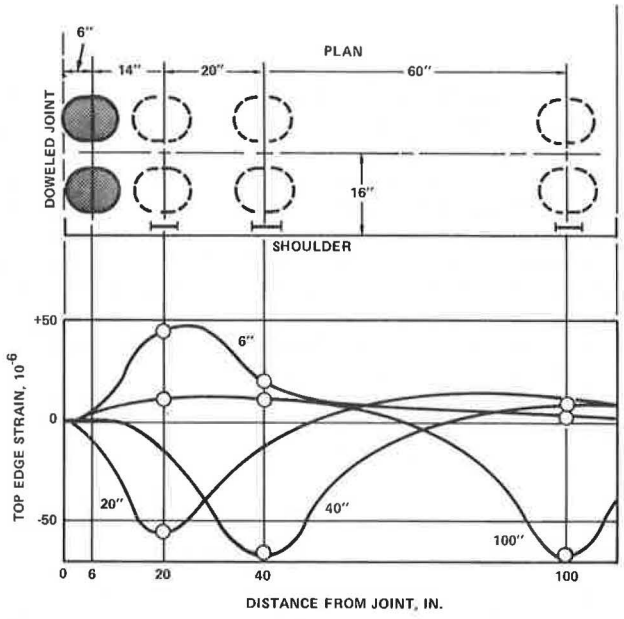

Figure 16. Corner deflections and rebounds of the end of the 500-ft slab (grouted tendons) during the first six vehicle crossings.

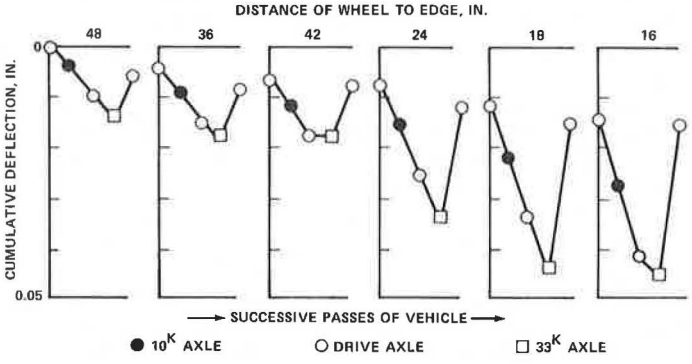

Figure 17. Corner deflections for different axle weights as the axles crossed the joints at various distances from the shoulder edge.

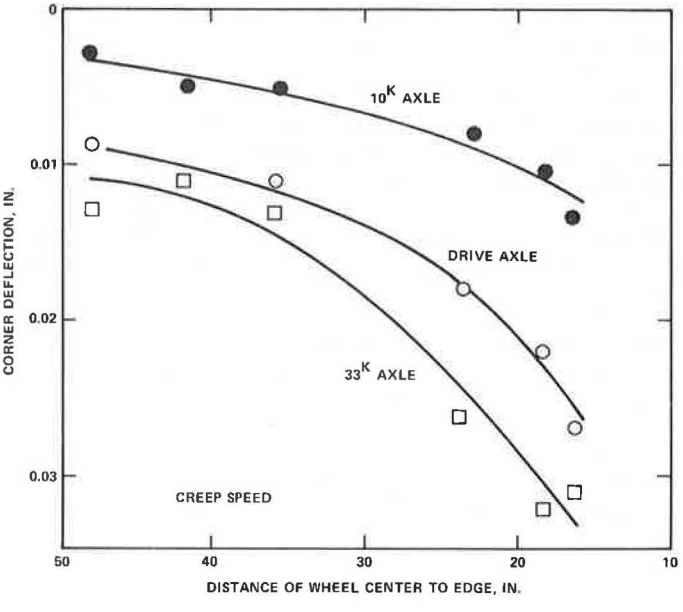

loads to cross that joint. Six consecutive crossings were made with the wheel center from 48 to 16 in. from the edge. The trucking sequence and the deflections measured with Benkelman beams are shown in Figure 16. Consolidation under the slab end is shown for these initial applications of a heavy axle load. For normal lane tracking, as represented by the first three runs, the consolidation amounted to 0.007 in. under the corner. The following three loads, tracking 24, 18, and 16 in. from the edge, increased the corner consolidation to 0.015 in. The corner deflections increased from about 0.010 in. for normal wheel tracking to 0.030 in. for the wheel 16 in. from the edge. These creep speed deflections are about one-half of the static deflections for the same axle load, as measured under the 19.5-kip stationary axle (Fig. 13).

The same data from the creep tests are replotted in Figure 17 to show the relation between corner deflections and the distance to the wheel track for the three axles of the truck. The three curves are consistent and indicate that the deflections under traffic will generally be less than 0.03 in. These deflections will probably decrease after the slab ends are fully seated by traffic.

CONCLUSIONS

The study supports the following conclusions:

1. The prestressed pavement was constructed in essential conformance to the design. The construction problems were remedied without major modifications although they suggest features that could be improved on future projects.
2. Average strand effectiveness, based on elongation, was approximately 90 percent for strand in steel tubing and 80 percent for plastic-enclosed strand. Wobble friction coefficients of 0.0006 and 0.0019 per ft of strand were indicated for the two types of tendons respectively.
3. Independent of temperature, the total length changes because of elastic shortening, shrinkage, and creep were less than 1 in. through 100 days of age. Shortening in the unstressed transverse direction was 70×10^{-6} in./in., whereas the longitudinal unit shortening approached values about twice that amount.
4. The double layer of polyethylene under the slab reduced the coefficient of subgrade friction to less than 0.5 for diurnal movements.
5. The slab ends move at a rate consistent with a slightly reduced apparent coefficient of thermal expansion. The expansion movement is offset from the contraction movement by an amount equal to the sum of the average tensile and compressive length changes produced by the frictional restraint stresses.
6. The effective prestress at midlength is from 135 to 180 psi in the 400- to 600-ft slabs and about 95 psi in the 760-ft slab. Subgrade friction for normal temperature drops does not overcome the prestress in the 400- to 600-ft slabs; however, at midlength in the 760-ft slab, a tension stress of about 100 psi could exist for normal temperature drops.
7. The longest slab (760 ft) suffered a transverse crack at about midlength during a sustained concrete temperature drop of 42 F to 16 F at 1½ months of age. The effective prestress at midlength of less than 100 psi was apparently inadequate for this slab length under the extreme environmental conditions.
8. The interiors of the slabs are essentially flat lying because of restrained warping strains. The slab ends curl upward and downward in response to thermal gradients. The prestress, applied below middepth, has apparently eliminated warping slab end uplift due to moisture gradients.
9. Corner deflections under a static axle load of 20 kip approached 0.04 in. at the transverse joints on the 6-in. cement-treated base.
10. Tensile stresses up to 300 psi in the concrete occur along the transverse joint and along the longitudinal edge within 40 in. from the corner for a static 20-kip axle at the joint, with one wheel at the corner. Along the edge and away from the joint, maximum longitudinal tensile load stresses are less than 50 psi under the 20-kip axles when the 200-psi prestress is present, exclusive of frictional stress.
11. The first dynamic loads caused consolidation under the joint as the slab end was seated.

12. Deflections under a 33-kip axle crossing a joint at creep speed were less than one-half of the deflections under the same stationary load.

ACKNOWLEDGMENT

This report is an abridgment of a Federal Highway Administration report (7).

The construction of this project was conducted and supervised by the FHWA Region 15 Demonstration Projects Division. The Pavement Systems Group, Office of Research, developed the design for prestressing and conducted the research study of the pavement.

Testing of the slabs with simulated aircraft loadings is being conducted by the U.S. Corps of Engineers, Waterways Experiment Station, Vicksburg, Mississippi, for the Federal Aviation Administration and will be reported separately.

REFERENCES

1. The AASHO Road Test: Report 5—Pavement Research. HRB Spec. Rept. 61E, 1962.
2. ACI Manual of Concrete Practice. American Concrete Institute, ACI 318-63, Ch. 26, 1968.
3. Methods for Reducing Friction Between Concrete Slabs and Cement-Treated Subbases. Cement and Concrete Research Institute, Portland Cement Assn., Sept. 1971.
4. Prestressed Concrete Pavement Demonstration at Dulles International Airport. Public Roads, Vol. 37, No. 1, June 1972.
5. Prestressed Road Slab Gets Tested. Engineering News-Record, Aug. 5, 1971.
6. Friberg, B. F. Investigations of Prestressed Concrete for Pavements. HRB Bull. 332, 1962.
7. Friberg, B. F. Prestressed Concrete Highway Pavement at Dulles International Airport, Research Progress Report to One Hundred Days. Federal Highway Administration, FHWA-RD-72-29.
8. Friberg, B. F. Sector Analysis for Concrete Pavement Load Stresses. Jour. Highway Div., Proc. ASCE, Paper 1153, Jan. 1957.
9. Thwing, J. W. Prestressed Concrete Pavement Construction. Federal Highway Administration, FHWA-RDDP-17-1, Feb. 1973.

PROBABILISTIC CONCEPTS AND THEIR APPLICATIONS TO AASHO INTERIM GUIDE FOR DESIGN OF RIGID PAVEMENTS

Ramesh K. Kher and Michael I. Darter, Center for Highway Research, University of Texas at Austin

Probabilistic design concepts have been applied to modify the AASHO Interim Guide for the Design of Rigid Pavement Structures; it is now possible to design for any specified level of reliability. The major objective for applying probabilistic concepts to pavement design is to make the design process sensitive to the many variabilities and uncertainties associated with the design, construction, and performance of rigid pavements. This provides a rational means of designing at varying levels of reliability depending on the pavement function. This method makes the design process closer to reality than the present deterministic method and, therefore, upgrades the current procedure. Variance models were developed for the performance equation of the AASHO Guide to predict variation in pavement performance due to statistical variations in traffic estimation, flexural strength and modulus of elasticity of concrete, concrete thickness, joint continuity, foundation modulus, initial serviceability index, and lack of fit of the AASHO performance equation. Estimates of the variations associated with each of the variables listed above are obtained by analysis of data from actual concrete pavement projects. A new revised nomograph is developed to include, among other things, a scale for reliability and a scale for the overall variance determined by the level of quality control exercised, variations associated with design parameters, and errors associated with traffic predictions. The variance models are also applied to determine the relative significance of the design factors associated with rigid pavement design and to quantify the effects of quality control on pavement performance.

•ONE of the most important areas of needed research with regard to the design of asphalt concrete pavement systems, as selected by a Highway Research Board advisory committee in a workshop held at Austin in December 1970, was stated as follows (25):

> So that designers can better evaluate the reliability of a particular design, it is necessary to develop a procedure that will predict variations in the pavement system response due to statistical variations in the input variables, such as load, environment, pavement geometry, and material properties including the effects of construction and testing variables. As part of this research it will be necessary to include a significance study to determine the relative effect on the system response of variations in the different input variables.

Designers of rigid pavements cannot help but rank this research need as one of the most important areas of their interest.

In this paper, probabilistic design concepts have been applied to the AASHO Interim Guide for the Design of Rigid Pavement Structures (1), making it now possible to design

Publication of this paper sponsored by Committee on Rigid Pavement Design.

a pavement for any specified level of reliability. The major purpose for applying probabilistic concepts to pavement design is to make the design much closer to reality than the present deterministic method, therefore upgrading the current procedure. This will provide engineers with means to design a pavement thickness at a desired level of reliability or confidence (i.e., the serviceability of the pavement will not decrease below a specified minimum throughout the design period for which the pavement is being designed).

During the past few years, several investigators (2-9) have suggested that probabilistic concepts be applied to the design and analysis of portland cement concrete and other structures. An excellent summary of these concepts is given in a series of four articles published by the American Concrete Institute (10-13) on the development of a probability-based structural code. The basic reason for the development of such a code is that the loads and resistances in a concrete structure are variable or probabilistic in that they cannot be estimated exactly and they change from point to point in the structure and the foundation soil. For the same reason, random failures in concrete pavement have been observed for many in-service highways and airports as well as the pavements at the AASHO Road Test.

In pavement design, several empirical safety and judgment factors have been applied in the past to "adjust" for the many uncertainties involved without quantitatively considering the magnitude of the uncertainties involved. This generally has resulted in an overdesign or underdesign, depending on the situation and the level of applied safety factor. If the current deterministic pavement design procedures were modified so that the safety factors applied depended on the magnitude of the variation of concrete properties, supporting soil properties, smoothness variations, and uncertainties in traffic estimation, a more realistic design would be achieved. The pavement could be designed for a desired level of reliability, depending on its function and other decision factors.

Whereas the AASHO Guide (1) has been selected to demonstrate the applicability of probabilistic concepts, and at the same time to modify it so that engineers can achieve a pavement design at any desired level of reliability, the concepts have been presented in a general format applicable to any other design model. The method provides a powerful tool to researchers to perform sensitivity analysis of various parameters of a model, to study the effects of quality control and material variability on the output of the model, and to design a structure at any desired level of reliability.

Probabilistic design concepts are discussed first and followed by a short review of the equations involved in the AASHO Guide with emphasis on the uncertainties involved. A derivation of the necessary probability models and a characterization of variabilities associated with concrete pavement design are then presented. A brief sensitivity and quality control analysis illustrating the effects of variability of design factors on pavement performance is then followed by a presentation of the modified nomograph and design procedure. Finally, the results are illustrated by a practical example problem.

PROBABILISTIC CONCEPTS APPLIED TO PAVEMENT DESIGN

The sole underlying reason for formulating a probability-based design procedure is to better account for the variabilities and uncertainties associated with loadings and resistances of a structure. Current design practices are deterministic in that all design factors are assumed to be exact quantities, not subject to variations. However, based on personal judgment and experience, specific safety factors have always been used to account, at least partially, for these uncertainties. These safety factors have generally been the reductions of working strengths of materials, designing for heaviest wheel load, or, in some cases, a gross increase in structure thickness based on personal judgment.

In essence, the three basic types of variations associated with portland cement concrete pavement design that must be considered are as follows:

1. Variability within a design section (or project if the pavement structural design remains the same throughout) such as in flexural strength or subgrade support along a pavement;

2. Variability between assumed average design values and those obtained "as constructed" including, for example, the difference of average measured flexural strength from that specified in design and specifications and/or unforeseen variations to which the pavement may be subjected during its design life, such as traffic and gain or loss of material strengths; and
3. Variability due to the lack of fit of the empirical equation used in the design procedure.

The basic way in which uncertainties in concrete pavement design can be accounted for is through reliability concepts. There are several ways to define the reliability of a pavement. Because the AASHO Guide is based on the serviceability concept, the following definition of reliability is proposed.

Reliability, R, is in general the probability that the pavement will have an adequate serviceability level for the design period. Specifically it may be defined as the expected percentage of length along a project (if the design is constant) that will maintain a serviceability level greater than the specified minimum for a design period. The expected percentage length of failure along a project would correspondingly be defined as 1 - R. Because the failure phenomenon is mostly due to the application of repeated loads, the reliability of a pavement structure will be determined mathematically from the basic concept that a no-failure probability exists when the number of load applications, N, that a given pavement section can withstand to a specified minimum serviceability index is not exceeded by the number of load applications, n, actually applied. Failure as used in this paper refers to a condition of the pavement when the serviceability index drops below its specified minimum level and some sort of repair maintenance or replacement is needed to restore the serviceability.

If the serviceability index is measured along an in-service pavement at any interval, perhaps every 0.2 mile, it is found to vary considerably down the roadway. Each short section will reach failure at different number of load applications because of the variational nature of material strengths, pavement thickness, pavement smoothness, joint conditions, and foundation support. Because of the random nature of fatigue failures, it has been assumed that N is a random variable and the distribution of log N to failure is approximately normally distributed.

The number of load applications that will be applied to a given pavement has been considered as an exact number. However, the actual traffic in most cases has been different from the estimated traffic. It is also assumed that the forecasting error is log normally distributed because of the nature of estimating procedures and the errors associated with various factors that are considered.

Reliability is defined as the probability that N will exceed n as presented in the following expression:

$$R = P[(\log N - \log n) > 0] = P(D > 0) \tag{1}$$

where $D = \log N - \log n$.

Because log N and log n are both normally distributed, D will also be normally distributed. Using bars above the expressions to represent their mean values, we can write the following equation as

$$\overline{D} = \overline{\log N} - \overline{\log n} \tag{2}$$

The standard deviation of D will be computed as s_D by the following equation:

$$s_D = \sqrt{s^2_{\log N} + s^2_{\log n}} \tag{3}$$

where

$s_{\log N}$ = standard deviation of log N, and
$s_{\log n}$ = standard deviation of log n.

Reliability is given by the following expression:

$$R = P[0 < (\log N - \log n) < \infty] = P(0 < D < \infty) \tag{4}$$

The transformation that relates D and the standardized normal variable Z is

$$Z = \frac{D - \overline{D}}{s_D} \tag{5}$$

For D = 0,

$$Z = Z_o = -\frac{\overline{D}}{s_D} = -\frac{\overline{\log N} - \overline{\log n}}{\sqrt{s^2_{\log N} + s^2_{\log n}}} \tag{6}$$

For $D = \infty$,

$$Z = Z_\infty = \infty \tag{7}$$

The expression for reliability may be rewritten as

$$R = P(Z_o < Z < Z_\infty) \tag{8}$$

The reliability may now be determined very easily by means of the normal distribution table. The area under the normal distribution curve between the limits of $Z = Z_o$ and $Z = \infty$ gives the reliability of a design.

An example for the calculation of reliability will be given here. If we assume that $(\overline{\log N}, s_{\log N}) = (7.100, 0.400)$ and $(\overline{\log n}, s_{\log n}) = (6.500, 0.200)$,

$$Z_o = -\frac{7.100 - 6.500}{\sqrt{(0.4)^2 + (0.2)^2}} = -1.342$$

From normal distribution tables the area from -1.342 to ∞ is 0.91. Therefore, R is 91 percent.

The applicability of these concepts is demonstrated in the following sections.

AASHO RIGID PAVEMENT DESIGN MODEL

The serviceability trends of the rigid pavement sections at the AASHO Road Test led to the following equation (15), which predicts the number of 18-kip single-axle load applications W that a pavement will sustain:

$$\log W = 7.35 \log (D + 1) + 0.05782 + \frac{G}{\beta} \pm \Delta \tag{9}$$

where

$$G = \log \frac{P1 - P2}{P1 - 1.5},$$

$$\beta = 1 + \frac{16.196 \times 10^6}{(D + 1)^{8.46}},$$

D = concrete thickness (in inches),
P1 = initial serviceability index, and
P2 = serviceability index of the pavement after sustaining W applications of 18-kip single-axle load applications.

The term Δ associated with the prediction Eq. 9 is called the "lack-of-fit" error. It is defined here as the error produced by the prediction equation not containing all the necessary parameters of design because of a lack of data or because the equation has not been fitted properly through the available data. Some of the causes of this lack of fit are very obvious. An excellent example is the lack of data that resulted in showing

that the effects of subbase thickness and amount of reinforcement were insignificant, and therefore these terms should be ignored. Other causes of this lack of fit are drastic linearizations, extrapolations, and assumptions used for the sake of achieving simplicity in data analysis. The errors also arise because of material variability, which will be dealt with in later sections. Errors arising because of material variabilities will be excluded from the definition of Δ.

To design rigid pavements with materials and conditions appreciably different from those that existed during the Road Test, an AASHO subcommittee on design (16) developed an additive term to Eq. 9 to account for different physical properties of pavement materials. The modified number of 18-kip single-axle applications, W_m, are given as

$$\log W_m = \log W + \log\left(\frac{f\delta}{215.625\ J} \times \frac{D^{0.75} - 1.1326}{\delta^{0.25} D^{0.75} - 18.423}\right)^b \tag{10}$$

where

$\delta = E/k$,
E = modulus of elasticity of concrete (in psi),
k = gross modulus of foundation reaction (in lb/in.^{3}),
f = flexural strength of concrete (in psi),
J = joint or crack efficiency coefficient, and
b = 4.22 - 0.32 P2.

It should be noted that Eq. 10 has an additional factor J termed as joint or crack efficiency coefficient. In the AASHO Guide design equation, this factor was eliminated by using a value of 3.2. This led to the major restriction on the use of the AASHO Guide that only pavements similar to AASHO Road Test pavements (jointed, free corners with no load transfer devices) can be designed by the AASHO Guide. In this paper, this factor will be treated as a variable so that other kinds of pavements can also be designed.

VARIANCE MODEL

Variance in log W_m can be predicted in terms of the variances of individual variables affecting log W_m. The general form of the variance model is given in the following paragraphs.

If x is a function of a series of variables $y_1, y_2, y_3, \ldots, y_n$, the variance V_x of response variable x can be written in the following general form in terms of individual variances $V_{y_1}, V_{y_2}, V_{y_3}, \ldots, V_{y_n}$:

$$V_x \approx \sum_{i=1}^{i=n} \left[\left(\frac{\partial x}{\partial y_i}\right)^2 V_{y_i}\right] \tag{11}$$

By applying the general Eq. 11 to the AASHO Guide model represented by Eq. 10, we obtain the following expression:

$$\begin{aligned} V_{\log W_m} = &\left(\frac{\partial \log W_m}{\partial f}\right)^2 V_f + \left(\frac{\partial \log W_m}{\partial J}\right)^2 V_J + \left(\frac{\partial \log W_m}{\partial P1}\right)^2 V_{P1} \\ &+ \left(\frac{\partial \log W_m}{\partial E}\right)^2 V_E + \left(\frac{\partial \log W_m}{\partial k}\right)^2 V_k + \left(\frac{\partial \log W_m}{\partial D}\right)^2 V_D \\ &+ \left(\frac{\partial \log W_m}{\partial \Delta}\right)^2 V_\Delta \end{aligned} \tag{12}$$

Each term in Eq. 12 represents the variance in log W_m contributed by the variable involved in that term. For example, variance in log W_m contributed by parameter f as

denoted by C_f can be given as follows using Eq. 10:

$$C_f = \left(\frac{\partial \log W_m}{\partial f}\right)^2 V_f = \left(\frac{b \log_{10} e}{f}\right)^2 V_f \tag{13}$$

Similarly, variances in log W_m contributed by parameters J, P1, E, k, D, and Δ as denoted by C_J, C_{P1}, C_E, C_k, C_D, and C_Δ respectively can be given as follows:

$$C_J = \left(\frac{-b \log_{10} e}{J}\right)^2 V_J \tag{14}$$

$$C_{P1} = \left(\frac{\log_{10} e}{\beta}\right)^2 \left(\frac{1}{P1 - P2} - \frac{1}{P1 - 1.5}\right)^2 V_{P1} \tag{15}$$

$$C_E = \left(\frac{b \log_{10} e}{4}\right)^2 \left[\frac{1}{E} - \frac{D^{0.75}}{(\delta^{0.25} D^{0.75} - 18.423) k^{0.25} E^{0.75}}\right]^2 V_E \tag{16}$$

$$C_k = \left(\frac{b \log_{10} e}{4}\right)^2 \left[\frac{E^{0.25} D^{0.75}}{(\delta^{0.25} D^{0.75} - 18.423) k^{1.25}} - \frac{1}{k}\right]^2 V_k \tag{17}$$

$$C_D = \left[\frac{7.35 \log_{10} e}{D + 1} + \frac{(1.3739 \times 10^8) G}{\beta^2 (D + 1)^{9.46}} + \frac{0.75 b \log_{10} e}{(D^{0.75} - 1.1326) D^{0.25}} - \frac{0.75 \delta^{0.25} b \log_{10} e}{D^{0.25} (\delta^{0.25} D^{0.75} - 18.423)}\right]^2 V_D \tag{18}$$

$$C_\Delta = V_\Delta \tag{19}$$

The total variance in log W_m (adding Eqs. 13 through 19) can be given as

$$V_{\log W_m} = C_f + C_J + C_{P1} + C_E + C_k + C_D + C_\Delta \tag{20}$$

Variances V_f, V_J, V_{P1}, V_E, V_k, V_D, and V_Δ are the squares of the respective standard deviations s_f, s_J, s_{P1}, s_E, s_k, s_D, and s_Δ associated with the variables. The standard deviation in log N as used in Eq. 3 can now be given as

$$s_{\log N} = \sqrt{V_{\log W_m}} \tag{21}$$

VARIABILITY CHARACTERIZATION

The probabilistic design approach requires estimates of the variations associated with the design parameters. Results have been obtained from actual concrete pavement projects to establish estimates of these variations. The design engineer should consider these as general values and should estimate the standard deviations of the design parameters for the specific project that is being designed. This section briefly summarizes available data of variations associated with concrete properties, joint load transfer, thickness, serviceability, subgrade support, lack of fit of design equation, and traffic forecasting.

Concrete Properties

The variations of concrete strength and modulus of elasticity have been measured in numerous field and laboratory studies in the past. The causes of these variations are attributed to two major factors: nonhomogeneous ingredients and nonuniform concrete production and placing. Property variations due to ingredients arise from changes in types and quantities of aggregates, cement, and water during concrete pavement construction. Variations due to concrete production occur during batching, mixing, transporting, placing, finishing, and curing of concrete.

Flexural strength data were obtained from 15 projects from the files of the Texas Highway Department and other sources. A plot of mean flexural strength versus standard deviation for each project is shown in Figure 1. An overall coefficient of variation of 10.7 percent was obtained from these data, a value that is very close to that obtained from the analysis of compressive strength data on 56 concrete projects throughout the United States. A typical histogram of the flexural strength data for one project is shown in Figure 2. The frequency distributions for most of the projects showed the flexural strength to be approximately normally distributed.

The modulus of elasticity variations were obtained from laboratory studies as well as from AASHO Road Test data. The standard deviation was found to increase with the mean as for compressive and flexural strengths. An overall coefficient of variation of 8.6 percent was obtained for the laboratory data and 12.8 percent for the AASHO Road Test concrete slabs.

Joint and Crack Continuity Coefficients

Structural efficiency of joints and cracks in providing deflection and stress relief at these locations in concrete pavements is a very critical factor in concrete pavement design. There are essentially three types of concrete pavements in wide use today: continuously reinforced pavements, jointed pavements without load transfer devices, and jointed pavements with load transfer devices. An empirical value of 3.2 was assigned to the J-term in the AASHO Guide for jointed pavements without load transfer units. This value was originally assigned by Spangler (17) in his empirical formula that represented the stress at a free corner. The stresses computed with this value matched closely with the stresses observed in warped corners at the Arlington Road Test. A value of 2.2 for this factor was suggested by Hudson and McCullough for continuously reinforced pavements (18). The J-term is not a measurable property but empirically represents the structural capability of a joint or a crack to transfer loads across them. The standard deviations were estimated by Treybig, McCullough, and Hudson (19) based on variability of deflections measured across joints. The resulting values are as follows:

Value of J	Description	Standard Deviation of J
3.2	Jointed pavement without load transfer units	0.13
2.2	Continuously reinforced pavements	0.19

Slab Thickness

Because of construction variations, the thickness of a concrete slab has always been found to vary throughout a project. Thickness of concrete is usually measured on construction projects for quality control purposes. Variability of the slab thickness is important in that localized, premature failures may occur, causing loss of serviceability and increase in pavement roughness.

Data showing the variation of concrete slab thickness were obtained for 27 pavement projects in four states, and the variances within the projects were pooled to obtain an overall average standard deviation for nominal pavement thicknesses. These standard deviations are given as follows:

Nominal Concrete Pavement (in.)	Standard Deviation	Number of Projects
8	0.32	14
9	0.29	8
10	0.29	5

As can be noted, the data do not indicate the standard deviation of concrete pavement thickness to be dependent on the average thickness for the range of thicknesses in common practice for concrete pavement construction.

An example of distribution of concrete slab thickness for an actual pavement as measured from cores taken from the pavement is shown in Figure 3. A normal distribution curve shown in this figure shows that the pavement thickness is approximately normally distributed along the project length.

Initial Serviceability Index

The initial serviceability index is a direct function of the smoothness of a pavement immediately after construction. A histogram showing the distribution of the initial serviceability indexes of 224 test sections is shown in Figure 4. The data approximately follow a normal distribution curve. Results show a standard deviation of 0.14, which may be considered a minimum value or the "best" obtainable value in the field because the Road Test pavements were constructed under controlled conditions. Normal pavement projects may be expected to have twice as great a standard deviation—about 0.3, as was measured for a newly constructed concrete pavement in Texas.

Foundation Modulus

Foundation support is represented by the modulus of reaction, k, in the AASHO Guide. This factor probably has the greatest variation because of the nonuniformity of soil support along and across a typical pavement. Any change in type of soil, compaction, moisture, and factors such as loss of support, erosion, and pumping causes variations in foundation support along a project and during numerous seasonal changes during the design life of a pavement.

Estimates of possible variation of the foundation modulus were obtained in rigid pavement projects in New York (20) and from the AASHO Road Test (15). The data show a general increase in standard deviation with increasing value of mean k and an overall coefficient of variation of 35 percent.

Lack of Fit of Design Equation

The basic design equation derived empirically from the AASHO Road Test data does not predict the exact life of all Road Test sections and therefore has a lack-of-fit error. This scattering of data is caused by the lack of fit of the equation (i.e., the equation does not contain all the necessary parameters or it is not in a proper form) and nonuniformity of design parameters in the Road Test pavements. The latter error is also called replicate error, which is the difference in pavement life between two replicate sections or pavements.

The total variation about the fitted design equation is given in the AASHO Road Test Report 5 (15). Total variance of errors in actual and predicted log of load applications is given as $V_{\Delta t}$.

$$V_{\Delta t} = (s_{\Delta t})^2 = (0.22)^2 = 0.0484$$

This total variance is made up of replication and lack-of-fit components:

$$V_{\Delta t} = V_{\Delta} + V_{\Delta(\text{replicates})} \tag{22}$$

The variance contributed only by lack of fit of the equation was determined by subtracting, from the total variance, the variance of error due to nonuniformity of design parameters at the Road Test. An analysis was made of 36 pairs of replicate sections used at the AASHO Road Test. The replicate error was estimated by taking the mean squared difference in log N of the replicate pairs at serviceability indexes of 3.5, 3.0, 2.5, and 2.0. Variance due to replicate errors was found as follows:

$$V_{\Delta(\text{replicates})} = 0.0131$$

Figure 1. Average flexural strength of concrete versus standard deviation for various projects.

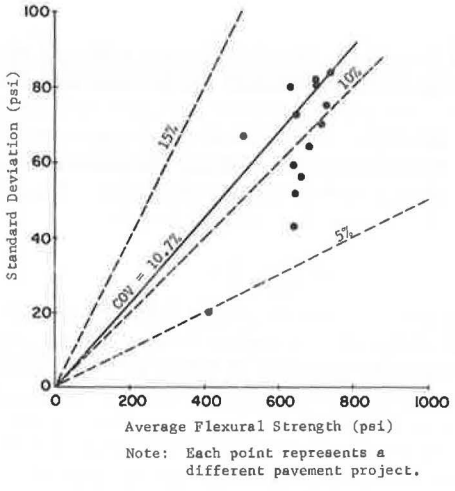

Figure 2. Frequency distribution of flexural strength for a concrete pavement project.

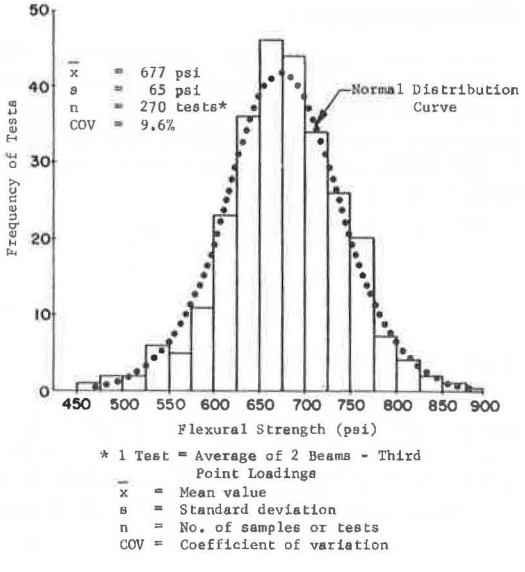

Figure 3. Frequency distribution of concrete slab thickness (22).

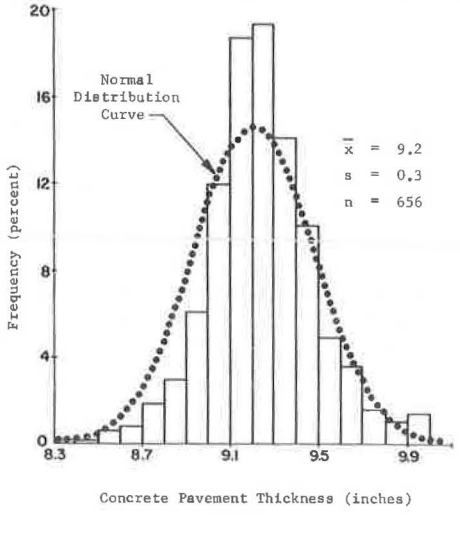

Therefore, the lack-of-fit variance was estimated as

$$V_{\Delta} = 0.0484 - 0.0131 = 0.0353 \quad (23)$$

It will be advantageous at this time to clarify the purpose of the preceding analysis, which in turn will clarify the overall purpose of this study. The objective is to determine for a new project the total variance of log N, which will consist of (a) total variance of error about the fitted design equation for the AASHO Road Test data (b) minus the variance due to nonuniformity of design parameters at the Road Test (c) plus the variance due to nonuniformity of design parameters for a new project.

Equation 23 encompasses items a and b, whereas item c is estimated by Eqs. 13 through 18.

Traffic Estimation

The AASHO Guide requires an estimate of the number of equivalent 18-kip single-axle load applications that the pavement will carry during its design life. There are many available methods to estimate this parameter, but each has considerable uncertainties associated with it. Basically, there are three types of uncertainties associated with forecasting this parameter:

1. Uncertainties involved in the estimation of total number of axles during pavement life, axle configurations, and axle weight distributions;
2. Uncertainties involved in equivalency factors used in the conversion of mixed traffic to equivalent applications of 18-kip single-axle loads; and
3. Uncertainties involved because of directional and lane distribution of traffic, lateral placement of loads, axle growth rate, and other unforeseen traffic increases during the life of a pavement.

A procedure has been developed (9) that gives an estimate of this error for the Texas Highway Department. Kentucky (21) analyzed the accuracy of its equivalent wheel load forecasting procedures and concluded the following: "...in some instances the actual accumulation may be somewhere between half and twice the predicted value but in the majority of cases will conform much closer." For general use, the following method is suggested to give an approximate estimate of the variance involved.

For a specific project, the average, maximum, and minimum number of 18-kip load applications that could pass during the pavement life should be estimated. This range should be selected to ensure that 95 percent of the time the values will fall between the maximum and minimum estimates. A conservative estimate of maximum and minimum equivalent applications could be approximately twice and half the average prediction respectively. The variance may then be calculated as follows (assuming n as log normally distributed):

$$V_{\log n} = \left[\frac{\log(\text{maximum applications}) - \log(\text{minimum applications})}{4}\right]^2 \quad (24)$$

SENSITIVITY ANALYSIS OF AASHO INTERIM GUIDE MODEL

Variance models developed in Eqs. 13 through 19 provide an excellent method for conducting a significance study to determine the relative effects of different input factors on the response of the model. The technique consists of determining the value of variance contributed by a variation in any input factor. This individual variance due to a factor, when computed as a percentage of the total variance contributed by all the factors, gives an estimate of the significance of that factor relative to the significance of the other factors.

The individual percentage-of-significance values for the factors were computed for 32 representative problems. Table 1 gives the percentage-of-significance value of each factor for each problem, the significance of a variable averaged over all the problems, and the range of such significance for each factor. The table demonstrates that the lack of fit of the AASHO data is the most important factor in the design model,

Figure 4. Frequency distribution of serviceability index after construction of AASHO Road Test pavements (23).

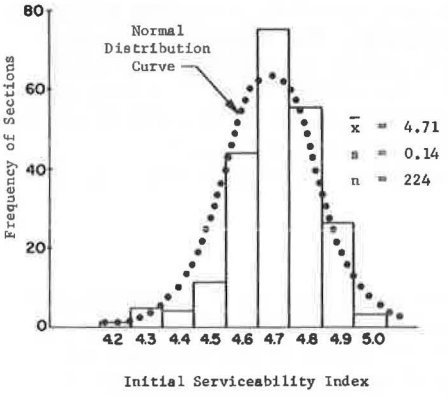

Table 1. Percentage-of-significance values.

Problem Number	Flexural Strength	Concrete Modulus	Concrete Thickness	Foundation Modulus	Continuity Coefficients	Initial Serviceability Index	Lack of Fit
1	24.1	0.8	14.2	2.1	19.9	0.3	38.6
2	26.0	0.4	8.1	1.1	21.5	1.4	41.6
3	26.0	0.3	8.5	0.8	21.5	1.4	41.6
4	23.0	3.7	6.8	10.3	19.0	0.3	36.9
5	23.8	2.3	9.5	6.4	19.7	0.3	38.0
6	25.7	1.1	6.7	3.0	21.2	1.3	41.1
7	25.8	0.7	7.4	2.0	21.4	1.3	41.3
8	27.0	1.3	14.3	3.5	10.5	0.3	43.2
9	27.0	0.9	15.8	2.4	10.5	0.3	43.1
10	29.3	0.5	9.2	1.3	11.4	1.5	46.9
11	29.3	0.3	9.6	0.9	11.5	1.5	46.9
12	25.6	4.1	7.6	11.4	10.0	0.3	41.0
13	26.5	2.6	10.6	7.2	10.4	0.3	42.4
14	28.9	1.2	7.6	3.3	11.3	1.5	46.2
15	29.1	0.8	8.3	2.3	11.4	1.5	46.6
16	23.9	1.1	13.7	3.1	19.8	0.1	38.3
17	23.9	0.8	15.1	2.1	19.8	0.1	38.3
18	26.2	0.4	8.3	1.1	21.6	0.5	41.9
19	26.2	0.3	8.6	0.8	21.6	0.5	41.9
20	22.9	3.7	7.5	10.2	18.9	0.1	36.7
21	23.6	2.3	10.3	6.4	19.5	0.1	37.8
22	25.9	1.1	6.8	3.0	21.4	0.5	41.4
23	26.0	0.7	7.5	2.0	21.5	0.5	41.7
24	26.7	1.2	15.3	3.5	10.4	0.1	42.8
25	26.7	0.8	16.8	2.3	10.4	0.1	42.7
26	29.5	0.5	9.3	1.3	11.5	0.6	47.3
27	29.6	0.3	9.7	0.9	11.6	0.6	47.3
28	25.5	4.1	8.3	11.3	9.9	0.1	40.7
29	26.3	2.6	11.4	7.1	10.3	0.1	42.1
30	29.1	1.2	7.7	3.4	11.4	0.6	46.6
31	29.4	0.8	8.4	2.3	11.5	0.6	47.0
32	24.1	1.1	12.8	3.1	19.9	0.3	38.6
Average	26.3	1.4	10.0	3.8	15.7	0.6	42.1
Range	22.9 to 29.6	0.3 to 4.1	6.8 to 16.8	0.8 to 11.4	9.9 to 21.6	0.1 to 1.5	36.7 to 47.3

followed by concrete flexural strength, continuity coefficient, concrete thickness, and foundation modulus.

EFFECTS OF QUALITY CONTROL

Quality control has always been a matter of great concern to the engineers supervising any construction project. The probabilistic analysis developed in this study made it possible to investigate the effects of varying amounts of quality control exercised in the construction of concrete pavements.

The effects of quality control are illustrated here for two areas of major concern: quality of concrete production and quality of pavement construction. The quality of concrete is represented, in the model, by its flexural strength and modulus of elasticity; the quality of pavement construction is represented by the three factors: concrete thickness, joint construction, and initial serviceability index (or smoothness of the pavement).

Based on the variability characterizations described in a previous section, the values of standard deviations were selected for each variable to represent poor, average, and good conditions of quality control. A 7-in. jointed pavement without load transfer devices was selected to illustrate the quality control analysis. It was found that this pavement could carry about 3.51 million 18-kip single-axle applications if no safety factor was used in the AASHO Guide. This, according to the variance analysis, corresponds to a reliability of 50 percent. With the help of the modified AASHO Guide design model, pavement thicknesses were computed that will carry 3.51 million applications at various levels of reliability up to 99.99 percent. The results obtained for the two examples are shown in Figure 5. The relative concrete thicknesses required for various levels of reliability are presented for poor, average, and good quality control conditions. The figure lists the standard deviations used for each variable to represent good and poor quality control with respect to concrete production and pavement construction. The figure also gives the standard deviations assigned to each variable to represent an average quality control.

It can be noted from Figure 5 that poor quality control requires higher pavement thickness for the same level of reliability than that required when an average quality control is exercised. Similarly, a good quality control can lead to a significant reduction in the required concrete thickness, or, in other words, a good quality control for a fixed pavement thickness can lead to having a higher level of reliability. Figure 5 also demonstrates that the effect on thickness of poor and good quality control varies with the level of required reliability.

Though the two examples previously given are studied in terms of required pavement thicknesses, monetary values can be assigned to these thicknesses, thus providing (for the first time in pavement design and construction) a powerful tool to quantitatively study the economics of quality control relative to pavement performance.

EFFECTS OF LACK-OF-FIT ERROR

Statistically derived relations always possess a certain lack-of-fit error because of the scatter of data around the developed regression equation. Pavement engineers have always used numerous empirical equations for the design of pavement structures but have never considered the lack-of-fit errors. Rather, they have adopted a tendency to consider these equations as completely deterministic. This has led to an inadequate designing process.

Lack-of-fit error associated with the AASHO Guide model has already been described in an earlier section. For the sake of demonstrating the significance of this error, Figure 6 is presented in which the required pavement thicknesses have been determined with and without the consideration of the lack-of-fit error. The example data and procedure of design are the same as those used for Figure 5 for the average quality control. As can be noted, significant differences in required thicknesses result for the pavements designed at various reliability levels, with and without lack-of-fit error.

Figure 5. Relative thicknesses required at various confidence levels for poor, good, and average quality control for concrete and construction quality.

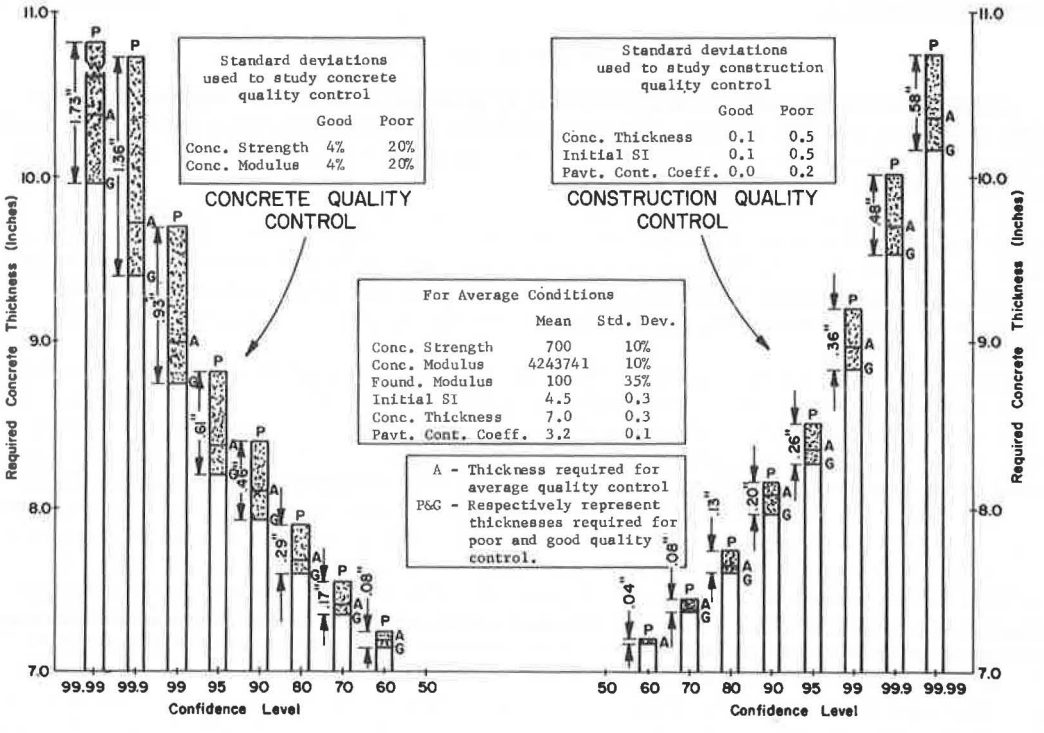

Figure 6. Relative thicknesses required at various confidence levels with and without the consideration of lack-of-fit error.

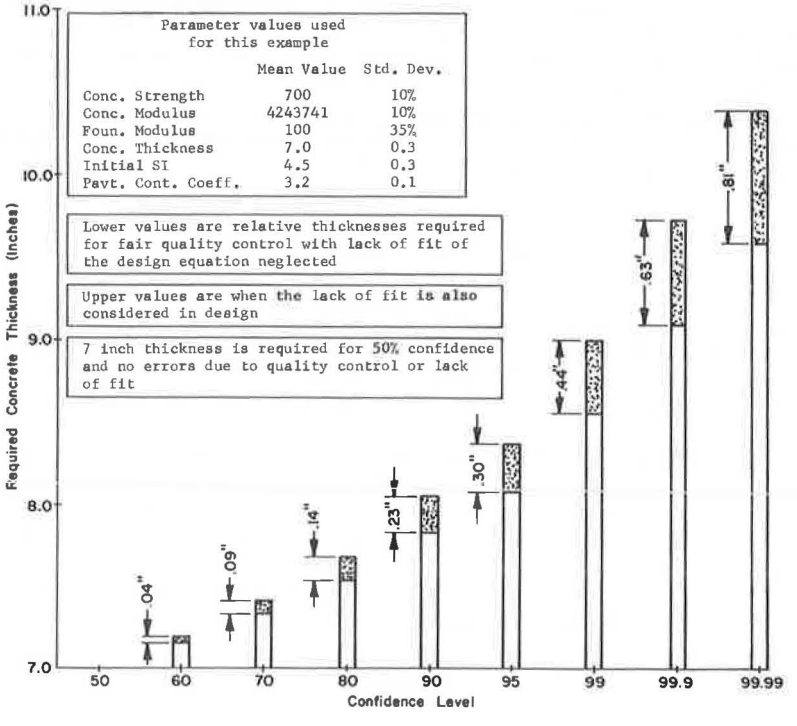

REVISED NOMOGRAPH

Based on the variance model developed in this research study, the AASHO Guide nomograph is modified (Fig. 7). The nomograph makes it possible to design a pavement thickness at any level of reliability taking into account the uncertainties associated with various parameters. This is achieved by two scales shown in the nomograph, a variance scale and a reliability scale. The two scales are combined in such a way that the designed thickness will stand a good chance of lasting the required number of applications with a reliability for which the pavement is designed.

Variance (excluding the variance due to traffic) can be theoretically computed by using Eqs. 13 to 20. However, Figure 8 has been developed so that the value of variance can readily be obtained. This figure has been developed using variability characterization and judgment factors and represents average conditions of scatter in material properties and other parameters. The following values of variability have been used to develop this figure:

1. Flexural strength, coefficient of variation = 10 percent;
2. Concrete modulus, coefficient of variation = 10 percent;
3. Concrete thickness, standard deviation = 0.3 in.;
4. Foundation modulus, coefficient of variation = 35 percent;
5. Initial serviceability index, standard deviation = 0.3; and
6. Continuity coefficient, standard deviation = 0.1 for JCP without load transfer units and 0.2 for CRCP and JCP with load transfer units.

The figure does not contain initial serviceability index and concrete modulus as variables because the sensitivity analysis showed that the effects of variabilities in these parameters are insignificant. Minimum serviceability index is a basic design criterion, and therefore no variation in this factor is considered.

Although the figure is developed from the best available data in connection with parameter variability, and therefore can be effectively used for design, the designers are encouraged to develop similar figures by using Eqs. 13 to 20 to suit their own construction conditions and quality controls.

The reliability scale presents 50 to 99.99 percent reliability. The designer can use any reliability in design. It has been observed during the use of this and other similar systems that the designers prefer to select this number based on their own judgments and the importance of highway facility under design. A thorough investigation of the old practice of using working stress as 0.75 times the flexural strength demonstrated that it corresponded to having reliability levels between 90 to 95 percent with the modified nomograph.

USE OF THE NOMOGRAPH

Concrete thickness can be designed with the use of the revised nomograph (Fig. 7) by going through the following steps:

1. Determine the overall variance by either of the following methods: Estimate standard deviation associated with each design factor, determine total variance according to Eq. 20, and add to it the variance due to error in traffic prediction; or estimate total variance by Figure 8 (an initial estimate of the required thickness will be needed to use this table), and add to it the variance due to error in traffic prediction using Eq. 24.
2. Estimate the design reliability level based on experience and judgment. The design reliability should depend on the "consequence of failure" to provide an adequate performance throughout the design period. The consequence of failure should be judged by user delay and accident costs during rehabilitation operations and other socio-economic and political effects. Thus, design reliability levels should be selected based on consideration of all these factors and not only the initial construction cost.
3. Select concrete thickness from nomograph in the following manner: (a) Join the reliability and variance to intersect at the TL 1; (b) draw a line through traffic and the point already established on TL 1 in step a to intersect TL 2; (c) go to TL 3 from TL 2

Figure 7. Nomograph for concrete pavement design at desired reliability level.

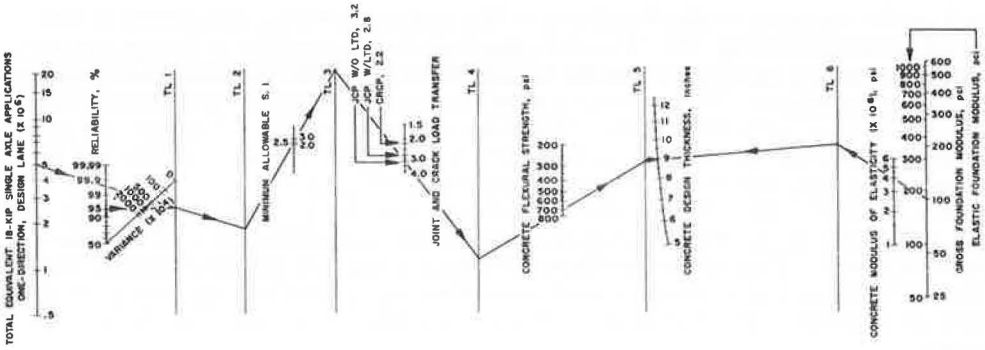

EXAMPLE PROBLEM

Traffic = 5,000,000 single axle equivalent 18-kip applications
Variance = 1,000 (corresponds to average quality control)
Minimum Allowable Serviceability Index = 2.5
Joint and Crack Load Transfer Coefficient = 3.2 (JCP w/o load transfer device - LTD)
Concrete Flexural Strength = 700 psi
Concrete Modulus of Elasticity = 4,000,000 psi
Gross Foundation Modulus = 100 pci

REQUIRED CONCRETE THICKNESS

Reliability	90	95	99	99.9	99.99
Thickness, inches	8.6	8.9	9.7	10.4	11.5

Concrete thickness required by original interim design guide using working flexural stress of .75 × 700 = 8.75 inches (corresponds to 92.5 percent reliability)

Figure 8. Variances (10^4) for use in modified AASHO Guide nomograph.

Concrete flexural strength, psi	Foundation Modulus, pci	Concrete Thickness, inches	JCP Without Load Transfer Devices				JCP With Load Transfer Devices				CRCP			
			6	8	10	12	6	8	10	12	6	8	10	12
600	25		775	718	684	661	866	809	775	752	935	879	845	822
	100		779	722	688	664	870	813	779	755	940	883	849	825
	300		821	742	700	673	912	833	791	764	982	903	861	834
	600		918	777	719	685	1009	868	810	776	1078	938	880	846
700	25		775	718	684	661	866	809	775	752	936	879	845	821
	100		778	721	687	664	869	812	778	755	938	882	848	824
	300		810	737	698	671	901	828	788	762	971	898	858	832
	600		886	766	714	682	977	857	805	773	1047	927	874	843
800	25		775	718	684	661	866	808	775	752	936	879	845	821
	100		776	720	687	663	867	811	778	754	937	881	847	824
	300		803	734	696	670	894	825	787	761	964	895	856	830
	600		865	759	710	679	956	850	801	770	1026	920	870	840
900	25		776	718	684	661	867	809	775	752	937	879	845	821
	100		776	720	686	663	867	811	777	754	936	881	847	824
	300		797	731	694	669	888	823	785	760	958	892	855	829
	600		849	753	706	677	940	844	797	768	1010	914	867	838

through minimum serviceability level; (d) go to TL 4 from TL 3 through joint and crack load transfer coefficient; (e) go to TL 5 from TL 4 through average concrete flexural strength (do not use any safety factor); (f) start now on the extreme right-hand side of the nomograph, and draw a line through foundation modulus and concrete modulus of elasticity to intersect TL 6; and (g) join the two points established in steps e and f on TL 5 and TL 6 respectively (this joining line will pass through concrete thickness scale and will intersect it at the required design concrete thickness).

EXAMPLE PROBLEM

An example problem solved for an actual project is demonstrated on the nomograph (Fig. 7). A jointed concrete pavement without load transfer devices has been designed to carry an expected 5 million equivalent 18-kip axle applications. Other pertinent input data are shown in the figure. The total overall variance used for this project is estimated to be 0.1, and a reliability level of 95 percent is used for the design. The required concrete thickness was estimated to be 8.9 in.

Concrete thicknesses required for reliability levels of 90, 99, 99.9 and 99.99 were also computed as shown in Figure 8. The respective thickness values were 8.6, 9.7, 10.4, and 11.5 in. The design was compared with the original method by designing the pavement using working stress equal to 0.75 times the flexural strength and the original nomograph. The required thickness was computed as 8.75 in., which corresponded to a reliability level of 92.5 percent for the new method.

CONCLUSIONS AND RECOMMENDATIONS

As concisely stated by Finn (24): "It is the role of research to improve and quantify and control the reliability factor in order to provide the most economic balance between performance requirements and costs." The procedure presented in this paper has attempted to further knowledge in achieving this overall goal. The reliability method of design has shown excellent promise, and it appears possible to incorporate the concepts of reliability into any design model as well as to conduct a significance study of the parameters of the model and to study the effects of quality control on pavement performance.

It is recommended that the modified nomograph be used for design so that it will be possible to consider variabilities associated with the design parameters and the lack-of-fit errors associated with the AASHO design equation.

ACKNOWLEDGMENTS

This investigation was conducted at the Center for Highway Research, University of Texas at Austin. The authors wish to thank the sponsors, the Texas Highway Department and the U.S. Department of Transportation, Federal Highway Administration.

The opinions, findings, and conclusions expressed in this publication are those of the authors and not necessarily those of the Federal Highway Administration.

REFERENCES

1. AASHO Interim Guide for the Design of Rigid Pavement Structures. AASHO Committee on Design, 1961.
2. Freudenthal, A. M. Safety, Reliability and Structural Design. Jour. Structural Div., Proc. ASCE, Vol. 87, No. ST3, March 1961, pp. 1-16.
3. Freudenthal, A. M., Garretts, J., and Shinozuka, M. The Analysis of Structural Safety. Jour. Structural Div., Proc. ASCE, Vol. 92, No. ST1, Feb. 1966, pp. 267-325.
4. Pugsley, A. G. The Safety of Structures. Edward Arnold Ltd., London, 1966, 156 pp.
5. Johnson, A. K. Strength, Safety, and Economical Dimensions of Structures. Royal Institute of Technology, Stockholm, 1953, 159 pp.
6. Pugsley, A. G. Concepts of Safety in Structural Engineering. Jour. Institution of Civil Engineers, London, Vol. 35, No. 4, March 1951, pp. 5-51.

7. Freudenthal, A. M. The Safety of Structures. Trans. ASCE, Vol. 112, 1947, pp. 125-180.
8. Freudenthal, A. M. Safety and the Probability of Structural Failure. Trans. ASCE, Vol. 121, 1956, pp. 1337-1397.
9. Darter, M. I., McCullough, B. F., and Brown, J. L. Reliability Concepts Applied to the Texas Flexible Pavement System. Highway Research Record 407, 1972, pp. 146-161.
10. Shah, H. C. The Rational Probabilistic Code Format. Proc. ACI, Sept. 1969.
11. Sexsmith, R. G., and Nelson, M. F. Limitations in Application of Probabilistic Concepts. Proc. ACI, Oct. 1969.
12. Benjamin, J. R., and Lind, H. C. A Probabilistic Basis for a Deterministic Code. Proc. ACI, Nov. 1969.
13. Cornell, C. A. A Probability-Based Structural Code. Proc. ACI, Dec. 1969.
14. Haugen, E. B. Probabilistic Approaches to Design. John Wiley and Sons, New York, 1968.
15. The AASHO Road Test: Report 5—Pavement Research. HRB Spec. Rept. 61E, 1962.
16. Langsner, G., Huff, T. S., and Liddle, W. J. Use of Road Test Findings by AASHO Design Committee. HRB Spec. Rept. 73, 1962.
17. Spangler, M. G. Stresses in the Corner Region of Concrete Pavements. Engineering Experiment Station, Iowa State College, Ames, Bull. 157, 1942.
18. Hudson, W. R., and McCullough, B. F. An Extension of Rigid Pavement Design Methods. Highway Research Record 60, 1964, pp. 1-14.
19. Treybig, H. J., McCullough, B. F., and Hudson, W. R. Sensitivity Analysis of the Extended AASHO Rigid Pavement Design Equation. Highway Research Record 329, 1970, pp. 20-33.
20. Bryden, J. E., and Phillips, R. G. The Catskill-Cairo Experimental Rigid Pavement: Construction and Materials Testing. New York State Department of Transportation, Res. Rept. 2, Dec. 1971.
21. Deacon, J. A., and Lynch, R. L. Determination of Traffic Parameters for the Prediction, Projection and Computation of EWL's. Kentucky Department of Highways, Final Rept. KYHPR-64-21, Aug. 1968.
22. Highway Quality Control Program, Statistical Parameters. Michigan Department of State Highways, Res. Rept. R-572, March 1966.
23. Fordyce, P., and Teske, W. E. Some Relationships of the AASHO Road Test to Concrete Pavement Design. Highway Research Record 44, 1963, pp. 35-70.
24. Finn, F. N. Observation of Distress in Full-Scale Pavements. HRB Spec. Rept. 126, 1971, pp. 86-90.
25. Structural Design of Asphalt Concrete Pavement Systems. HRB Spec. Rept. 126, 1971.

DISCUSSION

Mihai Rafiroiu, University of Michigan

In their report the authors deal with an extremely important problem: the reliability of the design and thus the behavior of highway pavements at an adequate serviceability index.

It should be appreciated that the study presented in this report was generally well conducted, and the results are very interesting from both theoretical and experimental points of view. It should also be noted that this study is one of the first done in the area of the stochastic design of highway pavements.

Although the study is remarkably accurate in all aspects, I would like to express some reservations and make some suggestions.

The authors assumed that both total traffic during the design period and forecasting error are log normally distributed, but it is noted that this assumption is valid only for a rather small number of cases.

It should also be stated that, if the variables follow the normal distribution, it is not theoretically possible to also follow the log-normal distribution. From a practical point of view, one can accept this approach only if the range of the values is very small.

The variance model that was adopted can be generally used only if either all the exponents of the variables are equal to one or there are no more than two variables with exponents of two. Usually, when the exponents of the variables are greater than one, the principles and methods of numerical calculus are used, which leads to quite different variance models.

The preceding statements are true only if all the variables are independent of one another. If not (and this is the case of Young's modulus that is related to Poisson's ratio or to the deviator stress for granular materials), only a step-by-step approach using the techniques of numerical calculus could be used to reach a solution.

Finally, the variance model differs among design methods, and only very general principles can be used.

RELATIVE EFFECTS OF STRUCTURAL VARIABLES ON THE PERFORMANCE OF CONTINUOUS PAVEMENTS

Adnan Abou-Ayyash and W. Ronald Hudson, Center for Highway Research, University of Texas at Austin

This paper describes a sensitivity analysis performed to establish the relative importance of structural variables on the performance of continuously reinforced concrete pavements. The experiment design for this study consisted of three basic variables: slab bending stiffness, subgrade modulus, and crack spacing. The discrete-element method of slab analysis was the mechanistic tool applied to obtain slab responses, i.e., deflections, principal moments, and stresses. For the range of variables studied, the analysis of variance showed that the most significant variables, which explained about 90 percent of the variation in deflection and principal moment (stress) responses, were slab bending stiffness and modulus of subgrade reaction. Although the first variable made a higher contribution to principal moments than to deflections, subgrade modulus had a contrasting effect. The orthogonal polynomial breakdown indicated that in a logarithmic model the linear effect of both subgrade modulus and slab bending stiffness is highly significant. Furthermore, interactions between these two design variables do occur, indicating that variations in deflections and principal moments are not defined by the main effect of design variables alone. The comparison between slab responses for an uncracked slab and a slab with 90 and 100 percent reduction in bending stiffness at crack locations indicated the importance of cracks and crack width on the behavior of continuously reinforced concrete pavements. As cracks widen to approach the hinge case, slab deflections increase significantly, but no appreciable drop is experienced in the principal moments. Indeed, cracks as narrow as possible are desirable for the successful performance of continuous pavements.

•A GENERAL discrete-element method for solution of discontinuous plates and slabs has been developed by Hudson and Matlock (1) and Stelzer and Hudson (2). The method is based on a physical model representation of a plate or slab by bars, springs, and torsion bars that are grouped in a system of orthogonal beams. Computer programs developed for the method are designated by the acronym SLAB. These programs can handle complex problems with combinations of load and a variety of discontinuities (cracks and joints) and support conditions.

Extensive use of SLAB programs has been made with two-way floor slabs that are continuous over many supports (3) and in the analysis of rigid pavements (4, 5). This paper describes the application of SLAB methods in a study of the relative importance of the structural variables associated with the design of continuous pavements. These variables include slab thickness, concrete modulus, modulus of subgrade reaction, loading position, and crack spacing.

FACTORIAL DESIGN EXPERIMENT

A sensitivity analysis is a procedure to determine the change in a dependent variable due to a unit change in an independent variable. It can be used to evaluate the effect of

Publication of this paper sponsored by Committee on Rigid Pavement Design.

a certain number of variables in the system and the interactions among them. In this research, a full factorial of the variables (Fig. 1) was evaluated. Both maximum deflections and principal moments were computed for variations in each variable in each block of the factorial (Fig. 1). Two solutions were made for each block: one for the loads on a crack and the second for loads between cracks. Figure 2 shows the loading and crack-spacing pattern for the 4- and 10-ft cases only. This work was performed for a 24- by 40-ft slab size and for two 9,000-lb wheel loads located at 2 and 8 ft from the slab edge respectively.

The number of slab problems to be solved can be decreased by combining the modulus of elasticity of concrete E and the slab thickness t into the bending stiffness factor, namely $\frac{Et^3}{12(1-\mu^2)}$. From the combination of the low, medium, and high levels of both E and t, the values shown in Figure 1 resulted for a Poisson's ratio of 0.20.

RESULTS AND ANALYSIS

Continuously reinforced concrete pavement is a type of pavement that takes care of volume change stresses by developing a regular pattern of very fine transverse cracks. These cracks or discontinuities have been analyzed theoretically by Abou-Ayyash, Hudson, and Treybig (4). It has been shown that the bending stiffness at cracked sections is reduced by 80 to 93 percent of the uncracked stiffness value. In this study, for the closed-crack case, a 90 percent reduction in bending stiffness is applied at crack locations, which corresponds to a 0.55 percent longitudinal reinforcement. The results from the 90 percent reduction were compared with the uncracked and hinge cases also.

Case 1: SLAB Program Results of Loads on the Crack

Maximum values of slab downward deflections and principal moments are shown in Figure 3.

The location of the maximum deflection was dependent on the relative magnitudes of the slab stiffness and the subgrade modulus. For the low level of stiffness, maximum deflection occurred 2 ft from the pavement edge, i.e., directly under the exterior 9,000-lb load. As stiffness increased, the maximum deflection was at the edge of the slab for low values of subgrade modulus. The effect of the subgrade was even more significant on high values of stiffness, as shown in Figure 3, where the maximum deflection occurred at the pavement edge for the low and medium levels of the subgrade modulus. So far as the principal moments are concerned, the maximum value was always under the interior load, which was 8 ft from the pavement edge.

Effect of Crack Spacing—Transverse cracks in continuously reinforced concrete pavements occur randomly, and in most cases they extend the whole width of the pavement. One of the principles of design of this pavement type is to provide sufficient reinforcement to keep the cracks tightly closed. In this study it was assumed that a very slight curvature is needed to bring the two parts of the slab in touch and hence allow the transfer of bending.

In light of this behavior, the variation in maximum deflection and principal moment with crack spacing and slab bending stiffness for a subgrade modulus of 40 lb/in.^{3} is shown in Figure 4. As noted, there is a slight change in both responses as the crack spacing increases over the range studied. However, it is worthwhile to note that these results were based on the same value of bending stiffness reduction at the crack location, whereas in reality the stiffness should vary with crack width. As is demonstrated later in this study, as crack width increases, and hence the reduction in stiffness increases, the influence of crack spacing becomes more important. Similar results were obtained for the other levels of the modulus of subgrade reaction.

Effect of Modulus of Subgrade Reaction—Modulus of subgrade reaction, as defined by Westergaard and others, plays an important role in the evaluation of deflections and stresses in pavement slabs and plates resting on soils. In light of the very small effect of crack spacing, nine deflection values were determined by averaging the deflection values corresponding to the three levels of stiffness and the three levels of subgrade

Figure 1. Factorial variables.

Modulus of subgrade reaction, lb/in²/in.	Crack Spacing, ft	Slab bending stiffness, (lb-in²)/in. 20 x 10^6	150 x 10^6	1125 x 10^6
40	4	×	×	×
	6	×	×	×
	8	×	×	×
	10	×	×	×
200	4	×	×	×
	6	×	×	×
	8	×	×	×
	10	×	×	×
1000	4	×	×	×
	6	×	×	×
	8	×	×	×
	10	×	×	×

Figure 2. Pavement loading and crack spacing pattern.

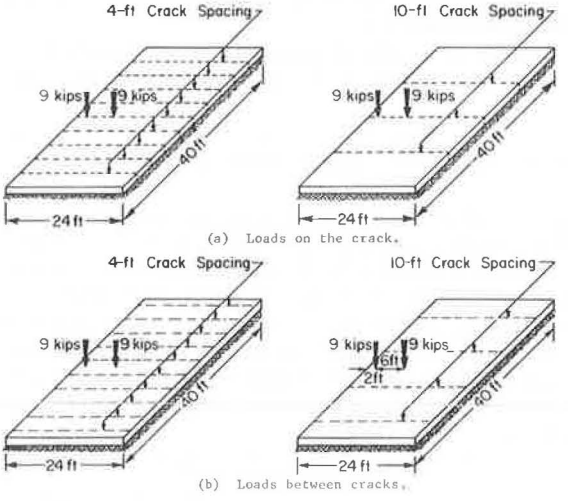

Figure 3. Maximum values of deflection (90 percent reduction, loads on the crack).

Modulus of subgrade reaction, lb/in²/in.	Crack Spacing, ft	Slab bending stiffness, (lb-in²)/in. 20 x 10^6	150 x 10^6	1125 x 10^6
40	4	0.0934 2117	0.0490* 2384	0.0248* 2587
	6	0.0886 2103	0.0485* 2374	0.0246* 2583
	8	0.0864 2099	0.0475* 2364	0.0245* 2582
	10	0.0859 2099	0.0464* 2357	0.0245* 2578
200	4	0.0330 1839	0.0166 2182	0.0086* 2430
	6	0.0321 1835	0.0158 2165	0.0085* 2432
	8	0.0320 1835	0.0153 2159	0.0084* 2413
	10	0.0320 1835	0.0151 2158	0.0083* 2406
1000	4	0.0131 1436	0.0057 1920	0.0029 2240
	6	0.0131 1436	0.0055 1914	0.0028 2223
	8	0.0131 1436	0.0054 1914	0.0027 2215
	10	0.0131 1436	0.0054 1914	0.0026 2213

+ All values occurred 8 feet from the pavement edge.

* Maximum deflection was at the pavement edge; otherwise, it was under the load, 2 feet from the edge.

NOTE: The upper value in each block is the deflection and the lower value is the principal moment.

Figure 4. Effect of slab bending stiffness and crack spacing on maximum principal moment.

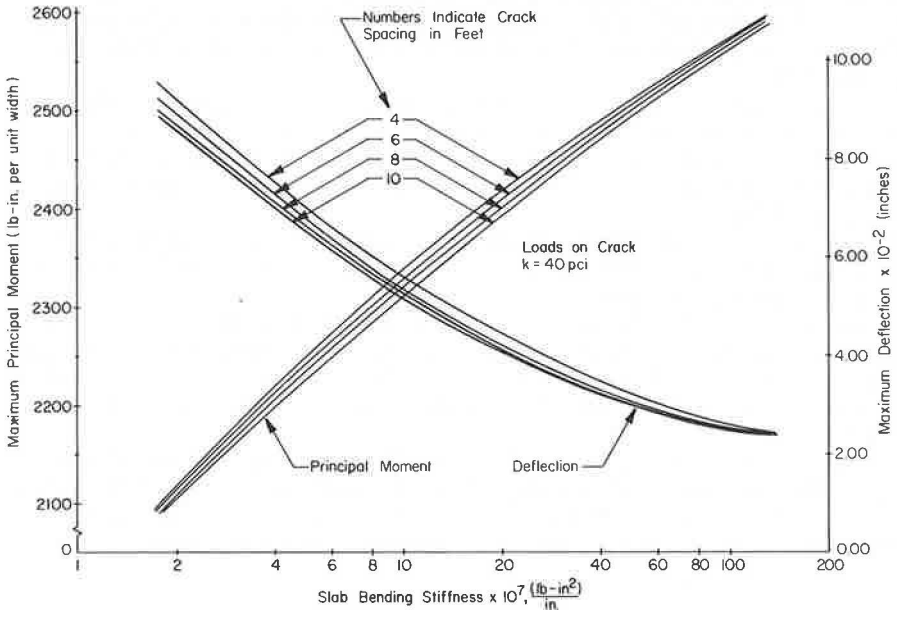

modulus. In other words, an average value of deflection was obtained corresponding to an average value of crack spacing.

The average values of maximum principal moment were determined on the same basis; the logarithmic influence of subgrade modulus on deflections and moments is shown in Figure 5. As shown, the effect of the subgrade modulus on deflection is higher than on principal moments. Slab deflection experiences an important and significant drop as subgrade modulus increases from low to medium levels. However, this deflection decrease tends to level off as the subgrade reaction exceeds the medium level and approaches the high side. This implies that, for the loading condition studied, moderate values of subgrade modulus are quite satisfactory. Furthermore, there is about a 10 percent drop in the value of the principal moment as k varies from one level to another.

Effect of Slab Bending Stiffness—As mentioned previously, the slab bending stiffness per unit width is defined by $\frac{Et^3}{12(1-\mu^2)}$. Obviously, the contribution of the thickness t to the magnitude of the stiffness term is more than the concrete modulus E.

The effect of bending stiffness on deflections and principal moments is shown in Figure 5. For the whole range of subgrade moduli, it can be seen that the influence of stiffness on principal moment is greater than on deflection. It is worthwhile to note that, for low values of subgrade modulus, the decrease in deflection as stiffness increases is highly significant and that, as the subgrade modulus increases, the influence of stiffness levels off. The logarithmic effect of the stiffness term is shown in a way similar to that for subgrade modulus.

Case 2: SLAB Program Results of Loads Between Cracks

In the case when the loads acted between cracks, the effect of crack spacing was greater than when the loads were on the crack. Except for this, results for these two load placements were quite similar. As expected, deflection values were lower for the case when the loads were between cracks, whereas higher values were obtained for principal moments.

Figure 6 shows the maximum values of deflections and principal moments respectively. Values of principal moment were 2 ft from the pavement edge for all ranges in the pavement design variables encountered. As was the case when the loads were on the crack, maximum deflection occurred either under the exterior load or at the pavement edge, depending on the relative values of the slab stiffness and the subgrade modulus.

Effect of Crack Spacing—The influence of crack spacing and slab stiffness on maximum deflections and principal moments for subgrade moduli of 40 and 200 lb/in.^{3} is shown in Figures 7 and 8. The effect of crack spacing on deflections is slight or practically negligible, whereas changes in principal moment for the low and medium levels of k are quite considerable.

Furthermore, this change in principal moment due to the spacing of the cracks increases with an increase in stiffness. The percentage of increase in the maximum moment between the 10- and 4-ft crack spacing (based on the 10-ft value) is about 18 percent. By comparing Figures 7 and 8, it can be seen that this percentage increase in the moment drops as k increases.

Effect of Subgrade Modulus and Bending Stiffness—For the purpose of demonstrating the effect of bending stiffness and subgrade modulus, average values of deflections and principal moments are shown in Figure 9.

The essential importance of the subgrade modulus in determining the amount of slab deflection is very well illustrated. Similar to the case where the loads are on the crack, the rate of change in deflection decreases as the subgrade modulus increases. About a 20 percent drop is experienced in the magnitude of the principal moment as k increases from one level to the next.

Although the subgrade modulus shows a higher contribution in the determination of deflection than principal moment, slab bending stiffness possesses a contrasting effect except for its effect on deflections for low values of subgrade modulus. Again, the logarithmic effect of stiffness as well as subgrade modulus is demonstrated.

Figure 5. Influence of slab bending stiffness and subgrade modulus on maximum deflections and principal moments for loads on the crack.

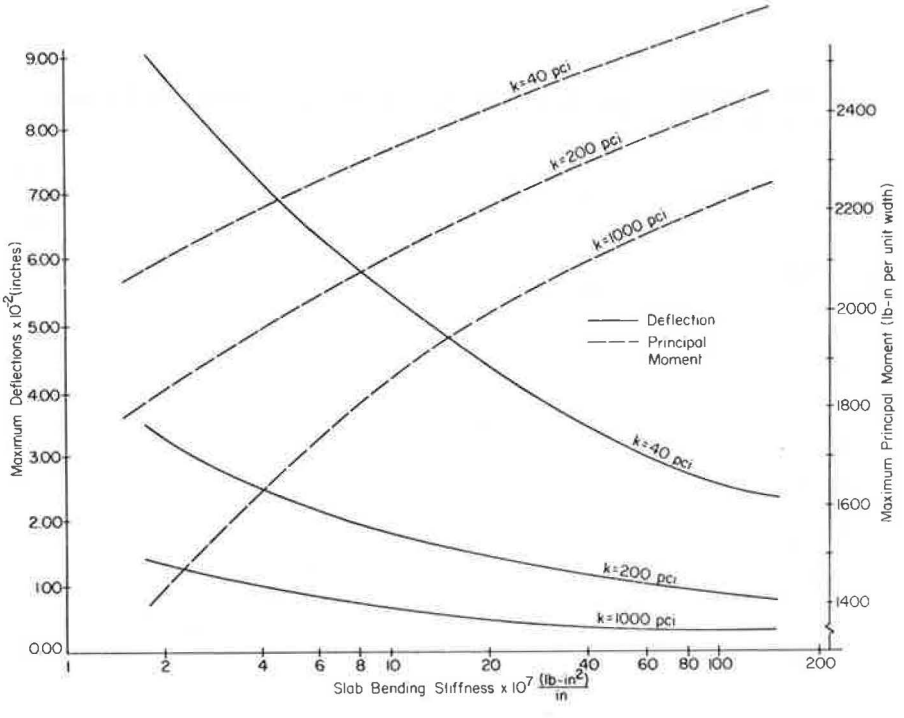

Figure 6. Maximum values of deflection (90 percent reduction, loads between the cracks).

Modulus of subgrade reaction, lb/in²/in.	Crack Spacing, Ft	Slab bending stiffness, (lb-in²)/in. 20×10^6	150×10^6	1125×10^6
40	4	0.0606 2239	0.0383* 2791	0.0223* 3585
	6	0.0589 2406	0.0354* 3049	0.0210* 3901
	8	0.0600 2427	0.0344* 3226	0.0203* 4130
	10	0.0604 2391	0.0345* 3320	0.0198* 4297
200	4	0.0220 1826	0.0109 2338	0.0070* 2940
	6	0.0225 1898	0.0104 2541	0.0064* 3206
	8	0.0223 1853	0.0105 2603	0.0062* 3398
	10	0.0220 1835	0.0106 2581	0.0062* 3518
1000	4	0.0098 1444	0.0038 1993	0.0020* 2441
	6	0.0097 1401	0.0038 2037	0.0019* 2666
	8	0.0096 1395	0.0038 1992	0.0019* 2767
	10	0.0096 1396	0.0037 1962	0.0019* 2771

+ All values occurred 2 feet from the pavement edge.

* Maximum deflection was at the pavement edge; otherwise, it was under the load, 2 feet from the edge.

NOTE: The upper value in each block is the deflection and the lower value is the principal moment.

Figure 7. Effect of slab bending stiffness and crack spacing on deflections and principal moments (k = 40 lb/in.^{3}).

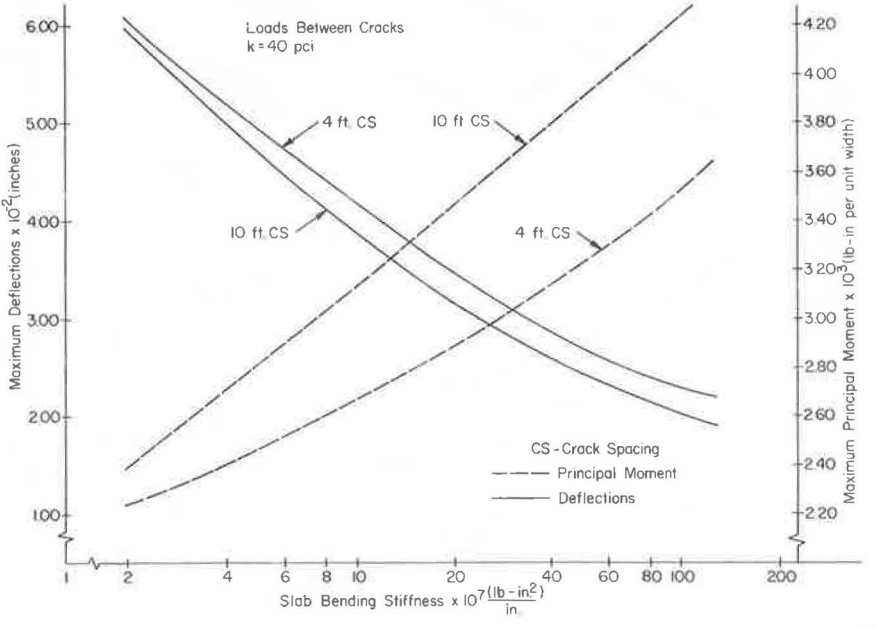

Figure 8. Effect of slab bending stiffness and crack spacing on deflections and principal moments (k = 200 lb/in.^{3}).

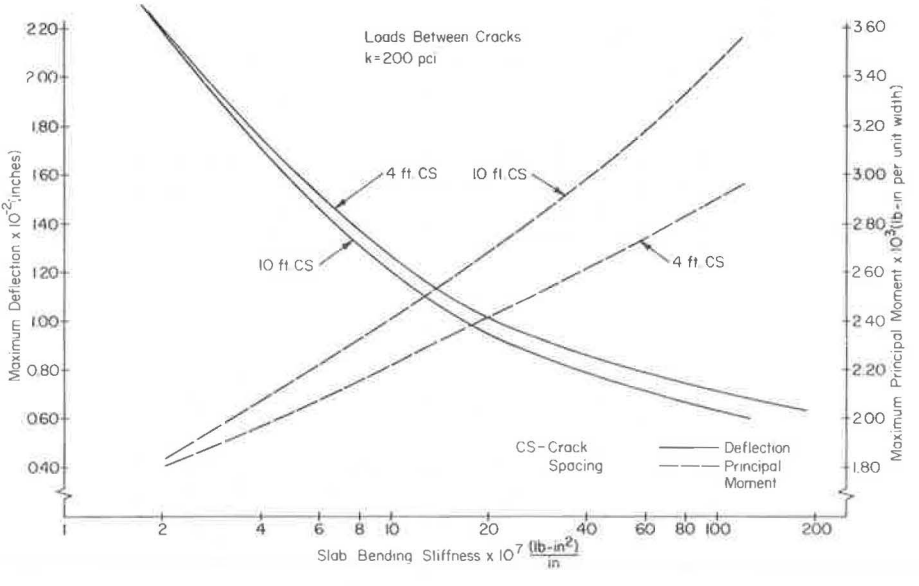

Analysis of Variance

To determine the sensitivity of the rigid pavement design variables, we made an analysis of variance (ANOVA) on the maximum values of deflections and principal moments for both load positions. The ANOVA considered the three design variables encountered, namely, slab bending stiffness, crack spacing, and subgrade modulus.

Table 1 gives the average contribution of the main effects of each variable and their interactions on deflections and principal moments for the loads on the crack. For the levels given to subgrade modulus, slab bending stiffness, and crack spacing, the highest average contribution in the variation in deflections (58.88 percent) was due to the main effect of the subgrade modulus. This was followed by bending stiffness, which accounted for 27.74 percent of the variation, and interaction of subgrade modulus and stiffness ($k \times D$), which accounted for 13.26 percent. The amount that the crack spacing contributed was negligible.

For the variation of principal moment, the main effect of slab stiffness was the largest (59.35 percent), and the main effect of the subgrade modulus was next. The effect of crack spacing was slight.

Results of the ANOVA for the loads between cracks were similar to the case when loads were on the crack (Table 2). It is worthwhile to note that the effect of crack spacing was higher when loads were between cracks. However, over the whole range of the variables studied, neither the main effect of crack spacing nor its interaction with either k or D nor both were highly significant.

ANOVA—Orthogonal Polynomial Breakdown

In a design experiment where the levels of factors are quantitative, it is often possible to extract more information on how the response variable might vary with the changing levels of the quantitative factor, e.g., how deflection varies with the modulus of subgrade reaction and whether or not there is a linear relation between subgrade modulus and deflection.

The use of orthogonal polynomials makes the analysis rather simple, provided the experiment is designed with equispaced quantitative levels. In the design experiment studied (Fig. 1), the levels of slab stiffness, as well as subgrade modulus, are equispaced logarithmically. That is, each level is obtained from the preceding one by a constant multiplier, which means that the levels progress geometrically. The multiplier was 7.5 for slab stiffness and 5.0 for subgrade modulus. The levels of crack spacing are also equispaced but constitute an arithmetic progression.

Loads on the Crack—Table 3 gives the ANOVA orthogonal breakdown for the deflection response for loads on the crack. In tabulating the orthogonal breakdown, effects that contributed less than 1 percent in response variation were neglected.

It is worthwhile to note that the levels of subgrade modulus are equispaced in the logarithm and that the linear effect refers to the deflection variation associated with log k and not k. Likewise, the quadratic effect is associated with $(\log k)^2$. Similar statements can be made concerning the stiffness term.

General ANOVA in Table 1 gives the average contribution of subgrade modulus to deflection as 58.88 percent. When this total effect is broken into its linear and quadratic log portions, it is seen that 54.40 percent of the deflection variation was due to the log linear effect and only 4.48 percent to the quadratic effect. In addition, the log linear effect of stiffness and the log linear interaction of k and D explain a substantial amount of the deflection response.

In the case of principal moments given in Table 3, the logarithmic linear effects of stiffness and subgrade modulus contributed around 97 percent. None of the quadratic log effects entered into the picture, and the first order interaction of D and k was not so high as in the deflection case.

Loads Between Cracks—Similar results were obtained for the case with loads between cracks. Table 4 gives the orthogonal breakdown of the pavement variables for deflections and principal moments. In both deflection and principal moment responses for loads on the crack, the effect of crack spacing was less than 1 percent, but this was true only for the deflection response when the loads were between cracks; on prin-

Figure 9. Influence of slab bending stiffness and subgrade modulus on maximum deflections and principal moments for the loads between cracks.

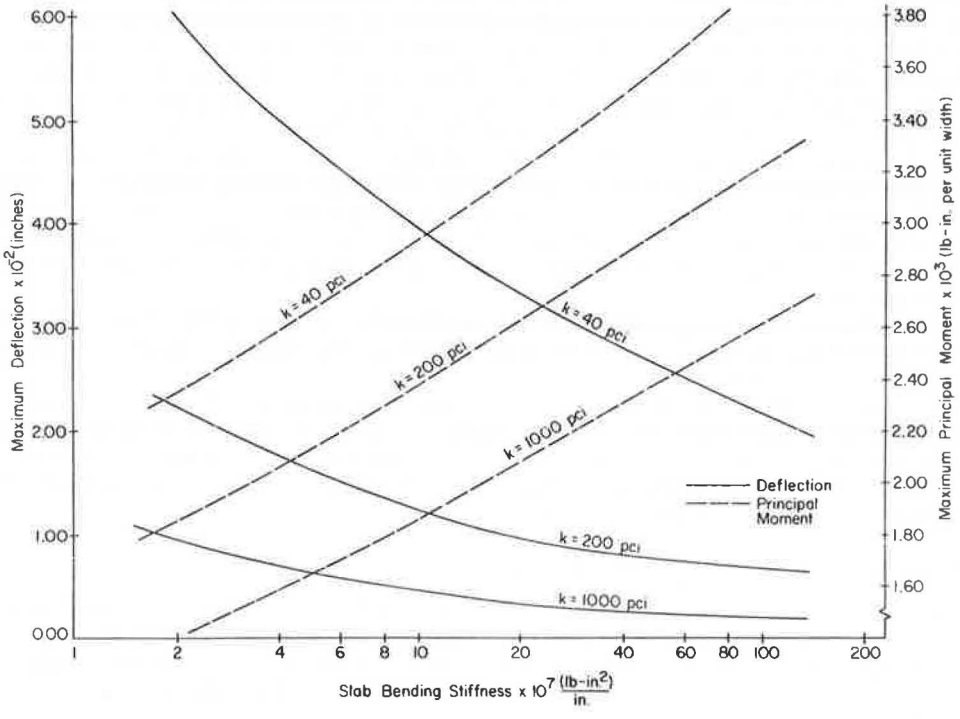

Table 1. General ANOVA for loads on crack.

Source of Variation	Degrees of Freedom	Sum of Squares x 10^3	Mean of Squares x 10^3	Average Contribution[a] (percent)
Maximum Deflections				
Log (subgrade modulus), log k	2	14.089	7.045	58.88
Crack spacing, CS	3	0.012	0.004	0.05
Log (bending stiffness), log D	2	6.637	3.318	27.74
Log k x CS interaction	6	0.010	0.001	0.04
Log k x log D interaction	4	3.173	0.793	13.26
CS x log D interaction	6	0.007	0.001	0.03
Log k x CS x log D interaction	12	—	—	—
Total	35	23.930		100.00
Maximum Principal Moments				
Log (subgrade modulus), log k	2	1,459.43	729.71	37.84
Crack spacing, CS	3	1.16	0.39	0.03
Log (bending stiffness), log D	2	2,288.75	1,144.38	59.35
Log k x CS interaction	6	0.20	0.03	—
Log k x log D interaction	4	105.68	26.42	2.74
CS x log D interaction	6	0.28	0.04	—
Log k x CS x log D interaction	12	0.59	0.04	—
Total	35	3,856.03		99.96

[a]Based on sum of squares.

Table 2. General ANOVA for loads between cracks.

Source of Variation	Degrees of Freedom	Sum of Squares × 10^3	Mean of Squares × 10^3	Average Contribution[a] (percent)
Maximum Deflections				
Log (subgrade modulus), log k	2	7.473	3.736	66.37
Crack spacing, CS	3	0.004	0.001	0.03
Log (bending stiffness), log D	2	2.705	1.352	24.04
Log k × CS interaction	6	0.006	0.001	0.05
Log k × log D interaction	4	1.069	0.267	9.50
CS × log D interaction	6	0.006	0.001	0.01
Log k × CS × log D interaction	12	—	—	—
Total	35	11.263		100.00
Maximum Principal Moments				
Log (subgrade modulus), log k	2	7,599.56	3,799.78	36.82
Crack spacing, CS	3	384.46	128.15	1.86
Log (bending stiffness), log D	2	12,121.70	6,060.87	58.73
Log k × CS interaction	6	123.98	20.66	0.60
Log k × log D interaction	4	133.45	33.36	0.65
CS × log D interaction	6	239.32	39.87	1.16
Log k × CS × log D interaction	12	36.02	3.00	0.18
Total	35	20,638.52		100.00

[a]Based on sum of squares.

Table 3. ANOVA orthogonal polynomial breakdown for loads on crack.

Source of Variation	Degrees of Freedom	Sum of Squares × 10^3	Mean of Squares × 10^3	Contribution (percent)
Maximum Deflections				
Log (subgrade modulus), log k	2	14.089		
Linear	1	13.016	13.016	54.40
Quadratic	1	1.073	1.073	4.48
Log (bending stiffness), log D	2	6.637		
Linear	1	6.415	6.415	26.77
Log k × log D interaction	4	3.173		
Linear × linear	1	2.881	2.881	12.02
Linear × quadratic	1	0.238	0.238	1.00
Residual	30	0.307	0.011	1.33
Total	35	23.930	23.634	100.00
Maximum Principal Moments				
Log (subgrade modulus), log k	2	1,459.43		
Linear	1	1,448.94	1,448.94	37.57
Log (bending stiffness), log D	2	2,288.75		
Linear	1	2,269.96	2,269.96	58.87
Log k × log D interaction	4	105.68		
Linear × linear	1	96.25	96.25	2.50
Residual	32	40.88	1.28	1.06
Total	35	3,856.03	3,816.43	100.00

Table 4. ANOVA orthogonal polynomial breakdown for loads between cracks.

Source of Variation	Degrees of Freedom	Sum of Squares × 10^3	Mean of Squares × 10^3	Contribution (percent)
Maximum Deflections				
Log (subgrade modulus), log k	2	7.473		
Linear	1	6.837	6.837	60.72
Quadratic	1	0.636	0.636	5.60
Log (bending stiffness), log D	2	2.705		
Linear	1	2.606	2.606	23.17
Log k × log D interaction	4	1.069		
Linear × linear	1	0.981	0.981	8.70
Residual	31	0.203	0.006	1.81
Total	35	11.263	11.066	100.00
Maximum Principal Moments				
Log (subgrade modulus), log k	2	7,599.56		
Linear	1	7,590.38	7,590.38	36.77
Crack spacing, CS	4	384.46		
Linear	1	346.55	346.55	1.68
Log (bending stiffness), log D	2	12,121.70		
Linear	1	12,096.98	12,096.98	58.62
Residual	32	604.61	18.89	2.93
Total	35	20,638.52	20,052.80	100.00

cipal moments, the linear effect of crack spacing was 1.68 percent of the total contribution, which still is not highly significant.

Comparison Between 90 Percent Stiffness Reduction and Full Slab

The effect of crack formation on structural members is an increase in the flexibility of the system. Generally, this will produce an increase in deflections and a decrease in moments or stresses. Because no contraction joints are provided in continuously reinforced concrete pavements, volume change stresses will cause random transverse cracks to develop. The influence of these transverse cracks on maximum deflection and principal moments is shown in Figures 10 and 11.

Values of maximum deflections and principal moments for the full slab case were compared with those of the 90 percent reduction in bending stiffness at the cracks for the two load placements. For low and medium levels of subgrade modulus, the increase in deflection when loads are on cracks is quite significant (Fig. 10). This indicates the detrimental effect of these transverse discontinuities on the pavement slab. It is worthwhile to note that the difference in principal moments between the cracked and uncracked slab increases as the relative stiffness of the slab to that of the subgrade increases (Fig. 11).

Comparison Between 90 and 100 Percent Reduction (Hinge) in Bending Stiffness

In this study, the cracks were analyzed as if they were completely closed. Deformations in the slab are thus resisted by some degree of moment transfer across the cracks as is customary in normal structural concrete analysis. In practice, however, slabs have crack openings of a finite width that varies primarily because of volume changes. Considering these finite crack widths would thus involve the nonlinear relation of no bending resistance until the crack closes at the top, at which time some bending resistance would then be felt. In this section, however, comparisons of deflections and principal moments are made between the two extreme cases: partial (closed crack) and zero (open crack) bending transfer across the transverse discontinuities.

Values of deflections and principal moments for the hinge case when the loads are on the crack are shown in Figure 12. A graphic representation is used to compare the ratios of deflections and principal moments in the hinge case with those in the 90 percent reduction case.

Figure 13 shows the change in deflections (expressed as a ratio of the values for the 100 to the 90 percent reductions) with the change in radius of relative stiffness for different crack-spacing patterns for loads on the crack. It is seen that, for high values of the radius of relative stiffness, as crack spacing decreases, changes in maximum deflections are highly significant. Obviously, this will emphasize the effect of the width of the crack on the behavior of the pavement structure. Deflections increase at a significant rate as the crack width increases. Hence, crack width should be given special consideration, and narrow cracks are indeed the desirable objective for successful performance of a continuously reinforced concrete pavement.

No significant difference in principal moments was evident between the 100 and 90 percent reductions when the loads were acting on the cracks. The same thing applies to deflections when loads were acting between cracks (Figs. 6 and 14). Comparing the values of principal moment for the loads between cracks (Figs. 6 and 14), certain differences resulted for high values of radius of relative stiffness (Fig. 15). The ratio of the two moment values approaches unity as crack spacing increases, and practically no difference is encountered in the range of 8 to 10 ft.

Therefore, the structural behavior of CRC pavement shows that crack width has a very important effect on the performance of such pavement. Because of the volume changes in the concrete mix, there is a direct relation between crack width and spacing. As crack spacing increases, crack width increases, which in turn causes significant changes in the pavement structure. Deflections increase at a high rate as crack width increases, causing several modes of distress. Furthermore, as shown in Figure 15, no significant drop is encountered in the principal moments between the partial and hinge cases for the 8- and 10-ft crack spacing.

Figure 10. Influence of bending stiffness and subgrade modulus on deflection for cracked and full (uncracked) slabs.

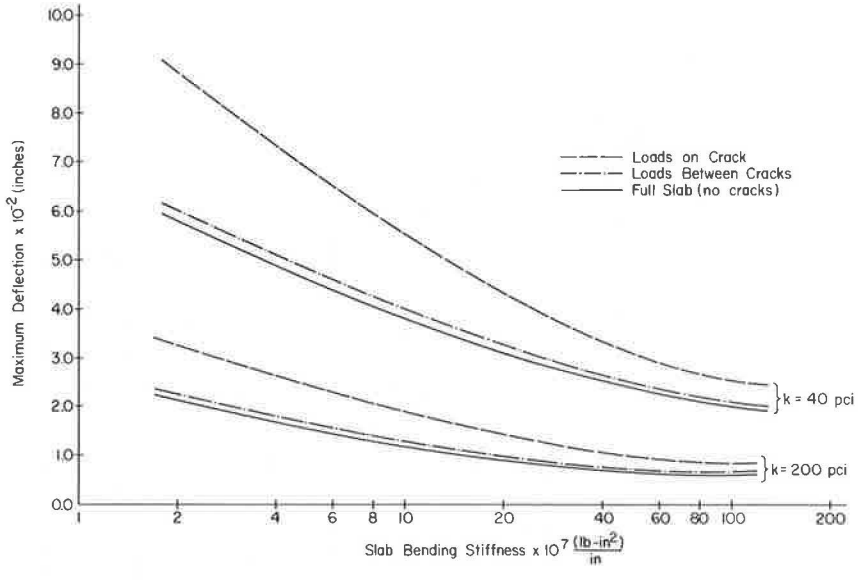

Figure 11. Influence of radius of relative stiffness on principal moments for cracked and uncracked slabs for loading (Fig. 5).

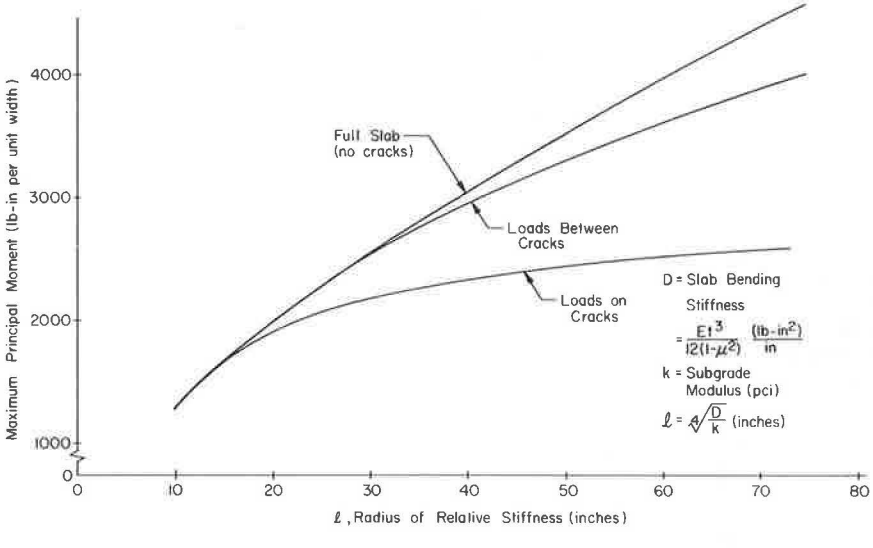

Figure 12. Maximum values of deflection (100 percent reduction, loads on the crack).

Modulus of subgrade reaction, lb/in²/in.	Crack Spacing, ℓ ℓ	Slab bending stiffness, (lb-in²)/in. 20 x 10^6	150 x 10^6	1125 x 10^6
40	4	0.1277 2096	0.0905* 2354	0.0643* 2554
	6	0.1087 2083	0.0741* 2331	0.0515* 2543
	8	0.1036 2079	0.0671* 2318	0.0438* 2535
	10	0.1030 2078	0.0598* 2312	0.0388* 2532
200	4	0.0380 1838	0.0246 2156	0.0176* 2402
	6	0.0362 1834	0.0202 2138	0.0141* 2380
	8	0.0362 1834	0.0188 2132	0.0121* 2365
	10	0.0362 1834	0.0185 2131	0.0111* 2358
1000	4	0.0139 1438	0.0068 1916	0.0046 2211
	6	0.0139 1438	0.0063 1909	0.0037 2190
	8	0.0139 1438	0.0063 1909	0.0034 2182
	10	0.0139 1438	0.0063 1909	0.0033 2180

+ All values occurred 8 feet from the pavement edge.

* Maximum deflection was at the pavement edge; otherwise, it was under the load, 2 feet from the egde.

NOTE: The upper value in each block is the deflection and the lower value is the principal moment.

Figure 13. Comparison of maximum deflections between the 100 and 90 percent reductions in bending stiffness at crack locations for loads on cracks.

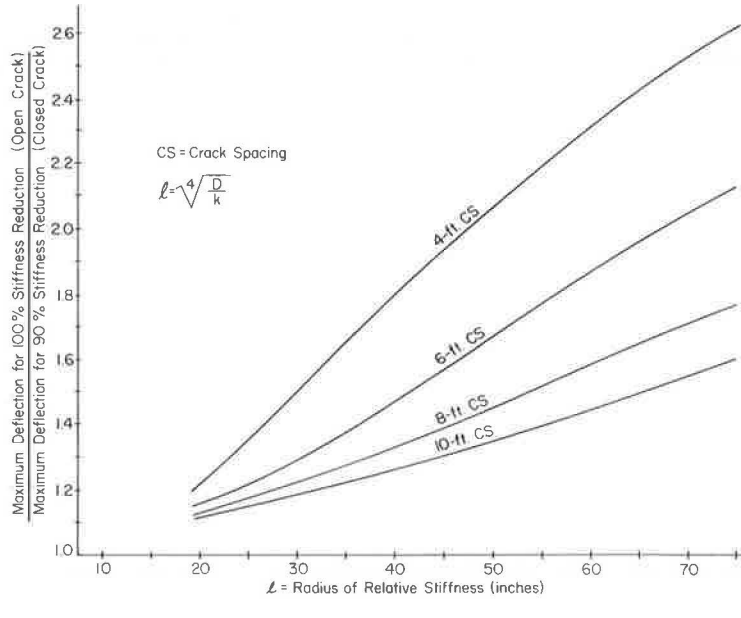

Figure 14. Values of maximum deflection (100 percent reduction, loads between cracks).

Modulus of subgrade reaction, lb/in²/in.	Crack Spacing, ft	Slab bending stiffness, (lb-in²)/in. 20 x 10^6	150 x 10^6	1125 x 10^6
40	4	0.0626 2159	0.0457* 2311	0.0330* 2430
	6	0.0594 2446	0.0375* 2828	0.0261* 3042
	8	0.0613 2487	0.0349* 3198	0.0225* 3558
	10	0.0619 2427	0.0350* 3398	0.0207* 3971
200	4	0.0221 1919	0.0116 2196	0.0087* 2332
	6	0.0228 1925	0.0105 2561	0.0070* 2876
	8	0.0226 1861	0.0107 2676	0.0064* 3294
	10	0.0221 1834	0.0109 2641	0.0063* 3560
1000	4	0.0099 1458	0.0037 2005	0.0022* 2226
	6	0.0097 1402	0.0038 2077	0.0019* 2647
	8	0.0096 1394	0.0038 2010	0.0019* 2840
	10	0.0096 1396	0.0038 1964	0.0020* 2852

+ All values occurred 2 feet from the pavement edge.

* Maximum deflection was at the pavement edge; otherwise, it was under the load, 2 feet from the edge.

NOTE: The upper value in each block is the deflection and the lower value is the principal moment.

Figure 15. Comparison of maximum principal moment between the 100 and 90 percent reductions in bending stiffness at crack locations for loads between cracks.

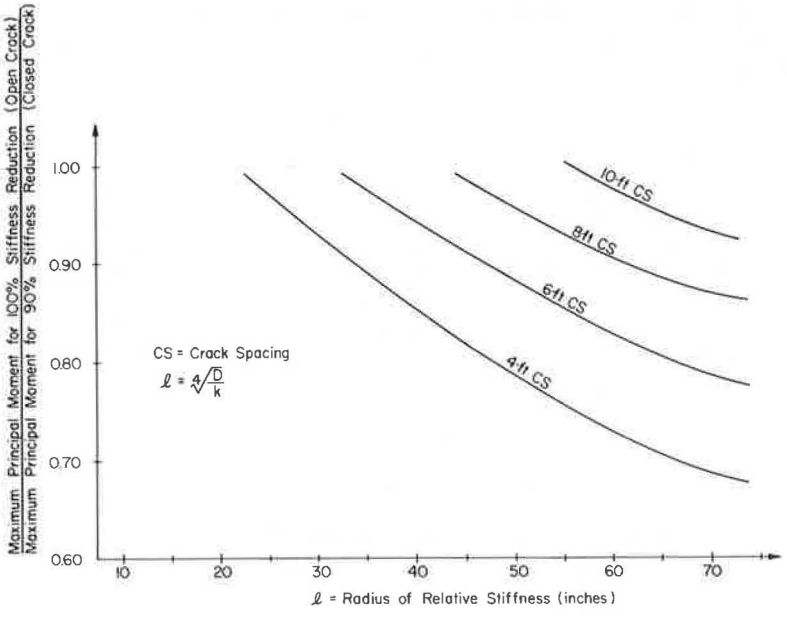

Discussion of Results

Transverse cracks are characteristic of continuously reinforced concrete pavements and significantly influence the behavior and performance of this pavement type. Comparison between the cracked and uncracked slab (Figs. 10 and 11) indicates that, when loads were on the crack, there was a substantial increase in slab deflections, whereas the drop in principal moment that occurred for loads between cracks was not highly significant. This illustrates the detrimental effects of these transverse discontinuities on the pavement structure.

According to SLAB program results, the modulus of subgrade reaction, as defined by Westergaard and others, plays an important role in the determination of deflections and principal moments (Figs. 5, 7, 8, and 9). Pavement deflections decrease at a significant rate as subgrade modulus increases. Furthermore, there is about a 10 percent decrease in the value of principal moment as k varies from one level to the next when loads are on the crack and about a 20 percent decrease for the case when loads are between cracks.

Although the subgrade modulus showed a higher contribution in the determination of deflections than principal moments, slab bending stiffness possessed a contrasting effect (Figs. 5, 7, 8, and 9). Hence, if the most important design criteria are pavement stresses, the thickness of the slab is the factor that requires the greatest consideration, and it is followed in importance by the modulus of subgrade reaction.

For the case when loads were on the crack, as crack spacing varied over the range studied (4 to 10 ft), a small change was encountered in deflections and principal moments (Fig. 4). For the second load placement investigated (i.e., loads between cracks), the effect of crack spacing on deflections was also slight or practically negligible, whereas changes in principal moments for the low and medium levels of k were significant (Figs. 7 and 8).

The ANOVA performed on the SLAB results has indicated that the main effects of slab bending stiffness and subgrade modulus contributed around 90 percent to the variation in each of the deflection and principal moment responses (Tables 1 and 2). It also showed the minor effect of crack spacing on the pavement behavior.

The polynomial orthogonal breakdown yielded similar results for the two load placements. The logarithmic linear effect of subgrade modulus and bending stiffness was highly significant and explained most of the variations in the pavement responses, deflections, and principal moments.

The comparison between the 90 percent (closed crack) and 100 percent (open crack) reduction in bending stiffness at the crack location indicated the importance of crack width on the behavior of continuously reinforced concrete pavements. Slab deflections increase at a high rate as crack width increases (Fig. 13), whereas no significant drop is encountered in principal moments.

CONCLUSIONS

This investigation was conducted to determine, by use of the discrete-element slab model, the sensitivity of pavement deflection and principal moment (or stress) to changes in design parameters. The conclusions are limited to the range of variables studied. These findings, however, can provide reasonable information to use in design, for selecting those variables that require the most intensive consideration and those that will yield the best results.

Based on changes in deflections and principal moments, the following conclusions have been drawn:

1. Higher principal moments or stresses are produced when loads are located between cracks than when loads are at the crack. The reverse is true for the deflection response.
2. The effect of the modulus of subgrade reaction on slab deflection is highly significant.
3. Principal moments or stresses are mainly dependent on, first, the stiffness of the slab and, second, the subgrade modulus.

4. As crack spacing increases, principal moment values for the loads placed between cracks approach those of the full slab case.
5. The effect of crack spacing on deflections and principal moments was greater for the case of 100 percent reduction in bending stiffness at crack location than it was for the 90 percent case.
6. The width of the crack has a big influence on the performance of continuously reinforced concrete pavements. The reduction of the bending rigidity of the slab and the consequent increase in the slab deflection as a result of an increase in crack width are important. Perhaps the requirement most necessary to the success of continuously reinforced concrete pavement is that the steel reinforcement hold transverse cracks as tightly as possible.
7. For the increments given to subgrade modulus, slab bending stiffness, and crack spacing, the analysis of variance and its orthogonal polynomial breakdown showed that (a) a definite logarithmic linear trend of subgrade modulus with deflection is observed as well as a tendency toward a logarithmic quadratic relation, (b) the linear effect of the log of bending stiffness on principal moments and deflections is quite significant, and (c) interactions do occur among design variables, indicating that the effect of any one design variable on deflections and principal moments is dependent on levels of the other two design variables.

RECOMMENDATIONS

Based on this investigation, the following recommendations are made:

1. Pavement design procedures should include greater consideration of the modulus of subgrade reaction because of its influence on deflections and stresses.
2. Stress criteria in present design procedures should be coupled with deflection criteria, which will enable the designer to ensure a pavement deflection less than the desired maximum.
3. Transverse cracks should be maintained very narrow in order to (a) prevent progressive infiltration of incompressible materials such as soil, which eventually might cause excessive compressive stress to develop in the pavement and thus produce blowups; (b) prevent appreciable amounts of surface water from reaching the subgrade; and (c) maintain effective aggregate interlock between the crack interfaces.

ACKNOWLEDGMENTS

The authors wish to thank the sponsors, the Texas Highway Department and the U.S. Department of Transportation, Federal Highway Administration, for their support of the research reported here. The contents of this report reflect the views of the authors, who are responsible for the facts and the accuracy of the data presented herein. The contents do not necessarily reflect the official views or policies of the Federal Highway Administration. This report does not constitute a standard, specification, or regulation.

REFERENCES

1. Hudson, W. R., and Matlock, H. Discontinuous Orthotropic Plates and Slabs. Center for Highway Research, Univ. of Texas at Austin, Res. Rept. 56-6, May 1966.
2. Stelzer, C. F., Jr., and Hudson, W. R. A Direct Computer Solution for Plates and Pavement Slabs (DSLAB 5). Center for Highway Research, Univ. of Texas at Austin, Res. Rept. 56-9, Oct. 1967.
3. Panak, J. J., and Matlock, H. A Discrete-Element Method of Multiple-Loading Analysis for Two-Way Bridge Floor Slabs (SLAB 30). Center for Highway Research, Univ. of Texas at Austin, Res. Rept. 56-13, Jan. 1970.
4. Abou-Ayyash, A., Hudson, W. R., and Treybig, H. J. Effect of Cracks on Bending Stiffness in Continuous Pavements. Highway Research Record 407, 1972, pp. 10-21.
5. Treybig, H. J., Hudson, W. R., and McCullough, B. F. Effect of Load Placement on Rigid Pavement Behavior. Jour. Transportation Engineering, Proc. ASCE, Vol. 97, No. TE4, Nov. 1971.

6. Richmond, B. S. Statistical Analysis, 2nd Ed. Ronald Press Co., New York, 1957.
7. Hicks, R. C. Fundamental Concepts in the Design of Experiments. Holt, Rinehart, and Winston, New York, 1964.
8. McCullough, B. F., and Treybig, H. J. Determining the Relationship of Variables in Deflection of Continuously Reinforced Concrete Pavement. Texas Highway Department, Res. Rept. 46-4, Aug. 1965.

FINITE-ELEMENT ANALYSIS OF CONCRETE SLABS AND ITS IMPLICATIONS FOR RIGID PAVEMENT DESIGN

Y. H. Huang and S. T. Wang, Department of Civil Engineering,
University of Kentucky

A finite-element method programmed for a high-speed computer was developed for determining the stresses in concrete slabs with load transfer at the transverse joints. The method is based on the classical theory of thin plates on Winkler foundations and yields numerical results that check closely with other available solutions as well as with the experimental measurements from the AASHO Road Test. Although a single value of the modulus of subgrade reaction can be selected to predict approximately the stresses for various slab thicknesses and axle loads, it was found that, under a given axle load, a better agreement between theoretical and experimental results could be obtained if greater subgrade moduli were used for thicker pavements, a fact contributing to the nonlinear behavior of subgrade soils. Numerical results are presented to illustrate the effect of loading position, load transfer, and loss of subgrade contact on critical stresses in rigid pavements. When load transfer is provided at the transverse joint, the most critical stress in highway pavements occurs when the load is near the edge and far from the joint. It is suggested that the edge stress, instead of the stress at the joint, be used for the design of highway pavements.

•THE determination of stresses due to wheel loads in concrete pavements has been a subject of major concern for more than four decades. In 1926 Westergaard (1), using the theory of elasticity by assuming the subgrade as a Winkler foundation, developed a mathematical method for determining the critical stresses in concrete highway pavements resulting from three cases of loading: load applied near the corner of a large slab, load applied near the edge of a large slab but at a considerable distance from any corner, and load applied at the interior of a large slab at a considerable distance from any edge. In extending the method to airport pavements, he later developed new formulas (2, 3) that give the stresses and deflections at an edge point far from any corner and at an interior point far from any edge. These formulas were then employed by Picket and Ray (4) for developing influence charts, which have been used by the Portland Cement Association (5, 6) for the design of highway and airport pavements.

In comparing the critical corner stress obtained from Westergaard's formula with that from field measurements, Pickett found that Westergaard's corner formula, based on the assumption that the slab and subgrade were in full contact, always yielded a stress that was too small. By assuming that part of the slab was not in contact with the subgrade, he developed a semi-empirical formula that was in good agreement with both theoretical and experimental results. Pickett's corner formula, with a 20 percent allowance for load transfer, was used previously by the Portland Cement Association (7) for the design of highway pavements.

All the preceding theoretical solutions are based on an infinitely large slab, with a load at the corner, on the edge, or in the interior, and therefore may not be applicable to today's 12-ft wide lanes with most traffic moving at some distance from slab edges

Publication of this paper sponsored by Committee on Rigid Pavement Design.

and corners. With the advent of high-speed computers and the powerful finite-element method, it is now possible to analyze rectangular slabs subjected to any wheel loads and boundary conditions. The purposes of this paper are (a) to present a finite element method programmed for a high-speed computer for determining the stress distribution in a rectangular concrete slab, with or without load transfer at the transverse joint; (b) to compare the results of the finite-element method with other theoretical solutions available as well as with the experimental measurements from the AASHO Road Test, so as to check the accuracy and validity of the method; and (c) to investigate the effect of loading position, load transfer, and loss of subgrade contact on the critical stress in some typical pavements, so as to shed light on current concepts of rigid pavement design.

The finite-element method presented here is quite different from the discrete-element method employed earlier by Hudson and Matlock (8) and later by Vesic and Saxena (9) for the analysis of concrete pavements. The discrete-element method is more or less similar to the finite difference method by considering the slab as an assemblage of elastic joints, rigid bars, and torsional bars. The finite-element method is based on the theory of minimum potential energy by dividing the slab into small elements interconnected only at a finite number of nodal points. The major advantages of the finite-element method are that elements of varying sizes can be easily incorporated in the analysis and that no special treatment is needed at a free edge. As a result, the finite-element method generally yields a stiffness matrix that is symmetric, positive, and definite, and the large number of simultaneous equations can be solved by an effective scheme, although this symmetric characteristic was not fully utilized in this study because of the assumption of load transfer at the joint.

DESCRIPTION OF METHOD

The finite-element method employed in this study is based on the classical theory of thin plates by assuming that the plane before bending remains plane after bending. In addition to the basic requirements that the slabs are homogeneous, isotropic, and elastic, it is further assumed that the subgrade acts as a Winkler foundation; i.e., the reactive pressure between subgrade and slab at any given point is proportional to the deflection at that point. The procedure follows essentially that of Zienkiewicz and Cheung (10, 11) and will not be presented here. Only the general approach, the treatment of doweled joints, and the capability of the computer program will be briefly described.

General Approach

Figure 1 shows a rectangular finite element with nodes i, j, k, and l. At each node, there are three fictitious forces and three corresponding displacements. The three forces are a vertical force, F_w; a couple about the x-axis, $F_{\theta x}$; and a couple about the y-axis, $F_{\theta y}$. The three displacements are the deflection in the z-direction, w; a rotation about the x-axis, θ_x; and a rotation about the y-axis, θ_y. These forces and displacements are related by

$$\begin{Bmatrix} F_i \\ F_j \\ F_k \\ F_l \end{Bmatrix} = [K] \begin{Bmatrix} \delta_i \\ \delta_j \\ \delta_k \\ \delta_l \end{Bmatrix} + kab \begin{Bmatrix} \delta'_i \\ \delta'_j \\ \delta'_k \\ \delta'_l \end{Bmatrix} \tag{1}$$

in which [K] = stiffness matrix, the coefficients of which depend on the dimensions, a and b, of the element and the Young's modulus and Poisson's ratio of the slab; k = modulus of subgrade reaction; and at any given node i is

$$F_i = \begin{Bmatrix} F_{wi} \\ F_{\theta xi} \\ F_{\theta xi} \end{Bmatrix}, \quad \delta_i = \begin{Bmatrix} w_i \\ \theta_{xi} \\ \theta_{yi} \end{Bmatrix}, \quad \delta'_i = \begin{Bmatrix} w_i \\ 0 \\ 0 \end{Bmatrix}$$

The stiffness matrix for a rectangular element was tabulated by Zienkiewicz and Cheung (10) and is used in the present analysis. By superimposing the stiffness matrices over all elements and replacing the fictitious nodal forces with the statistical equivalent of the externally applied loads, a set of simultaneous equations was obtained for solving the unknown nodal displacements. The nodal moments and stresses were then computed from the nodal displacements, using the stress matrix tabulated by Zienkiewicz and Cheung (10). Because the stresses at a given node computed by means of one element might be different from that by the neighboring elements, the stresses in all adjoining elements were computed and their average values obtained.

Doweled Joints

The finite-element analysis of concrete slabs with doweled joints as developed here is believed to be original and provides an effective method for solving this complex problem. Figure 2 shows a load applied on the left slab of a two-slab system connected by dowel bars at the joint. If no dowels are provided at the joint, each slab will act independently, and it is only necessary to consider the left slab. When dowels are provided, part of the wheel load will be transferred from the left slab to the right slab. The efficiency of load transfer can be defined as

$$L = \frac{w_r}{w_l} \times 100 \qquad (2)$$

in which L = efficiency of load transfer, w_l = deflection of the left or loaded slab at the joint, and w_r = deflection of the right or unloaded slab at the joint. When no dowels are used, $w_r = 0$, and the efficiency of load transfer is zero. When $w_l = w_r$, or both slabs deflect the same amount at the joint, the efficiency of load transfer is 100 percent.

For the ease of explanation, each slab is divided into two elements (Fig. 2). There are a total of 12 nodes, each having three unknown displacements, or a total of 36 equations. These equations can be obtained by first assuming the discontinuity of the two slabs at the joint, so neither moment nor shear can be transferred through the joint. For example, let us look at the three equations at node 4. The 10th equation gives the vertical force, the 11th equation gives the couple about the x-axis, and the 12th equation gives the couple about the y-axis. The corresponding equations at node 7 are the 19th equation for the vertical force, the 20th equation for the couple about the x-axis, and the 21st equation for the couple about the y-axis. Because dowel bars cannot transmit moments from one slab to the other, the addition of the dowel bars will make no change in the 11th, 12th, 20th, and 21st equations. However, because of the transfer of shear, the sum of the vertical forces given by the 10th and 19th equations must be equated to the external force applied at node 4. In other words, the 10th and 19th equations are combined to form a new equation replacing the original 10th equation. The original 19th equation is then replaced by Eq. 2, which is written as

$$w_4 = \frac{100}{L} w_7 \qquad (3)$$

Because two original equations are replaced by two new equations, the total number of equations remains unchanged. The same procedure can be applied to nodes 5 and 8 as well as nodes 6 and 9. This modification destroys the symmetry of the stiffness matrix and results in an upper half band being greater than the lower half, so both the upper and lower bands must be stored. The Gauss elimination method with banded matrix provided by the IBM scientific subroutine package was used in this study to solve the simultaneous equations.

Computer Program

A general computer program was developed for determining the stresses in a pavement system composed of a series of up to three slabs connected by dowels at the transverse joints. The three slabs are used because this is a general case with the

loads applied on the middle slab, which is connected at each end to a neighboring slab by dowel bars. The use of more than three slabs is not necessary because the additional slabs are far from the load and have practically no effect on the stresses in the loaded slab. When the loads are applied near the transverse joint, only two slabs are generally sufficient, and the slab at the far end can be ignored.

Figure 3 shows the finite-element network of a three-slab system under a single- or tandem-axle load, which will be subjected to later analysis. The input parameters, which control the size and division of the slabs in this case, are number of slabs = 3; number of y-coordinates = 7; number of x-coordinates for slab 1 = 4; number of x-coordinates for slab 2 = 7; number of x-coordinates for slab 3 = 4; y-coordinates = 0, 17, 34, 57, 80, 105, and 144 in.; x-coordinates = 0, 70, 130, 180, 180, 232, 256.5, 281, 305.5, 330, 360, 360, 400, 470, and 540 in. The same program can be used for two slabs by setting the number of horizontal coordinates for slab 1 to 0, and for one slab by setting the number of horizontal coordinates for both slab 1 and slab 3 to 0; the horizontal coordinates must also be changed accordingly.

The tire imprints are converted to rectangular areas, and the coordinates of their sides must be given, so that the program can distribute the wheel loads among adjacent nodes by statics (10, 11). The program can compute several different loadings at the same time. The additional computer time due to these additional loads is very small because Gauss elimination of the coefficient matrix is carried out only once regardless of the number of loads involved.

If the problem to be solved exhibits symmetry with respect to one or both axes, it is only necessary to consider one-half or one-quarter of the pavements, which saves a great deal of computer time.

The program can be used to investigate the effect of partial subgrade contact on stress distribution. The nodal numbers at which subgrade reaction resulting from loss of subgrade contact does not exist can be assigned, and the second term on the right side of Eq. 1 will be automatically eliminated at these nodal points when forming the simultaneous equations.

The program was written in FORTRAN IV for the IBM 360 computer, Model 65, available at the University of Kentucky.

COMPARISON WITH AVAILABLE SOLUTIONS

To check the accuracy of the finite-element method and the correctness of the computer program, it is desirable to compare the finite-element solutions with other theoretical solutions available, especially with those involving discontinuities such as the stress at the free edge of a slab. Westergaard's original work and Pickett and Ray's influence charts can be used for such purposes. Because these available solutions are based on an infinite slab, a very large slab was used in the finite-element analysis.

Westergaard's Solutions

The finite-element solutions were obtained by using a large slab, 20ℓ long by 10ℓ wide, where ℓ is the radius of relative stiffness. Because the problem is symmetrical with respect to the y-axis, only one-half of the slab was considered. The slab was divided into rectangular finite elements as shown in Figure 4. The x-coordinates are 0, $\pi\ell/8$, $\pi\ell/4$, $\pi\ell/2$, $\pi\ell$, 5ℓ, 7ℓ, and 10ℓ, and the y-coordinates are 0, $\pi\ell/4$, $\pi\ell/2$, $\pi\ell$, $1.5\,\pi\ell$, $2\,\pi\ell$, $2.5\,\pi\ell$, and 10ℓ. The Poisson's ratio of the concrete is 0.25, as was assumed by Westergaard.

Figure 4 shows a comparison between Westergaard's exact solutions for an infinite slab with a concentrated load, P, on one edge far from any corner, as indicated by the solid curves, and the finite-element solutions, as indicated by the small circles. The moment, M, and deflection, w, along the edge of slab and the deflection at a distance of $\pi\ell/4$ and $\pi\ell/2$ from the edge are presented. It can be seen that the finite-element solutions check very closely with Westergaard's results, thus indicating the accuracy of the authors' finite-element formulation.

Figure 1. Rectangular plate element.

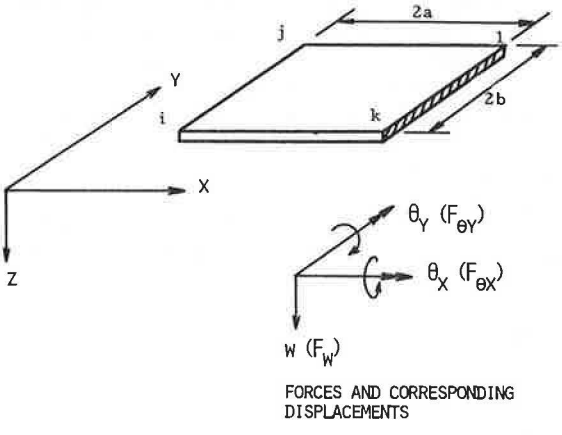

Figure 2. Two-slab system with doweled joint.

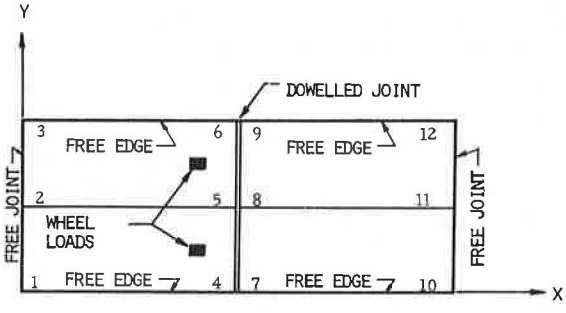

Figure 3. Three-slab system with doweled joints.

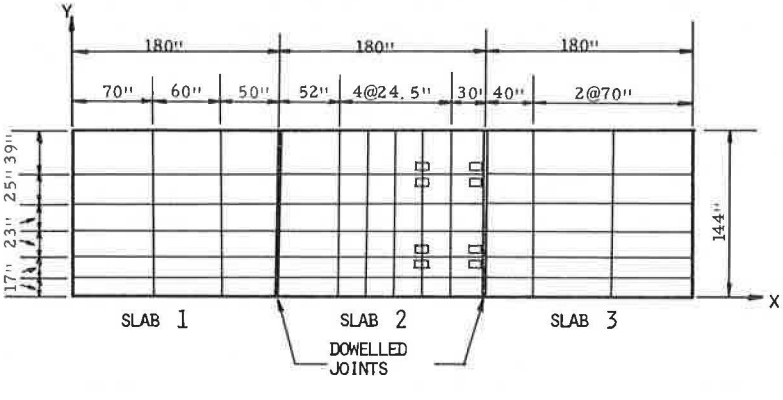

PCA's Solutions

The Portland Cement Association has made use of the influence chart developed by Pickett and Ray (4) for determining the stress on a pavement edge due to tire loads. Figure 5 (12) shows the application of the chart for determining the moment at point 0 under a 36-kip tandem-axle load having an 11.5-in. dual-tire spacing, a 49-in. tandem-axle spacing, and a 71-in. spacing between the centers of the two sets of dual tires. The load on each tire is 4,500 lb. The actual contact area is 67 in.^{2}, consisting of a rectangle with two rounded ends, but was converted to a rectangle of 6.79 by 9.87 in. The Poisson's ratio of the concrete is 0.15.

The moment, M, at point 0 in Figure 5 (due to each of the tire loads) can be determined from the number of blocks enclosed by each tire imprint, tabulated as N-counts in the figure, by

$$M = \frac{q\,\ell^2\,N}{10{,}000} \tag{4}$$

in which q = contact pressure = 67.2 psi and ℓ = 50 in. As tire 1 yields the same moment as tire 2 and tire 5 the same as tire 6, there are actually six different tire positions, some close to point 0 and some far from it, which can be used for comparison.

In the finite-element analysis, only one-half of the slab was considered because the problem could be made symmetric by placing an image tire on the left corresponding to each tire on the right. The moment thus determined was divided by two to give the moment resulting from one tire only. The horizontal and vertical coordinates for finite-element subdivisions were 0, 24, 48, 72, 96, 128, 160, 208, and 300 in.

Table 1 gives a comparison of the moments at point 0 due to six different tire positions. It can be seen that the finite-element solutions check quite well with the influence chart solution, especially when the tire is close to point 0. The large discrepancy for tire 7 is due to the fact that this tire straddles between positive and negative blocks and covers only two blocks. The percentage of discrepancy would become zero if the block enclosed was counted as 1.2 instead of the two blocks counted by the PCA.

COMPARISON WITH AASHO ROAD TEST

Although the finite-element solutions check very closely with other available solutions, the comparison is based on a large slab with free edges. Because no theoretical solutions are available for rectangular slabs with load transfer at the joint, it is desirable to compare the finite-element solutions with experimental measurements so that the validity of the method as applied to actual pavements with doweled joints can be tested. The results of the stress measurements from the AASHO Road Test (13) provide an excellent opportunity for making such comparisons.

In the AASHO Road Test, two series of experiments were made to measure the stresses in concrete slabs. The first was conducted on the main traffic loops where the stress due to moving traffic was measured at a single point on the pavement edge far from any joint. The second was conducted on the nontraffic loop where the stresses due to a rapidly oscillating load were measured at 15 different points distributed over a 6- by 6-ft area at one corner. The length of slabs consisted of 15-ft nonreinforced sections and 40-ft reinforced sections. It was found that reinforcing, or slab length, had very little effect on the stresses measured, so only the 15-ft slab was employed in the finite-element analysis.

The slabs were 15 ft long and 12 ft wide with dowels at the transverse joints and tie bars at the longitudinal joint. Because the dowels were much larger bars spaced at 12 in. in centers and the tie bars were smaller and spaced at 30 in. apart, it was assumed in the finite-element analysis that the efficiency of load transfer was 100 percent at the transverse joint and 0 percent at the longitudinal joint, or the longitudinal joint was treated as a free edge.

In computing theoretical stresses, it is necessary to know the Young's modulus and the Poisson's ratio of concrete and the modulus of subgrade reaction, k. The Young's moduli of concrete, as measured at the AASHO Road Test, were 6.25×10^6 psi for dy-

Figure 4. Comparison of finite-element solution with Westergaard's exact solution.

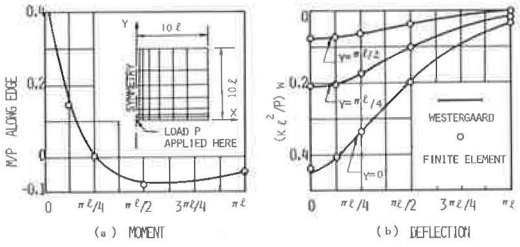

Figure 5. Contact imprints on influence chart and corresponding N-count.

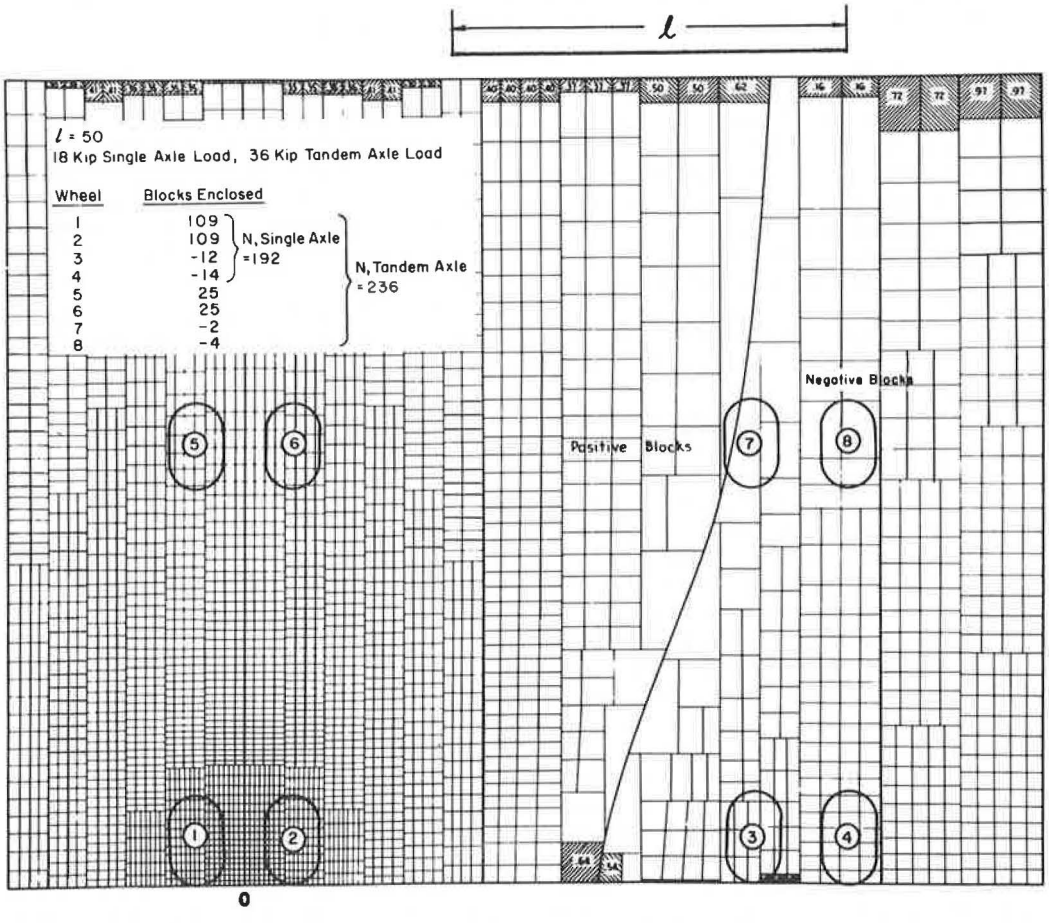

namic loads and 5.25×10^6 psi for static loads, and the Poisson's ratio was found to be 0.28. Because the type of loading does not have significant effect on the Young's modulus, a dynamic modulus of 6.25×10^6 psi was used in the finite-element analysis as well as in the conversion from the measured strains to stresses.

The determination of the subgrade k-values is much more difficult because they change appreciably with the time of the year and the type of loading. The k-values on the subbase obtained by the plate bearing test at the AASHO Road Test varied from 85 to 135 lb/in.^{3}, but these were measured during the spring when the subgrade was weak and by static or gradually applied loads. Because the stresses were measured at the AASHO Road Test mostly during the summer and fall and under dynamic or vibratory loads, larger k-values should be used.

In comparing theoretical stresses with the results of the AASHO Road Test, Vesic and Saxena (9) indicated that the k-values should be inversely proportional to the thickness of the slab and suggested the use of 90.4 lb/in.^{3} for a 5-in. slab, 47.5 lb/in.^{3} for a 9.5-in. slab, and 36.2 lb/in.^{3} for a 12.5-in. slab. These k-values are too small for the reasons discussed previously. If these values are used in the finite-element analysis, the results do not check with the test data, as will be illustrated later.

Dynamic Edge Stress

In the AASHO Road Test, the dynamic strain at the edge of pavement 7.5 ft from the joint was measured under various single- and tandem-axle loads, moving mostly at 5 mph with the center of the dual at a distance of 20 in. from the pavement edge. Statistical equations were developed by the Highway Research Board (13) to predict the dynamic edge strains for various axle loads, slab thicknesses, and temperature gradients. These strains can be converted to stresses using a dynamic Young's modulus of 6.25×10^6 psi as determined from the AASHO Road Test.

The finite-element network is shown in Figure 6. Because of symmetry, only one-half of the pavement was considered. The x-coordinates for the finite-element grid were 0, 30, 60, 90, 130, 190 and 270 in.; the y-coordinates were 0, 20, 40, 70, 90, 110, and 144 in.

Figure 6 shows a comparison of the edge stress when the temperature in the slab is uniform or the temperature gradient is zero. It can be seen that the experimental measurements (as indicated by the solid curves) check reasonably well with the finite-element solutions (as indicated by the dotted curves) for a variety of loads and slab thicknesses when a k-value of 300 lb/in.^{3} is assumed. Nearly in every case, the experimental curves have a steeper slope than the theoretical curves. The curves can be made more compatible by increasing the stress in thinner slabs by decreasing the k-value, or by decreasing the stress in thicker slabs by increasing the k-value. In other words, the k-values should increase with the increase in slab thickness. This is in contradiction to the contention by Vesic and Saxena (9) that the k-values to be used should increase with the decrease in slab thickness. Their conclusion is valid only when the subgrade soils are linearly elastic. In order to obtain solutions based on Winkler foundation comparable to those based on elastic solid, we must increase the k-value with decreasing thickness. However, because the subgrade soils are not linearly elastic and are much stiffer under small stresses and deflections, it is not difficult to explain why under a given load the k-value should increase with the increase in thickness.

The selection of a k-value of 300 lb/in.^{3} needs explanation. This value appears quite reasonable for the conditions of the subgrade and subbase and the types of loading available at the AASHO Road Test. It is well known that the stress in concrete slabs depends on the radius of relative stiffness, ℓ, which is a function of the ratio between Young's modulus of concrete and the k-value of the subgrade. If a k-value of 300 lb/in.^{3} is considered too high, it is quite possible that a Young's modulus of 6.25×10^6 psi is also too high. Thus, the same stress would be obtained if both were reduced proportionately. In fact, the k-value is a fictitious parameter not characteristic of soil behavior. If a k-value that gives a good prediction of the stress for various axle loads and slab thicknesses can be found, it is a most reasonable value to be used. Fortunately,

the value of k does not have a large effect on the computed stress. If a smaller k-value were used, the finite-element solutions, as indicated by the dotted curves, would move slightly upward, but the general trend still remains the same.

Stress Distribution Under Vibratory Loads

In the AASHO Road Test, a rapidly oscillating load at a frequency of 6 cps was applied to the pavement through two wooden pads, each having 11- by 14-in. area and spaced on 6-ft centers. The center of the outer pad was placed 1 ft from the pavement edge, thus simulating a single-axle load in the traffic loops. The major and minor principal strains at 15 points, distributed over a 36-ft^2 region bounded by the pavement edge and a transverse joint, were determined. These strains were then converted to principal stresses, and graphs of the major and minor principal stresses were published by the Highway Research Board (13).

Four loading positions were employed, with the center of the load at a distance of 0.5, 2, 4, and 6 ft from the transverse joint. The loading position, the location of points at which stresses were measured, and the finite-element subdivisions are shown in Figure 7. Because the slab on the left of the loaded slab has very little effect on stress distribution, only two slabs were considered with 100 percent load transfer at the transverse joint and 0 percent at the longitudinal joint. A k-value of 900 lb/in.^{3}, which is three times greater than the 300 lb/in.^{3} used previously for computing the edge strain, was assumed because the vibratory load was applied at a frequency of 6 cps, which is much faster than the vehicle speed of 5 mph.

Figure 8 shows a comparison of principal stresses for three cases: a 5-in. slab with 12,000-lb axle load, 9.5-in. slab with 22,400-lb axle load, and 12.5-in. slab with 30,000-lb axle load. In line with the sign convention used in the finite-element analysis, the stress is considered positive when the surface is in compression and negative when in tension, which is opposite to the sign convention reported by the Highway Research Board (13). The finite-element solutions are indicated by the solid lines for the major principal stresses and dotted lines for the minor principal stresses. The experimental data, which were obtained from the graphs of major and minor principal stresses published by the Highway Research Board, are indicated by the small circles. For loading position 1, the stresses are those along the joint. For other loading positions, they are under the respective axle at various distances from the edge.

Figure 8 shows that the finite-element solutions check quite well with the experimental measurements, except for the minor principal stress in the 5- and 9.5-in. slabs. Although it is possible to improve the agreement between theoretical and experimental data for loading position 1 by decreasing the efficiency of load transfer for the 5-in. slab to 40 percent and the 9.5-in. slab to 50 percent, these corrections do not improve significantly the situation for other loading positions. It is believed that these discrepancies are due to the curling of slabs because the experimental data were taken during the early morning hours when the corners and edges of the slab were curled upward and part of the slab is not in contact with the subgrade. Even if this curling effect were not considered, the agreement in stress distribution between theoretical and experimental data is certainly surprising and clearly indicates the applicability of the method for predicting the stresses in concrete pavements.

A k-value of 900 lb/in.^{3} seems rather large and falls outside the range recommended for use in practical design. However, if the concrete has a Young's modulus of 6.25×10^6 psi, as determined at the AASHO Road Test, the only way to make the theoretical and experimental results comparable is by the use of a large k-value. The solutions presented are certainly correct as can be proved by using the influence chart shown in Figure 5 for loading position 4, which is quite far away from the joint. For example, let us work with the 9.5-in. pavement. For a k-value of 900 lb/in.^{3}, the maximum stress on pavement edge determined from the influence chart is 183 psi, which checks with the 182 psi obtained by the finite-element method, even though the former assumes a Poisson's ratio of 0.15 and the latter 0.28. If a k-value of 47.5 lb/in.^{3}, as suggested by Vesic and Saxena (9), is used, the stress obtained from the influence chart is 332 psi, which is much greater than the observed stress of 181 psi. It appears that

Table 1. Comparison of moments.

Tire Number	Moment (in.-lb) By Influence Chart	By Finite-Element Method	Percentage of Discrepancy
2	1,831	1,861	+1.6
3	-202	-204	+1.0
4	-235	-260	+10.6
6	420	393	-6.4
7	-33	-20	-39.4
8	-67	-73	+9.0

Figure 6. Comparison of theoretical and experimental stresses at pavement edge.

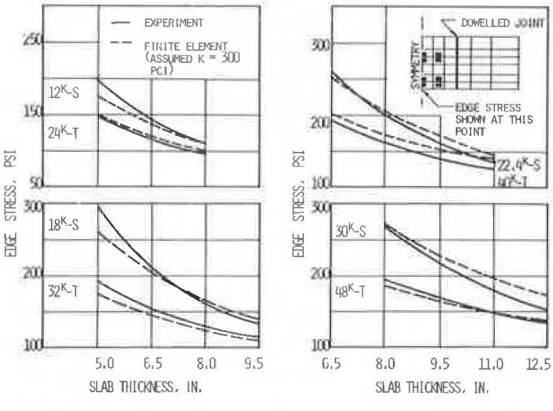

Figure 7. Loading positions and finite-element grid.

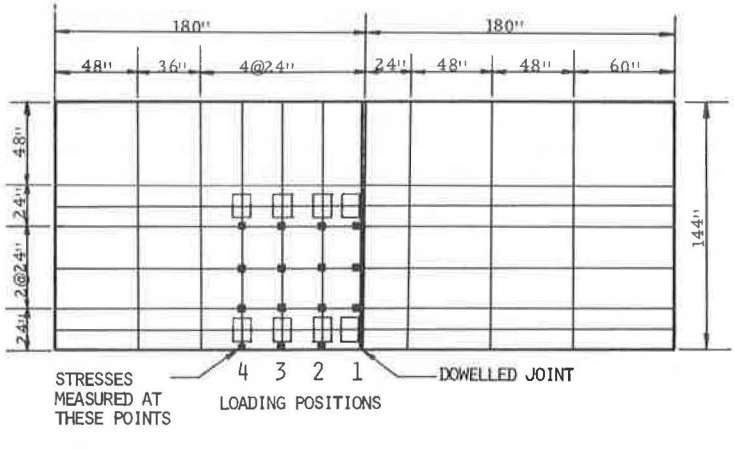

under a vibratory load the use of 900 lb/in.^{3} for k-value is more reasonable than that of 47.5 lb/in.^{3}. However, it should be reiterated that the exact value of k is not important; the most important question is whether a k-value can be found that gives a good prediction on the stress distribution for various axle loads and slab thicknesses. This study clearly shows that such a k-value does exist and that the finite-element method presented here gives a reasonable prediction of the stress distribution in concrete pavements.

IMPLICATIONS FOR PAVEMENT DESIGN

The computer program developed in this study is very effective in solving stresses in concrete pavements. Results accurate enough for design purposes can be obtained even if a coarse network is used. For the system shown in Figure 3, it took only 20 sec of compiling time and 1 min of execution time to calculate the stresses at various nodal points under 16 different loading positions. By running the program on some typical cases, interesting conclusions, which may or may not be in agreement with current design concepts, were obtained.

Critical Loading for Airport Pavements

The design method for airport pavements as developed by PCA (6) is based on interior loads because it is considered that the most critical stress in a slab occurs when the load is in the interior of the slab rather than at the doweled joint. The computer program can be used to determine how much greater the stress at the interior will be as compared to the stress at the joint. For example let us use a 12.5-in. slab with a Young's modulus of 4×10^6 psi, a Poisson's ratio of 0.15, a subgrade k-value of 100 lb/in.^{3}, and a single wheel load of 40,000 lb applied over a rectangular area 11.74 by 17.04 in. If the load is applied at the center of a 15- by 15-ft slab with a given efficiency of load transfer at two opposite joints, the maximum interior stress will be 332 psi for 100 percent efficiency, 331 psi for 80 percent efficiency, and 320 psi for 0 efficiency. If the load is applied adjacent to the joint midway between two corners, the maximum stress at the joint will be 289 psi for 100 percent efficiency, 323 psi for 80 percent efficiency, and 600 psi for 0 efficiency. This indicates that the efficiency of load transfer has relatively small effect on the interior stress but a large effect on the stress at the joint. The stress at the joint can be kept smaller than that in the interior by installing a very effective load transfer device, (e.g., one more than 70 percent efficient). Teller and Sutherland (14) investigated the efficiency of various joints and found that in many cases the deflections at the joint for both the loaded and the unloaded slabs were equal, thus indicating that this efficiency could be easily obtained in the field.

Critical Loading for Highway Pavements

In view of the fact that, on modern pavements with 12-ft lanes, traffic has moved inward from outside corners and edges, PCA (5, 12) has discontinued the use of the corner formula for pavement design. With the outer face of the exterior tire mostly about 2 ft from the pavement edge, PCA indicated that the most critical loading position was at the transverse joint, and design curves based on the influence charts shown in Figure 5 were developed for determining the maximum stress at the joint. PCA's conclusion was based on two simplifying assumptions: There is no load transfer at the joint, and the load is applied far from the corners, so that the influence chart for an infinite slab applies. Both assumptions yield a stress at the joint, as determined by the PCA method, considerably greater than the actual stress. The negligence of load transfer for highway pavements is inconsistent with PCA design method for airport pavements, which relies heavily on the load transfer at the joint. The following example illustrates the effect of loading positions on the critical stress.

Let us use a concrete pavement having a thickness of 7 in., a Young's modulus of 4×10^6 psi, a Poisson's ratio of 0.15, and a subgrade k-value of 100 lb/in.^{3}. The pavement is subjected to a typical 18-kip single-axle load and a 36-kip tandem-axle load.

According to PCA (12), the most critical stress occurs when the load is at the transverse joint and is 285 psi for single axle and 336 psi for tandem axle. The pavement was subjected to finite-element analysis using the finite-element network shown in Figure 3. The center of the outer dual is 34 in. from the edge, or the face of the tire 2 ft from the edge. The load moves from left to right, and the maximum major and minor principal stresses, when the single axle (or the front axle of the tandem) is at various distances from the joint, are given in Table 2. The efficiencies of load transfer for the two extreme cases of 0 and 100 percent are assumed. It can be seen that, if no load transfer is provided, the most critical stress takes place when the load is nearest the transverse joint. However, the computed stresses of 221 psi for single axle and 230 psi for tandem axle are much smaller than the 285 and 336 psi computed by PCA, as a direct result of PCA's assumption that the slab is infinitely wide and the load is far from the corner. If complete load transfer is provided, the most critical stress occurs when the load is at a considerable distance from the joint. The critical stresses of 225 psi for single axle and 207 psi for tandem axle are also smaller than those by PCA. The smaller stress under the tandem-axle load is caused by the compensative effect of the two axles. The actual stress of only 104 psi at the joint with 100 percent load transfer under the 18-kip single-axle load is far below the 285 psi by PCA.

The preceding discussion should not be interpreted that the current PCA method gives a design that is too conservative because there are other factors that may cause an increase in stress. The exterior tire may be closer to the pavement edge than the 2 ft assumed in the finite-element analysis. Pumping of the subgrade, blowing of the subbase, and curling of the slab may result in the loss of subgrade contact. It will therefore be interesting to investigate these extreme cases and compare the critical stresses with those by PCA.

Loss of Subgrade Contact

It is well known that concrete slabs are curled upward in early morning when the top of the slab is colder than the bottom, thus resulting in unsupported edges and corners. Loss of subgrade support may also be caused by pumping and blowing. If the conditions of contact at various points are known, the stresses in the slabs can be determined by the finite-element analysis using a method of successive approximations. However, for a qualitative comparison of critical stresses between full and partial contact, it is assumed that the two rows of nodes (Fig. 3), one on and the other next to the pavement edge, are not in contact with the subgrade; therefore, the reactive pressure at these points can be neglected.

Table 3 gives the effect of subgrade contact on critical stresses in the extreme case when the outer face of the tire is adjacent to the pavement edge. It was found that the maximum major principal stress always occurs when the load is far from the joint, whereas the maximum minor principal stress always occurs when the load is at the joint. Note that, when the pavement and subgrade are in full contact, the maximum major principal stress is always greater than the maximum minor principal stress, indicating that the critical stress occurs when the load is far from the joint. The critical stress of 391 psi for single axle is much greater than the 285 psi by PCA, whereas that of 343 psi for tandem axle is only slightly greater than the 336 psi by PCA. When the outside edge of pavement is not in contact with the subgrade, the critical stresses increase considerably, especially the minor principal stresses; however, the most critical stress still occurs when the load is far from the joint, except in the case of the tandem-axle load when no load transfer is provided.

It can be seen that, when the outer tire is nearest the pavement edge and the edge is not in contact with the subgrade, the critical stresses obtained by the finite-element method are much greater than those by PCA. Because most traffic does not travel near to the edge, except on modern freeways in urban areas, the actual stress should be much smaller. To avoid the difficulty involved in evaluating the loss of subgrade contact, it is suggested that full contact be assumed in the design of pavements. However, the assumed position of the outer tire should vary with the lane width and the type of highways and be closer to the pavement edge than anticipated to take into account the additional stress due to curling and the loss of subgrade contact.

Figure 8. Comparison of theoretical and experimental distribution of major and minor principal stresses.

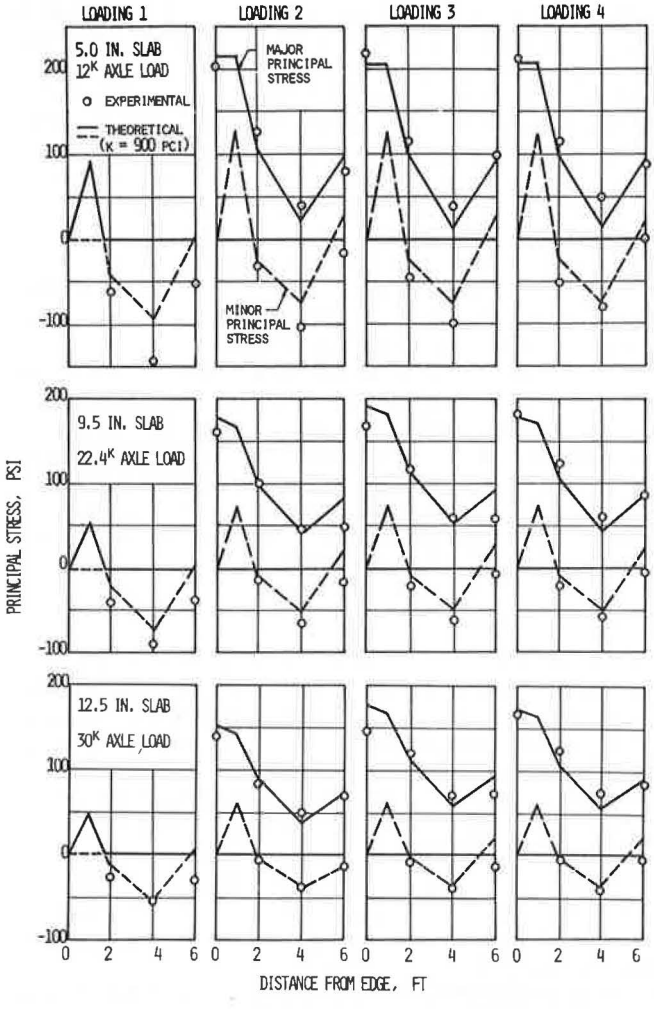

Table 2. Critical stresses with outer tire 2 ft from edge.

Distance From Axle to Joint (in.)	18-Kip Single Axle				36-Kip Tandem Axle			
	0 Percent Load Transfer		100 Percent Load Transfer		0 Percent Load Transfer		100 Percent Load Transfer	
	Major (psi)	Minor (psi)	Major (psi)	Minor (psi)	Major (psi)	Minor (psi)	Major (psi)	Minor (psi)
79	220	-27	218	-29	189	-21	192	-26
54.5	211	-37	225[a]	-40	198	-21	207[a]	-23
30	150	-54	200	-37	166	-57	197	-59
5.7	221[a]	-152	104	-66	230[a]	-121	160	-54

[a]Most critical stress for each case.

Table 3. Effect of subgrade contact on critical stresses.

Condition of Contact	18-Kip Single Axle				36-Kip Tandem Axle			
	0 Percent Load Transfer		100 Percent Load Transfer		0 Percent Load Transfer		100 Percent Load Transfer	
	Major (psi)	Minor (psi)	Major (psi)	Minor (psi)	Major (psi)	Minor (psi)	Major (psi)	Minor (psi)
Full	376	-237	391	-104	314	-262	343	-127
Partial	450	-413	501	-204	406	-634	508	-310

In view of the facts that load transfer is always provided in pavements and the critical stress always occurs when the load is far from the transverse joint, it is suggested that the edge stress, instead of the stress at the joint as recommended by PCA, be used for design of highway pavements. It is recognized that the old PCA design method based on the corner loading was used for a long time and gave reliable results. The current PCA method generally yields a critical stress comparable to that in the old method and therefore should also ensure a satisfactory service. However, the authors do not agree with PCA on the way in which this critical stress is obtained. When the outer face of the exterior tire is 2 ft from the pavement edge, designated by PCA as case I loading, the critical loading position is definitely not at the doweled joint but at a considerable distance from the joint. It is believed that comparable results could be obtained from the edge stress by placing the exterior tire a few inches from the edge. The use of edge stress for highway pavement design has the following advantages: It is in line with the use of interior stress for airport design because both assume that sufficient load transfer has reduced the stress at the joint to make it no longer critical; the edge stress is not affected significantly by the size of slab and the efficiency of load transfer at the transverse joint, so the influence chart developed by Pickett and Ray can still be used; lane width can be taken as a factor of design by specifying different distances between the outer tire and the pavement edge for various lane widths; and loss of subgrade contact at the pavement edge has less effect on edge stress than on stress at the joint, and the additional resultant edge stress can be more easily estimated.

CONCLUSIONS

A finite-element method programmed for a high-speed computer was developed for determining the stresses in concrete slabs with load transfer at the joints. The method is very efficient and checks closely with Westergaard's theoretical solutions as well as with those obtained from Pickett and Ray's influence chart. By the judicious selection of an appropriate k-value, it was found that the finite-element solutions also checked reasonably well with the stresses measured experimentally at the AASHO Road Test, thus verifying the validity of the method. Although a single k-value was used to compute the stresses for various slab thicknesses and axle loads, a comparison of the dynamic edge stresses clearly shows that under a given axle load the subgrade k-value should increase with the increase in slab thickness. This can be explained from the nonlinear behavior of subgrade soils because the thicker the slab is, the less the pressure on the subgrade is and the stiffer the soils are.

Numerical data are presented to illustrate the effect of loading position, efficiency of load transfer, and loss of subgrade contact on critical stresses. An analysis of the data results in the following conclusions:

1. In airport pavements, the most critical stress occurs when the load is in the interior of the slab. Stress due to loading at the joint can be kept smaller than the critical stress in the interior by use of load transfer devices having an efficiency of more than 70 percent at the joints.
2. In highway pavements with the outer face of the tire 2 ft from the edge, the most critical stress occurs when the load is at the transverse joint if no load transfer is provided, but at a considerable distance from the joint if load transfer is provided.
3. In highway pavements with the outer face of the tire adjacent to the edge and the slab in full contact with the subgrade, the most critical stress occurs when the load is at a considerable distance from the joint, regardless of the efficiency of load transfer.
4. In highway pavements with the outer tire adjacent to the edge and part of the slab not in contact with the subgrade, the most critical stress may occur at the transverse joint if no load transfer is provided. However, if load transfer is provided, the most critical stress occurs when the load is at a considerable distance from the joint.
5. In view of the fact that load transfer is always provided in pavements and the critical stress always occurs when the load is far from the transverse joint, it is suggested that the edge stress, instead of the stress at the joint as recommended by PCA, be used for the design of highway pavements.

ACKNOWLEDGMENTS

The study reported here was part of a faculty research program sponsored by the Department of Civil Engineering, University of Kentucky. The support given by the University of Kentucky Computing Center for use of an IBM 360 computer is appreciated.

REFERENCES

1. Westergaard, H. M. Stresses in Concrete Pavements Computed by Theoretical Analysis. Public Roads, April 1926, pp. 25-35.
2. Westergaard, H. M. Stress in Concrete Runways of Airports. HRB Proc., Vol. 19, 1939, pp. 197-202.
3. Westergaard, H. M. New Formulas for Stresses in Concrete Pavements of Airfields. Trans. ASCE, Vol. 113, 1948, pp. 425-444.
4. Pickett, G., and Ray, G. K. Influence Charts for Concrete Pavements. Trans. ASCE, Vol. 116, 1951, pp. 49-73.
5. Thickness Design for Concrete Pavements. Concrete Information, Portland Cement Assn., 1966.
6. Design of Concrete Airport Pavements. Portland Cement Assn., 1955.
7. Concrete Pavement Design for Roads and Streets Carrying All Classes of Traffic. Portland Cement Assn., 1951.
8. Hudson, W. R., and Matlock, H. Analysis of Discontinuous Orthotropic Pavement Slabs Subjected to Combined Loads. Highway Research Record 131, 1966, pp. 1-48.
9. Vesic, A. S., and Saxena, K. Analysis of Structural Behavior of AASHO Road Test Rigid Pavements. NCHRP Rept. 97, 1970.
10. Zienkiewicz, O. C., and Cheung, Y. K. The Finite Element Method in Structural and Continuum Mechanics. McGraw-Hill, 1967.
11. Cheung, Y. K., and Zienkiewicz, O. C. Plates and Tanks on Elastic Foundations: An Application of Finite Element Method. Internat. Jour. of Solids and Structures, Vol. 1, 1965, pp. 451-461.
12. Load Stresses at Pavement Edge, A Supplement to Thickness Design for Concrete Pavements. Concrete Information, Portland Cement Assn., 1969.
13. The AASHO Road Test: Report 5—Pavement Research. HRB Spec. Rept. 61E, 1962.
14. Teller, L. W., and Sutherland, E. C. The Structural Design of Concrete Pavements: Part 4—A Study of the Structural Action of Several Types of Transverse and Longitudinal Joint Designs. Public Roads, Vol. 17, 1936, pp. 143-171.

CORRELATION OF KENTUCKY CBR'S AND SOIL SUPPORT VALUES

Tommy C. Hopkins and Robert C. Deen, Kentucky Department of Highways

Several ASTM and Kentucky CBR tests were performed at different molding moisture contents and compactive energies on the AASHO embankment soil, four representative Kentucky soils, and one soil from Ohio. These data were compared to CBR data previously reported. For CBR's ranging from about 4 to 12, a relation was developed between Kentucky and ASTM CBR's. Within this range, Kentucky and ASTM CBR's are approximately equal. Molding specimens under the static pressure of 2,000 psi (as used in the Kentucky CBR procedure) produced specimens with initial dry densities that averaged about 6 percent higher than those obtained by AASHO T 99-57. CBR's and axial swell values were also higher. For soil specimens molded at the same initial dry density, CBR's of statically compacted specimens are distinctively lower than those observed for dynamically compacted specimens. For relatively small decreases in initial dry densities, there were very large decreases in CBR's. Three different correlations between Kentucky CBR's and the AASHO Road Test soil support values were developed. The first relation was made by assuming a logarithmic scale between Kentucky CBR's of 5.2 and 100, which corresponded to values on the soil support scale of 3 and 10 respectively. The Kentucky CBR of 5.2 was determined by performing tests on the AASHO road subgrade soils. For practical purposes, the AASHO Road Test crushed-stone base material was assumed to be a "100 percent CBR material" (this assumption was based on CBR data previously reported). The second correlation was obtained by assuming a logarithmic scale between Kentucky CBR's of 5.2 and 90, corresponding to values on the soil support scale of 3 and 10 respectively. The third relation was constructed through computations using the Kentucky flexible pavement design curves and the AASHO design chart ($P_t = 2.5$).

•SUBGRADE strengths of the upper 3 ft of the embankment soils at the AASHO Road Test were expressed in terms of a dimensionless, hypothetical soil support parameter (1). The AASHO Road Test sections were constructed on only one soil, giving one point on the soil support scale. This point was assigned a value of 3. A second point was established on the soil support scale from observations and analysis of the performance of various sections having crushed-stone bases sufficiently thick to make the effect of the subgrade insignificant. This second point on the soil support scale was established and arbitrarily assigned a value of 10. A linear scale was assumed between the soil support values of 3 and 10 and extended to 1.

The AASHO Road Test scheme did not specify a test method for determining soil support capacity of a given soil. However, some means to correlate the hypothetical soil support values (S) and strength values resulting from a selected test method would be desirable. Correlation of Kentucky CBR's and soil support values was the main con-

Publication of this paper sponsored by Committee on Flexible Pavement Design.

cern of this study. Such correlation would provide a basis for comparing flexible pavement designs from the AASHO Road Test with those based on Kentucky design criteria. Another intent was to compare CBR data reported by Shook and Fang (2) with Kentucky CBR data and CBR data obtained using other test methods so as to provide a means for making closer comparisons among various design criteria employing the CBR parameter.

Correlation curves C and D in Appendix A of the AASHO guide (1), which relate Kentucky CBR values and soil support values, are misleading because the conditions outlined for molding the CBR specimens are not the same as specified in the Kentucky CBR test procedure. The Kentucky CBR specimen is molded using static rather than dynamic compaction, and the CBR specimen is soaked until swell virtually ceases. Seed and Chan (3) presented data that indicated that the method—static, dynamic, or kneading—of compaction yields soil specimens with differing soil structures. When comparing samples prepared by static compaction and kneading compaction, there was a marked difference in the stress-strain relations for samples compacted "wet of optimum." Data showing the effect, if any, of different soil structures on CBR strengths were not available.

KENTUCKY CBR TEST PROCEDURE

Currently, there is not an AASHO or ASTM standard CBR test procedure involving static compaction. Static compaction, however, is suggested as an alternate compaction method for preparing test specimens for permeability, consolidation, volume-change expansion pressure, and triaxial compression tests. Static compaction does influence the structure of soils; i.e., the physical properties of specimens prepared with static compaction differ from those of specimens compacted dynamically or by types of kneading methods (4).

The CBR test procedure used in Kentucky was modeled by Baker and Drake (5) after a procedure suggested by Stanton (6). Significant changes made by Baker and Drake consisted of soaking the specimen until axial swell virtually ceases, molding the specimen to "Proctor conditions" using a 2,000-psi pressure, correcting the CBR load-deflection curve, and loading a 5-lb surcharge weight on the specimen at the start of penetration.

Most agencies specify a 4-day soaking period (2). Chamblin (7) noted in a study of the effect of soaking period on CBR strengths that, for a 4-day soaking period, there was a large decrease in CBR; for longer soaking periods, there was only a slight further decrease in CBR. Nevertheless, permitting swell to virtually cease does ensure an "extremely critical condition," comparable probably to the worst situation in the field.

In the Kentucky CBR procedure, the specimens are intended to conform to conditions of AASHO T 99-57, method A (compactive energy of 12,375 ft-lb/ft^3). However, observations (8) and data presented in this report suggest that the compactive effort of 2,000 psi is apparently greater than the compactive effort of AASHO T 99-57, method A. Consequently, the molded specimen has a higher density and a moisture content that is at or near optimum moisture content of AASHO T 99-57, method A.

During soaking, Stanton's method (6) specified a 10-lb surcharge weight; in the Kentucky procedure, a 17.5-lb surcharge weight is used. In the Kentucky method, a 5-lb annular weight is used during penetration to center the piston; in Stanton's method, such weight was used only for the case of granular materials.

Another feature added to the Kentucky method was the correction of the load-penetration curve. Because of irregularities in the surface or in distribution of moisture near the surface, it is usually necessary to plot load versus depth of penetration (ordinate and abscissa respectively). If necessary, the abscissa zero point is corrected for any concave-upward tendency in the curve near the origin.

It is customary in most CBR test procedures to select the CBR value at either 0.1- or 0.2-in. deflection. In the Kentucky method, the minimum CBR value is chosen from

CBR's occurring at 0.1-, 0.2-, 0.3-, 0.4-, and 0.5-in. penetration. Baker and Drake (5) noted in developing pavement thickness design curves that the minimum field and laboratory CBR's afforded the best correlation with pavement performance.

PREPARATION OF CBR SPECIMENS

Characteristics of the different methods used in molding CBR specimens for the study reported here are given in Table 1. Method 1 (AASHO T 99-61, method A) was used to determine the moisture-density relations of each of the soils investigated. These relations were used in preparing the Kentucky CBR specimens, method 5. Basically, method 1 consisted of compacting three equal layers of soil in a 4-in. mold, each layer receiving 25 blows from a 5.5-lb hammer dropped 12 in.

CBR specimens for testing under ASTM D1883-61T were prepared in three different ways. Method 2 (AASHO T 99-61, method B) involved compacting three equal layers of soil in a 6-in. mold with each layer receiving 56 blows from a 5.5-lb hammer dropped 12 in. Method 3 was the same as method 2, except that the height of the sample was 5 in. instead of 4.59 in. Method 4 (AASHO T 180-57, method B) consisted of compacting five equal layers of soil in a 6-in. mold with each layer receiving 56 blows from a 10-lb hammer dropped 18 in.

CBR specimens for testing under the Kentucky CBR procedure were prepared in two different ways. Method 5 involved compressing the total sample under a static pressure of 2,000 psi. Method 5 differed slightly from the Kentucky CBR testing routine. Normally, values of optimum moisture content and maximum dry density of method 1 are used to calculate the amount of material for specimen preparation. In this study, however, the moisture content was varied over a wide range of values. Method 6 was basically the same as method 5; however, the specimens were not molded under a static load of 2,000 psi but were molded to a predetermined height (volume).

LABORATORY RESULTS

Soil samples were secured from stockpiled embankment material located at the AASHO Road Test site, four different locations in Kentucky, and one location in Ohio. The Kentucky samples were representative of a range of Kentucky soils. A portion of each sample was submitted to a routine laboratory testing program consisting of specific gravity, Atterberg limits, grain size analysis, and standard compaction (method 1). All tests were performed in accordance with AASHO standard test methods. A summary of classification data for the six soils is given in Table 2. Included in the table are mean values reported by Shook and Fang (2) for the AASHO Road Test subgrade soil.

From 8 to 14 Kentucky CBR tests were performed on each of the soil samples from the six locations in accordance with method 5. However, moisture contents of the samples were varied in order to obtain a moisture content-dry density curve. A total of 67 Kentucky CBR tests were performed. A total of 56 CBR tests were performed on each of the six soil samples in accordance with ASTM D1883-61T. The number of tests performed on each of the six soils ranged from 8 to 29. The specimens were molded according to method 2. An additional 20 CBR tests were performed on specimens compacted according to method 3. Dry density-, CBR-, and axial swell-molding moisture content curves for the samples from the six locations are shown in Figures 1 through 6.

Five ASTM CBR tests were performed on the AASHO Road Test sample compacted in accordance with method 4 (Figs. 1 and 10). Four Kentucky CBR tests were performed on the Fayette County soil using a static compactive effort other than 2,000 psi (method 6). The intent of these tests was to duplicate the moisture content-dry density curve obtained using method 2 and to observe the resulting effects on CBR's. These data are shown in Figure 3. Also shown in Figure 1 are the results of two ASTM CBR tests performed on specimens compacted by method 4, with the exception that the compactive energies were 11,992 and 24,992 ft-lb/ft^3.

General relations between ASTM CBR's and Kentucky CBR's determined for various molding conditions are shown in Figure 7.

Table 1. Compaction methods used to prepare CBR specimens.

Item	AASHO T 99-61, ASTM D 698-66T			AASHO T 180-51, ASTM D 1557-66T	Standard Kentucky CBR	Altered Kentucky CBR
	Method A Method 1	Method B Method 2	Method B Method 3	Method B Method 4	Method 5	Method 6
Mold						
Diameter, in.	4	6	6	6	6	6
Height, in.	4.59	4.59	5.00	4.59	Variable	Predetermined
Volume, ft^3	1/30	1/13.33	1/12.23	1/13.33	Variable	Predetermined
Rammer						
Weight, lb	5.5	5.5	5.5	10.0		
Free drop, in.	12.0	12.0	12.0	18.0		
Face diameter, in.	2.0	2.0	2.0	2.0		
Layer						
Total number	3	3	3	5	1	1
Surface area, $in.^2$	12.57	28.27	28.27	28.27	28.27	28.27
Compacted thickness, in.	1.7	1.7	1.7	1.0	Variable	Predetermined
Compaction effort						
Blows per layer	25	56	56	56	2,000 psi	Variable
Energy, $ft\text{-}lb/ft^3$	12,375	12,317	11,301	55,986	Static compression	Static compression
Material						
Maximum size	No. 4	No. 4	No. 4	No. 4	3/4 in.	3/4 in.
Correction for oversize	No	No	No	No	Yes	Yes

Table 2. Summary of classification data.

Soil Sample	Classification			Atterberg Limits		Moisture-Density Relation (AASHO T 99-61)		Grain Size Distribution (percent finer)							Specific Gravity
	AASHO	Unified	Textural	Liquid Limit (percent)	Plasticity Index (percent)	Optimum Moisture Content (percent)	Maximum Dry Density (lb/ft^3)	No. 4	No. 40	No. 200	0.05 mm	0.02 mm	0.005 mm	0.002 mm	
AASHO Road Test[a]	A-6(9)	CL	Clay	27.7	12.6	13.5	119.2	96.6	88.6	75.5	72.3	61.9	40.3	27.6	2.72
AASHO Road Test (Kentucky)	A-6(11)	CL	Clay	32.5	15.7	14.0	117.0	97.0	90.0	79.5	76.5	65.5	45.0	32.0	2.68
Ohio	A-6(8)	CL	Clay loam	30.0	12.0	16.8	111.7	95.0	86.0	71.0	58.0	45.0	30.0	21.0	2.71
Fayette County (Maury series)	A-6(12)	CL	Clay loam	34.5	13.5	19.8	100.5	100.0	94.0	79.0	76.0	61.0	30.0	20.0	2.69
Clark County (Eden series)	A-6(13)	CL	Silty clay	36.5	12.0	21.5	98.6	100.0	98.0	91.0	88.0	75.0	44.0	31.0	2.71
Fulton County (Calloway series)	A-4(8)	ML	Silt loam	26.1	1.0	16.6	107.3	100.0	98.0	78.0	70.0	40.0	17.0	13.0	2.66
Adair County (Baxter series)	A-7-5(19)	CH	Clay	61.0	34.0	24.0	96.2	92.3	89.3	87.6	82.0	74.0	58.0	50.0	2.77

[a]Mean values (2).

Figure 1. CBR data, AASHO Road Test soil sample.

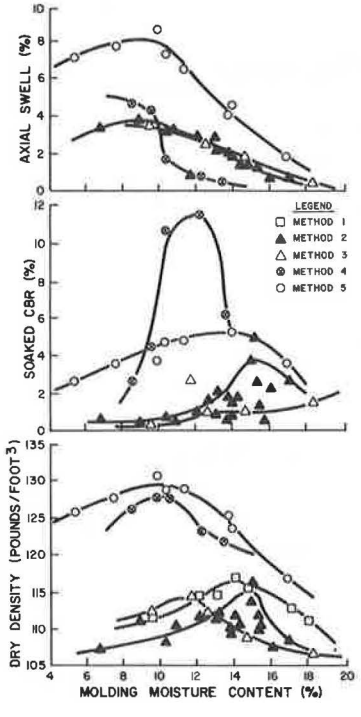

Figure 2. CBR data, Ohio soil sample.

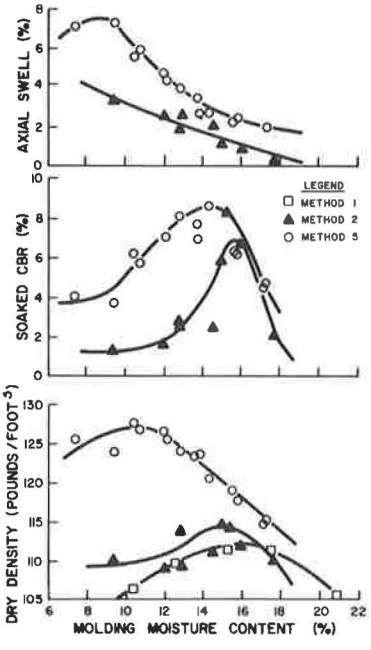

Figure 3. CBR data, Fayette County soil sample.

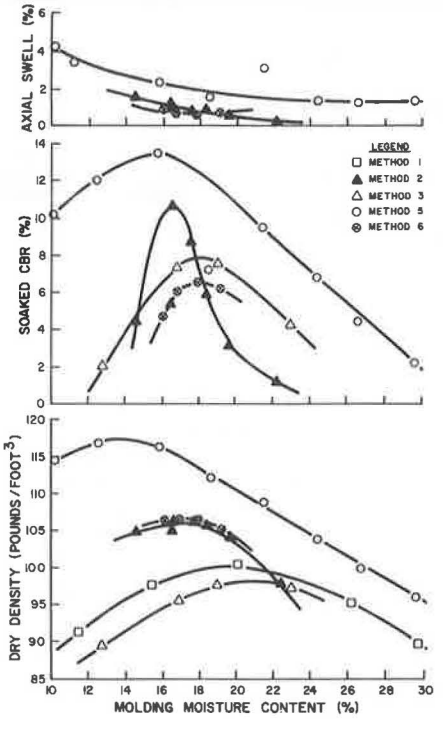

Figure 4. CBR data, Clark County soil sample.

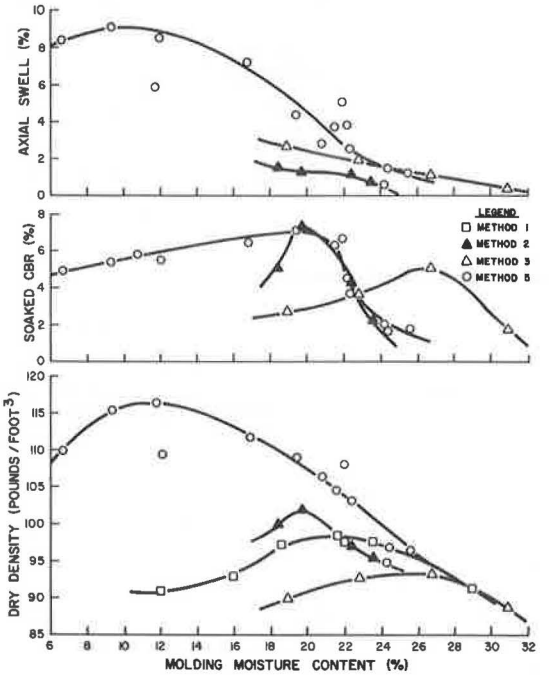

Figure 5. CBR data, Fulton County soil sample.

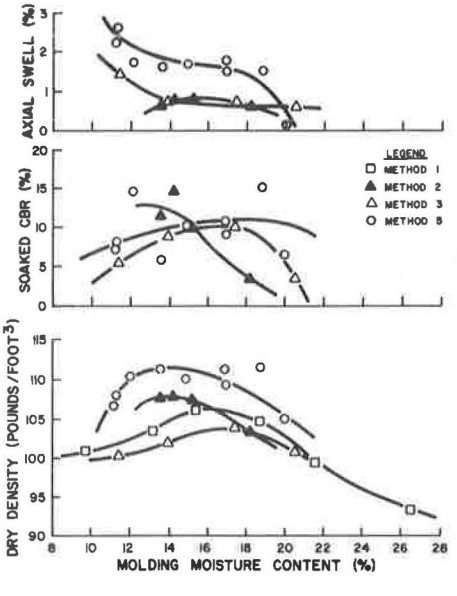

Figure 6. CBR data, Adair County soil sample.

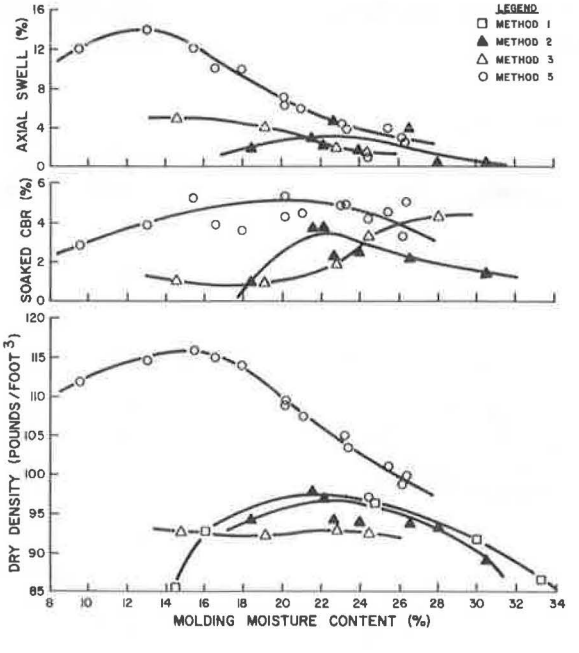

AASHO ROAD TEST CBR DATA

Twenty-eight agencies reported (2) CBR data on the embankment soil at the AASHO Road Test. Most reported only one CBR value. Seven agencies reported more than one CBR value, usually for varying conditions of compactive effort, moisture content, and dry density.

For conditions of similar testing, various plots of the reported CBR data (2) and data reported here were made. These data are shown and compared in Figures 8 through 12.

Seven agencies reported (2) CBR values for specimens molded under static compaction in accordance with Stanton's suggested CBR test procedure, but the static pressure of 2,000 psi was not always used. These data and the dry density-, CBR-, and swell-moisture content curves from Figure 1 are compared in Figure 8. The CBR test procedures of the Utah (8), Oklahoma (9), and Missouri agencies are practically the same as Kentucky's method, although it is not exactly evident which method of compaction is used to determine optimum moisture and maximum dry density; presumably each method refers to methods 1 or 2 because "standard compaction" is commonly referred to in each of the procedures except Oklahoma's. Each of these agencies compact their CBR specimens under a static pressure of 2,000 psi. Note in Figure 8 that the reported Utah CBR value of 5.0 fits the Kentucky data; Oklahoma's CBR value is close, but Missouri's differs significantly, mainly because of the relatively low dry density. In a later report (8), Utah correlated a dynamic CBR of 2.8 with a soil support of 3. In the Illinois CBR procedure, the specimen is molded statically to a predetermined optimum moisture content, and maximum dry density is derived in accordance with methods 1 or 2. Illinois's reported CBR of 4 differs from the Kentucky value, although the dry density value falls near the Kentucky moisture content-dry density curve. This agency in a later report (10) showed a correlation between its CBR and soil support of 3. Alabama's CBR procedure specifies molding of at least three specimens at different moisture contents under a static load of 2,000 psi to determine three points on the moisture content-dry density curve. Optimum moisture content and maximum dry density are determined by using this curve. A CBR test is performed on a specimen molded at these conditions. As shown in Figure 8, the reported CBR of 4.5 is in fair agreement with the Kentucky value, although Alabama's dry density is higher. Information on New Jersey's CBR testing method was not available.

In Figure 9, CBR data for specimens compacted in accordance with method 2, reported by Shook and Fang (2), and data shown in Figure 1 are compared. Although there is some scatter of the data, notable trends are evident.

Other CBR data reported by Shook and Fang (2) and data given here for specimens compacted in accordance with method 4 are shown in Figures 10 through 12. In Figures 11 and 12, the CBR data are for specimens molded with compactive energies of 24,992 and 11,992 ft-lb/ft^3. In Figure 10, the data are for specimens molded with 55,986 ft-lb/ft^3 of energy. Again, notable trends are apparent.

In Figure 13, relations between soaked CBR's and different compactive energies are presented for the AASHO embankment soil. Note that a 5 percent decrease in dry density produces a relatively large decrease in CBR's. Even a 2 percent decrease in dry density decreases the CBR's from 20 to 50 percent. The CBR values for the 98 and 95 percent compaction curves were on the "wet side of optimum moisture content." Generally, the "dry-side" CBR values could not be read from Figures 10 through 12.

KENTUCKY CBR-SOIL SUPPORT CORRELATION CURVES

From the Kentucky CBR tests performed on soil samples obtained from a stockpile at the AASHO Road Test, a Kentucky CBR of 5.2 was found to correspond to a soil support value of 3.0. Crushed-stone base material at the AASHO Road Test site having a soil support value of 10.0 was not available for determining a Kentucky CBR; consequently, a value had to be established by other means. In reviewing CBR data reported by Shook and Fang (2), indications were that the crushed-stone base material could be considered a "100 percent CBR material" for practical purposes. States such as Alabama, Illinois, Oklahoma, and Utah, which used static compaction in preparing test

Figure 7. Kentucky-ASTM CBR curves.

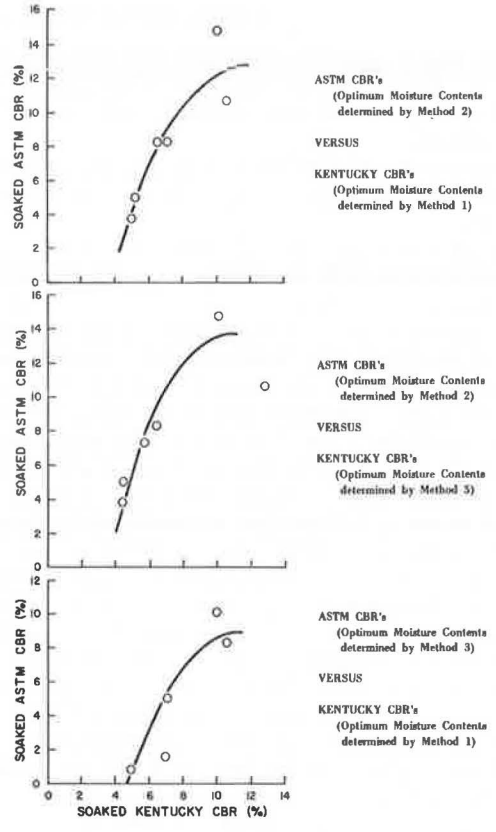

Figure 8. CBR data, AASHO soil sample (static compaction).

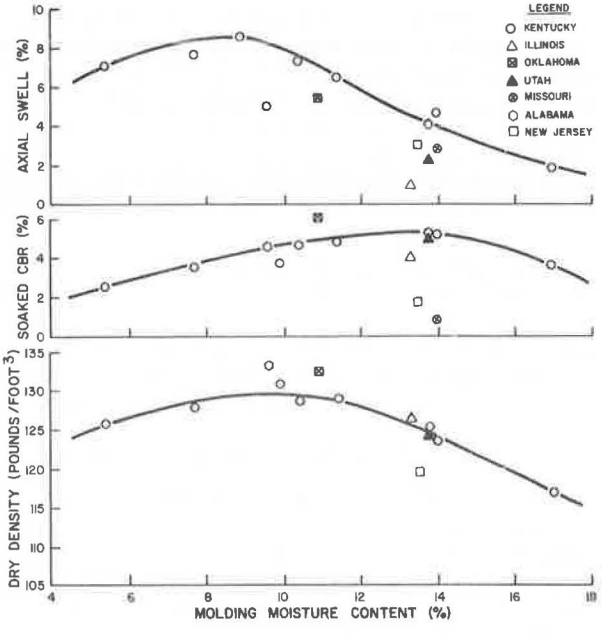

Figure 9. CBR data, AASHO soil sample (method 2).

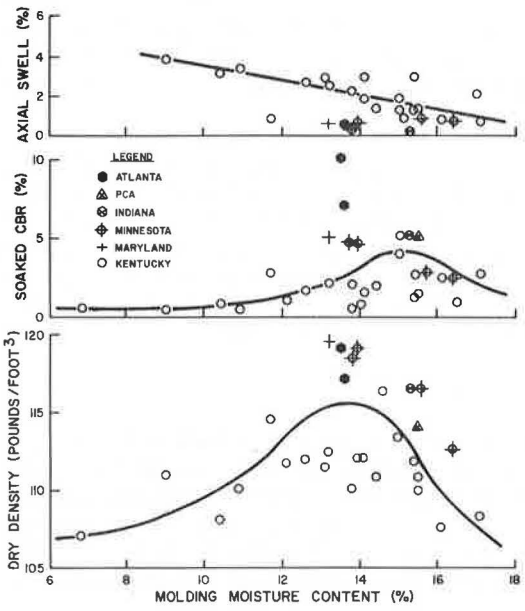

Figure 10. CBR data, AASHO soil sample (method 4).

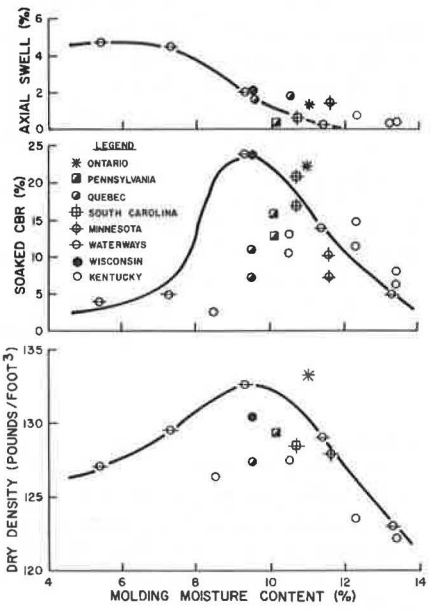

Figure 11. CBR data, AASHO soil sample (method 4, 25 blows per layer).

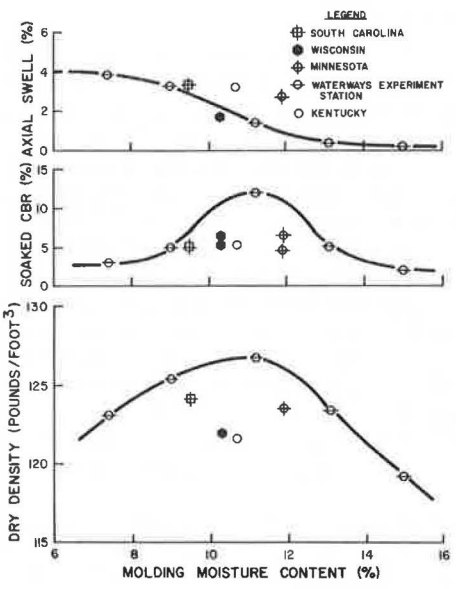

Figure 12. CBR data, AASHO soil sample (method 4, 12 blows per layer).

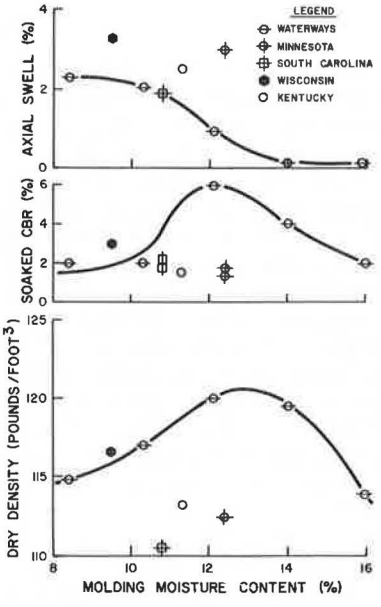

specimens, reported CBR values of 145, 202, 200, and 180 respectively although these states did not necessarily use these CBR's in their CBR-soil support correlation curves.

The Kentucky CBR-soil support correlation curve A (Fig. 14) was drawn by assuming a logarithmic scale between Kentucky CBR's of 5.2 and 100, corresponding to values on the soil support scale of 3 and 10 respectively. Correlation curve B was constructed by assuming a logarithmic scale between Kentucky CBR's of 5.2 and 90 and soil support values of 3 and 10 respectively.

Kentucky CBR-soil support correlation curve C (Fig. 14) was constructed in the following manner. A number of Kentucky CBR's covering the range from 3 to 90 were assumed. Equivalent axle loads (EAL's) were also assumed for a broad range of traffic conditions representing Kentucky design cruves IA through XII. The assumed EAL's were converted to AASHO-equivalent daily 18-kip axle load applications. The assumed Kentucky CBR's and EAL's and Kentucky flexible pavement design curves (11, 12) were used to obtain several combined pavement thicknesses. The structural numbers (SN) for the pavement systems obtained were calculated from the formula (1)

$$SN = a_1d_1 + a_2d_2$$

where a_1 and a_2 = coefficients of pavement components (equivalency factors), and d_1 and d_2 = thicknesses of bituminous surface course and base course. Values for a_1 of 0.36 and a_2 of 0.18 were used to compute the structural numbers. These values of a_1 and a_2 are currently used in pavement analyses in Kentucky. With these values of structural numbers and assumed EAL's, the AASHO design chart (serviceability index, P = 2.5) was used to determine values for the soil support corresponding to each assumed Kentucky CBR.

Comparisons of several trial pavement designs were made using the correlations shown in Figure 14, the AASHO design chart, and the Kentucky flexible pavement design charts. A range of traffic data and Kentucky CBR's were assumed for these designs. The results of these computations are given in Table 3.

SUMMARY OF FINDINGS

Classification data (Table 2) for the AASHO Road Test sample secured from a stockpile at the AASHO site were practically the same as mean classification data reported by Shook and Fang (2). Hence, the stockpile sample tested was essentially the same as that used in the embankment at the AASHO Road Test site. The two methods used to determine the Kentucky CBR of the AASHO Road Test soil, which has been assigned a soil support value of 3, produced similar results. From laboratory tests, a Kentucky CBR of 5.2 (Figs. 1 and 8) was obtained. Computations produced a value of 5.7 based on 1958 design curves (11) and 6.2 based on 1971 curves (12). For practical purposes, the AASHO Road Test crushed-stone base material, assigned a soil support value of 10, was assumed to be a 100 percent CBR material. Computed CBR values from the 1958 and 1971 curves for this material were 90 and about 80 respectively. Correlation curves were drawn using this CBR and soil support points of reference as shown in Figure 14. Based on CBR data reported by Shook and Fang and the data shown in Figures 10 through 12, CBR's of the AASHO soil for compactive energies of 55,986 (method 4), 24,992, and 11,992 (close to method 2 compactive energy) ft-lb/ft^3 appear to be 24, 12, and 6 respectively. For method 2, the CBR value (Fig. 9) of the AASHO soil appears to be about 5.

Pavement thicknesses determined from the AASHO design charts and the correlation curves (Fig. 14) relating Kentucky CBR's and soil support values and those determined from the 1958 and 1971 Kentucky design charts are reasonably similar (Table 3). Generally, the 1971 design curves yield slightly thicker pavements than those determined from either the 1958 Kentucky design curves or the AASHO charts and the correlation curves (A, B, and C).

Molding CBR specimens statically under a 2,000-psi pressure and in a manner specified in the Kentucky CBR procedure (method 5) produces CBR specimens with higher initial dry densities and higher CBR's and axial swell values than those specimens

Figure 13. CBR-compactive energy curves.

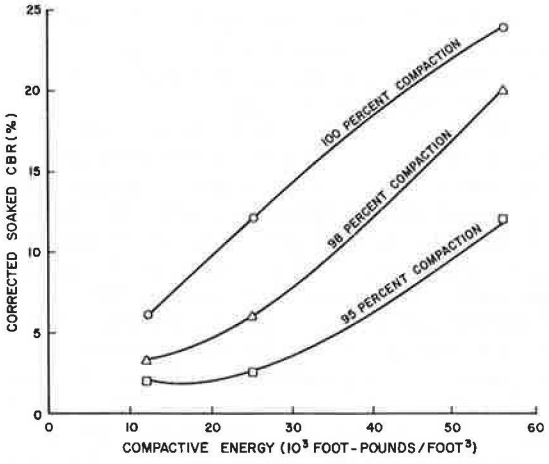

Figure 14. Soil support value-Kentucky CBR curves.

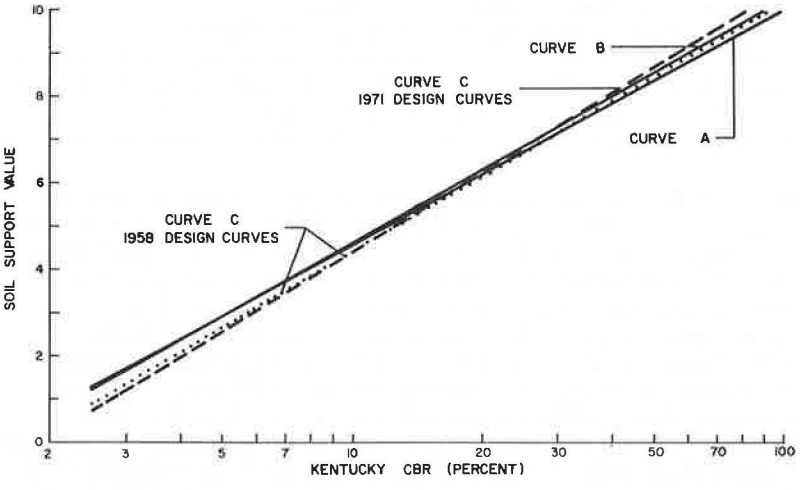

Table 3. Comparison of pavement thicknesses.

Assumed Traffic				Kentucky Designs[b]		AASHO Designs[d], Correlation Curves							
						A		B		C(1958)		C(1971)	
Traffic Curve	Kentucky EAL's	AASHO EAL's[a]	Assumed Kentucky CBR	1958	1971[c]	S	T	S	T	S	T	S	T
II	3.2×10^4	4.4	3	12.5	14.9	1.7	11.3	1.6	11.5	1.3	12.0	1.2	12.2
			5	9.8	12.6	2.9	9.6	2.9	9.6	2.6	10.0	2.5	10.1
			9	7.7	9.5	4.3	7.8	4.3	7.8	4.1	8.0	4.1	8.0
			15	6.5	6.6	5.5	6.4	5.6	6.3	5.4	6.5	5.5	6.4
VI	5.0×10^5	68	3	20.9	21.7	1.7	17.6	1.6	17.9	1.3	18.6	1.2	18.8
			5	17.3	19.0	2.9	15.1	2.9	15.1	2.6	15.7	2.5	15.8
			9	14.4	15.6	4.3	12.5	4.3	12.5	4.1	12.9	4.1	12.9
			15	12.4	12.7	5.5	10.6	5.6	10.5	5.4	10.8	5.5	10.6
X	8.0×10^6	1.1×10^3	3	27.2	29.2	1.7	26.9	1.6	27.1	1.3	28.1	1.2	28.2
			5	23.1	25.6	2.9	23.0	2.9	23.0	2.6	23.8	2.5	24.2
			9	19.5	22.0	4.3	19.5	4.3	19.5	4.1	19.9	4.1	19.9
			15	17.0	19.1	5.5	16.7	5.6	16.4	5.4	17.0	5.5	16.7
XII	3.2×10^7	4.4×10^3	3	29.8	36.1	1.7	32.7	1.6	33.1	1.3	34.4	1.2	34.6
			5	25.2	31.7	2.9	28.5	2.9	28.5	2.6	29.6	2.5	29.8
			9	21.5	27.0	4.3	24.0	4.3	24.0	4.1	24.6	4.1	24.6
			15	18.9	23.7	5.5	20.9	5.6	20.6	5.4	21.1	5.5	20.9

[a]Equivalent daily 18-kip axle loads.
[b]Total pavement thicknesses in inches.
[c]One-third of total thickness composed of asphaltic concrete.
[d]AASHO flexible pavement design chart for p = 2.0, one-third of total thickness composed of asphaltic concrete, and total pavement thickness in inches.

molded dynamically in accordance with methods 2 or 3 (Figs. 1 through 6). At method 2 optimum moisture contents, dry densities of specimens obtained by the Kentucky method (method 5) ranged from about 3 to 10 percent higher than the maximum dry densities obtained by method 1, and they averaged about 6 percent higher.

In the Kentucky CBR tests, the maximum CBR occurred slightly to the wet side of optimum moisture content. Maximum Kentucky CBR's generally occurred near the peak of the method 1 molding moisture content-dry density curve. For the dynamically compacted samples, the maximum CBR usually occurred at optimum conditions. Generally, for samples compacted at 2,000 psi and for method 1 optimum moisture contents, Kentucky CBR's in the range from 4 to 12 were approximately the same as or lower than CBR's of specimens molded by method 2, although in two cases they were slightly higher. Kentucky CBR's averaged about 15 percent lower than method 2 CBR's. The comparatively higher axial swells associated with the Kentucky CBR's are apparently a partial result of the elastic rebound of the specimens, the fact that the specimens are soaked until swell virtually ceases, and the absence of shear strains during compaction.

As shown in Figures 2 through 5, method 2 maximum dry densities were slightly higher and optimum moisture contents were lower than those obtained by method 1. In the case of the Adair County soil (Fig. 6), the maximum dry densities and optimum moisture contents for methods 1 and 2 were about the same. For samples molded in accordance with method 3, dry densities were slightly lower, optimum moisture contents higher, and CBR's lower than those obtained by method 2.

Influence of the method of compaction—static or dynamic—on CBR values is strongly indicated in Figure 3. In this series of tests, specimens were molded statically (method 6) to conform with the dry density-molding moisture content curve obtained by method 2. Static compaction pressures ranged from a high of 180 to a low of 99 psi. CBR's obtained in this manner were as much as 40 percent lower than those resulting from method 2.

As reported by Shook and Fang (2), average maximum densities and optimum moisture contents of the as-constructed embankment soil at the AASHO Road Test site were generally lower than those obtained from method 1, and field CBR's were also lower. For "optimum construction," the embankment had a dry density of 117 lb/ft^3. For method 1 compaction, the dry density was 119 lb/ft^3. Hence, the as-constructed dry density was about 2 percent lower than method 1 dry density. As shown in Figure 13, a 2 percent decrease in dry density resulted in a 20 to 50 percent decrease in CBR. For "P_{20} as constructed" (20th percentile, or density below which 20 percent of test values lie, or moisture content above which 20 percent lie), a density of 112 lb/ft^3 and a CBR of 2 were reported. The P_{20} field dry density was about 6 percent lower than method 2 dry density, and P_{20} field CBR of 2 was 60 percent lower than method 2 CBR of 5. In Figure 13, a 5 percent decrease in dry density results in roughly a 50 to 60 percent decrease in CBR. Consequently, the apparent discrepancies between field and laboratory CBR's (dynamic compaction) may be the result of differences in field and laboratory densities and moisture contents.

REFERENCES

1. The AASHO Road Test. HRB Spec. Rept. 73, 1962.
2. Shook, J. F., and Fang, H. Y. Cooperative Materials Testing Program at the AASHO Road Test. HRB Spec. Rept. 66, 1961.
3. Seed, H. B., and Chan, C. K. Structure and Strength Characteristics of Compacted Clays. Jour. Soil Mechanics and Foundations Div., Proc. ASCE, Vol. 85, No. SM5, Part 1, Oct. 1959.
4. Johnson, A. W., and Sallberg, J. R. Factors Influencing Compaction Tests Results. HRB Bull. 319, 1962.
5. Baker, R. F., and Drake, W. B. Investigation of Field and Laboratory Methods for Evaluating Subgrade Support in the Design of Highway Flexible Pavements. HRB Proc., 1948.
6. Stanton, T. E. Suggested Method of Test for Bearing Ratio and Expansion of Soils. Procedures for Testing Soils, ASTM, Sept. 1944.

7. Chamblin, B. B. The Effect of Soaking Time on CBR Value. Virginia Council of Highway Investigation and Research, Feb. 1960.
8. Sorbe, V. K. The Repeatability of Test Results Using Various California Bearing Ratio Procedures and the Resistance R-Value. Materials and Tests Div., Utah State Department of Highways, Aug. 1967.
9. Laboratory California Bearing and Expansion Test. Oklahoma State Highway Commission.
10. Chastain, W. E., and Schwartz, D. R. AASHO Road Test Equations Applied to the Design of Bituminous Pavements in Illinois. Illinois Department of Public Works and Buildings, Oct. 1964.
11. Drake, W. B., and Havens, J. H. Kentucky Flexible Pavement Design Studies. Engineering Experiment Station, Univ. of Kentucky, Bull. 52, June 1959.
12. Deen, R. C., Southgate, H. F., and Havens, J. H. Structural Analysis of Bituminous Concrete Pavements. Kentucky Department of Highways, May 1971.

ESTIMATION OF 18-KIP EQUIVALENT ON PRIMARY AND INTERSTATE ROAD SYSTEMS IN VIRGINIA

N. K. Vaswani and D. E. Thacker, Virginia Highway Research Council

For flexible pavement design purposes, the Virginia Department of Highways uses the AASHO method of determining the 18-kip equivalent single-axle load. The evaluation of the EAL-18 is based on on-location truck axle weight studies. These studies are expensive and time-consuming and hence are not used for pavement reevaluation and rehabilitation. For this reason, a method by which the EAL-18 could be economically and quickly estimated from the routinely available records seemed desirable. These records are the yearly traffic count on each section of the primary, Interstate, and arterial systems and the yearly record of the weights of vehicles using these systems. In this investigation, several methods were tried to determine the best one for estimating the EAL-18 from routine available records. A method involving three equations was considered the best for the following reasons: It provides a very good correlation with the AASHO method, data for estimating the EAL-18 are readily available from the yearly reports published by the Virginia Department of Highways (and those of most other states), and the method accounts for the weight and count of two-axle, six-tire single units, three-axle single units, and tandem trailer trucks separately, thus providing greater accuracy in the evaluation. It is shown that, even if the estimated EAL-18 deviates greatly from the AASHO value, the effect on the ultimate pavement design is very little. The approach could be used to develop traffic projections in cases where load meter studies are not feasible, for example, on roads with heavy traffic where vehicles can be counted but not weighed.

•IN VIRGINIA, for flexible pavement design purposes, the AASHO Interim Guide for Design of Flexible Pavements (1) is used to determine the 18-kip equivalent single-axle load (EAL-18) applications for a given roadway. The evaluation of the EAL-18 requires a truck weight study to obtain necessary axle weight distribution data, load equivalency factors, and a traffic count by vehicle classification. The required truck weight study is perhaps the most difficult task and is a major drawback in applying the AASHO method.

For pavement rehabilitation in Virginia, the truck weight study usually is not made. For the design of new flexible pavements, on-location weight studies of other roads—which are assumed to be carrying the same type of traffic—are utilized. These on-location studies usually are carried out in 1 day. Thus, the accuracy obtained in applying the AASHO method rests largely on the 1-day truck weight study and on the evaluator's judgment in choosing the appropriate weight study to reflect the axle-weight distribution for the proposed pavement design. In addition to these drawbacks, the on-location weight study is an expensive process.

The study reported here was conducted to provide less complex and less expensive methods of estimating the EAL-18 for a given flexible pavement road, methods that would eliminate the on-location truck weight study, at least for pavement rehabilitation purposes.

Publication of this paper sponsored by Committee on Flexible Pavement Design.

STUDY PURPOSE

The purpose of this investigation was to determine a suitable method for estimating the EAL-18 for a given road (as would be obtained by the AASHO method) for the rehabilitation or design of primary and Interstate roads.

For estimating the EAL-18 in Virginia, it was proposed to use data readily available to all divisions and districts of the Virginia Department of Highways, for example, the yearly reports on average daily traffic volumes (2) and truck weight studies (3).

VARIABLES AND SCOPE

The variables considered in this investigation were as follows:

1. Vehicle count;
2. Average vehicle weight, i.e., the weight of all the vehicles divided by the number of vehicles;
3. 18-kip equivalent—either in terms of the 18-kip equivalent (EAL-18) for a given roadway or as the average 18-kip equivalent for each vehicle (EAL-18/vehicle); and
4. Vehicle classification in two types—by axle weight as given in the W-4 table of the truck weight reports (3) and by type of vehicle as given in the yearly traffic volume reports (2).

Other variables, such as the ratio of empty to loaded vehicles, legal axle and gross truck weights, and seasonal changes in traffic patterns, were assumed to have a negligible effect on the evaluation in Virginia and hence were considered constant. The major activities of the area, such as coal mining, do have an effect on the evaluation but were not considered in the mathematical analysis, though an arbitrary provision was made for heavy loads in coal mining areas. A distinction was made between rural and suburban areas, but the difference was so little that this distinction has been ignored and is not reported here.

The annual truck mileage is constantly increasing and will affect the forecast of the total vehicle count but does not affect the conversion of the present traffic into EAL-18 values.

In accordance with the practice of the Virginia Department of Highways, the load equivalency factors were taken directly from the AASHO Guide (1) for flexible pavements for structural number of 5 and a serviceability index of 2.5.

The methodology of estimation was established by adopting the following data:

1. On-location, 1-day truck weight studies on 93 projects in 21 suburban and 72 rural areas for 1963 through 1966,
2. W-3 and W-4 tables from the truck weight study reports for 1961 through 1970,
3. Average daily traffic volumes on Interstate, arterial, and primary roads for 1960 through 1970, and
4. Traffic data on 412 flexible pavement projects for 1960 through 1970.

METHODOLOGY FOR ESTIMATING EAL-18

The first step in determining the methodology was to calculate the EAL-18 for each of the 93 on-location truck weight studies by use of the AASHO Guide procedure. The EAL-18 values obtained by other methods were correlated with the EAL-18 values from the AASHO method, based on the assumption that the results obtained by the AASHO method were the true values.

In all methods, automobiles—which hardly add to the total EAL-18 value—were not considered. The W-4 table method accounts for two-axle, four-tire (2A-4T) vehicles by weight and volume. This type of vehicle was therefore considered in the W-4 table method. However, it has been determined that the EAL-18 due to 2A-4T vehicles does not add appreciably to the total EAL-18 value; on the contrary, consideration of it leads to poor correlations between the traffic count and the total EAL-18 value. The 2A-4T vehicles, therefore, were not considered in any of the methods other than the W-4.

W-4 Table Method

The first method investigated was the W-4 table method. This method does not require the determination of mean ADT values, the average number of axles per vehicle, or the distribution of vehicle weight groups in percentages as does the AASHO method, but it is similar to the AASHO method in its use of equivalency factors and weight ranges. It provides a means of determining the EAL-18 for each type of vehicle, which is not provided by the AASHO method.

The correlation between the W-4 and AASHO methods is shown in Figure 1. This figure shows that the two methods correlate extremely well, with a correlation coefficient of 0.99. It also shows that the EAL-18 determined by the AASHO method is about 1.25 times the EAL-18 value obtained from the W-4 method.

Asphalt Institute Method

The Asphalt Institute method (AI) is given by Shook and Lepp (4) and is based on the principle that trucks having two axles and six tires (2A-6T) or heavier are the prime developers of the EAL-18 and that vehicles lighter than these have a negligible effect on the final evaluation of the EAL-18. They use a model equation as follows:

$$\log (\text{EAL-18}) = a + b \log S + c \log W + d \log N \quad (1)$$

where

a, b, c, and d = constants;
S = legal single-axle load limit (18 for Virginia);
W = average heavy truck gross weight (2A-6T and heavier); and
N = number of heavy trucks (2A-6T and heavier).

Using an S-value of 18 for Virginia and the values of the constants as given by Shook and Lepp, we can reduce Eq. 1 as follows:

$$\log [\text{EAL-18(AI)}] = -6.413 + 1.334 \log W + 1.051 \log N \quad (2)$$

where [EAL-18(AI)] = EAL-18 obtained by the Asphalt Institute method. Equation 2 was applied to each of the 93 on-location studies by the following two methods. In the first method, the equation was applied separately to each of five types of vehicles: 2A-6T, three-axle single unit, three-axle trailer truck, four-axle trailer truck, and five-axle trailer truck. The EAL-18's for each of the five types were then summed to obtain the total EAL-18 for each weight study. In the second method, the average weight of the trucks (2A-6T and heavier) for each project was determined, and then the equation was applied to get the total EAL-18 directly. The values obtained from each of these methods were independently correlated with the values obtained from the AASHO method. It was found that there was very little difference between the two methods. The correlation coefficients, R, and standard errors of estimation, E_s, were almost identical ($R = 0.97$ and $E_s = 76.8$ for the first method, and $R = 0.971$ and $E_s = 77.8$ for the second). The correlation between the EAL-18's from the first method and the EAL-18's from the AASHO method is shown in Figure 2. This correlation shows that the EAL-18 determined by the AASHO method is about 1.42 times that obtained from the Asphalt Institute method by using Eq. 2.

Modified Asphalt Institute Method

New values of coefficients a, b, c, and d for the Asphalt Institute model Eq. 1 were determined by using a computerized multiple regression analysis. The dependent variable in the equation was the EAL-18 of each of the 93 on-location weight studies obtained from the AASHO method. The independent variables were W, the average weight of the combined types of vehicles (two-axle, six-tire and heavier) for each weight study, and N, the vehicle count (again, two-axle, six-tire and heavier). The resulting equation was

Figure 1. Correlation of the EAL-18 values obtained by the W-4 and AASHO methods.

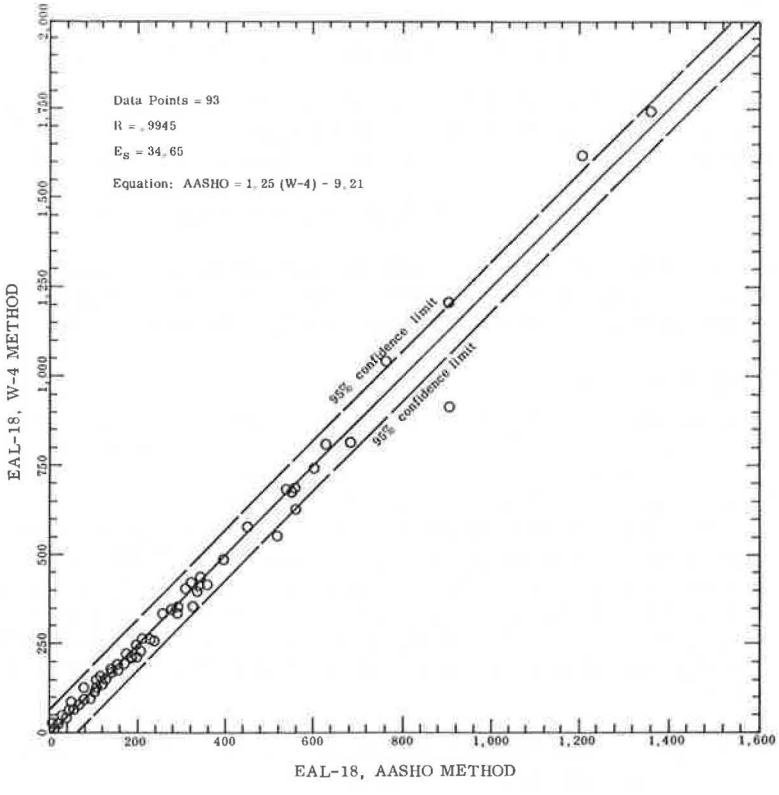

Figure 2. Correlation of the EAL-18 values obtained by the Asphalt Institute and AASHO methods.

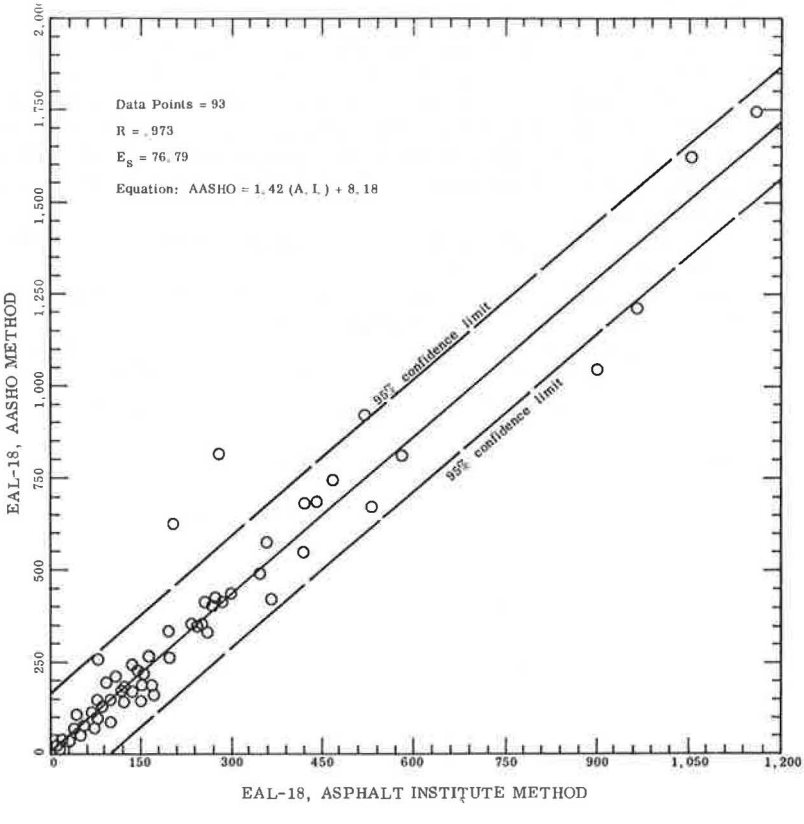

$$\log [\text{EAL-18(mod. AI)}] = -8.483 + 1.873 \log W + 0.99 \log N \quad (3)$$

where [EAL-18(mod. AI)] = EAL-18 obtained by modified AI method. The correlation between the EAL-18 obtained by the modified AI method and the AASHO method is shown in Figure 3 and is expressed by the following equation.

$$[\text{EAL-18(AASHO)}] = 0.894\ [\text{EAL-18(mod. AI)}] + 24.79 \quad (4)$$

where [EAL-18(AASHO)] = EAL-18 obtained by the AASHO method.

Equation 4, or Figure 3, has a correlation coefficient of 0.98, which shows that the modified AI method correlates extremely well with the AASHO method.

Percent Method

In developing the percent method, a percentage distribution of the number of vehicles for different weight groups in each of the five vehicle classifications was made for the 93 on-location studies. The Appendix shows this distribution and gives values of EAL-18 per vehicle for each vehicle classification.

The values of EAL-18 per vehicle for each vehicle classification were applied to each of the 93 on-location studies, and the EAL-18 for each of the 93 on-location studies was determined. The EAL-18 values so obtained were correlated with the EAL-18 values obtained from the AASHO method. This correlation is shown in Figure 4. The correlation coefficient is 0.94, which shows that this method correlates extremely well with the AASHO results, though it has a high standard error of estimate; i.e., E_s = 116.72.

If one assumes that the EAL-18 per vehicle as determined by this method holds for all projects, the total EAL-18 for any project could be obtained if the vehicle count by each vehicle classification is known.

Five-Equation Method

In an attempt to remove weight as a variable, each of the 93 on-location studies was divided into five vehicle classifications as follows: two-axle, six-tire single unit; three-axle single unit; three-axle trailer truck; four-axle trailer truck; and five-axle trailer truck. For each classification under each study, the numbers and average weights of the vehicles and EAL-18's were determined. The EAL-18's were determined by the W-4 table method. This method was adopted because of its high correlation with the AASHO method and because the AASHO method cannot give an EAL-18 for each vehicle classification.

By multiple regression analysis, a general equation for each vehicle classification was developed. The equations for the respective classifications are shown as Eqs. 5 through 9. Each of these equations has two independent variables, i.e., W, the average weight of vehicle, and N, the vehicle count.

The data for determining W in each of the five equations could be obtained either from the 93 on-location studies or from the W-3 tables. In this evaluation, W-3 tables were used (as discussed later) and Eqs. 5a, 6a, 7a, 8a, and 9a were obtained:

For two-axle, six-tire, single-unit vehicles,

$$\log (\text{EAL-18})_1 = -21.34 + 4.991 \log W_1 + 0.99 \log N_1 \quad (5)$$

$$= -0.70 + 0.99 \log N_1 \quad (5a)$$

For three-axle, single-unit vehicles,

$$\log (\text{EAL-18})_2 = -0.74 + 0.043 \log W_2 + 1.00 \log N_2 \quad (6)$$

$$= -0.55 + 1.00 \log N_2 \quad (6a)$$

For three-axle trailer trucks,

Figure 3. Correlation of EAL-18 values obtained by the modified Asphalt Institute and AASHO methods.

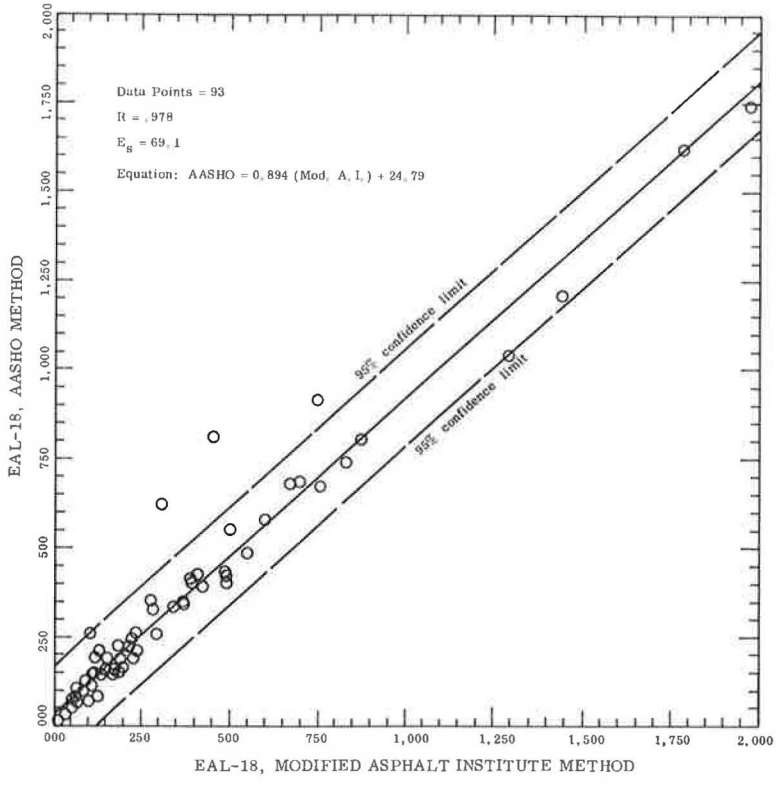

Figure 4. Correlation of EAL-18 values obtained by the percent and AASHO methods.

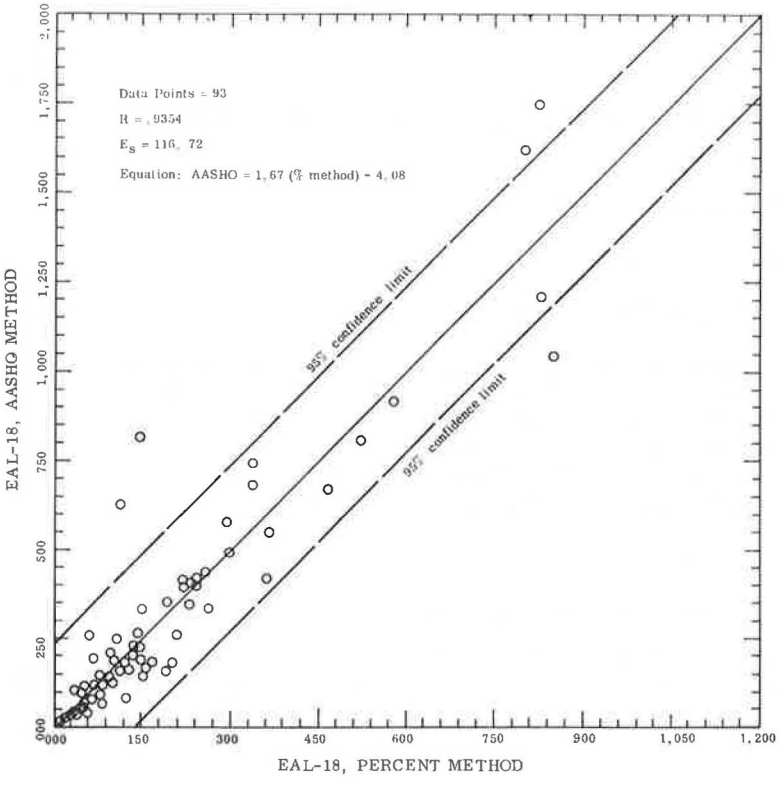

$$\log (\text{EAL-18})_3 = -0.04 - 0.101 \log W_3 + 1.05 \log N_3 \quad (7)$$

$$= -0.49 + 1.05 \log N_3 \quad (7a)$$

For four-axle trailer trucks,

$$\log (\text{EAL-18})_4 = -0.08 - 0.078 \log W_4 + 1.11 \log N_4 \quad (8)$$

$$= -0.44 + 1.11 \log N_4 \quad (8a)$$

For five-axle trailer trucks,

$$\log (\text{EAL-18})_5 = -0.02 - 0.035 \log W_5 + 0.97 \log N_5 \quad (9)$$

$$= -0.18 + 0.97 \log N_5 \quad (9a)$$

In Eqs. 5 through 9a, subscripts 1 through 5 for the EAL-18, W, and N show the five vehicle classifications for the EAL-18, the average weight of vehicles, and number of vehicles in each classification respectively.

The sum of EAL-18_1 through EAL-18_5 would give the total value of EAL-18 by the five-equation method. This value could be represented by [EAL-18(5-eq.)].

The correlation between this five-equation method and the AASHO method is shown in Figure 5. The correlation coefficient is 0.94, which shows that this method correlates extremely well with the AASHO method.

Three-Equation Method

The three-equation method is a simple reduction of the five-equation method. Instead of using an equation for each of the axle groups in the three classifications of tractor semitrailers, an equation was developed to cover all tractor semitrailers (three-, four-, and five-axle trucks). The equations for the single-unit vehicles (two-axle six-tire, and three-axle) remain the same as Eqs. 5a and 6a as follows:

$$\log (\text{EAL-18})_1 = -0.70 + 0.99 \log N_1 \quad (5a)$$

and

$$\log (\text{EAL-18})_2 = -0.55 + 1.00 \log N_2 \quad (6a)$$

The equation developed for trailer trucks having three, four, and five axles is as follows:

$$\log (\text{EAL-18})_T = -13.92 + 3.00 \log W_T + \log N_T \quad (10)$$

Based on the W_T values given in Table 1,

$$\log (\text{EAL-18})_T = \log N_T - 0.0578 \quad (10a)$$

where W_T and N_T are the average weight and the number of trailer trucks respectively.

The sum of $(\text{EAL-18})_1$, $(\text{EAL-18})_2$, and $(\text{EAL-18})_T$ would give the value of EAL-18 by the three-equation method. This value could be represented by [EAL-18(3-eq.)].

The correlation between this three-equation method and the AASHO method is shown in Figure 6. The correlation coefficient of 0.98 shows that this method correlates extremely well with the AASHO method. The correlating equation is as follows:

$$[\text{EAL-18(AASHO)}] = 16 + 1.22\ [\text{EAL-18(3-eq.)}] \quad (11)$$

SELECTION OF THE METHOD FOR USE

The investigation showed that, given the necessary information, the following methods enable good estimations of the AASHO EAL-18 for a given project. The correlation

Figure 5. Correlation of EAL-18 values obtained by the five-equation and AASHO methods.

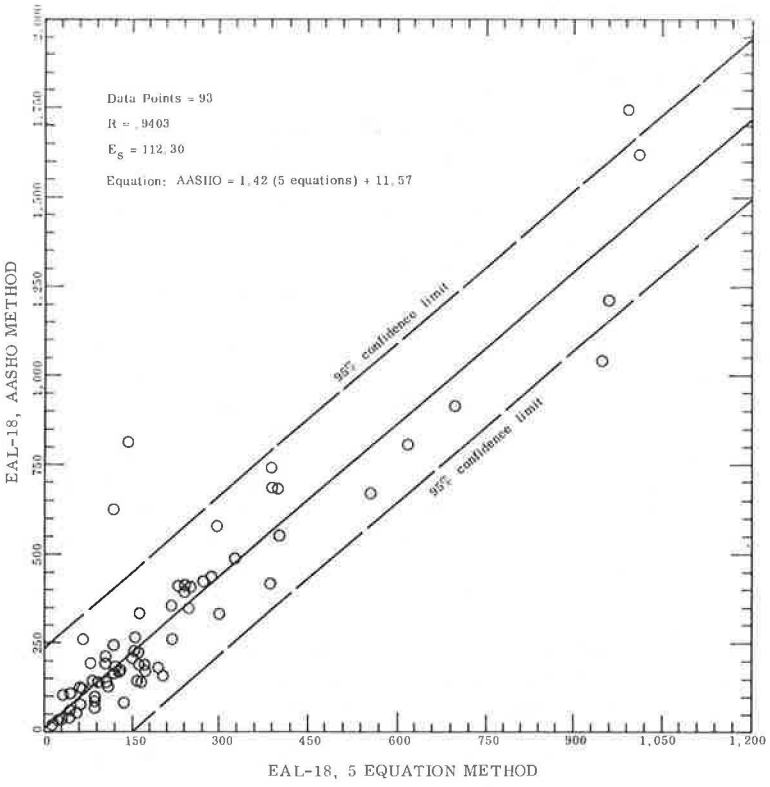

Table 1. Average vehicle weight by classification.

Vehicle Classification	Average Vehicle Weight (lb)
Single unit (two axles, six tires)	13,705
Single unit (three axles)	25,980
Tractor semitrailers (three, four, and five axles)	41,760

coefficient, R, and standard error of estimate, E_s, are also given for each method:

1. Percent method—R = 0.94, E_s = 117;
2. W-4 table method—R = 0.99, E_s = 35;
3. Five-equation method—R = 0.94, E_s = 112;
4. Modified Asphalt Institute method—R = 0.98, E_s = 69; and
5. Three-equation method—R = 0.98, E_s = 63.

The percent method requires the percentage of vehicle count in different vehicle weight groups for each vehicle classification to determine the EAL-18 for each vehicle classification as shown in the Appendix. If at a later date the weights of vehicles in each vehicle classification change, there will be no way to modify the values of EAL-18 per vehicle unless a study similar to the 93 on-location study is made. This method is therefore considered less useful than the other methods where the average weight of a vehicle instead of the EAL-18 per vehicle is an independent variable. This method is, therefore, not recommended for use on a long-term basis.

In the W-4 table method, axle counts by each weight classification need to be known. This information is not obtainable for any project without the collection of data on the site. This method, therefore, cannot be used for estimation purposes.

In the remaining three methods, the independent variables are the average weight of all vehicles (two-axle, six-tire or heavier), or the average weight of all vehicles in each vehicle classification, and the vehicle count. The average weights for all vehicles and the average weights by vehicle classification can be obtained from the W-3 tables in Virginia's truck weight study reports. The vehicle count for any Interstate or primary highway is obtainable from Virginia's annual daily traffic volume reports.

In the traffic volume reports, the trailer trucks are not categorized as three-, four-, and five-axle, which information is needed for the five-equation method. The five-equation method might, therefore, be difficult to apply in many cases. Consequently, this method is not recommended for general purposes of estimation.

The annual truck weight study reports of the Virginia Department of Highways show that, from 1963 to 1970, there was no tendency toward an overall increase or decrease in truck weights. Thus, the average truck weights during this period as obtained from the W-3(03) and W-3(04) tables are given in Table 1 and could be used for estimating the EAL-18 for any project.

The average weights given in Table 1 could be applied directly in the three-equation method. For the modified Asphalt Institute method, the average weight of the vehicle, W, is obtained as follows:

$$W = \frac{N_1W_1 + N_2W_2 + N_3W_3}{N_1 + N_2 + N_3} \tag{12}$$

where N_1, N_2, and N_3 are the counts, and W_1, W_2, and W_3 are the weights of 2A-6T vehicles, three-axle single units, and trailer trucks respectively.

In the three-equation method, Eqs. 5a, 6a, and 10a are obtained from Eqs. 5, 6, and 10 by the use of the truck weights given in Table 1. The average weights given in Table 1 could be used for design throughout Virginia, except in the coal mining areas of the Bristol district. In the coal areas, permits for higher than conventional wheel and truck loads are issued free of charge. The permits limit the weight on single and tandem axles to 24,000 and 36,000 lb as compared to the conventional maximum permissible weights of 20,000 and 32,000 lb on single and tandem axles respectively.

The values given in Table 1 could be used for design, with the stipulation that they could be exceeded by 20 percent in the coal areas. If the weight values are changed, Eqs. 5, 6, and 10 should be used for the three-equation method.

The correlations between the three-equation and modified AI methods in Figures 3 and 6 show that, though their correlation coefficients with the AASHO method are the same, the standard error of estimate in the three-equation method is slightly lower than that in the modified AI method.

To further evaluate the choice between these two methods, we selected 412 satellite projects designed between 1960 and 1970. Their traffic counts were obtained from the

Virginia reports of average daily traffic volumes. In these traffic volume data, buses are given separately. The buses are classed as either school buses of the 2A-6T type or commercial buses with three axles. Because these data are collected on working days only and between 8 a.m. and 5 p.m., almost all the school buses are counted, whereas not all the commercial buses are counted. Thus, 70 percent of the buses counted were assumed to be of the 2A-6T class, and the remaining 30 percent were assumed to be three-axle vehicles. It is, however, recommended that for general application 80 percent of the buses counted should be considered to be of the 2A-6T class and the remaining 20 percent in the three-axle vehicle class. This breakdown is necessary for the three-equation method but is not needed for the modified AI method.

For determining the [EAL-18(3-eq.)] for each project, Eqs 5a, 6a, and 10a were used. For determining the [EAL-18(mod. AI)] for each project, Eq. 3 was used. The EAL-18 values so obtained by these two methods were correlated with each other. The correlation coefficient was 0.995 with a standard error of estimate of 15.8. This is an excellent correlation. The relation between the EAL-18 values obtained by the two methods was found to be

$$[\text{EAL-18(mod. AI)}] = 13 + 1.2\ [\text{EAL-18(3-eq.)}] \tag{13}$$

The total truck traffic consisting of 2A-6T and heavier vehicles was correlated with the EAL-18 obtained by each of these two methods by the use of their equations.

In the three-equation method, the correlation coefficient was 0.92 with a standard error of 80. The correlation equation was as follows:

$$[\text{EAL-18(3-eq.)}] = -7 + 0.7\ (N_1 + N_2 + N_T) \tag{14}$$

This correlation is shown in Figure 7. In the modified AI method, the correlation coefficient was 0.88 with a standard error of 96.

The two correlations show that the three-equation method is statistically slightly better than the modified AI method, but both methods would give very good estimated values. The authors, however, feel that by use of different equations for different vehicle types, as in the three-equation method, one can obtain better estimates of the EAL-18 than from one equation for trucks as in the modified AI method.

The three-equation method is therefore recommended as the best choice for estimating the [EAL-18(AASHO)]. For ease of application of this method, the three equations have been translated into a graphical form as shown in Figure 8. The sum of three values obtained on the y-axis of this figure for the three traffic categories gives the total 18-kip equivalent obtained from the three categories. This value, when used with Eq. 11, would give the estimated AASHO 18-kip equivalent.

This three-equation method is under further review by the Virginia Department of Highways for use on new projects. Fourteen new projects so evaluated have given a correlation coefficient of 0.97 and a standard error of estimate of 66.

QUICK METHOD FOR CONVERTING VEHICLE COUNT TO EAL-18

For the easy conversion of the traffic count to the [EAL-18 (AASHO)], Eqs. 14 and 11 and [EAL-18(3-eq.)] could be combined. Based on these two equations

$$[\text{EAL-18(AASHO)}] = 16 + 1.22\ [-7 + 0.7\ (N_1 + N_2 + N_T)]$$

$$= 7.46 + 0.85\ (N_1 + N_2 + N_T) \tag{15}$$

$$= 7.46 + 0.85 \tag{16}$$

This shows that the EAL-18 obtained by the AASHO method is about 0.85 times the total 2A-6T and heavier truck traffic.

Figure 6. Correlation of EAL-18 values obtained by the three-equation and AASHO methods.

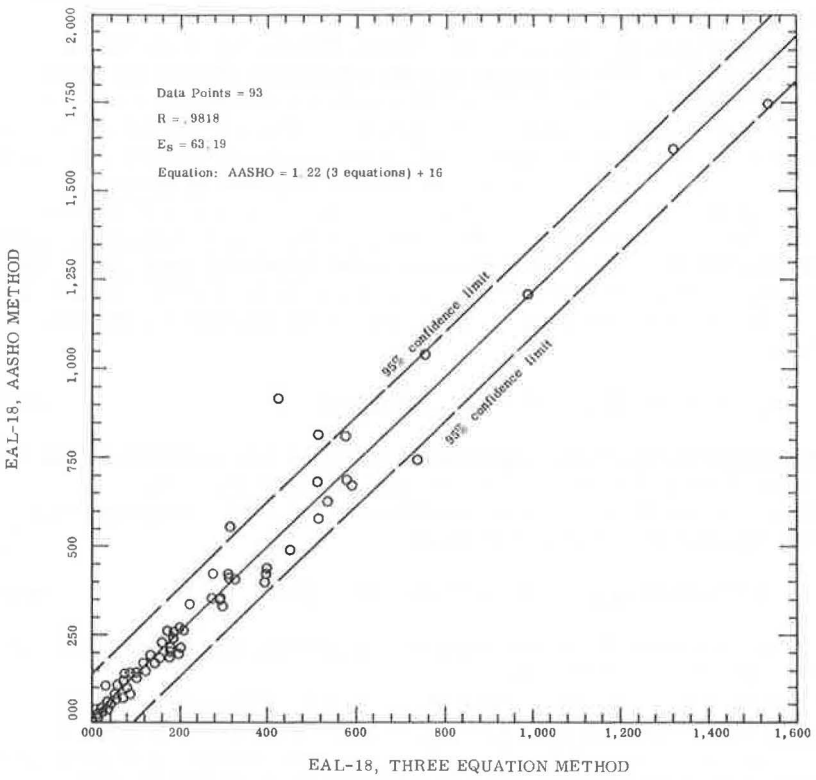

Figure 7. Correlation of EAL-18 obtained by the three-equation method and the total truck traffic (2A-6T and heavier).

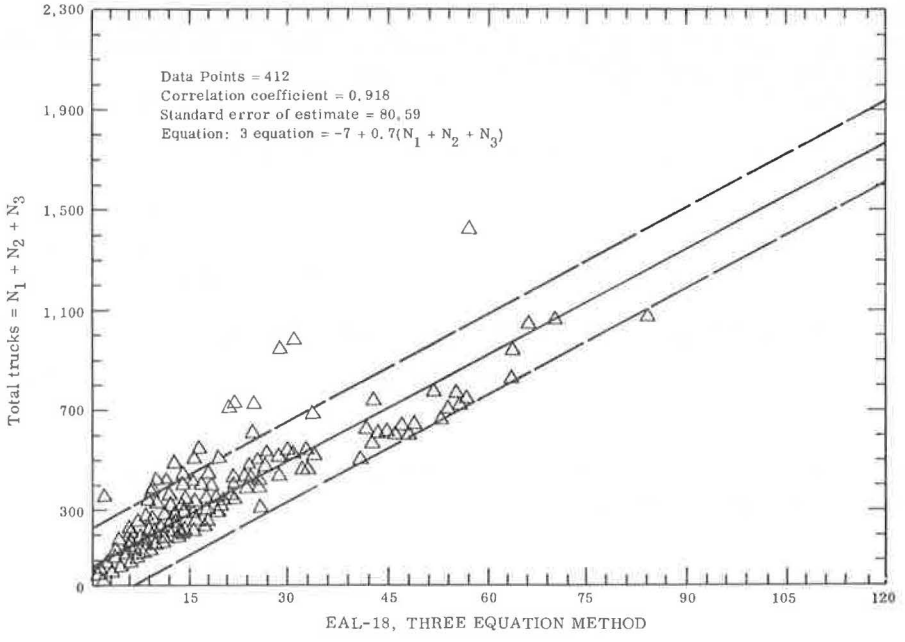

Figure 8. Evaluation of EAL-18 by three-equation method.

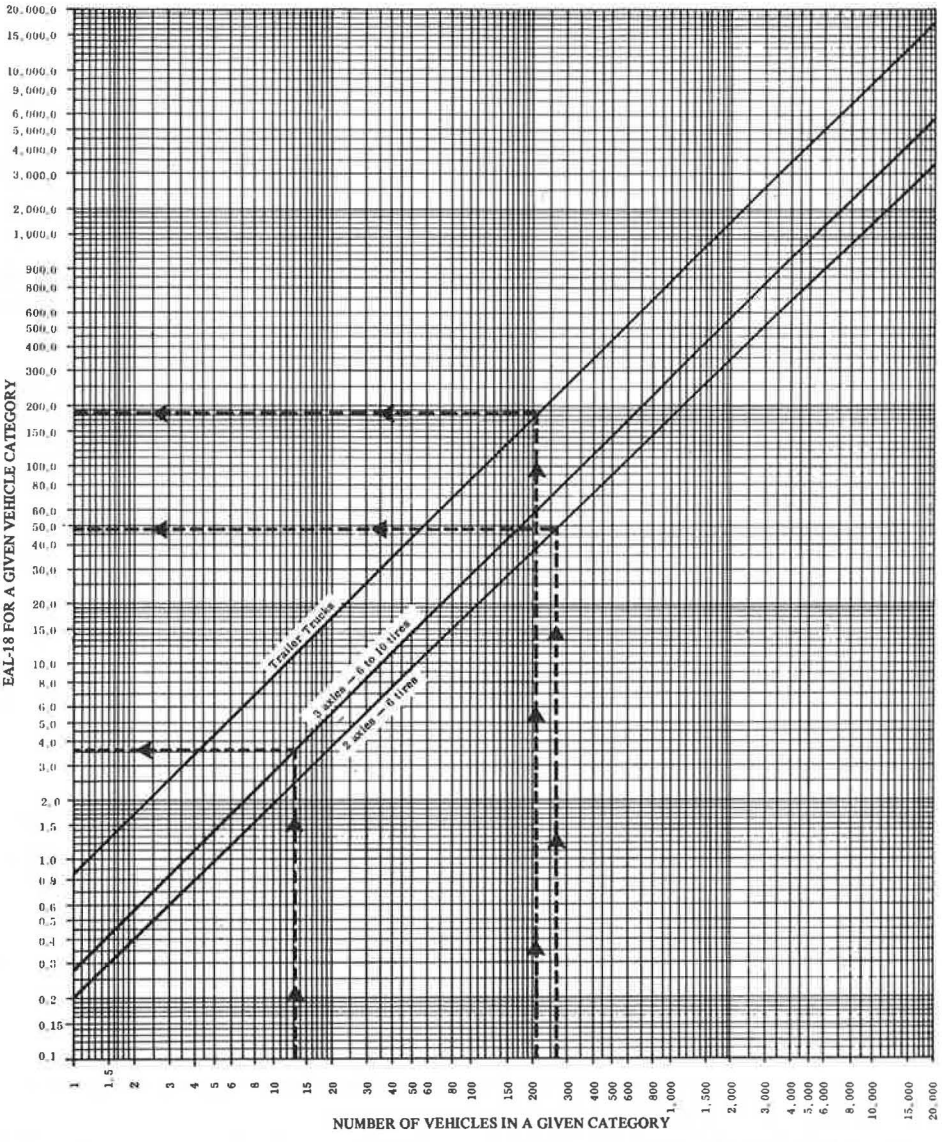

Figure 9. Correlation of thickness index (D) by three-equation and AASHO methods.

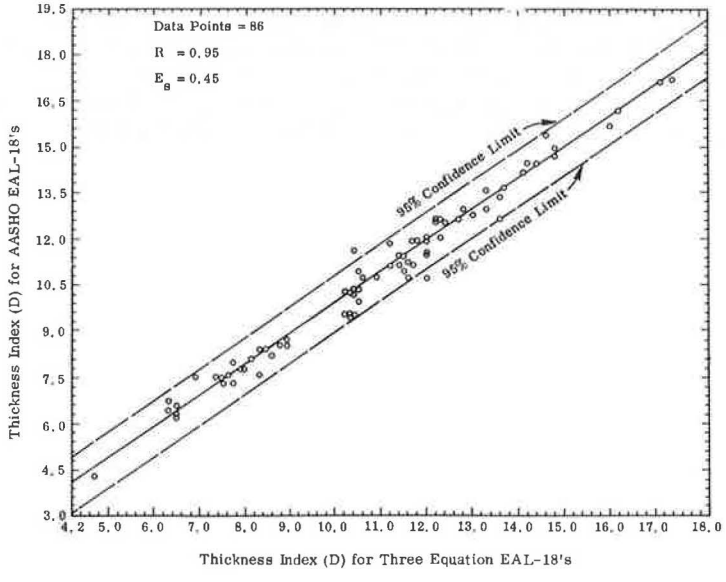

EFFECT OF ESTIMATING THE EAL-18 ON PAVEMENT DESIGN

As mentioned before, in Virginia the AASHO method is used for pavement design only. Though it was found that the estimated EAL-18 values have an excellent correlation with the AASHO values on a statistical basis, it was necessary to confirm the maximum possible deviation a designer is likely to encounter in using the estimated method as compared to the AASHO method currently used.

In Virginia for the design of primary, Interstate, and arterial roads, the pavement design method developed by Vaswani (5) is used. In this method, the thickness index (or structural number) of the pavement is determined.

The estimated values of EAL-18 obtained from the three-equation method were used to determine the thickness index (or structural number) for each of 86 projects chosen from the 93 projects considered in this investigation. The soil support values for all pavements were assumed to be 10 in the design chart of Vaswani's method. Given the soil support and EAL-18, the thickness indexes obtained were correlated with the thickness indexes obtained by using the AASHO EAL-18 method. The correlation graph is shown in Figure 9. The correlation coefficient of 0.97 and standard error of estimate of 0.45 show that the estimated value enables pavement design from estimated EAL-18 values.

CONCLUSION AND RECOMMENDATION

It is concluded that the small errors resulting from calculating or estimating EAL-18 values do not significantly affect the ultimate pavement design. It is recommended that the three-equation method be used for estimating the EAL-18 when load meter studies are not feasible.

ACKNOWLEDGMENT

The assistance received from the Traffic and Safety Division of the Virginia Department of Highways is gratefully acknowledged. Thanks go to K. H. McGhee and H. T. Craft of the Virginia Highway Research Council for reviewing the report. The study was conducted under the general supervision of J. H. Dillard, head of the Council, and was financed from state research funds.

The opinions, findings, and conclusions expressed in this report are those of the authors and not necessarily those of the sponsoring agencies.

REFERENCES

1. AASHO Interim Guide for the Design of Flexible Pavement Structures. AASHO Committee on Design, 1961.
2. Average Daily Traffic Volumes on Interstate, Arterial and Primary Routes. Virginia Department of Highways, Richmond.
3. Truck Weight Study. Virginia Department of Highways, Richmond.
4. Shook, J. F., and Lepp, T. Y. Method for Calculating Equivalent 18-Kip Load Applications. Highway Research Record 362, 1971, pp. 87-95.
5. Vaswani, N. K. Recommended Design Method for Flexible Pavements in Virginia. Virginia Highway Research Council, Charlottesville, March 1969.

APPENDIX

EVALUATION OF EAL-18 PER VEHICLE BY WEIGHT GROUP IN EACH VEHICLE CLASSIFICATION

Vehicle classification	Single Unit				Tractor Semi-Trailer					
No. of vehicles	2A-6T		3-axle		3-axles		4-axles		5-axles	
	19,355		4,472		3,841		11,509		2,519	
Percent No. of vehicles	46.5%		10.8%		9.2%		27.5%		6%	
Vehicle Weight Group in kips	% count	EAL-18/veh	% count	EAL-18/veh	% count	EAL-18/veh	% count	EAL-18/veh	% count	EAL-18/veh
(1)	(2)	(3)	(4)	(5)	(6)	(7)	(8)	(9)	(10)	(11)
11 - 12	17	.1273								
12 - 13	47	.1432	3.5	.118	2.5	.1201	—	—	—	—
13 - 14	19	.1555								
14 - 15	7	.1687								
15 - 16	10	.1867	—	—	—	—	—	—	—	—
15 - 20	—	—	10	.2036	7.5	.2199				
20 - 25	—	—	26	.2884	26	.2880	8	.2641	—	—
25 - 30	—	—	32.5	.3736	36	.3609	9	.3853	—	—
30 - 35	—	—	13	.4547	23.5	.4596	18.5	.4614		
35 - 40	—	—	12	.5483	4.5	.5455	29.5	.5900	18	.5149
40 - 45	—	—	3	.7637			23	.6984		
45 - 50	—	—	—	—	—	—	9	.7867	33	.7218
50 - 55	—	—	—	—	—	—			18	.8718
55 - 60	—	—	—	—	—	—	3	.8443	10.5	.9608
60 - 65	—	—	—	—	—	—	—	—	13.5	.9715
65 - 75	—	—	—	—	—	—	—	—	7	1.1604
TOTALS	100	.149	100	.369	100	.357	100	.572	100	.801

% count = Percent number of vehicles in each vehicle classification in the 93 on-location studies

EAL-18/vehicle = Average 18-kip equivalent of a vehicle

STIFFNESS HISTORY OF ASPHALT CONCRETE SURFACES IN ROADS

Mohamed Y. Shahin and B. Frank McCullough, Center for Highway Research, University of Texas at Austin

A system for predicting the stiffness history of an asphalt concrete pavement layer throughout its design analysis period has been developed. The system uses standard material properties and environmental inputs to predict the daily changes in stiffness due to temperature variations and also the long-term changes in stiffness due to hardening of the asphalt cement binder. This system was developed as part of an overall system for the prediction of low-temperature and thermal-fatigue cracking in flexible pavements. The following procedures and models were developed from actual projects and other research results: models to estimate the asphalt concrete stiffness from the ordinary laboratory measurements, procedure to estimate the loading time for temperature, and models to predict the in-service aging of asphalts. The system has been used in predicting low-temperature and thermal-fatigue cracking and has shown a good degree of reliability.

•PROPER estimation of asphalt concrete stiffness is essential for calculating thermal stresses and fatigue distress due to traffic loading and temperature cycling and for determining flexible pavement design in general. If the stiffness is too low, load distress may develop; if it is too high, temperature cracks are likely to occur. The calculation of thermal stresses and fatigue distress in flexible pavements demands the estimation of many values of asphalt concrete stiffness at many temperatures. For example, the calculation of thermal stresses on an hourly basis for a single year will demand the estimation of 8,640 (360 × 24) stiffness values. Therefore, the model for estimating the asphalt concrete stiffness should be in a form that can be programmed.

It is an established fact that asphalt concrete is neither elastic nor viscous but viscoelastic; i.e., its stiffness is a function of temperature and loading time. Moreover, the aging of asphalt adds an important dimension to the stiffness of the asphalt concrete. In this research effort, a system for estimating the asphalt concrete stiffness as a function of temperature, loading time, and age has been developed. The following are the constituents of the system:

1. Models to estimate the asphalt concrete stiffness from the ordinary laboratory measurements,
2. Procedure to estimate the loading time for temperature, and
3. Models to predict the in-service aging of asphalts.

The system has been used in predicting low-temperature and thermal-fatigue cracking (1) and has shown a good degree of reliability.

ASPHALT CONCRETE STIFFNESS

There are three approaches to characterizing the behavior of viscoelastic materials: models, direct measurements, and indirect measurements. The last approach is utilized here in estimating asphalt concrete stiffness. This choice is based on the belief

Publication of this paper sponsored by Committee on Flexible Pavement Design.

that Van der Poel's method (2) can be computerized to fit in the overall system for predicting the history of the asphalt concrete stiffness.

Several investigators have investigated the accuracy of the Van der Poel and Heukelom and Klomp nomographs. Pell and McCarthy (3) reported that the general stiffnesses computed by Van der Poel compared reasonably well with those measured on actual samples. Monismith (4) also checked laboratory-determined stiffness values with both laboratory compacted samples and samples cut from in-service pavements. The results showed reasonable agreement with those determined from Heukelom and Klomp.

Van der Poel (2) also independently checked the accuracy of his nomograph and concluded that the difference in measured stiffness values of an asphalt and the stiffness obtained from the nomograph seldom exceeded a factor of 2.

The concept of stiffness was introduced by Van der Poel (2) as follows:

$$\text{Stiffness modulus (S)} = \frac{\text{tensile stress}}{\text{total strain}} \tag{1}$$

The nomograph for estimating the asphalt stiffness was derived by Van der Poel from experimental data from two types of tests: constant stress (static creep test in tension) and dynamic test with an alternating stress of constant amplitude and frequency.

Van der Poel's nomograph was modified slightly by Heukelom and Klomp (5), in that the stiffness is determined in kg/cm^2 instead of N/m^3, and the lines for negative penetration indexes are in a different location. This modified nomograph is shown in Figure 1. The determination of the asphalt stiffness from the nomographs published by Van der Poel and Heukelom and Klomp requires three parameters: loading time, test temperature minus softening-point temperature, and penetration index of the asphalt.

The stiffness of the asphalt concrete mixture depends on the stiffness of the asphalt and the volume concentration of the aggregate. Heukelom and Klomp gave the following equation to estimate the stiffness of the asphalt concrete when the stiffness of the asphalt cement is determined from their nomograph (Fig. 1):

$$S_{mix} = S_{ac}\left[1.0 + \left(\frac{2.5}{n}\right)\left(\frac{C_v}{1.0 - C_v}\right)\right]^n \tag{2}$$

where

$$n = 0.83 \log_{10}\left(\frac{4 \times 10^5}{S_{ac}}\right);$$

S_{mix} = stiffness of asphalt concrete mixture, kg/cm^2;
S_{ac} = stiffness of asphalt cement, kg/cm^2; and
cv = volume concentration of the aggregate.

The volume concentration of the aggregate in a mixture is defined as follows:

$$C_v = \frac{\text{volume of compacted aggregate}}{\text{volume of (asphalt + aggregate)}} \tag{3}$$

This equation can be substituted by an equivalent equation (Eq. 4) by replacing the terms with values that can be measured on an asphaltic concrete core cut from a pavement or a compacted laboratory sample.

$$C_v = \frac{1}{1 + C} \tag{4}$$

Figure 1. Nomograph for predicting the stiffness modulus of asphaltic bitumens (5).

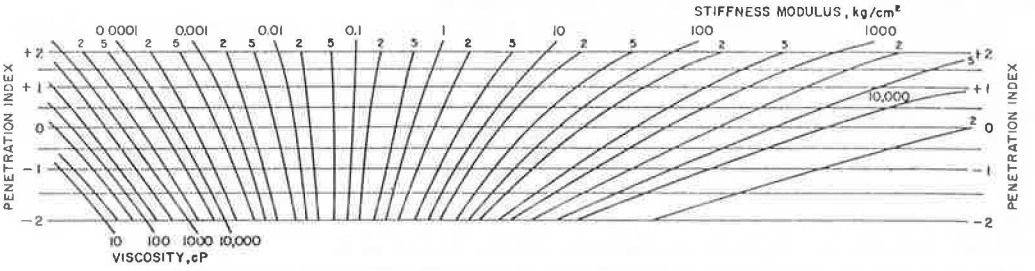

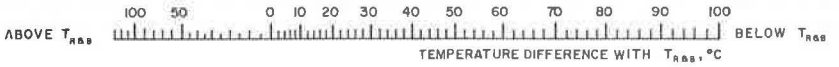

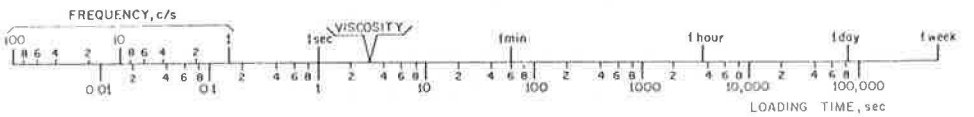

where

$$C = \left(\frac{W_a}{W_g}\right) \times \left(\frac{G_g}{G_a}\right) = (\text{percentage of asphalt by weight of aggregate}/100)\left(\frac{G_g}{G_a}\right),$$

W_a = weight of asphalt,
W_g = weight of aggregate,
G_a = specific gravity of asphalt, and
G_g = specific gravity of aggregate.

The relation shown in Eq. 2 is applicable to well-compacted mixtures with about 3 percent air voids. For mixtures with air voids greater than 3 percent, Draat and Sommer (6) derived a correction to be applied to the C_v:

$$C_v' = \frac{C_v}{1 + H} \tag{5}$$

where H = actual air voids - 0.03.

After a review of the literature and also personal contact with Van der Poel, it was found that no equation has been developed since the nomograph was first published in 1954. As a result, a predictive mode was developed through the use of regression methods. The method selected was the stepwise regression because it was felt that this method provides the best selection of independent variables. The dependent variable was chosen as the $\log_{10}$ of stiffness because the stiffness varies over many orders of magnitude. The independent variables selected were loading time t, temperature of test minus softening-point temperature T, penetration index PI, log t, log T + 101, log PI + 3, t^2, T^2, PI^2, t^3, T^3, PI^3, all two-way interactions of these variables, and other combinations of these factors that seemed theoretically reasonable.

As explained in Draper and Smith (7), the stepwise regression procedure starts with the simple correlation matrix and enters into regression the independent variable X most highly correlated with the dependent variable Y, $\log_{10}$ (stiffness). Using partial correlation coefficients, it then selects as the next variable to enter regression that X-variable whose partial correlation with the response Y is highest, and so on. The procedure reexamines "at every stage of the regression the variables incorporated into the model in previous stages" (7). The program does this by testing every variable at each stage as if it had entered last.

The overall goals for the prediction equation were as follows:

1. The final equation should explain a high percentage of the total variation ($R^2 \geq 0.98$),
2. The standard error of the estimate should be less than 0.20 (this value being a log) to ensure a small coefficient of variation,
3. All estimated coefficients should be statistically significant with $\alpha \leq 0.05$, and
4. There should be no discernible patterns in the residuals.

An attempt to characterize the entire nomograph with a single regression equation was first made. A large factorial grouping of data as shown in Figure 2 was taken from the nomograph in Figure 1. The data represent loading time from 10^{-2} to 10^{-5} sec, PI from -2 to +2, and $T_{test} - T_{R\&B}$ from +50 to -100 C. After many attempts to obtain a suitable prediction equation that met the goals listed, and after not being able to reduce the standard error of the estimate to an acceptable level, we decided to split the nomograph into two parts and fit a separate equation to each part. Almost all of the stiffness values of practical significance to a pavement design engineer are greater than the 10 kg/cm^2 of the asphalt cement. This is approximately 400 kg/cm^2 for a mix with C_v of 0.86, which equals about 5,700 psi. Therefore, a regression equation was derived using the data shown in Figure 2 with stiffness values less than 10 kg/cm^2, and another regression equation was built using all data that had stiffness values greater than 10 kg/cm^2. Acceptable prediction equations were then obtained for each portion of the data that met all of the goals set for the regression equations.

The following equations were obtained with the corresponding statistics:

1. For a stiffness value of 10^{-7} to 10^{1} kg/cm^2, the prediction model is

$$\log_{10} S = -1.35927 - 0.06743(T) - 0.90251 \log(t) + 0.00038(T^2) - 0.00138(T \times \log t) + 0.00661(PI \times T) \quad (6)$$

where

T = test temperature minus softening-point temperature, deg C;
t = loading time, sec; and
PI = penetration index.

The corresponding statistics are $R^2 = 0.99$, standard error of estimate = 0.1616, and n = 126 data points. The range of factors is PI = -2 to +2, T = +50 to -100 C, and t = 10^{-2} to 10^{5} sec.

2. For a stiffness value of 10 to 20,000 kg/cm^2, the prediction is

$$\log_{10} S = -1.90072 - 0.11485(T) - 0.38423(PI) - 0.94259 \log(t) - 0.00879(T \times \log t) - 0.05643(PI \times \log t) - 0.02915(\log t)^2 - 0.51837 \times 10^{-3}(T^2) + 0.00113(PI^3 \times T) - 0.01403(PI^3 \times T^3) \times 10^{-5} \quad (7)$$

The corresponding statistics are $R^2 = 0.98$, standard error of estimate = 0.1638, and n = 79 data points. The range of factors is PI = -1.5 to +2.0, T = +50 to -100 C, and t = 10^{-2} to 10^{5} sec.

The models were verified by plotting the stiffness values obtained from the nomograph against the stiffness as calculated from Eqs. 6 and 7. The results shown in Figures 3 and 4 indicate that the models are reliable.

The following guidelines are given for using the equations to predict asphalt stiffness:

1. Use Eq. 6 only to predict stiffness from 10^{-7} to 10 kg/cm^2, and use Eq. 7 only to predict stiffness from 10 to 2×10^{4} kg/cm^2. The user should not employ predictions that fall outside of these limits.
2. The ranges given for T, t, and PI should not be exceeded. It was found that Eq. 7 values of stiffness obtained when the PI was -2 were not accurate enough, so use of the equation is limited to a PI of -1.5 or greater.

Equations 6 and 7 can be used to estimate the asphalt concrete stiffness using Eq. 2.

LOADING TIME FOR ESTIMATING ASPHALT STIFFNESS

Asphalt stiffness is partly dependent on the loading time. For traffic, the loading time can be physically measured or estimated; so far as temperature is concerned, the thermal loading time has been a question to be answered by engineering judgment. Most engineers have considered the thermal loading time as the time corresponding to the temperature interval, ΔT (Eq. 8), used for calculating the thermal stresses.

Although this may seem logical initially, it does not appear that it actually is. Instead, thermal loading time is fictitious and depends mainly on the rate of temperature drop and the asphalt concrete mixture properties. This can be shown by using the experimental work performed by Monismith et al. (8). In this experiment, an asphalt concrete beam was subjected to a temperature drop, and the developed thermal stresses were measured. The properties of the mixture are given in Table 1.

The specimens were subjected to a temperature drop from 75 to 35 F. The calculations were simplified by assuming the temperature drop to be linear (Fig. 5). A factorial experiment was then designed for the estimation of thermal stresses under different loading times and temperature intervals (Fig. 6). Equation 8, after Hills and Brien (9), was used for the calculations:

Figure 2. Factorial data obtained from nomograph (5) (in kg/cm^2).

Loading Time, seconds / Penetration Index of Asphalt / T test - TRB, °C		10^{-2}	10^{-1}	10^{0}	10^{1}	10^{2}	10^{3}	10^{4}	10^{5}
+50	-2	3.3E-3	4.0E-4	4.2E-5	5.0E-6	4.0E-7	7.0E-8	1.0E-8	1.0E-9
	-1	7.2E-3	9.5E-4	1.0E-4	1.1E-5	9.5E-7	1.0E-7	1.8E-8	2.0E-9
	0	1.3E-2	1.7E-3	2.0E-4	2.1E-5	2.0E-6	2.3E-7	3.0E-8	5.1E-9
	+1	2.0E-2	2.8E-3	4.0E-4	4.4E-5	4.0E-6	5.0E-7	5.1E-8	7.1E-9
	+2	2.7E-2	4.2E-3	5.7E-4	7.7E-5	5.5E-6	1.0E-6	6.1E-8	1.0E-8
+20	-2	1.3E-1	1.6E-2	1.8E-3	1.8E-4	1.8E-5	1.9E-6	1.9E-7	4.1E-8
	-1	2.0E-1	2.3E-2	2.9E-3	2.9E-4	3.0E-5	2.9E-6	2.9E-7	5.1E-8
	0	2.3E-1	3.0E-2	3.8E-3	4.1E-4	4.6E-5	5.0E-6	4.7E-7	7.1E-8
	+1	2.4E-1	3.5E-2	4.9E-3	5.7E-4	7.2E-5	7.0E-6	6.5E-7	1.0E-7
	+2	2.4E-1	4.1E-2	6.0E-3	8.5E-4	1.1E-4	1.1E-5	1.0E-6	2.0E-7
-10	-2	3.0E1	3.7E0	4.0E-1	4.4E-2	3.9E-3	4.6E-4	5.0E-5	5.0E-6
	-1	1.4E1	2.0E0	2.8E-1	3.4E-2	3.4E-3	4.0E-4	4.2E-5	4.6E-6
	0	7.7E0	1.4E0	2.2E-1	3.0E-2	3.0E-3	3.8E-4	4.2E-5	4.6E-6
	+1	5.0E0	1.1E0	1.9E-1	2.6E-2	2.9E-3	4.0E-4	5.0E-5	4.7E-6
	+2	4.0E0	9.0E-1	1.6E-1	2.4E-2	3.0E-3	4.6E-4	6.0E-5	5.0E-6
-40	-2	1.2E4	5.0E3	1.4E3	2.2E2	2.2E1	2.5E0	3.5E-1	3.7E-2
	-1	1.7E3	5.7E2	1.9E2	3.8E1	4.9E0	6.0E-1	8.0E-2	8.5E-3
	0	5.7E2	2.1E2	6.0E1	1.1E1	1.9E0	2.5E-1	4.0E-2	4.5E-3
	+1	2.5E2	8.5E1	2.5E1	4.9E0	1.0E0	1.6E-1	2.3E-2	3.0E-3
	+2	1.02E2	3.9E1	1.15E1	3.2E0	6.0E-1	1.1E-1	1.7E-2	2.0E-3
-70	-2	2.6E4	2.3E4	2.0E4	1.8E4	1.7E4	1.3E4	5.6E3	1.4E3
	-1	2.0E4	1.6E4	1.2E4	6.7E3	2.4E3	1.0E3	3.0E2	7.0E1
	0	1.1E4	7.0E3	3.7E3	1.6E3	6.0E2	2.3E2	6.2E1	1.1E1
	+1	5.1E3	2.3E3	1.35E3	5.0E2	2.0E2	6.5E1	1.7E1	3.5E0
	+2	2.1E3	1.05E3	5.0E2	1.9E2	7.0E1	2.2E1	6.7E0	1.7E0
-100	-2	3.3E4	3.2E4	3.10E4	3.0E4	2.9E4	2.6E4	2.4E4	2.1E4
	-1	3.1E4	2.9E4	2.8E4	2.5E4	2.2E4	1.9E4	1.7E4	1.2E4
	0	2.7E4	2.5E4	2.1E4	1.9E4	1.4E4	1.1E4	5.5E3	2.3E3
	+1	2.2E4	1.9E4	1.3E4	9.0E3	6.0E3	3.2E3	1.6E3	7.0E2
	+2	1.5E4	1.0E4	6.1E3	4.9E3	2.4E3	1.1E3	5.0E2	1.9E2

Figure 3. Comparison of stiffness of asphalt obtained manually from nomograph and stiffness of asphalt predicted from regression Eq. 8.

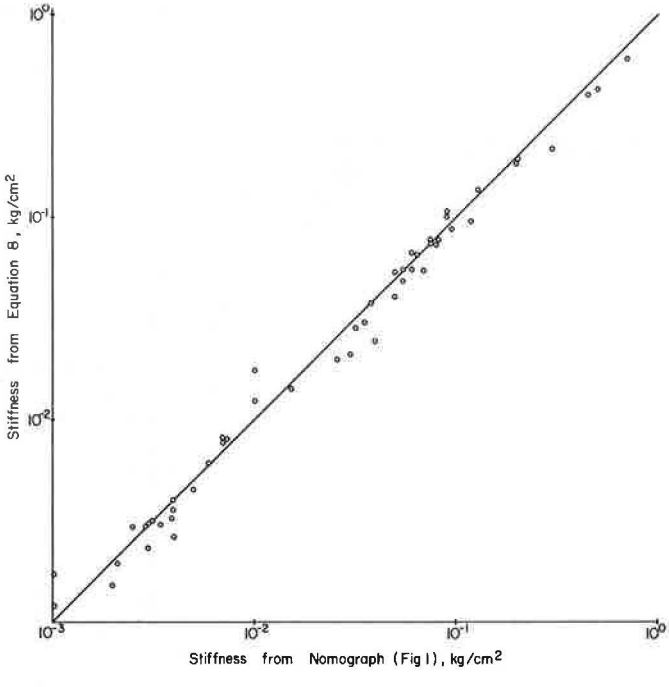

Figure 4. Comparison of stiffness of asphalt obtained manually from nomograph and stiffness of asphalt predicted from regression Eq. 9.

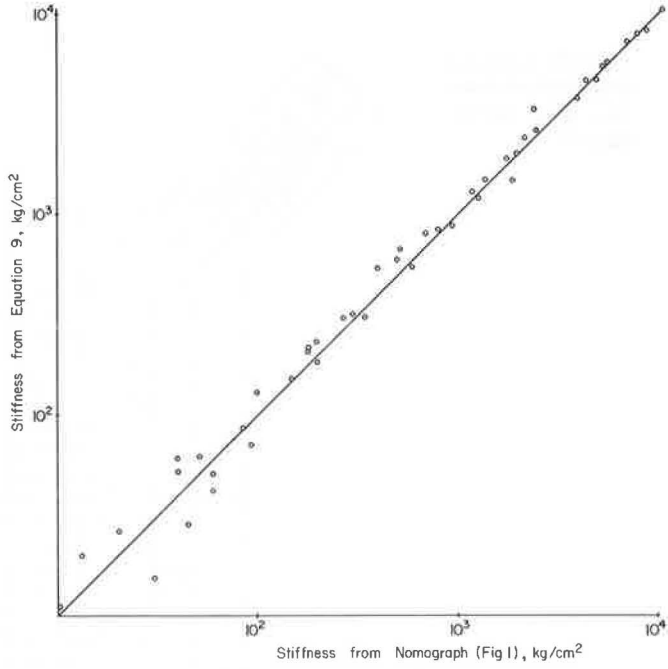

Table 1. Asphalt concrete mixture properties.

Property	Value
Recovered penetration at 77 F, 100 grams, 5 sec	31[a]
Recovered softening point, ring and ball, deg F	132[a]
Percentage of asphalt by weight of aggregate	5.1
Average density of the compacted specimens, lb/ft³	152
Average thermal coefficient of contraction, deg F	1.35×10^{-5}

[a]Estimated.

Figure 5. Measured and assumed asphalt concrete specimen temperatures for thermal stress calculations.

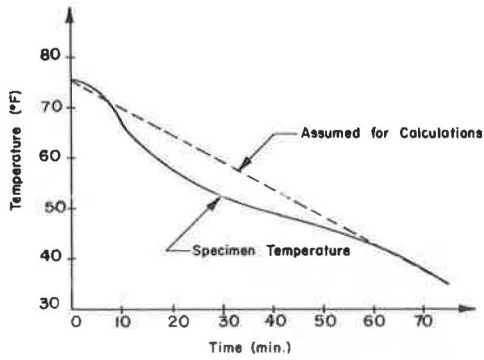

Figure 6. Calculated thermal stresses (in psi).

(Temperature drop 75-35°F, period of 4500 seconds)

Temperature Interval, °F \ Loading Time, seconds	10	100	1000
.04	96.51	34.02	7.18
.4	96.43	34.08	7.25
4.0	96.67	33.55	7.42
5.0	95.72	32.94	7.91
8.0	95.95	33.19	4.91
10.0	94.61	34.66	4.81
20.0	93.16	32.54	4.11
40.0	75.73	11.06	2.37

$$\sigma = \alpha \sum_{T_o}^{T_f} \Delta T \times S(t, \overline{T}_\Delta) \qquad (8)$$

where

α = average coefficient of thermal contraction over the temperature range;
$S(t, \overline{T}_\Delta)$ = stiffness modulus, at the midpoint of the temperature interval ΔT and a loading time t; and
T_o and T_f = initial and final temperatures of the temperature drop.

Figure 7 shows the results of the calculations. The figure seems to indicate the following conclusions:

1. A temperature interval as large as 20 F will result in an acceptable approximation, and
2. The choice of the appropriate loading time is more important than the temperature interval.

Because of the preceding conclusions, a more rational approach for estimating the actual thermal loading time was developed and is summarized as follows:

1. Estimate the average rate of daily pavement temperature drop from U.S. Weather Bureau reports.
2. Experimentally determine the developed thermal stresses in an asphalt concrete beam in a reasonable period of time by subjecting it to the rate of temperature drop estimated in step 1. This can be performed by putting the asphalt concrete beam in an environmental chamber in the laboratory and using the technique described by Monismith et al. (8) or Tuckett et al. (10) or any similar technique.
3. Calculate the developed thermal stress for the same temperature conditions (step 2) by using different loading times.
4. Plot the relation between the loading time and the corresponding thermal stress for the tested asphalt concrete mixture.
5. Find the actual thermal loading time by locating the measured thermal stress (step 2) on the graph (step 4).

The application of the method for the previous example is shown in Figure 8. The thermal stresses were calculated for different loading times at a temperature interval of 4 F. The measured thermal stress, 27.5 psi, was found on the vertical axis, and the actual loading time was estimated as 155 sec. By using this value of loading time, a comparison was made between the calculated and measured thermal stresses (Fig. 9).

In the same figure, the thermal stresses calculated by the conventional method $\left(\text{loading time} = \frac{\text{total time}}{\text{number of intervals}} = 450 \text{ sec}\right)$ are shown.

Figure 9 shows the following:

1. When the difference between the assumed and the actual specimen temperatures is recognized, it is obvious that the agreement between the measured and calculated thermal stresses (based on the proposed method for estimating the thermal loading time) is good. At the beginning of the test, where the actual rate of temperature drop was higher than the assumed value, the observed rate of thermal stresses buildup was also higher than the calculated rate. However, at the end of the test, the reverse was true.
2. The maximum thermal stress calculated by the conventional method is almost half the measured value in this example.

Generally speaking, the conventional method can predict different values of thermal stresses depending on the engineering judgment in choosing the size of the temperature interval.

Figure 7. Maximum thermal stresses for a linear temperature drop of 75 to 35 F in 4,500 sec.

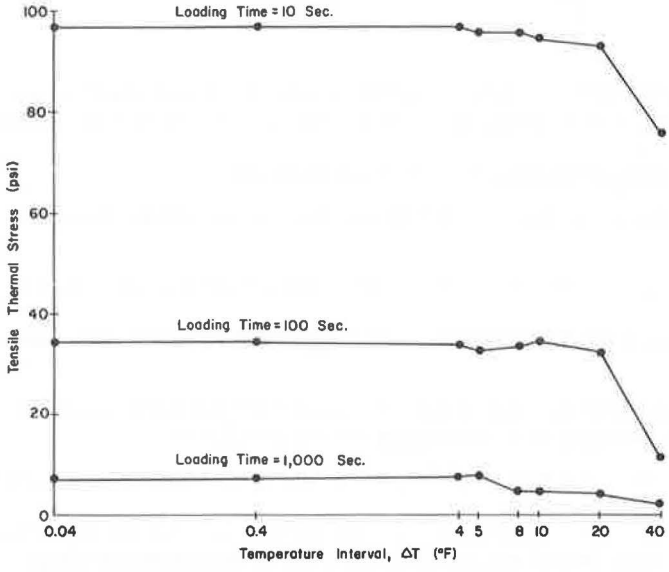

Figure 8. Estimation of the actual thermal loading time.

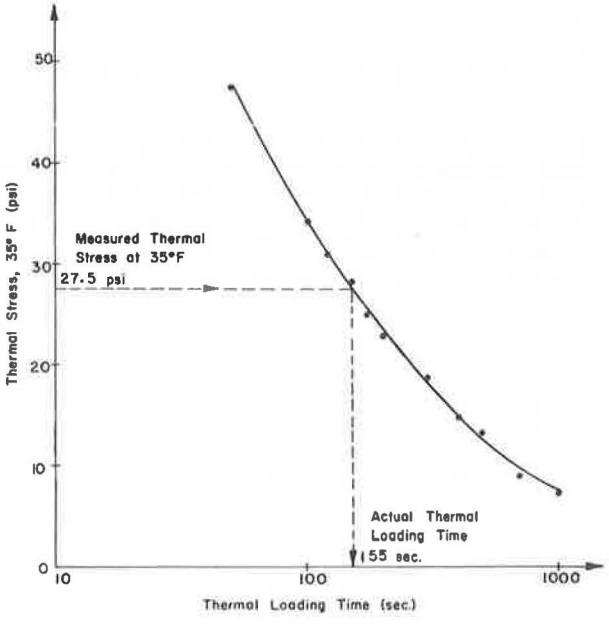

IN-SERVICE AGING OF ASPHALTS

In the previous sections, a model was developed to estimate the stiffness of asphalt, knowing its penetration and softening point. In this section, the history of penetration and softening point is investigated, and models to estimate the aging effect are developed. The intention is to use these models in conjunction with the asphalt stiffness model to estimate the stiffness of asphalt concrete mixtures as a function of temperature, loading time, and age.

Sources of Data Used in Developing the Asphalt Aging Models

In developing the models, a stepwise regression computer program (11) was used. An extensive search was conducted for projects all over the United States where asphalt hardening studies had been conducted. The data from these projects were difficult to correlate and use because different asphalt properties were measured at each one. The locations and the references used in developing the penetration and the softening-point aging models are as follows:

1. Penetration—California (8, 12, 13, 14), Delaware (15), Utah (16, 17), and Pennsylvania (18); and
2. Softening point—California (8, 12, 13, 14) and Delaware (15).

Penetration Aging Model

The purpose of developing the model is to predict the penetration of the in-service asphalt (at any time after construction) from the ordinary laboratory measurements. An acceptable prediction equation was obtained using the stepwise regression technique. The following is the equation with the corresponding statistics:

$$\text{Pen (time)} = -48.258 - 2.561\sqrt{\text{TIME}} + 0.1438\ (\text{OPEN}) - 8.466\ (\text{VOID})\ (\text{XTIME}) + 1.363\ (\text{TFOT}) + 0.9225\ (\text{OPEN})\ (\text{XTIME}) \quad (8)$$

where

time = time placement of the asphalt concrete mixture, months;
XTIME = $1/(\sqrt{\text{TIME}} + 1)$;
OPEN = original penetration, 100 grams, 5 sec, 77 F;
VOID = initial percentage of voids in the asphalt concrete mixture (preferably after mixture placement and compaction); and
TFOT = thin-film oven test, percentage of original penetration.

The corresponding statistics are number of cases, 93; number of variables in the model, 5; mean of the dependent variable (penetration), 49.5; standard error for residuals, 13.1; coefficient of variation, 26.51 percent; multiple R, 0.922; and multiple R^2, 0.85.

This model is valid only for the following ranges of the different variables: time, 1 to 100 months; original penetration, 60 to 240; percentage of voids, 3.8 to 13.6; and TFOT (original penetration < 100), 55 to 70 percent; (original penetration 100 to 175), 45 to 70 percent; and (original penetration > 175), 30 to 70 percent.

The model explains 85 percent of the variability of the dependent variable (penetration).

Also, the model shows a coefficient of variation of 26.5 percent. This value resulted not only from a lack of fit but also from unexplained errors (measured errors, human variations, replications, etc.). Welborn (19) reported that, in some projects where the mean penetration was 46.7, the standard deviation reached 17.6, which gives a coefficient of variation of about 38 percent.

Figure 10 shows the relation between estimated and measured values of penetration for the 93 cases used to predict the model. The effect of the variation of each of the individual factors in the model (Eq. 8) is discussed in the following paragraphs.

With both the initial voids (9 percent) and the TFOT (60 percent) as constants, Figure 11 shows the decrease of penetration with time for five different original penetration values. From the figure, the following observations can be made:

Figure 9. Comparison between measured and estimated tensile thermal stresses.

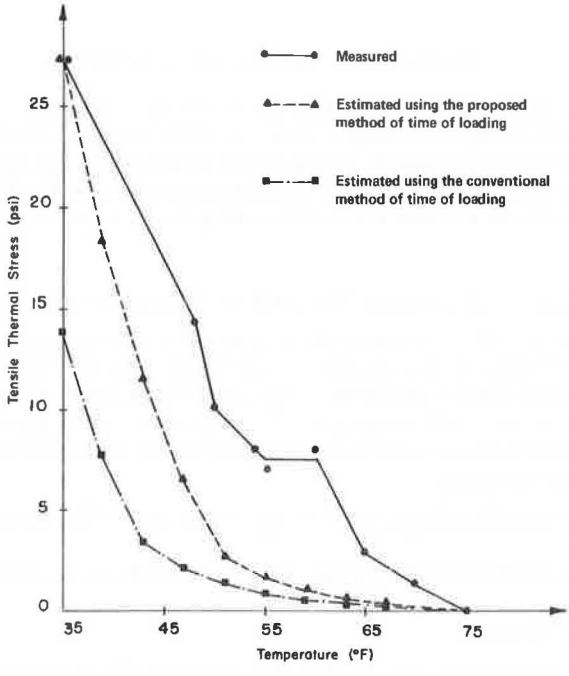

Figure 10. Measured in-service penetration versus predicted values from the penetration model.

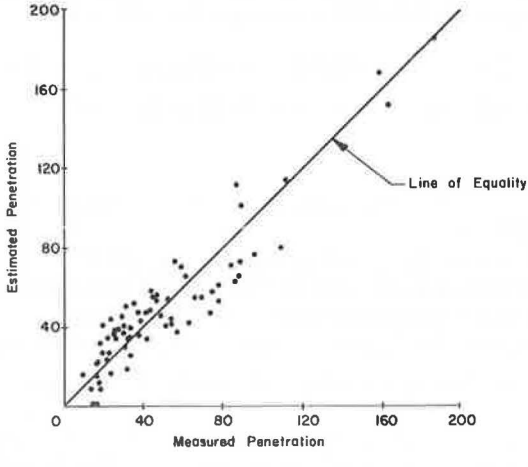

Figure 11. Effect of original penetration on in-service values of penetration as predicted from penetration model.

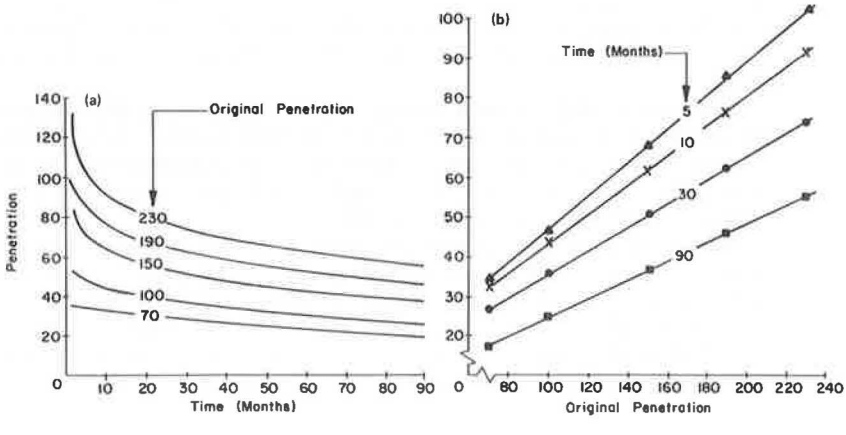

1. The higher the original penetration is, the higher the rate of initial hardening (Fig. 11a) is;
2. The rate of hardening decreases considerably with time for all values of original penetration (Fig. 11a); and
3. The penetration at a given time is a linear function of the original penetration (Fig. 11b).

Based on an original penetration of 100 and a TFOT of 60 percent, Figure 12 shows the effect of five levels of voids on asphalt hardening. The higher the percentage of voids is in the asphalt concrete mixture, the higher is the hardening of the asphalt. Vallerga and Halstead (20) concluded the following: "In pavements of below 2 percent voids, field aging during 11 to 13 years appeared to have been negligible. Above this level, hardening increased with air voids."

Field observations have shown a direct correlation between the percentage of original penetration from the TFOT and the percentage of original penetration after field mixing. In addition, laboratory results from different asphalts have shown that the higher the original penetration is, the lower the percentage of original penetration after the TFOT is. Therefore, the developed penetration model was used to analyze the behavior of two different asphalts having different original penetrations under different TFOT percentages (Fig. 13). As expected, more hardening occurred during the mixing process for asphalts exhibiting a lower percentage of original penetration after the TFOT.

Softening-Point Aging Model

The purpose of this model is to predict the softening point of the in-service asphalt (any time after construction) from the ordinary laboratory measurements. An acceptable prediction equation was obtained using the stepwise regression technique. The following is the equation with the corresponding statistics:

$$TRB\ (TIME) = -4.632 + 3.162\ TIME + 1.585\ (ORB) - 0.93\ (TFOT) \qquad (9)$$

where

TIME = time from placement of the asphalt concrete mixture, months;
ORB = original ring and ball temperature, deg F; and
TFOT = thin-film oven test, percentage of original penetration.

The corresponding statistics are number of cases, 49; number of variables in the model, 3; mean of the dependent variable, 134.4; standard error for residuals, 4.8; coefficient of variation, 3.6 percent; multiple R, 0.93; and multiple R^2, 0.87.

This model is valid only for the following ranges of the different variables: time, 1 to 100 months; original ring and ball temperature, 99 to 125 F; and TFOT, 30 to 70 percent.

With only three variables in the model, the multiple $R^2 = 0.87$ indicates that the model is satisfactory. It can be seen that the voids did not enter the final model, which can be explained by the fact that the 49 cases have percentages of voids that are relatively high.

A plot of measured versus estimated values of the softening point for the 49 cases used to predict the model is shown in Figure 14.

The behavior of the model for different values of each factor in the mathematical equation was studied by programming the model and varying the factors one at a time with the others held constant. Figure 15 shows the increase of softening point with time for three different original softening points (100, 110, and 120 F) and a constant value of TFOT (60 percent).

Figure 16 shows the same concept for three different values of TFOT (40, 50, and 60 percent) and a constant initial softening point (110 F).

Factors Considered But Not Used in the Final Models

For different reasons, several variables were considered but not used in the final models (Eqs. 8 and 9).

Climatography Factors—The following factors were considered: solar radiation on

Figure 12. Effect of five levels of voids on asphalt hardening.

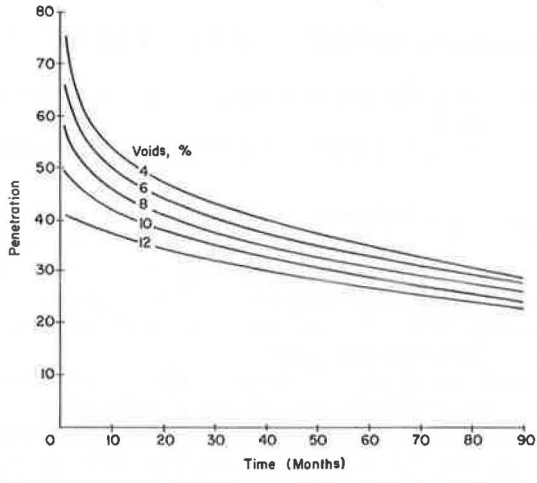

Figure 13. Effect of TFOT on in-service values of penetration as predicted from penetration model.

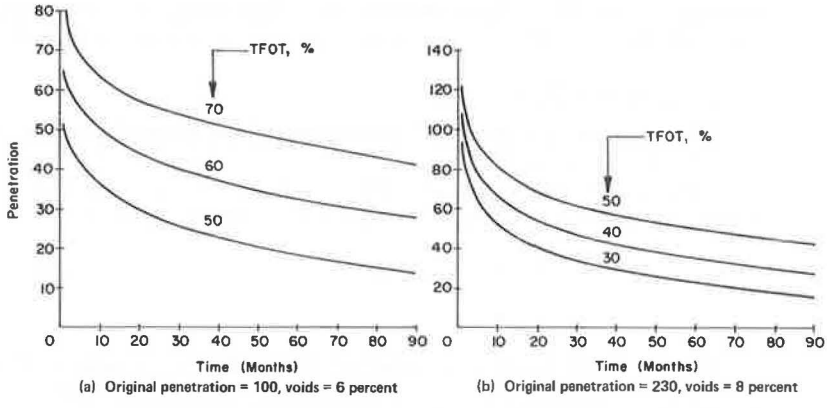

Figure 14. Measured in-service softening point versus predicted values from the softening-point model.

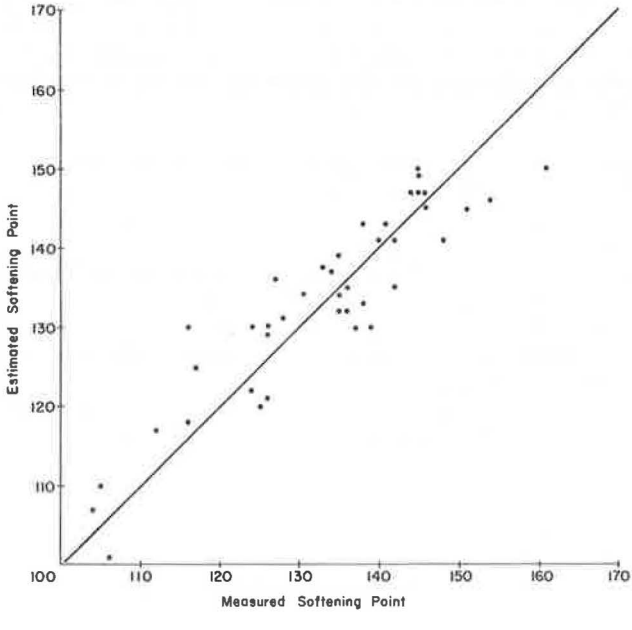

annual basis, wind velocity, number of days > 90 F, average annual temperature, and average annual daily range of temperatures.

The most significant environmental variable that showed a high correlation with asphalt hardening was the solar radiation. However, because of the limited number of geographical locations, it was decided not to include it in the final models, but it should be considered in future investigations.

Inverse Gas-Liquid Chromatography—IGLC is a new technique developed by Davis et al. (21). In this test, the asphalt is absorbed on the surface of an inert support and placed in a chromatography column. Different chemical test compounds are injected individually into the column. Based on the retention time for a nonreactive material of the same molecular weight as the test compound, a parameter known as the interaction coefficient (Ip) is computed. The higher the value of Ip is, the higher is the reaction of the test compound with the asphalt. An extension of this technique was introduced by Davis and Peterson (22). The extension suggests the oxidation of the asphalt in the chromatography column before injecting the chemical test compounds.

In developing both asphalt hardening models (penetration and softening point), Ip resulting from injecting phenol into oxidized asphalt showed extremely high correlation with asphalt hardening. The IGLC test values were not included in the final aging models because of the shortage of test locations where the test was performed. The IGLC is believed to hold a promise for improved prediction of asphalt hardening and thus should be given attention in future research studies.

Asphalt Components—The five components of asphalt are asphaltness A, nitrogen bases N, first "acidaffins" A1, second acidaffins A2, and paraffins P. The ratio $(N + A1)/(P + A2)$ was proposed by Rostler to express the ratio between more reactive components to the less reactive ones. None of the variables showed a significant correlation with asphalt hardening (penetration and softening point). Gotolski et al. (18) concluded the following about asphalt components: "In the overall picture, the asphaltene content or that of any of the other single components does not determine the performance of asphalts."

Percentage of Asphalt—The percentage of asphalt in the asphalt concrete mixture showed a correlation with asphalt hardening whenever it was considered without considering the effect of the percentage of air voids in the mixture. However, whenever the percentage of voids enters the models, the percentage of asphalt loses its significance. This is logical because the percentage of voids and percentage of asphalt are known to be related to each other.

Asphalt Viscosity—Viscosity is not included in final aging models because asphalt viscosities were determined under different conditions for all the projects used to develop the models, and it was difficult to match the viscosity results from all the projects. A specific viscosity test and test conditions should be established and specified for future studies.

Penetration Index—The penetration index suggested by Pfeiffer and Van Doormaal (23) correlated with asphalt hardening. However, because of the limited range of the penetration indexes reported in the different projects, this factor was omitted from the final models.

PREDICTION OF ASPHALT CONCRETE STIFFNESS

The usefulness of the system can be shown by estimating the asphalt concrete stiffness at the normal monthly average air temperatures, for a period of 5 years (starting from the month of July), for the cities of El Paso and Los Angeles. It should be noted that using the air temperature for the calculations is misleading because the asphalt concrete temperature is different from the air temperature (1). However, the purpose of this example is to illustrate the use of the system only.

The asphalt concrete properties and loading time used for the calculations are given in Table 2. The normal monthly average air temperatures for the cities of El Paso and Los Angeles are given in Table 3. Figure 17 shows the results of the calculations, from which one may conclude the following:

1. There is a sudden increase in the modulus during the first month, mainly because

Figure 15. Effect of original softening point on in-service values of softening point as predicted from softening-point model.

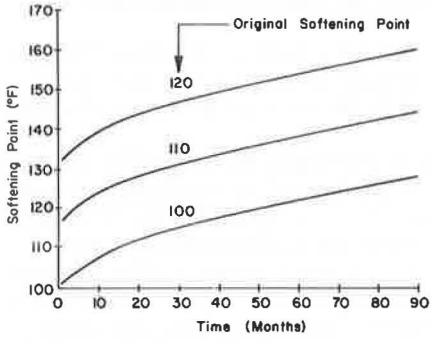

Figure 16. Effect of TFOT on in-service values of softening point as predicted from softening-point model.

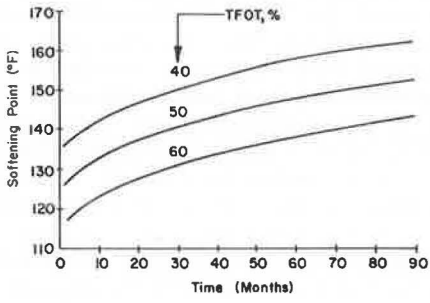

Table 2. Assumed asphalt concrete mixture properties and loading times.

Property	Value
Original penetration at 77 F, 100 grams, 5 sec	95
Original softening point, deg F	115
Percentage of original penetration after TFOT	60
Percentage of air voids	5
Volume of concentration of the aggregate	0.87
Time of loading, sec	100

Table 3. Normal monthly average temperatures.

City	July	Aug.	Sept.	Oct.	Nov.	Dec.	Jan.	Feb.	Mar.	April	May	June
El Paso	81.9	80.4	74.5	64.4	51.2	44.1	42.9	49.1	54.9	63.4	71.9	81.0
Los Angeles	69.1	69.1	68.5	64.9	61.6	56.9	54.4	55.2	57.0	59.4	62.0	64.8

Figure 17. Example of the variation of the monthly average asphalt concrete stiffness as estimated from the system.

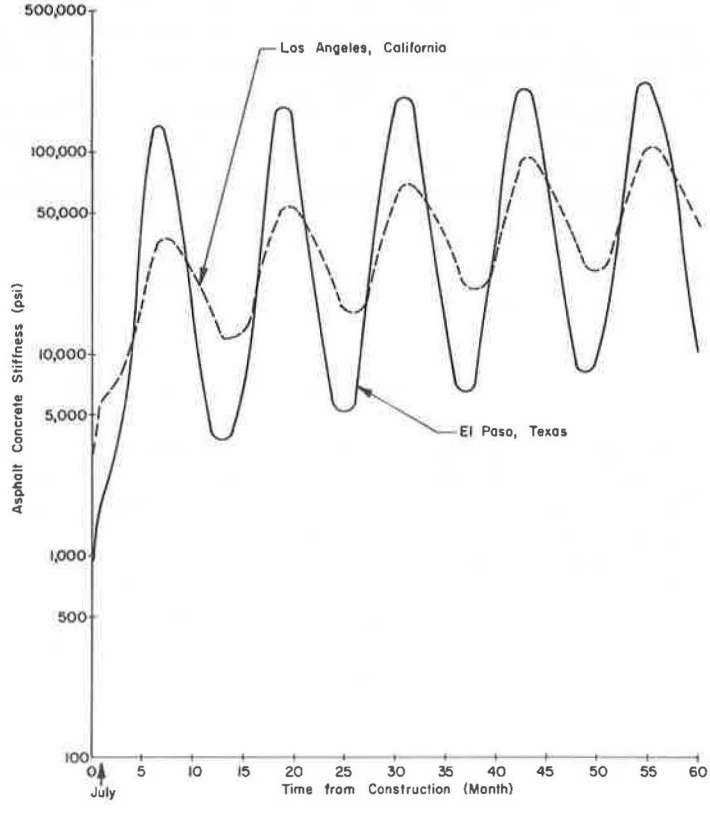

of the hardening of asphalt that occurs during the mixing process;

2. The range of the annual stiffness variation is different among locations, depending on the annual temperature range;

3. Considering a single stiffness value for the purpose of design of an asphalt concrete surface is inadequate;

4. Because low stiffness is the most critical for traffic loads, the asphalt concrete stiffness during the first July after construction is the one to be considered; and

5. Because high stiffness is the most critical for temperature, the asphalt concrete stiffnesses during December and January, several years from construction, are the ones to be considered.

SUMMARY AND RECOMMENDATIONS

In this research effort, a system for predicting asphalt concrete stiffness history has been developed. The main constituents of the system are the asphalt concrete stiffness and aging models. The objective of the system is to help analyze the different modes of distress in asphalt concrete surfaces. The system has been utilized in predicting low-temperature and thermal-fatigue cracking due to daily temperature cycling (1), and it has shown a good degree of reliability.

In addition, it is recommended that the system be used in conducting the following studies:

1. The establishment of a rational specification for asphalt concrete mixture design,

2. The provision of a tool to differentiate among the different asphalt sources in a particular location, and

3. The advancement of the fatigue distress studies due to traffic loads (24).

ACKNOWLEDGMENTS

This investigation was conducted at the Center for Highway Research, University of Texas at Austin. The authors wish to thank the sponsors, the Texas Highway Department and the Federal Highway Administration, U.S. Department of Transportation.

The contents of this report reflect the views of the authors, who are responsible for the facts and the accuracy of the data presented herein. The contents do not necessarily reflect the official views or policies of the Federal Highway Administration. This report does not constitute a standard, specification, or regulation.

REFERENCES

1. Shahin, M. Y. Prediction of Low-Temperature and Thermal-Fatigue Cracking in Flexible Pavements. Univ. of Texas at Austin, PhD dissertation, Aug. 1972.
2. Van der Poel, C. A General System Describing the Viscoelastic Properties of Bitumens and Its Relation to Routine Test Data. Jour. of Applied Chemistry, Vol. 4, May 1954.
3. Pell, P. S., and McCarthy, P. F. Amplitude Effect of Stiffness of Bitumen and Bituminous Mixes Under Dynamic Conditions. Rheologia Acta, Vol. 2, No. 2, 1962.
4. Monismith, C. L. Asphalt Mixture Behavior in Repeated Flexure. Univ. of California, Berkeley, IER Rept. TE-65-9, Nov. 1965.
5. Heukelom, W., and Klomp, A. J. G. Road Design and Dynamic Loading. Proc., AAPT, Vol. 33, Feb. 1964, pp. 92-125.
6. Van Draat, W. E. F., and Sommer, P. Ein Gerat zur Bestimmung der Dynamischen Elastizitattsmoduln von Asphalt. Strasse und Autobahn, Vol. 35, 1966.
7. Draper, N. R., and Smith, H. Applied Regression Analysis. John Wiley and Sons, New York, 1966.
8. Monismith, C. L., Secor, G. A., and Secor, K. E. Temperature Induced Stresses and Deformations in Asphalt Concrete. Proc., AAPT, Vol. 34, Feb. 1965, p. 248.
9. Hills, J. F., and Brien, D. The Fracture of Bitumens and Asphalt Mixes by Temperature Induced Stesses. Proc., AAPT, Vol. 35, Feb. 1966, p. 292.
10. Tuckett, G. M., Jones, G. M., and Littlefield, G. The Effects of Mixture Variables

on Thermally Induced Stresses in Asphaltic Concrete. Proc., AAPT, Vol. 39, Feb. 1970, p. 703.
11. STEP-01: Statistical Computer Program for Stepwise Multiple Regression. Center for Highway Research, Univ. of Texas at Austin, 1968.
12. Hveem, F. N., Zube, E., and Skog, J. Progress Report on the Zaca-Wigmore Experimental Asphalt Test Project. Symposium on Paving Materials, ASTM, Spec. Tech. Publ. 277, 1959, pp. 3-45.
13. Skog, J. Results of Cooperative Test Series on Asphalts From the Zaca-Wigmore Experimental Project. Symposium on Paving Materials, ASTM, Spec. Tech. Publ. 277, 1959, pp. 46-51.
14. Zube, E., and Skog, J. Final Report on the Zaca-Wigmore Asphalt Test Road. Presented to Materials and Research Dept., California Division of Highways, 1959.
15. Kenis, W. J., Sr. Progress Report on Changes in Asphaltic Concrete in Service. HRB Bull. 333, 1962, pp. 39-65.
16. Beteson, W. B. Rubber in Asphalt, Field and Laboratory Performance Testing. Internat. Symposium on the Use of Rubber in Asphalt Pavements, Salt Lake City, May 1971.
17. Liddle, W. J., Jones, G. M., Peterson, D. E. Use of Synthetic Rubber-in-Asphalt Pavement to Determine Mixture Behavior and Pavement Performance. Materials and Tests Div., Utah State Highway Department, Interim Rept., Dec. 1969.
18. Gotolski, W. H., Ciesielski, S. K., and Heagy, L. N. Progress Report on Changing Asphalt Properties of In-Service Pavements in Pennsylvania. Proc., AAPT, Vol. 33, Feb. 1964, pp. 285-319.
19. Welborn, J. Y. Asphalt Hardening: Fact and Fallacy. Public Roads, Vol. 35, No. 12, Feb. 1970, pp. 279-285.
20. Vallerga, B. A., and Halstead, W. J. Effects of Field Aging on Fundamental Properties of Paving Asphalts. Highway Research Record 361, 1971, pp. 71-92.
21. Davis, T. C., Peterson, J. C., and Haines, W. E. Inverse Gas-Liquid Chromatography: A New Approach for Studying Petroleum Asphalts. Analytical Chemistry, Vol. 38, No. 2, Feb. 1966, pp. 241-243.
22. Davis, T. C., and Peterson, J. C. An Adaptation of Inverse Gas-Liquid Chromatography to Asphalt Oxidation Studies. Analytical Chemistry, Vol. 38, No. 13, Dec. 1966, pp. 1938-1940.
23. Pfeiffer, J. P., and Van Doormaal, P. M. The Rheological Properties of Asphaltic Bitumen. Jour. Institute of Petroleum Technology, Vol. 22, 1936.
24. Jain, S. P., McCullough, B. F., and Hudson, W. R. Flexible Pavement System—Second Generation, Incorporating Fatigue and Stochastic Concepts. Texas Highway Department; Texas Transportation Institute, Texas A&M Univ.; and Center for Highway Research, Univ. of Texas at Austin, Res. Rept. 123-10, Dec. 1971.

LAYER ANALYSIS OF THE BRAMPTON TEST ROAD AND APPLICATION TO PAVEMENT DESIGN

Nabil I. Kamel and W. Phang, Ministry of Transportation and Communications, Ontario; and
Jack Morris and R. C. G. Haas, University of Waterloo, Ontario

Considerable attention has been devoted, during the past decade, to developing a pavement design system based on structural analysis concepts. The implementation of a design system requires a structural model that will calculate the serviceability-age history of various alternative strategies. Consequently, it is essential to relate the structural analysis outputs of stresses, strains, and deflections to the subsequent performance of the pavement under different traffic and environmental conditions. One objective of a recent study of the Brampton Test Road was to develop these relations for conditions in southern Ontario. BISTRO and CHEVRON computer programs were used in iterative procedures to calculate pavement structural response of stresses, strains, and deflections of each of the Brampton Test Road sections. The moduli values required for the analysis were derived from laboratory test data provided by The Asphalt Institute. These calculated structural responses were then correlated to observed pavement behavior and performance measurements of the test sections. Charts to predict serviceability losses as a function of traffic, type of base material, and vertical stress level on subgrade surface are developed. A good relation is found between the measured Benkelman beam rebounds and calculated subgrade surface deflection. Equivalencies of various types of base materials are developed based on equal loss of serviceability. Finally, the paper presents a structural design system for flexible pavements based on use of layered analysis techniques. It also discusses, through an example problem, how this fits into overall pavement management systems.

•THE development of comprehensive pavement design and management systems has received considerable attention in Canada and the United States during the past few years (1-12). Currently, authorities in Texas, Ontario, and other jurisdictions are attempting to implement working systems of pavement management (1-3).

A major component of any pavement management system is the structural design phase. Here, the primary outputs that must be predicted by the designer are performance (i.e., serviceability-age history) and the associated cost and benefit implications, as shown in Figure 1. The structural analysis outputs of stress, strain, and deformation must then be linked with serviceability history. Today, a fundamental method of predicting pavement performance under different traffic and environmental conditions is needed.

In southern Ontario, the Brampton Test Road was constructed in 1965 primarily to compare the performance of a variety of base materials. Extensive data on material properties, traffic, climate, and performance were available (13-17). Hence a unique opportunity was provided to relate structural response and performance in a controlled experiment over a period of time. As a result, an investigation (18, 19) was undertake

Publication of this paper sponsored by Committee on Theory of Pavement Design.

to determine whether structural analysis could be used to predict the serviceability-age histories of the various pavement designs used at Brampton Test Road. The purpose of this paper is to report the findings of this investigation. More specifically it reports the following:

1. The basic material characteristics required for a structural method of analysis;
2. The analysis of stresses, strains, and deflections for the Brampton test sections employing computerized, non-linear-elastic layered techniques;
3. The relations between the structural responses obtained in step 2 and the observed behavior and performance;
4. The establishment of equivalencies for the Brampton materials, based on the criterion of equal terminal serviceability; and
5. The application of the results obtained in steps 3 and 4 to a pavement design and management system.

STRUCTURAL ANALYSIS OF THE BRAMPTON TEST ROAD

Structural Analysis Model

Since the 1960 AASHO Road Test, pavement researchers have devoted considerable attention to developing a "rational" method of pavement design based on stresses, strains, and deflections throughout the pavement system. Ideally, the constitutive equations of the materials should be determined and the pavement modeled accordingly. Up to the present time, it has not been possible to follow this approach because of the complex nature of the pavement structure. The current situation has been summarized by Morris, Kamel, and Haas (20). It is concluded that a non-linear-elastic layered solution is the most convenient and reliable means of obtaining the structural responses within a pavement system. In this study, CHEVRON and BISTRO multilayered elastic computer programs were employed, and iterative procedures were used to account for the nonlinear characteristics of the materials.

Material's Characterization

The Brampton Test Road was constructed during August and September 1965 as a full-scale experiment. Details of the project construction, objectives, and principal findings to date are presented elsewhere (13-15). The experiment consists of 36 test sections and incorporates five types of base as shown in Figure 2.

Repeated load triaxial compression tests on the unbound and stabilized materials were conducted by The Asphalt Institute (16, 17). During the testing, appropriate ranges of temperature, stress, moisture content, density, etc., were selected to simulate the field conditions.

The test sections composed of cement-treated bases suffered from shrinkage fracture early in the experiment and were not considered in this investigation.

The elastic response of unbound and emulsion stabilized materials can be described by the resilient modulus, M_R (21, 22), the ratio of the repeated deviator stress to the rebound or recoverable axial strain. The characteristics of the unbound materials based on The Asphalt Institute's test are shown in Figure 3. In keeping with previous research workers (23, 24), M_R is shown as a function of deviator stress, σ_d, for the clay subgrade and of confining stress, σ_3, in the case of the granular materials. The results of the repeated load triaxial tests on the bituminous stabilized sand at three test temperatures are shown in Figure 4.

The response of an asphaltic material is generally described by the stiffness modulus, S, as defined by Van der Poel (25). This parameter can be obtained either by "direct" means from laboratory measurements or by "indirect" methods based on Van der Poel's nomograph and its modifications (9). For this study, indirect estimation of stiffness was employed using McLeod's modified method (26). The stiffness-temperature relations obtained, based on a loading time of 0.03 sec, which corresponds to traffic moving at 60 mph (27), are shown in Figure 5.

Asphalts are thermoplastic materials; i.e., their stress and strain responses under load are time- and temperature-dependent. Consequently, the structural response of a

Figure 1. Gross output of pavement system in terms of performance and value.

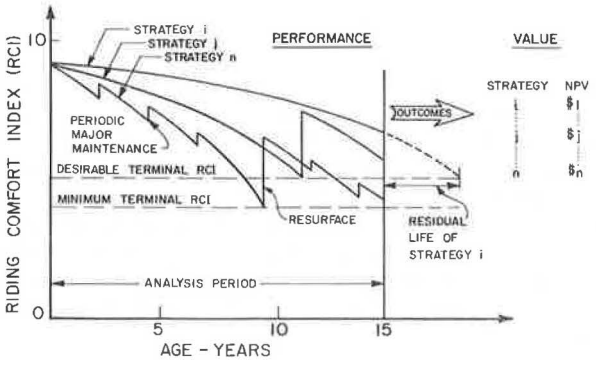

Figure 2. Layout of experimental pavement sections.

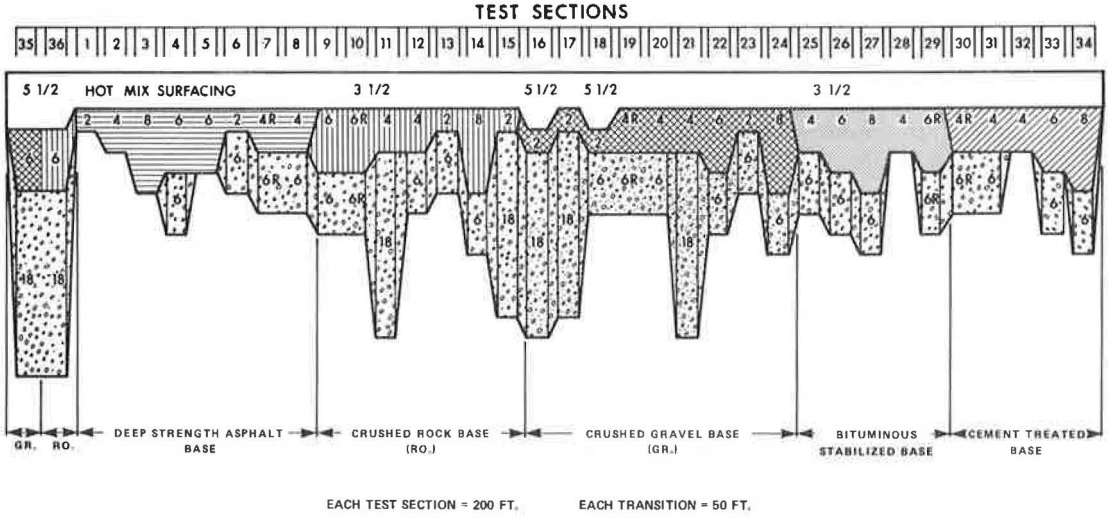

EACH TEST SECTION = 200 FT. EACH TRANSITION = 50 FT.

LEGEND

R. = REPLICATED (I.E. DUPLICATED DESIGN)

GR. = CRUSHED GRAVEL BASE

RO. = CRUSHED ROCK BASE

Figure 3. Resilient moduli of Brampton unbound materials.

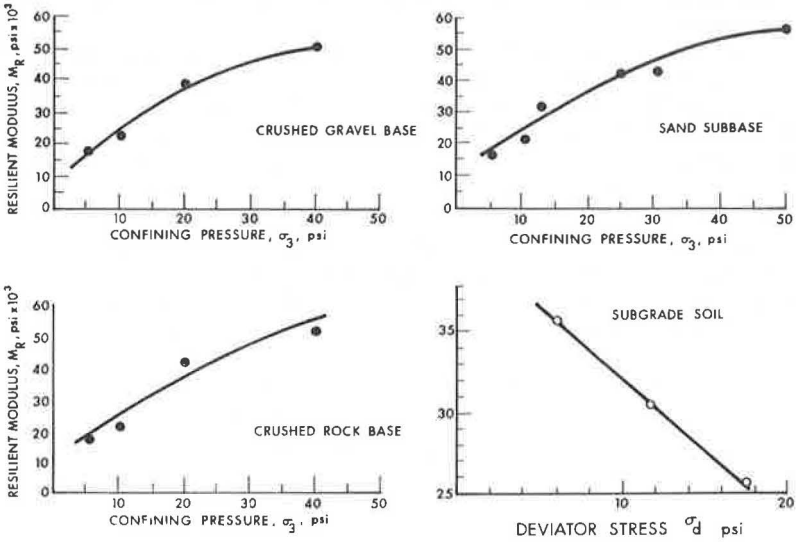

pavement depends on the temperature distribution within the asphaltic concrete. In recent years, considerable effort has been devoted toward developing realistic models for the determination of temperature distribution within asphaltic concrete pavements (28-30). Southgate's approach (28), which appears to give reasonable results and is easy to apply, was adopted for this investigation.

An earlier study (15) indicated that the pavement of the Brampton Test Road is at its annual weakest condition in the month of June. The average maximum air temperature in June (70 F) was used to determine the temperatures at middepth of the asphaltic concrete surface, binder, and base courses. The corresponding stiffness modulus for each layer was then obtained from Figure 5.

Structural Analyses

The structural analyses of the Brampton test sections were performed primarily by means of the CHEVRON computer program. This approach assumes that each layer is composed of linear-elastic and homogeneous material; but, as shown in the previous section, the moduli of unbound and stabilized materials are stress-dependent. This difficulty can be overcome by using an iterative process as follows:

1. Assume moduli for the layers,
2. Calculate the horizontal and vertical stresses at the middepth of the base and subbase and those at the surface of the subgrade,
3. Use the calculated stresses in step 2 to get the corresponding M_R value for each layer using the material characterization curves shown in Figure 3,
4. Compare the assumed values of M_R in step 1 with the calculated values in step 3, and
5. Repeat the previous steps until the assumed and calculated values of the moduli are approximately equal.

CHEVRON does not provide subgrade strains, so BISTRO was employed for this calculation. The results are given in Table 1.

STRUCTURAL ANALYSIS-PAVEMENT PERFORMANCE RELATIONS

Pavement Serviceability and Performance

This section first considers pavement serviceability and performance in general terms and then considers the performance of the Brampton sections.

The best-known procedure for defining and obtaining serviceability was developed at the AASHO Road Test by Carey and Irick (10). Their concept of present serviceability rating (PSR) explicitly recognized the road user by means of a panel rating procedure. PSR was then correlated to a set of physical measurements called present serviceability index (PSI). The integration of PSI over time or load applications was termed the performance.

The Roads and Transportation Association of Canada (RTAC, formerly the Canadian Good Roads Association) concurrently developed the present performance rating (PPR) along similar lines except that it used a 10-point rather than a 5-point scale (31, 32). In 1968, the Pavement Management Committee of RTAC changed the term PPR to riding comfort index (RCI) (33). The new term recognized that serviceability is only an evaluation of riding comfort quality and does not include structural condition or safety characteristics. RCI is employed throughout this paper.

Attempts to model RCI in Canada have not been highly successful. At Brampton, RCI was estimated from correlations between RCI and a roughness index profilometer patterned after the British Road Research Laboratory design (34, 35). A typical set of RCI-time relations obtained by this method is shown in Figure 6.

RCI-Traffic-Vertical Stress on Subgrade Relations

The observed performance, in terms of annual RCI values, is related to calculated structural response, in particular the vertical stress on subgrade surface, σ_v. Vertical subgrade stress has been used as the principal structural response variable because

Figure 4. Resilient modulus-confining pressure relation for bituminous-stabilized sand.

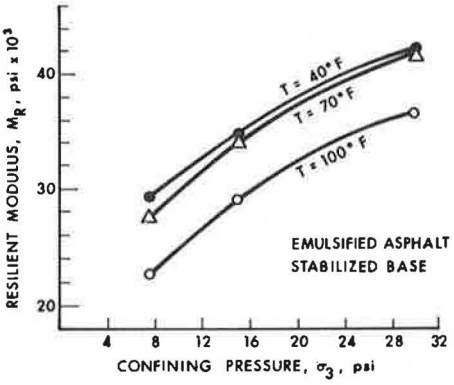

Figure 5. Asphalt concrete stiffness moduli-temperature relations.

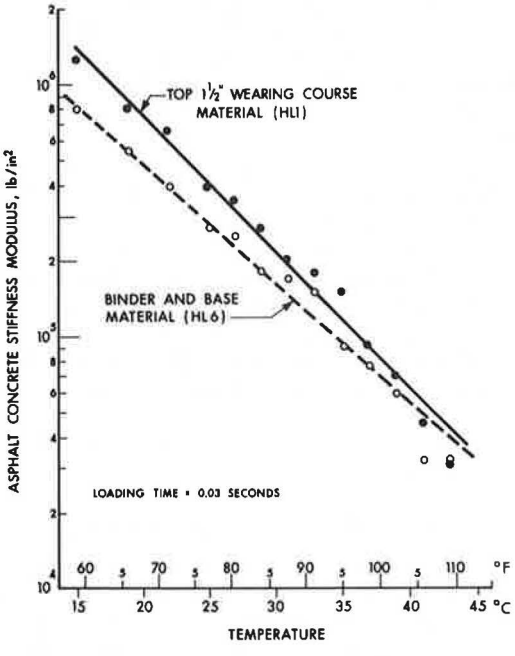

Table 1. Summary of results of layer analyses.

Section Number	Base	Subbase	Surface Deflection (in.)	Subgrade Deflection (in.)	Vertical Stresses on Subgrade Surface (psi)	Vertical Strain on Subgrade Surface (in./in. x 10^{-3})
1	Full-depth asphalt concrete	None	0.0183	0.0172	30.3	0.917
2			0.0134	0.0120	20.7	0.609
3			0.0096	0.0074	12.0	0.292
5			0.0104	0.0088	14.6	0.398
4	Deep asphalt concrete	6-in.	0.0103	0.0064	9.32	0.229
6			0.0172	0.0110	18.00	0 573
7, 8			0.0128	0.0083	12.90	0.352
9, 10	Crushed rock	6-in.	0.0241	0.0095	14.90	0.505
12			0.0226	0.0108	17.20	0.601
13			0.0240	0.0133	20.60	0.792
14			0.0236	0.0083	12.60	0.405
11	Crushed rock	18-in.	0.0249	0.0053	7.04	0.205
15			0.0232	0.0056	8.07	0.227
36			0.0211	0.0046	5.28	0.148
16	Crushed gravel	18-in.	0.0208	0.0053	6.71	0.187
17			0.0227	0.0056	8.04	0.225
21			0.0278	0.0056	7.30	0.214
35			0.0216	0.0047	5.37	0.150
18	Crushed gravel	6-in.	0.0181	0.0099	15.40	0.499
19, 20			0.0240	0.0109	17.50	0.629
22			0.0247	0.0090	14.70	0.580
24			0.0223	0.0080	12.50	0.384
25	Bituminous-stabilized	6-in.	0.0210	0.0102	16.70	0.561
26, 29			0.0211	0.0086	13.40	0.429
27			0.0200	0.0076	11.70	0.342
28	Bituminous-stabilized	None	0.0241	0.0189	28.60	1.230

Note: Using 9-kip single wheel load acting uniformly over a circular area of about 12 in. in diameter. Poisson's ratio of approximately 0.4 was assumed.

it is a good indicator of pavement load-carrying capacity; it also appears to give the best relations. The results indicate that the test sections can be classified into four groups: full-depth asphaltic concrete sections; asphalt concrete base sections that include subbase materials, i.e., deep-strength construction; granular base sections involving crushed-rock and crushed-gravel bases, i.e., conventional construction; and bituminous stabilized base sections.

Typical results, those obtained for the granular base sections, are shown in Figure 7. These RCI-σ_v-age relations can be drawn in a more meaningful form by plotting RCI-age (or traffic) curves for various levels of σ_v. The results for the four pavements are shown in Figure 8. The relations demonstrate the effect of σ_v on the serviceability history. It can be seen that RCI decreases more rapidly as the vertical stress on the subgrade surface increases. The rate of the decrease depends on the pavement type. The full-depth sections are the least sensitive to increasing in σ_v, and the bituminous stabilized base sections are the most sensitive.

These relations can be used to develop loss of performance curves for the various levels of σ_v. If normal scales are employed, good linear relations, as shown in Figure 9, are obtained. If the lines are extended to the left, then for each pavement type a different but relatively constant serviceability loss occurs at zero load applications. This loss is to be expected because of the effects of climate, foundation movements, and aging.

RCI-Traffic-Benkelman Beam Rebound Relations

The Benkelman beam has been used for many years as a means of measuring the in situ structural response of a pavement to load, and considerable technology has been developed on the basis of the method (1, 31). The Ontario pavement management system (1) employs structural design models that are derived principally from Benkelman beam experience.

Figure 10 shows the good correlations obtained between calculated subgrade surface deflections and measured initial mean peak Benkelman beam rebounds. Two distinct patterns emerge—one for the full-depth sections and the other for the remaining pavement types.

A complete description of this phase of the analysis is given elsewhere (36, 37). Briefly, a linear relation between log RCI and accumulated equivalent 18-kip single-axle loads for various Benkelman beam rebounds was found. Charts that predict performance loss as a function of traffic, type of base material, and pavement strength, as indicated by Benkelman beam rebound, have been developed (37). The type of model obtained in this analysis agrees with that obtained by Painter (38) when analyzing AASHO pavements of various strengths. It was also found that, for all pavement types other than the full-depth sections, sections with an initial peak rebound of 0.05 in. should lose 4.0 units of RCI after some 0.5 million applications of equivalent 18-kip single-axle loads. This result agrees with the findings of the CGRA after an extensive study of Canadian roads (31).

DEVELOPMENT OF BASE LAYER EQUIVALENCIES

The concept of layer equivalency is an integral part of design procedures currently employed by a number of agencies, including the Ministry of Transportation and Communications, Ontario. The RCI-age (or traffic)-vertical subgrade stress relations, previously developed, were therefore utilized as a basis for evaluating the equivalencies of various types of bases.

Basic Criterion

In the past, the equivalencies of various materials have generally been based on equal structural response (e.g., stresses, strains, deflections, etc.). Phang (15) for example established the equivalencies of the Brampton base materials on the basis of a peak Benkelman beam deflection of 0.05 in. Pavement deflection varies with age (1), and therefore equivalencies based on this criterion are also time-dependent. Further-

Figure 6. Time relations for typical Brampton RCI.

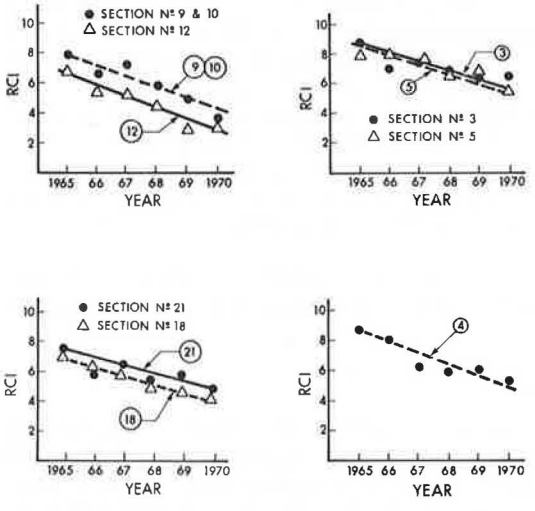

Figure 7. RCI and vertical compressive stresses on subgrade surface for crushed-rock and crushed-gravel base sections.

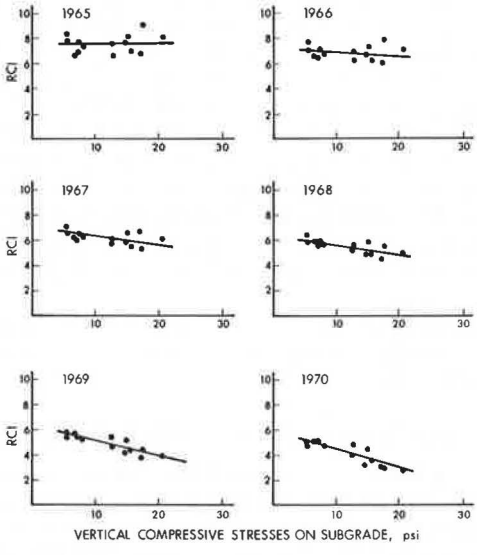

Figure 8. Performance history of Brampton base materials at various vertical stresses on subgrade surface.

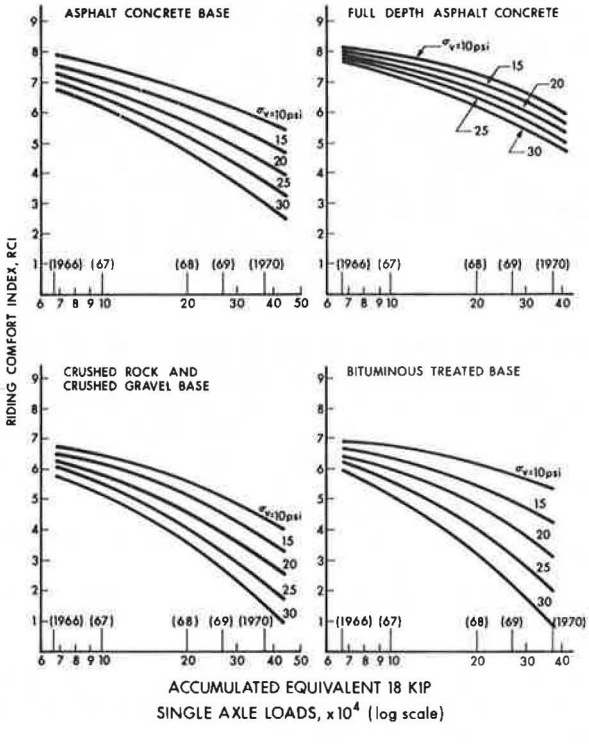

more, pavement strength does not vary proportionately with thickness; therefore, if the deflection criterion is varied from 0.05 in. to, say, 0.02 or 0.10 in., significantly different equivalencies may be found.

In this study, the serviceability-age relations of the Brampton sections have been established in terms of the vertical stresses on the subgrade surface. Therefore, equivalencies can be developed on the basis of equal terminal serviceability. This criterion seems to be more realistic because pavement performance must be the end concern. Equivalencies based on this criterion enable the engineer to generate thickness combinations without having to consider the problem of strength differences.

Equivalencies based on terminal serviceability, however, may also vary depending on the level of terminal serviceability selected. The philosophy of varying the terminal RCI with the function or class of the pavement has been discussed in detail by Haas, Kamel, and Morris (37). Three terminal serviceability levels, 5.5 for major highways and freeways, 4.5 for secondary highways, and 3.5 for township roads, are recommended.

The data available at this time only permit the development of equivalencies for secondary highways, i.e., a terminal serviceability of 4.5 as represented by the Brampton Test Road.

Layer Equivalencies for Secondary Highways

A terminal serviceability of 4.5 has been recommended for secondary highways (37). The initial RCI of most newly constructed pavements lies between 8 and 9. If the initial RCI is assumed to be 8.5, then the basic criterion can be considered as a loss of RCI equal to 4.0. Figure 9 shows RCI loss-traffic relations for various stress levels and pavement types. A horizontal line corresponding to an RCI loss of 4.0 has been drawn, and the lines of different stress levels, σ_v, have been extended to intersect this basic criterion line. The points of intersection provide the relations between accumulated equivalent 18-kip single-axle loads and vertical stresses on the subgrade for a loss of 4.0 units of RCI. The results obtained for each type of base are shown in the upper portion of Figure 11. In constructing the relation for the bituminous stabilized base, a very large accumulated traffic number was found at the 10-psi level. This point resulted from considerable extrapolation and therefore was neglected when the curve was drawn. The lower part of Figure 11 shows the relation between stress level and equivalent base thickness (i.e., actual base thickness plus transformed subbase) for each pavement type. Subbase thicknesses have been converted into equivalent base thicknesses, using the following equivalencies suggested by Phang (14): 1 in. of subbase = 0.57 in. of granular base = 0.57 in. of bituminous stabilized base = 0.23 in. of asphalt concrete base.

The relations shown in Figure 11 are based on sections that have a constant thickness of asphalt concrete surface equal to $3\frac{1}{2}$ in.

Canadian studies (31) show that secondary pavements may reach a terminal RCI of 4.5 after 0.5 million applications of equivalent 18-kip single-axle loads. The Brampton Test Road provides similar evidence. If the upper portion of Figure 11 is entered at 0.5 million load applications, then the stress levels corresponding to 4.0 units of RCI loss can be determined. The example shown in Figure 11 indicates that a granular base pavement will lose 4.0 units of RCI if the subgrade surface is stressed to 7.5 psi. The lower portion of Figure 11 can then be used to determine the corresponding equivalent base thickness. For the example considered, 13.5 in. of base thickness is required to maintain a subgrade surface stress of 7.5 psi. The equivalent base thicknesses for other pavement types are 12.5 in. of bituminous stabilized base, 6.7 in. of asphalt concrete base (with subbase), and 4.0 in. of asphalt concrete (without subbase, i.e., full depth). The equivalencies based on these results are given in Table 2.

The values obtained are very close to those employed by the Ministry of Transportation and Communications of Ontario at the present time, except for the full-depth asphalt concrete. Here, the superior behavior of the asphaltic concrete base without subbase is reflected in a granular base equivalency of 3.4 compared to 2.0 when the subbase was included.

Figure 9. Loss of RCI for various base materials and vertical stresses on subgrade surface.

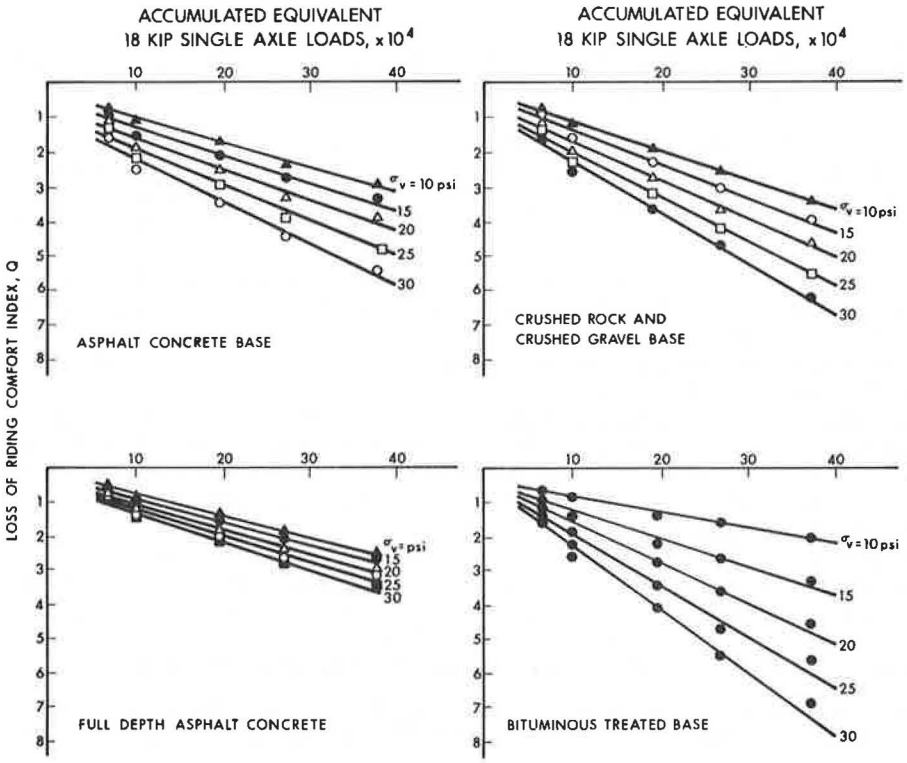

Figure 10. Calculated subgrade surface deflections and measured initial mean-peak Benkelman beam rebounds.

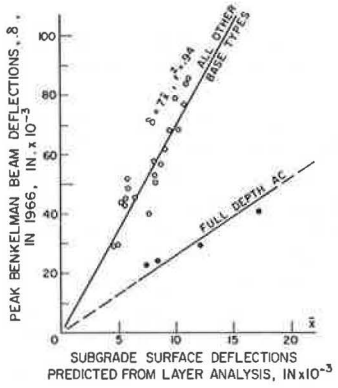

Figure 11. Brampton Test Road materials relations.

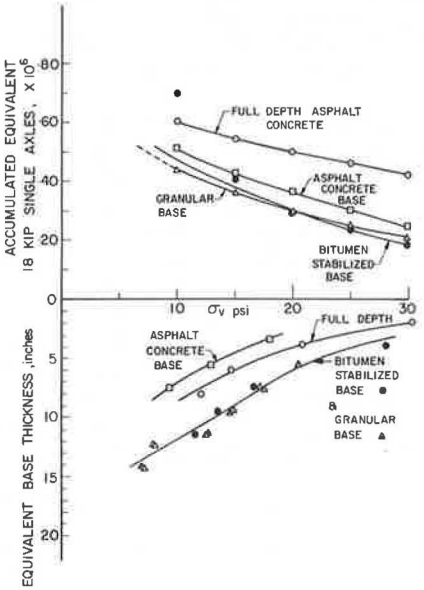

APPLICATION OF RCI-AGE (OR TRAFFIC) RELATIONS TO THE PAVEMENT DESIGN SYSTEM

In the previous section, it was shown that the RCI-age (or traffic) relations for various pavement strategies involving Brampton materials could be based on two approaches: the calculated vertical stress on the subgrade surface and the initial peak Benkelman beam rebound (37).

The application of these results to a pavement design system is shown in Figure 12. The diagram shows a simplified flow chart of the major steps required in the design process and includes the two alternative approaches. The method employed for a particular design situation should be governed primarily by the size and importance of the project.

The second approach, based on Benkelman beam rebound, will not be detailed here. The method has been developed to give a set of "second-generation" structural models for the Ontario pavement management system (1) and is described elsewhere (37).

The first alternative employing calculated vertical stress on the subgrade surface is illustrated by the following example problem.

A two-lane highway is to be designed (using a flexible pavement) for a design traffic number (DTN) of 200 in both directions. The location is in a region similar to that of Brampton, and similar materials are to be used. Repeated load triaxial compression test results on samples simulating the field conditions (in terms of density, water content, etc.) are as shown in Figures 3 and 4.

The stiffness modulus for the asphalt concrete, for a range of temperatures and for a loading time of 0.03 sec, is shown in Figure 5. Temperature records show that the average maximum air temperature at the project is about 70 F in June, and the corresponding pavement surface temperature is about 85 F.

In accordance with Figure 12, the designer proceeds in the following steps:

1. Consider the available base and subbase materials. For the purposes of this example, assume that this was restricted to an asphalt concrete base and a sand subbase.
2. Generate an array of possible layer thickness combination alternatives within established constraints for minimum and maximum layer thicknesses. Even for one base and subbase alternative, this can result in a very large number of arrays. A computerized approach is desirable. For the purposes of this example, consider the following thicknesses as one possible combination: surface layer, $3\frac{1}{2}$ in. of asphalt concrete; base layer, 2 in. of asphalt concrete; subbase, 6 in. of sand; and subgrade, natural clay soil of "infinite" depth.
3. Perform the structural analyses as detailed in earlier sections of this paper. The final output after iterating the CHEVRON program gives a vertical stress on the subgrade surface, σ_v, of 18 psi.
4. Predict the performance of each alternative. For this example, assume that the initial RCI is 8.5 and the terminal RCI is set at 4.5. This corresponds to a loss of 4.0 units of RCI to the first overlay. Figure 9 shows that the pavement type considered here will lose 4.0 units of RCI at a σ_v level of 18 psi after approximately 4×10^5 accumulated equivalent 18-kip single-axle loads. For a DTN of 100 (in one direction), the expected design life would be $(4 \times 10^5)/(100)\ (365) = 11$ years.
5. The design problem is not complete until a final design strategy has been recommended. This paper has concentrated on those components of the design phase of pavement management that deal primarily with the structural models and their inputs. However, as shown in Figure 12, overlay designs must be completed for each alternative to the end of the analysis period, and an economic evaluation must be conducted (i.e., expected materials, construction, and maintenance costs must be estimated for each strategy). The designer can then recommend an optimal strategy.

SUMMARY AND CONCLUSIONS

The purpose of this investigation was to determine whether structural analysis could be applied to the design of pavements in terms of predicting serviceability-age history.

Table 2. Brampton Test Road layer equivalencies.

Type of Material	Equivalencies of Granular Base (in.)
1.0 in. of granular base (crushed gravel or crushed rock)	1.0
1.0 in. of sand subbase	0.6
1.0 in. of bituminous-stabilized base	1.1
1.0 in. of asphalt concrete base (with subbase)	2.0
1.0 in. of asphalt concrete base (without subbase, i.e., full depth	3.4

Note: 1 in. of granular base ≃ 1 in. of bituminous stabilized base, ≃ 2 in. of sand subbase, ≃ ½ in. of asphalt concrete base, and, ≃ ⅓ in. of full-depth asphalt concrete.

Figure 12. Pavement design system.

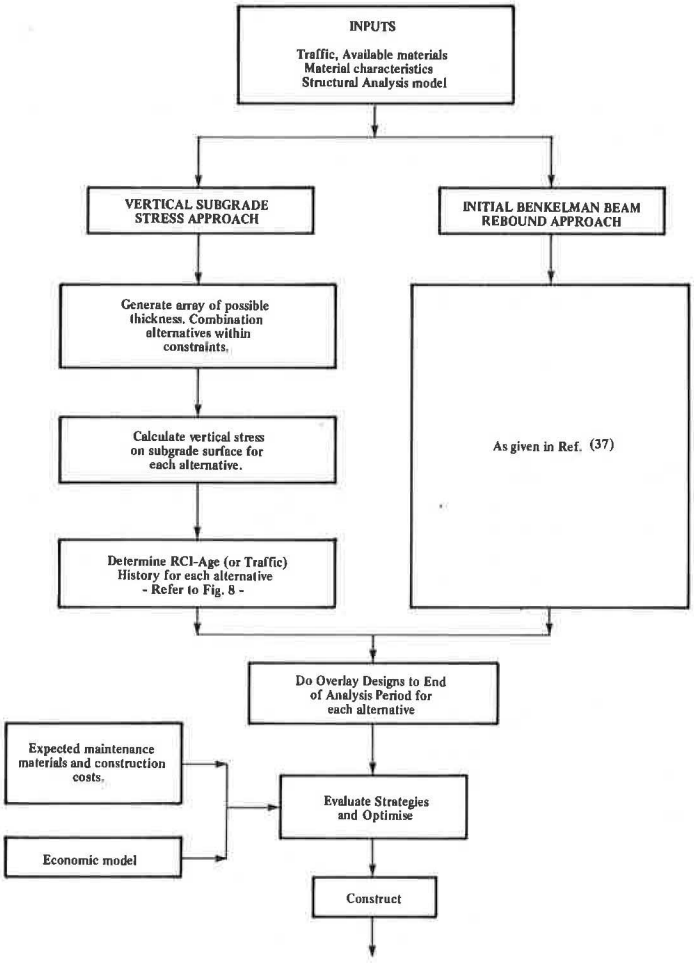

This goal was fulfilled through layer analyses of the various pavement designs employed at the Brampton Test Road, in the following manner:

1. The basic properties of the five pavement materials under consideration, for input to the layer analyses, were established from laboratory test results on the original materials.
2. The structural responses of the various pavement sections in terms of stresses, strains, and deflections under simulated traffic loading, were calculated by iterative, linear-elastic, computerized, layered-system models known as CHEVRON and BISTRO.
3. The calculated structural responses of step 2 were related to the observed performance [in terms of the serviceability-age (or traffic) histories] and to the measured behavior (in terms of Benkelman beam rebounds).
4. It was demonstrated that layer equivalency values could be developed using layer system analysis and a criterion of equal terminal serviceability. The results indicated that, for full-depth pavements, 1 in. of asphalt concrete can conservatively be considered equivalent to 3 in. of granular base.
5. The relations developed in step 3 were demonstrated to be applicable for use in designing pavements; in other words, layer analysis results can be used by the designer to predict the serviceability-age (or traffic) history of pavement strategy.

ACKNOWLEDGMENTS

The work reported in this paper was sponsored primarily by the Ministry of Transportation and Communications, Ontario. The authors wish to thank The Asphalt Institute for making the laboratory test data on the Brampton materials available. The CHEVRON and BISTRO computer programs were provided through the courtesy of the Chevron Asphalt Company and Koninklijke/Shell-Laboratorium, Amsterdam, respectively.

REFERENCES

1. Phang, W. A., and Slocum, R. Pavement Investment Decision Making and Management System. Ministry of Transportation and Communications, Ontario, Rept. RR174, Oct. 1971.
2. Hudson, W. R., et al. A Systems Approach Applied to Pavement Design and Research. Texas Highway Department; Texas A&M Univ.; and Center for Highway Research, Univ. of Texas at Austin, Res. Rept. 123-1, March 1970.
3. Brown, J. L., Buttler, L. J., and Orellana, H. E. A Recommended Texas Highway Department Pavement Design System User's Manual. Texas Highway Department; Texas A&M Univ.; and Center for Highway Research, Univ. of Texas at Austin, Res. Rept. 123-2, March 1970.
4. Haas, R. C. G., and Hutchinson, B. G. A Management System for Highway Pavements. Proc., Australian Road Research Board, 1970.
5. Pavement Management Committee, Roads and Transportation Assn. of Canada. Output Measurements for Pavements Management Studies in Canada. Third Internat. Conf. on Structural Design of Asphalt Pavements, London, Sept. 1972.
6. Kasianchuk, D. A., Terrel, R. L., and Haas, R. C. G. A Design System for Minimizing Fatigue, Permanent Deformation and Shrinkage Fracture Distress of Asphalt Pavements. Third Internat. Conf. on Structural Design of Asphalt Pavements, London, Sept. 1972.
7. Haas, R. C. G., and Hudson, W. R. The Importance of Rational and Compatible Pavement Performance Evaluation. HRB Spec. Rept. 116, 1971, pp. 92-109.
8. Haas, R. C. G., Hudson, W. R., McCullough, B. F., and Brown, J. L. Developing a Pavement Feedback Data System. Highway Research Record 407, 1972, pp. 162-172.
9. Haas, R. C. G. A Working Method for Designing Asphalt Pavement to Minimize Low-Temperature Shrinkage Cracking. Asphalt Institute, Dec. 1971.
10. Carey, W. N., Jr., and Irick, P. E. The Pavement Serviceability Performance Concept. HRB Bull. 250, 1960.

11. Haas, R. C. G., and Anderson, K. O. A Design Subsystem for the Response of Flexible Pavements at Low Temperatures. Proc. AAPT, 1969.
12. Jain, S. P., McCullough, B. F., and Hudson, W. R. Flexible Pavement System—Second Generation, Incorporating Fatigue and Stochastic Concepts. Texas Highway Department; Texas Transportation Institute, Texas A&M Univ.; and Center for Highway Research, Univ. of Texas at Austin, Res. Rept. 123-10, Dec. 1971.
13. Schonfeld, R. Construction of a Full-Scale Experiment as Part of a Unit-Price Contract. Ministry of Transportation and Communications, Ontario, Rept. RR-119, 1969.
14. Phang, W. A. Four Years Experience at the Brampton Test Road. Department of Highways, Ontario, Rept. RR-153, Oct. 1969.
15. Phang, W. A. The Effect of Seasonal Variation on the Performance of Selected Base Materials. Department of Highways, Ontario, Rept. IR-39, April 1970.
16. Kallas, B. F. The Brampton, Ontario Experimental Base Project. Interim Rept., unpublished, Feb. 1967.
17. Kallas, B. F. The Brampton, Ontario Experimental Base Project. Interim Rept., unpublished, Sept. 1967.
18. Kamel, N. I. Performance Analyses of the Brampton Test Road Using Elastic Layered Theory. Univ. of Waterloo, MASc thesis, Dec. 1971.
19. Kamel, N. I. Pavement Design System in Ontario—Second Generation Incorporating Use of Elastic Layer Theory. Transport Group, Civil Engineering Dept., Univ. of Waterloo, July 1972.
20. Morris, J., Kamel, N. I., and Haas, R. C. G. The Development of Design Procedures for Ontario Flexible Pavements. Symposium on Applications of Solid Mechanics, Univ. of Waterloo, June 1972.
21. Morris, J. An Experimental Investigation of the Vertical Stresses in Two-Layered Systems. Univ. of Melbourne, MEngSc thesis, 1961.
22. Terrel, R. L. Factors Influencing the Resilient Characteristics of Asphalt Treated Aggregates. Univ. of California, Berkeley, PhD dissertation, 1967.
23. Dehlen, G. L. The Effect of Non-Linear Material Response on the Behavior of Pavements Subjected to Traffic Loads. Civil Engineering Dept., Univ. of California, Berkeley, PhD thesis.
24. Seed, H. B., Chan, C. K., and Lee, C. E. Resilient Characteristics of Subgrade Soils and Their Relation to Fatigue Failures in Asphalt Pavements. Institute of Transportation and Traffic Engineering, Univ. of California, 1963.
25. Van der Poel, C. A General System Describing the Visco-Elastic Properties of Bitumens and Its Relation to Routine Test Data. Shell, Bitumen Reprint 9, 1954.
26. McLeod, N. W. Prepared Discussion of Ste. Anne Test Road. Canadian Technical Asphalt Assn., 1969.
27. Barksdale, R. D. Compressive Stress Pulse Times in Flexible Pavements for Use in Dynamic Testing. Highway Research Record 345, 1971, pp. 32-44.
28. Southgate, H. F. An Evaluation of Temperature Distribution and Its Relationship to Pavement Deflection. Kentucky Department of Highways, 1968.
29. Kallas, B. F. Asphalt Pavement Temperatures. Highway Research Record 150, 1966, pp. 1-11.
30. Barber, E. S. Calculation of Maximum Pavement Temperatures From Weather Reports. HRB Bull. 168, 1957.
31. A Guide to the Structural Design of Flexible and Rigid Pavements in Canada. Road and Transportation Association of Canada, 1965.
32. Manual on Pavement Investigations. Canadian Good Roads Assn., Tech. Publ. 11, 1959.
33. Wilkins, E. B. Outline of a Proposed Management System for the C.G.R.A. Pavement Design and Evaluation Committee, Proc. Canadian Good Roads Assn., 1968.
34. Chong, G. Measurement of Road Rideability in Ontario. Department of Highways, Ontario, Rept. IR-29, 1969.
35. Scott, W. J. Roads and Their Riding Qualities. Jour. Institute of Civil Engineers, Road Engineering Design, Road Rept. 25, 1947.

36. Kamel, N. I. Applying Structural Analysis of the Brampton Test Road to Pavement Investment Decision Making and Management System. Ontario Joint Transportation and Communications Research Program, Univ. of Waterloo, 1972.
37. Haas, R. C. G., Kamel, N. I., and Morris, J. Brampton Test Road: Analyses of Performance by Elastic-Layer Theory and Application to Pavement Design and Management System in Ontario. Ontario Joint Transportation and Communication Research Program, Final Rept., July 1972.
38. Painter, L. J. Analyses of AASHO Road Test Data by the Asphalt Institute. Proc. First Internat. Conf. on Structural Design of Asphalt Pavements, 1962.

FRACTURE (ULTIMATE STRENGTH) ANALYSES OF ASPHALT PAVEMENT LAYERS RESULTING FROM TRAFFIC LOADING

Y. M. Salam, American University of Beirut, Lebanon; and
C. L. Monismith, University of California, Berkeley

This paper presents analyses of fractures occurring in asphalt pavement structures due to excessive single-wheel loads and to braking tractions applied at the pavement surface. Specific solutions using a plane-stress finite-element idealization wherein nonlinear material responses and bond effects at layer interfaces could be considered are presented for cracking in an asphalt concrete bridge deck surfacing, for development of cracking in an asphalt concrete layer over a cement-treated base that was cracked due to load, and for cracking resulting from tractions imposed on an airfield pavement by a braking aircraft. The bridge deck surfacing incorporated two different support conditions, rigid and flexible, and two sets of material characteristics. For the flexible-support condition, the bituminous surfacing failed by compression and the stiffer material ruptured at a lower load; for the rigid-support condition, the stiffer material failed in tension at a higher load than the low-modulus material, which exhibited a compressive failure. The effect of low bond strength on this latter condition was to shift the failure condition from compression to a mixed mode. The ultimate strength of a pavement containing cement-treated base was determined by tensile fracture of the cement-treated base followed by subsequent cracking of the upper portion of the asphalt concrete layer. Braking tractions in a runway pavement resulted in lowering the total load to failure by increasing the tensile stresses at the heel of the loaded area. A weak interface also resulted in a further decrease of the total fracture loads.

•ASPHALT pavements can exhibit cracking that may result from both traffic-load- and non-traffic-associated causes. Table 1 gives some potential causes of fracture of this type. Cracking resulting from fatigue has received considerable attention in recent years (1) as has cracking resulting from thermal stresses associated with low temperatures (1). Some methodology has also been presented to illustrate procedures whereby cracking due to shrinkage in cement-treated materials can be estimated (2, 3).

Little information has been presented in the area of traffic-load-associated cracking due to excessive single loads or slippage distress resulting from braking tractions. This, perhaps, has been due in part to the limited nature of the initial distress resulting from these causes (1). It may also be due to the fact that no suitable method of analysis exists to examine the ultimate strength capabilities for realistic (three-dimensional) situations.

This paper will present an initial attempt of the analysis of such problems in the pavement area, the format for which is shown in Figure 1, and will examine specific solutions for cracking in an asphalt concrete bridge deck surfacing, development of cracking in an asphalt concrete layer over a cement-treated base that was cracked due to load, and cracking resulting from tractions imposed on an airfield pavement by a

Publication of this paper sponsored by Committee on Theory of Pavement Design.

braking aircraft. It should be noted that the analysis will be restricted to plane stress conditions but permits the idealization of nonlinearity of material response and bond effects at layer interfaces.

METHOD OF ANALYSIS

The method of analysis, the results of which are presented here, provides a format for studying the effect of progressive loading on pavement systems with emphasis on ultimate behavior. This type of loading results, at the higher levels of load, in decreased structural stiffness resulting from material nonlinearity and cracking and fracturing of individual elements resulting from limiting tension or compression strength criteria. As will be seen, fracturing, stresses, and displacements can successively be predicted.

When asphalt concrete is subjected to large stresses (near the ultimate strength), a nonlinear constitutive law is observed for a wide range of temperatures and loading times (7). Nonlinearity may also result because of local characteristics (e.g., voids) that act as stress raisers leading to local failures that amplify the global response into the nonlinear range.

When a pavement is monotonically loaded, a set of displacements will occur within and between the different layers. The force-displacement relations are determined by the element stiffnesses (of the discrete system), the internal connectivity between elements, and the external boundary conditions. As the load is increased, changes in element stiffnesses occur because of decreased material modulus at higher stresses or propagation of existing starter cracks. Such cracking results in the redefinition of the pavement being analyzed because a different internal stress distribution results and reorientation of the principal stresses occurs. This process is affected to varying degrees by differences in layer material response and prior loading history.

A finite-element idealization of bond-slip behavior has been suggested by Ngo and Scordelis (4) in conjunction with reinforced concrete. The interface is idealized by a series of linkage elements each containing two springs, one acting parallel to the direction of slip and the other perpendicular to it. The two springs may be uncoupled so that their behavior could be independent, or they could be made to interact if considered appropriate. This concept was further used by Nilson (5) for the finite-element analysis of reinforced concrete. The method employed here used the procedure developed by Franklin (6), who combined bond-slip behavior with material nonlinearity to analyze reinforced concrete frames and panels under plane stress states. The procedure is essentially an incremental iterative solution that provides for the cracking of individual material elements, with stress redistribution in the surrounding elements by iteration. Within each load increment, a number of iterations are performed to improve the stiffness value for that increment, with the initial stiffness derived from the previous increment, and an initial stiffness introduced to start the analysis.

The incremental procedure provides the bounds that isolate and identify successive failures. The external load is kept constant, whereas the solution is iterated to establish equilibrium of the system within a specified increment.

The fracturing of an element results in partial or total loss of the element stiffness. In addition, it will cease to carry part or all of the imposed loads, with the corresponding fraction of the released strain energy redistributed into the surrounding elements. This process of unloading may be explained as follows: Suppose that an element fails at increment i - 1 the total element nodal forces are $\{S_1\}$ and the total nodal deflections are $\{v_1\}$, with a corresponding element sitffness $[k_1]$. When the element fractures, a new element stiffness $[k_2]$ results with a corresponding release of forces at the nodes. Thus, for fixed nodes, equilibrium is achieved for the fractured element at a new set of nodal forces $\{S_2\}$ given by $\{S_2\} = [k_2]\{v_1\}$ with $\{S_f\} = \{S_1\} - [k_2]\{v_1\}$. $\{S_f\}$ is the element fracture release force accompanying a total or partial release of strain energy depending on whether or not $[k_2]$ is zero. Combining the forces $\{S_f\}$, the self-equilibrating vector of node fracture forces, the increment equation takes the form: $\{R\} + \{R_f\} = [K]\{r\}$, with $\{R_f\}$ appearing as an additional external loading. The iterations are performed until convergence occurs. Within this

context, fracture is considered as a factor that disturbs the rate of convergence of the iteration process. The system stiffness is allowed to adjust before the following load increment is applied, and the process is terminated when extensive structural damage occurs.

Because the program required extensive computer (CDC 6400) time (approximately 3 min per run), a relatively small-sized finite-element mesh was utilized. The problems investigated showed that the accuracy of the stress distribution predictions dropped with excessive cracking. (After failure of the first few elements had occurred, the rate of convergence of stiffnesses dropped, and the accuracy of the stresses predicted in the remaining intact elements decreased.)

The material properties required for the analysis were obtained from a laboratory study (7) and included stress-strain characteristics as well as ultimate tensile and compressive strengths.[1] Stress and strain curves were divided into eight linear portions for input to the computer program. Element fracturing, stress patterns, and displacements were determined in each of the problems investigated.

EXAMPLES OF THE STRUCTURAL ANALYSIS

Because of the complexity of the analysis used to obtain the results presented in this section, the examples have been selected on the basis of simplicity, computer time efficiency, and practicality as permitted by the plane stress state. Exact duplication of actual conditions is not possible at this time, and details that might have obscured the procedure or complicated the analysis were excluded.

The examples have been chosen to permit the comparison of pavement response under different boundary conditions and with different material properties. However, it must be recognized that the loads at fracture that have been estimated should be examined more on a comparative basis than in the absolute sense.

Cases examined in the computations include the following:

1. Asphalt concrete bridge deck surfacing with flexible support and rigid support (temperature of asphalt concrete at 68 and 40 F),
2. Asphalt concrete over a cement-treated base, and
3. Thick asphalt concrete runway pavement with vertical load only and with vertical load combined with braking traction (fixed bond at interface between pavement and underlying layer and weak interface).

Asphalt Concrete Bridge Deck Surfacing

Preliminary analyses indicated that the response of the asphalt concrete surfacing is a function of the rigidity of the supporting girder, with a flexible girder having the potential to induce a stress pattern differing markedly from that resulting from a rigid support. Both conditions were investigated with the same finite-element mesh but with differing boundary conditions.

Figure 2 shows the finite-element idealization representing a 5-in. thick half-section of a 14-in. girder with a 4-in. asphalt concrete cover. This section width was chosen because of its compatibility with plane stress states. A rigid support was obtained with roller A in place, whereas the flexible condition was obtained by deleting roller A. The girder was assumed to be linear elastic with a modulus of 30×10^6 psi (representative of structural steel). Linearized stress-strain characteristics of the asphalt concrete are shown in Figure 3. In addition, the biaxial strength envelopes shown in Figure 4 were used as failure criteria and were incorporated in the program. Characteristics of the bond between asphalt concrete and steel were not available. Accordingly, the interface was assigned a constant stiffness modulus equal to half the initial stiffness of the asphalt concrete, and bond effects were analyzed for the rigid support condition at 68 F.

[1] The original manuscript of this paper included Appendix A, Characteristics of Asphalt Concrete, and Appendix B, Incremental Iteration Method. The appendixes are available in Xerox form at cost of reproduction and handling from the Highway Research Board. When ordering, refer to XS-47, Highway Research Record 466.

Table 1. Categories of fracture in asphalt pavements.

General Cause	Specific Causative Factor	Visual Manifestation of Distress
Traffic-load associated	Repetitive traffic loading	Fatigue
	Horizontal forces, e.g., braking loads at pavement surface	Slippage
	Single or comparatively few excessive loads	Longitudinal or transverse cracks or both
Non-traffic associated	Thermal changes	Transverse cracks (relatively uniformly spaced)
	Shrinkage of treated materials (e.g., of cement-treated base)	Transverse cracks (relatively uniformly spaced)
	Moisture changes	Transverse cracks (relatively uniformly spaced)

Note: Table contains only a partial listing.

Figure 1. Fracture subsystem.

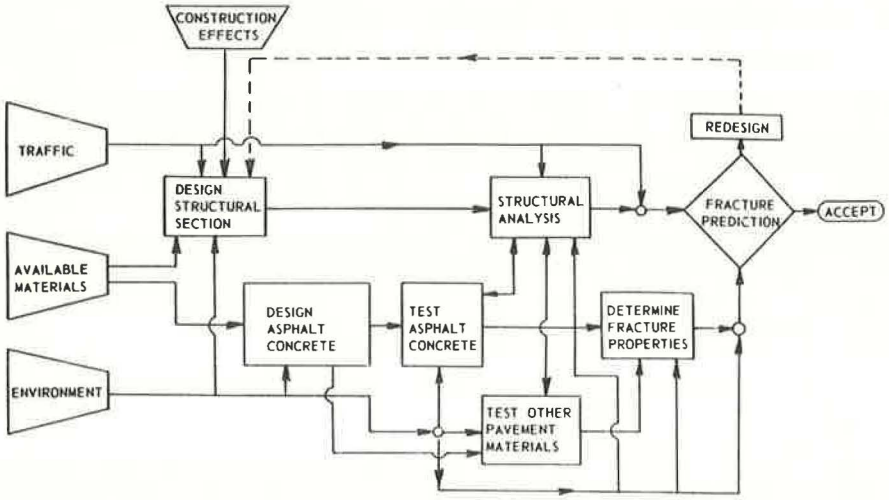

Figure 2. Finite-element idealization of bridge deck.

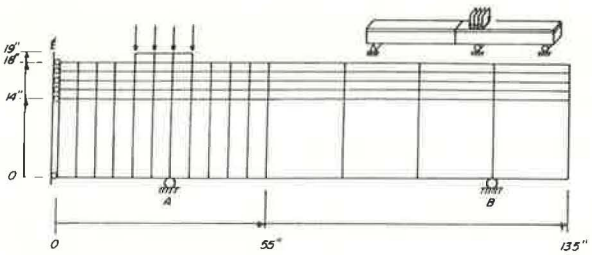

Figure 3. Asphalt concrete mix stress and strain data.

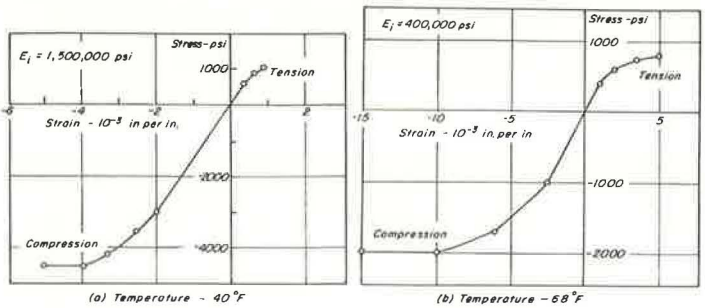

Load was applied to the surfacing through a loading strip 15 in. in length over four nodal points (Fig. 2). Braking forces were simulated by applying a horizontal load that was made equal to one-half of the vertical load. For a particular case, large load increments were first used to determine approximately the ultimate value; the problem was then rerun using smaller increments near the ultimate load.

Flexible Support—Results of the analyses for this condition are shown in Figures 5 through 7 for a mix temperature of 40 F and in Figures 8 through 10 for a mix temperature of 68 F. Generally, the response of the asphalt concrete is determined by the deflection of the supporting girder, and large compressive stresses are induced throughout the depth of the asphalt-bound layer. These stresses are increased in the region ahead of the loaded area because of the horizontal component of the load.

For the 40 F condition, Figure 5 shows the variation in horizontal strains and vertical deflections at the surface of the asphalt concrete prior to failure (load of 80 kip) along the girder. Figure 6 shows the distribution of the minimum stresses (maximum compressive stress for the individual elements) at the onset of fracture.

Figure 7 shows the sequence of fracture, which is indicated by the numbers 1, 2, 3, and 4 in the critical area when the total vertical load reached 84 kip. As would be anticipated (Fig. 6), the first elements to fail were those immediately ahead of the load, followed by those at the heel. At this temperature, distress occurs in compression due to the high compressive strains, and the failure area appears reasonably well distributed under the loaded area.

At 68 F, because the asphalt concrete is less stiff, larger deflections are tolerated (Fig. 8). At a load of 120 kip, at which failure was imminent, similar trends in stresses to those observed at 40 F were obtained (Fig. 9). In this instance, the stress at the toe of the load is almost twice that at the heel. As seen in Figure 10, failure occurs more extensively in this area at a load of about 140 kip.

Rigid Support—The same finite-element mesh as for the flexible condition was used to solve this problem. Figures 11 through 13 show the results of the analysis for a mix temperature of 40 F, and Figures 14 through 16 show the results for 68 F. In addition to the cases illustrated in these figures, a case was analyzed, as noted earlier, to study the effect of bonding between the asphalt concrete and the supporting member by assigning a stiffness at the interface equal to one-half that of the asphalt concrete. Results of this analysis for a mix temperature of 68 F are shown in Figures 17 and 18.

For the 40 F case (Fig. 11), the horizontal strains are tensile at the rear of the load and compressive in front of it. For this situation, the tensile condition is critical.

For a load of 160 kip, Figure 12 shows minimum and maximum stress distributions in the asphalt concrete beneath the loaded plate. The maximum compressive stress was approximately 2,100 psi, whereas the maximum tensile stress was about 850 psi. If these conditions were plotted in Figure 4, it would be noted that the tensile stress is more critical.

The sequence of fracture under a load of 200 kip is shown in Figure 13 and, as noted previously, is initiated on the tensile side. This figure also shows the directions of the maximum and minimum stresses prior to failure and illustrates the effect of the horizontal load on the orientation of stresses.

At 68 F, the compression effects are more pronounced because the ratio of compression to tensile strength is lower than at 40 F. Figure 14 shows the distribution of strains and deflections for a load of 136 kip (onset of fracture), and Figure 15 shows the corresponding stress distributions. The sequence of fracture at 140 kip is shown in Figure 16, indicating the stronger influence of compression in contributing to distress (as compared to 40 F, Fig. 13).

The influence of bonding between the asphalt concrete and the support is shown in Figures 17 and 18. At the onset of cracking, the stress distribution was similar to the case of fixed bond, but failure occurred at a lower load (112 kip). However, the cracking appeared to shift slightly to the tension side as shown in Figure 17. The difference between the fixed bond and the weak interface is shown more clearly in Figure 18 where the horizontal strain 1 in. above the interface is plotted with the applied load.

Figure 4. Asphalt concrete mix biaxial strength envelopes.

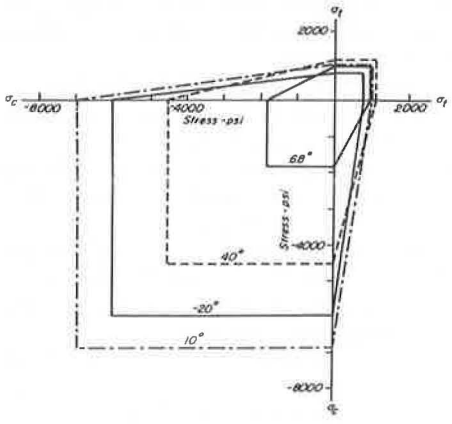

Figure 5. Horizontal strains and vertical deflections at surface of asphalt concrete cover, flexible support (40 F).

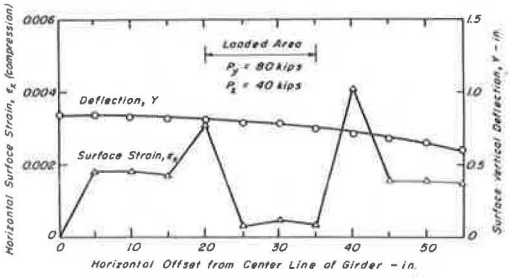

Figure 6. Distribution of maximum compressive stresses in asphalt concrete surfacing, flexible support (40 F).

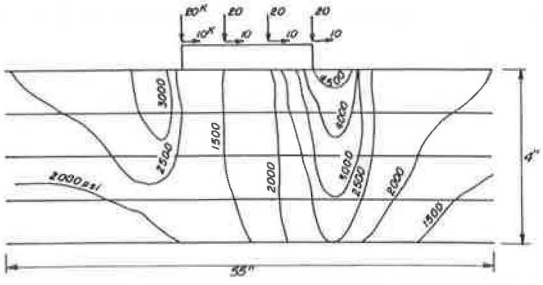

Figure 7. Fracture sequence in asphalt concrete surfacing, flexible support (40 F).

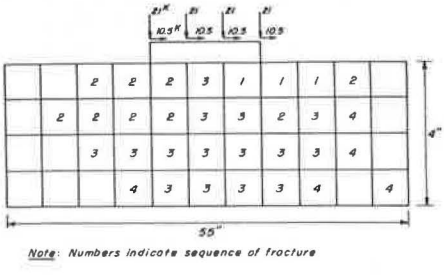

Figure 8. Horizontal strains and vertical deflections at surface of asphalt concrete cover, flexible support (68 F).

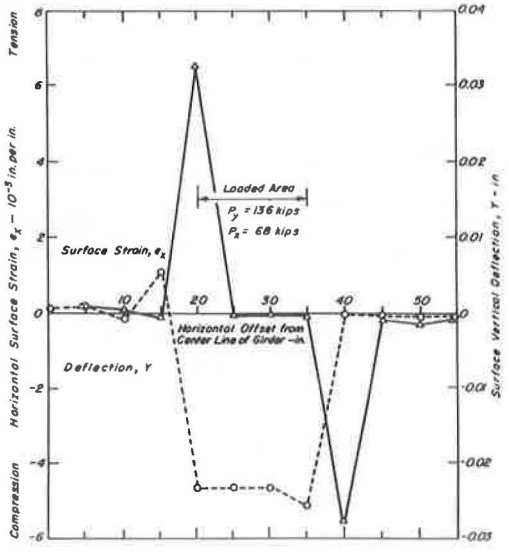

Figure 9. Distribution of maximum compressive stresses in asphalt concrete surfacing, flexible support (68 F).

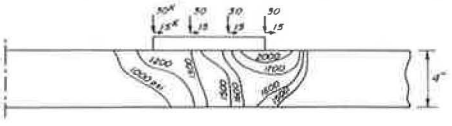

Figure 10. Fracture sequence in asphalt concrete surfacing, flexible support (68 F).

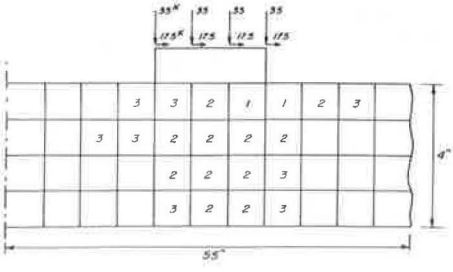

Figure 11. Horizontal strains and vertical deflections at surface of asphalt concrete cover, rigid support (40 F).

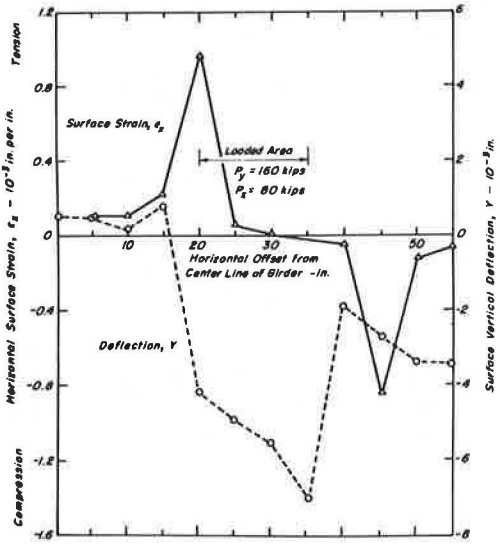

Figure 12. Distribution of minimum and maximum stresses in asphalt concrete surfacing, rigid support (40 F).

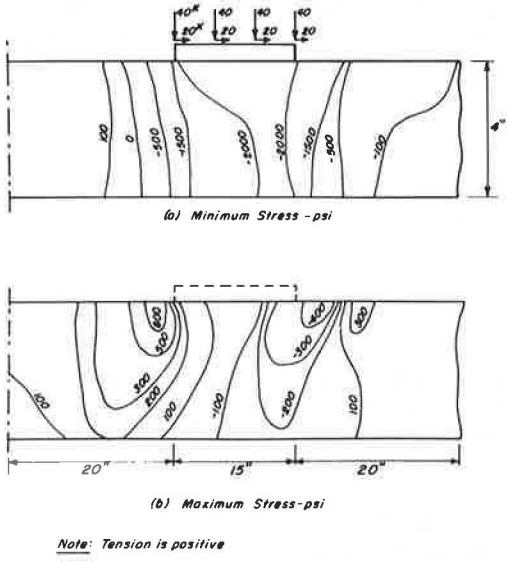

Figure 13. Sequence of fracture and orientation of maximum and minimum stresses prior to fracture in asphalt concrete surfacing, rigid support (40 F).

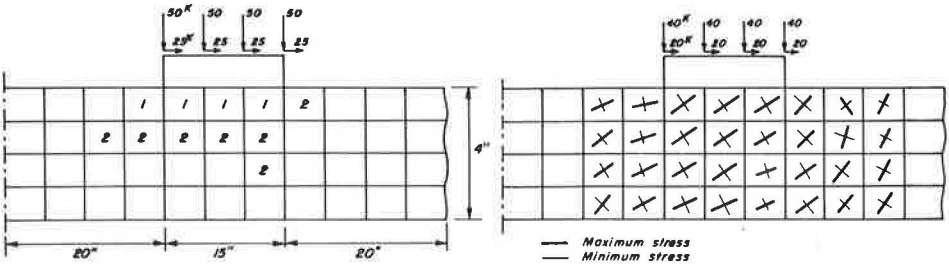

Figure 14. Horizontal strains and vertical deflections at surface of asphalt concrete cover, rigid support (68 F).

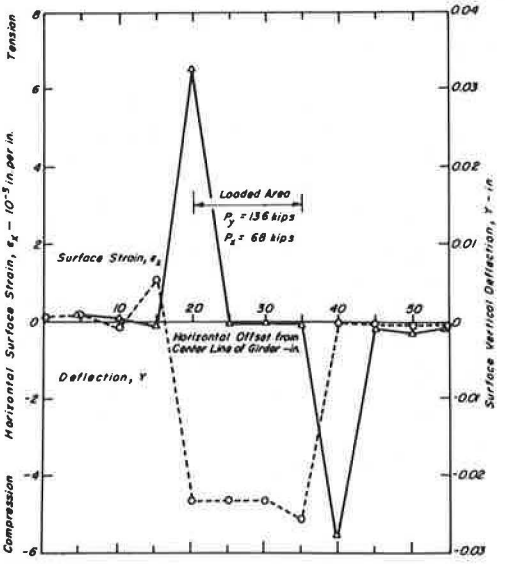

Summary and Comment

Effects of boundary conditions on the ultimate load-carrying capabilities of an asphalt concrete layer on a bridge deck may be summarized as follows:

Condition	Load to Failure (kip)	Mode of Failure
Flexible support		
40 F	84	Compression
68 F	120	Compression
Rigid support		
40 F	200	Tensile
68 F	140	Compression
68 F (weak interface)	112	Mixed

For the flexible support conditions, the maximum deflections, Y, were approximately 0.85 in. (Fig. 5) and 1.4 in. (Fig. 8). These values are in the range that might be expected in practice, e.g., allowable maximum of 1.5 in. for steel bridges of 100-ft spans ($^1/_{800}$ of the span length) and 0.75 in. for concrete bridges with 50-ft spans. For the rigid case, the deflection, Y, is very small (Figs. 11 and 14).

Asphalt Concrete Layer Over a Cement-Treated Base

The analysis described in this section is restricted to studying fracture progression in an asphalt concrete surface as the result of cracking of the underlying cement-treated base because of excessive loading.

The finite-element mesh used is shown in Figure 19. For this analysis, the pavement has been idealized as a composite beam 5 in. in width consisting of an 8-in. thick asphalt concrete layer and a 10-in. thick cement-treated base symmetrically located on a subgrade strip 10 in. in width. (This dimension was chosen to impart stability to the foundation layer relative to its extent in the vertical plane and its low modulus.) Load was applied at two nodal points of a 10-in. long plate (Fig. 19).

Stress-strain characteristics in tension and compression at 68 F for the asphalt concrete are the same as those used in the previous example (Fig. 3b). The stress-strain relation for the cement-treated base was obtained from data developed by Pretorius (2) (Fig. 20). An elastic modulus of 10,000 psi was used for the subgrade.

Variation of the vertical deflection at the surface of the pavement with horizontal offset measured from the centerline of the beam is shown in Figure 21 for a load of 20 kip (onset of cracking). Fracture occurred at a load of 22 kip in the sequence shown in Figure 22. The first element to crack was element 1 of the cement-treated base. Further cracking in the cement-treated base occurred adjacent to element 1 together with tensile fracture at the upper layers of the asphalt concrete surface. Further failures took place subsequently in the bottom layers.

This type of cracking has also been reported by Pretorius (2) based on the analysis of stresses in the pavement, idealized in the form of a prismatic space, after the cement-treated base had cracked due to shrinkage stresses.

Cracking Due to Braking Stresses Applied at Pavement Surface

This analysis is concerned with the development of stresses in the asphalt concrete layer due to braking stresses (representative of an aircraft loading) applied at the pavement surface. A friction factor between tire and pavement of 0.5 has been assumed, and both horizontal and vertical components of load have been applied at the same time.

The finite-element representation is shown in Figure 23, the pavement consisting of an asphalt concrete beam 5 in. wide and 20 in. deep on a subgrade strip 10 in. wide. As seen in the figure, the load (representative of a heavy aircraft load) was applied through an elastic plate 20 in. in length. Properties of the asphalt concrete were those shown in Figure 3a (a temperature of 40 F was assumed for this example); a subgrade stiffness of 10,000 psi was utilized.

Figure 15. Distribution of minimum and maximum stresses in asphalt concrete surfacing, rigid support (68 F).

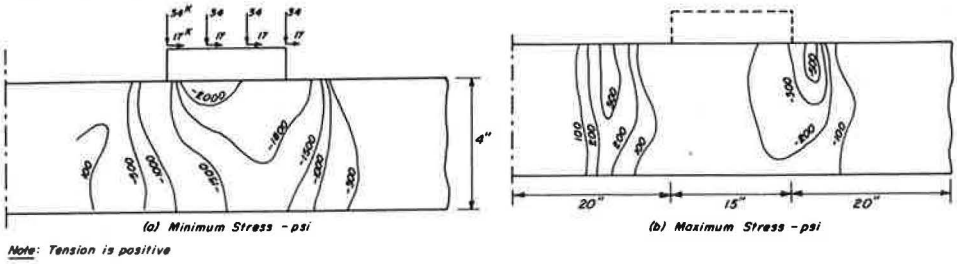

Figure 16. Sequence of fracture and orientation of maximum and minimum stresses prior to fracture in asphalt concrete surfacing, rigid support (68 F).

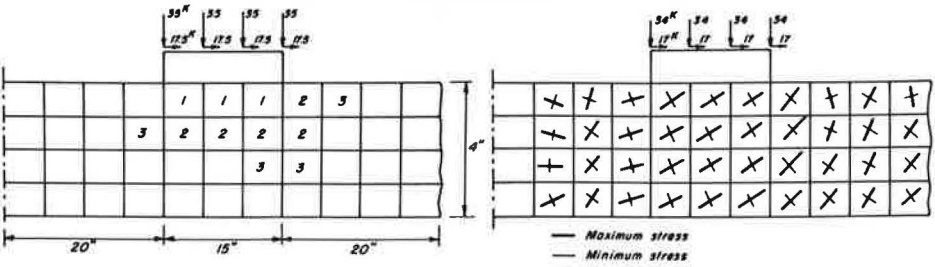

Figure 17. Sequence of fracture in asphalt concrete surfacing with weak interface, rigid support (68 F).

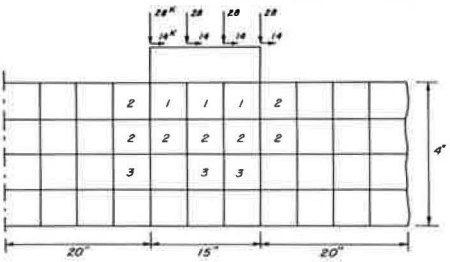

Figure 18. Effect of weak interface on strength of asphalt concrete surfacing, rigid support (68 F).

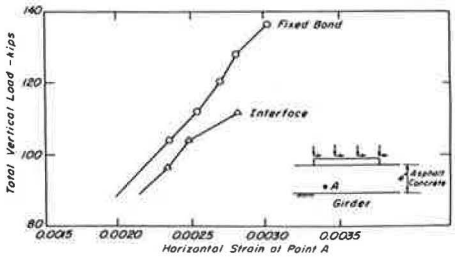

Figure 19. Finite-element mesh for pavement section with cement-treated base.

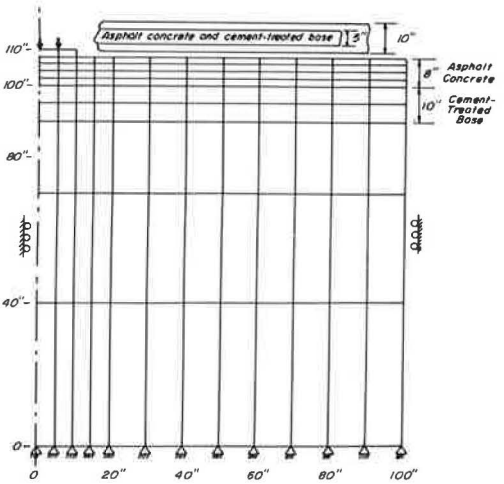

Figure 20. Stress-strain data for cement-treated base.

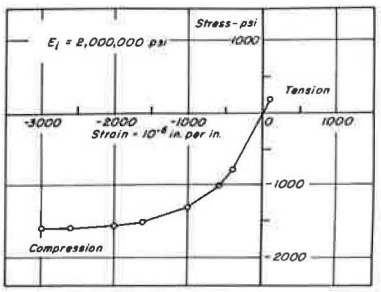

Figure 21. Variation of surface deflection with distance from centerline of load.

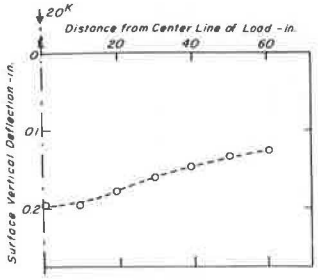

Figure 22. Sequence of fracture in pavement containing cement-treated base.

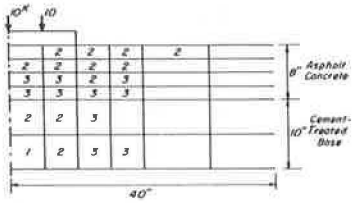

Figure 23. Finite-element idealization of runway pavement for braking tractions.

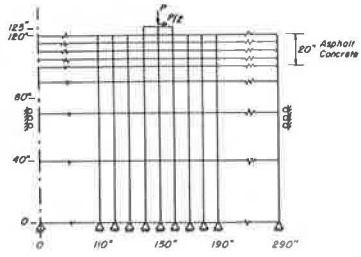

Figure 24. Influence of 44-kip vertical load applied to surface of 20-in. thick asphalt concrete layer (40 F).

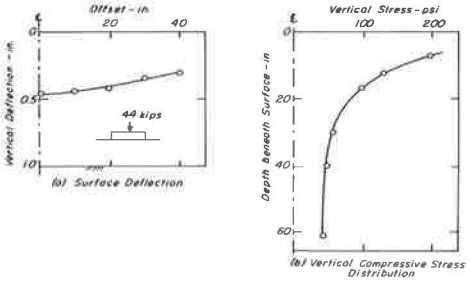

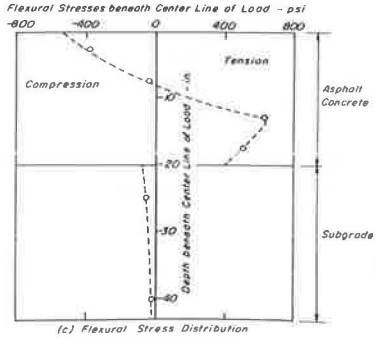

Figure 25. Fracture sequence in 20-in. asphalt concrete runway pavement for vertical loads (40 F).

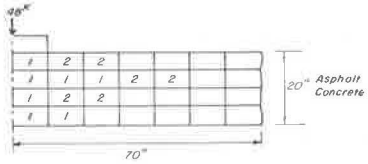

Figure 26. Horizontal stress distribution in 20-in. thick asphalt concrete runway pavement under braking tractions prior to cracking (40 F).

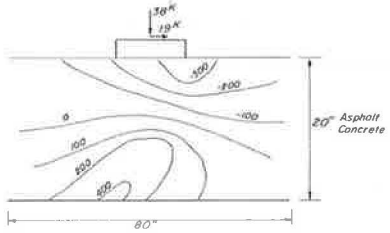

Figure 27. Fracture sequence in 20-in. thick asphalt runway pavement subjected to braking tractions.

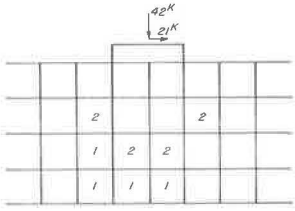

Figure 28. Variation of the horizontal strain at point A with applied loads for fixed-bond and weak-interface conditions.

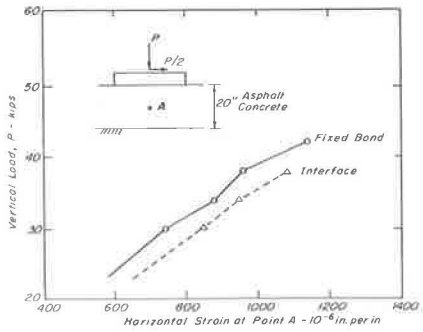

An analysis was first accomplished for only the vertical loading condition. Figure 24 shows the results of this analysis: surface deflection (Fig. 24a), vertical stress as a function of depth (Fig. 24b), and distribution of flexural stresses with depth (Fig. 24c).

The truncation of the tensile stresses at the bottom of the asphalt concrete might have resulted from forces released by those elements due to crack initiation. Figure 25 shows the sequence of cracking that occurred symmetrically over the full depth of the section at a total load of 48 kip.

Stress estimates including the effect of horizontal tractions are shown in Figure 26. In this figure, the horizontal (flexural) stress distribution for a vertical load of 38 kip is shown; it can be seen that the distortion of the flexural stress field has resulted from the compressive stresses at the toe of the load plate and tensile stresses at the heel. Fracture occurred in tension below the heel at a load of 42 kip (Fig. 27).

The effect of a weak interface between the asphalt concrete pavement and the subgrade was analyzed. The stress distribution and the fracture sequence were similar to the fixed bond condition, but the fracture load was slightly lowered. Horizontal strains were higher in the case of the weak interface as shown in Figure 28.

SUMMARY

In this paper, methodology for performing ultimate strength analyses for certain pavement structures has been briefly summarized. For simplicity, only plane stress conditions have been utilized.

The procedure involves an incremental loading pattern with solution iteration within each load increment. Predictions of cracking, stress distributions, and displacements were obtained for three examples.

The bridge deck surfacing incorporated two different support conditions, rigid and flexible, and two sets of material characteristics. For the flexible-support condition, the asphalt surfacing failed by compression and the stiffer material ruptured at a lower load. In the rigid-support condition, the stiffer material failed in tension at a higher load than the low-modulus material, which exhibited a compressive failure. The effect of low bond strength on this latter condition was to shift the failure condition from compression to a mixed mode.

The ultimate strength of a pavement containing cement-treated base was determined by tensile fracture of the cement-treated base followed by subsequent cracking of the upper portion of the asphalt concrete layer.

Braking tractions in a runway pavement resulted in lowering the total load to failure by increasing the tensile stresses at the heel of the loaded area. A weak interface also resulted in a further decrease of the total fracture loads.

Although the analyses presented here are restricted to plane stress conditions and can only be considered as a pilot study, they illustrate how critical areas can be defined in pavement structures (for example, the bridge deck pavement wherein two boundary conditions and two sets of materials were analyzed) and may thus provide some insight to techniques to minimize load associated fracture.

ACKNOWLEDGMENTS

The investigation was supported by the Federal Highway Administration. This agency has not reviewed the research findings.

REFERENCES

1. Structural Design of Asphalt Concrete Pavement Systems. HRB Spec. Rept. 126, 1971.
2. Pretorius, P. C. Design Considerations for Pavements Containing Soil-Cement Bases. Univ. of California, Berkeley, PhD dissertation, 1970.
3. George, K. P. Shrinkage Characteristics of Soil-Cement Mixtures. Highway Research Record 255, 1968, pp. 42-58.
4. Ngo, D., and Scordelis, A. C. Finite Element Analysis of Reinforced Concrete Beams. Jour. of American Concrete Institute, Vol. 64, March 1967.

5. Nilson, A. H. Finite Element Analysis of Reinforced Concrete. Univ. of California, Berkeley, PhD thesis, 1967.
6. Franklin, H. A. Nonlinear Analysis of Reinforced Concrete Frames and Panels. Univ. of California, Berkeley, PhD thesis, 1970.
7. Salam, Y. M. Characterization of Deformation and Fracture of Asphalt Concrete. Univ. of California, Berkeley, PhD dissertation, 1971.

SENSITIVITY ANALYSIS TO DETERMINE THE RELATIVE INFLUENCE OF MATERIALS CHARACTERIZATION ON A FATIGUE-DAMAGE MODEL

Wayne S. Smith and Keshavan Nair, Materials Research and Development, Oakland, California

The concept of and a procedure for conducting a deterministic sensitivity analysis to establish the relative influence of materials characterization on the prediction of the fatigue performance of asphalt concrete pavements are presented. The effects of isotropic linear-elastic materials characterization on fatigue performance prediction are compared with the effects associated with construction, environment, and fatigue criteria variability. The results of the study have permitted an evaluation of the adequacy of an isotropic linear-elastic characterization of the three most common types of materials used in flexible pavement construction (asphalt concrete, untreated granular base course, and subgrade) for three typical structural sections and for a range of temperatures. For several specific structural sections and environments, it was found that improved material characterization beyond isotropic linear elasticity could significantly reduce the uncertainty (variation) of fatigue life prediction. However, both the construction control of air voids in the asphalt concrete and the inherent variability in the experimental definition of the fatigue criteria themselves always contributed more uncertainty to the prediction of fatigue performance than the uncertainty contribution associated with linear isotropic materials characterization.

•IT is generally accepted that the level of characterization of pavement materials has reached a degree of sophistication such that further refinements would require considerable investments in time and money. Before making such commitments, it is pertinent to ask whether, in the present context of the state of development of pavement design and performance prediction models, further refinements are necessary.

The adequacy of a characterization can be measured by the degree to which deviations from the idealized material behavior influence the objective of predicting pavement performance and must be measured relative to the influence on performance of variations in other inputs. In order to do this, a sensitivity analysis was conducted under contract with FHWA. Implicit in the sensitivity results is that the pavement design method used is based on a layered system representation that directly accounts for the influence of individual layer properties and temperature on pavement performance.

GENERAL CONCEPT AND PROCEDURE FOR CONDUCTING SENSITIVITY ANALYSIS

Let us consider a system with the following three essential components: inputs, a law of transformation, and outputs. Outputs are generally considered in the context of the performance of the system being modeled. The basic concept in a sensitivity analysis is to relate variations in input to variations in the output. In general, a reduction in the uncertainty (variation) of the inputs will result in a reduced variation in the outputs. However, because the effect on the output of each input is not the same, it is not necessarily logical that each input be defined to the same degree of accuracy (level of

Publication of this paper sponsored by Committee on Theory of Pavement Design.

uncertainty). For example, a variation of 50 percent in one input may have the same effect on the output as a 1 percent variation in some other input.

A rigorous treatment of the uncertainties would require that the problem be considered in probabilistic terms. A closed-form probabilistic pavement performance prediction model is currently being evaluated by FHWA. However, it was not available at the time this study was initiated. Hence, the sensitivity analysis was conducted deterministically by considering ranges of variation from average values of the inputs. These variations in the inputs will be referred to as input uncertainties for the sake of brevity in the remainder of the paper.

It should be recognized that all system models represent idealizations of a real physical system, and, therefore, the system model within whose framework the sensitivity analysis is conducted is, in itself, an approximation. The accuracy of the overall model, in terms of the factors that are included or omitted, has a bearing on the desired accuracy of the various components of the model. This line of reasoning leads to the conclusion that it is necessary to develop a complete system model prior to conducting any sensitivity analysis. However, because a complete model of a pavement system was not available at the time this study was conducted, it was necessary to consider the specific subsystems that were available. Because materials characterization is primarily an input to the structural subsystem, it is within the context of the structural subsystem that a sensitivity analysis with respect to materials characterization was conducted.

The procedure utilized for conducting the sensitivity analysis is shown in Figure 1. It should be recognized that the entire sensitivity analysis is conducted within the context of the performance (failure) prediction model that has been selected. The subsequent sections discuss the sensitivity analysis in accordance with the steps shown in Figure 1.

SELECTION OF PERFORMANCE (FAILURE) PREDICTION MODEL

The failure mode considered in this study was fatigue due to repeated application of vehicle loads. This model can be defined by describing the inputs considered, the failure model, and the structural analysis model.

Inputs to the Sensitivity Analysis

The following inputs were considered in the sensitivity analysis: traffic, material constitutive equations, material failure characteristics, environment, structural section, and construction effects.

In this sensitivity study, only initial design was considered; hence, maintenance effects were not included in the subsystem. Traffic volume was not directly considered, and the performance of the pavement system was measured in terms of the number of repetitions needed to cause failure. The life or performance of the pavement, in terms of time, is dependent on the volume of traffic. No particular volume of traffic was assumed in the analysis.

Failure Model

Although local conditions may cause variations in pavement behavior, it is generally agreed that cracking due to the repeated action of traffic (fatigue) is a major contributor to pavement distress (1). Because fatigue cracking is of major significance in the failure of pavement systems, it is logical that this initial sensitivity analysis of materials characterization be conducted utilizing the fatigue components of the structural subsystem.

The fatigue criteria developed at the University of California at Berkeley by Monismith and his associates were utilized to predict the initiation of cracks in the pavement. These criteria are well documented in the literature (2, 3, 4, 5).

Structural Analysis Model

The structural analysis of the pavement system was performed using a layered, isotropic, linear-elastic boundary value representation of the pavement system. Although

other boundary value representations that are possibly more representative of a pavement system are available (e.g., non-linear-elastic layered system, and linear-viscoelastic layered systems), the linear-elastic representation was selected because it could adequately reflect the fatigue behavior of a pavement system if proper consideration was given to the effect of temperature, load duration, and stress levels on the material properties. In addition, information concerning material properties and failure characteristics is most commonly analyzed and reported assuming linear-elastic behavior. Furthermore, this representation is the most commonly used and widely understood.

For the purpose of determining the controlling strain value used for fatigue life prediction, both isotropic linear viscoelasticity and isotropic linear elasticity can be considered equivalent if proper consideration is given in the latter characterization to temperature and load duration effects. Viscoelastic theory provides for the dependence of the material properties on temperature and load duration directly in the theory. If elastic theory is used, the material properties must be selected based on the temperature and load duration of interest.

TYPICAL STRUCTURAL SECTIONS

Three pavement section geometries representative of possible design alternatives for a major highway were considered. The pavement sections range from full-depth asphalt concrete to a thin-surfaced layer of asphalt concrete over an untreated base course material. These sections are representative of a highway built on a relatively weak subgrade (CBR $\cong$ 3, E $\cong$ 5,000 psi, and R $\cong$ 15) with a relatively high traffic volume (DTN $\cong$ 550 and TI $\cong$ 10.5). The geometry of the actual sections analyzed is shown in Figure 2.

MATERIAL TYPES AND AVERAGE PROPERTIES

The three types of materials that are most prevalent in the asphalt pavement section (asphalt concrete surfacing, untreated granular base course, and subgrade) were investigated in the sensitivity analysis.

Asphalt Concrete

The average asphalt concrete properties used (6, 7) are shown in Figure 3. The asphalt concrete specimens were subjected to a range of simultaneously cycled axial and radial stress varying from 70-psi compression to 70-psi tension for axial stress and 0- to 70-psi compression for radial stresses. The average elastic modulus of the asphalt concrete was taken from the dotted line shown in Figure 3 for each temperature analyzed. An average value of Poisson's ratio of 0.4 was assumed for all temperatures analyzed.

Untreated Base Course

It was recognized that the modulus and Poisson's ratio of untreated base course material are strongly affected by stress level (6, 8). However, the material was taken to be linearly elastic in accordance with the structural analysis model selected. The results of this sensitivity analysis will yield the effect of assuming a constant linear-elastic modulus and a constant average Poisson's ratio. The average values of modulus and Poisson's ratio selected were based on experimental results and preliminary structural analysis of the pavement section geometries using a layered "ad hoc" non-linear-elastic boundary value representation. These results indicated that a realistic average modulus value was 10,000 psi, and the average Poisson's ratio was selected as 0.3.

Subgrade

The selection of average properties for the subgrade material was restricted by the geometry of the structural sections and traffic volume chosen for the sensitivity analy-

Figure 1. Procedure for conduct of sensitivity analysis.

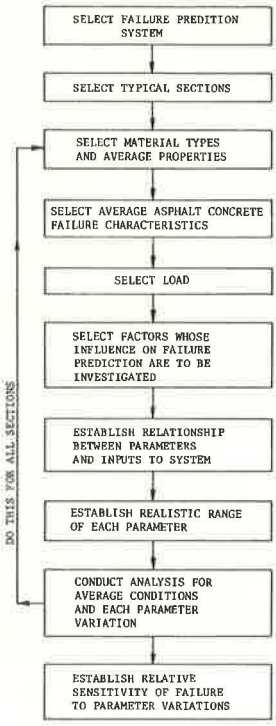

Figure 2. Geometries of structural sections.

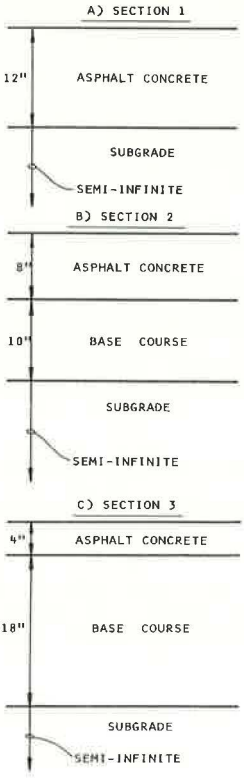

Figure 3. Temperature dependence of asphalt concrete modulus (6, 7).

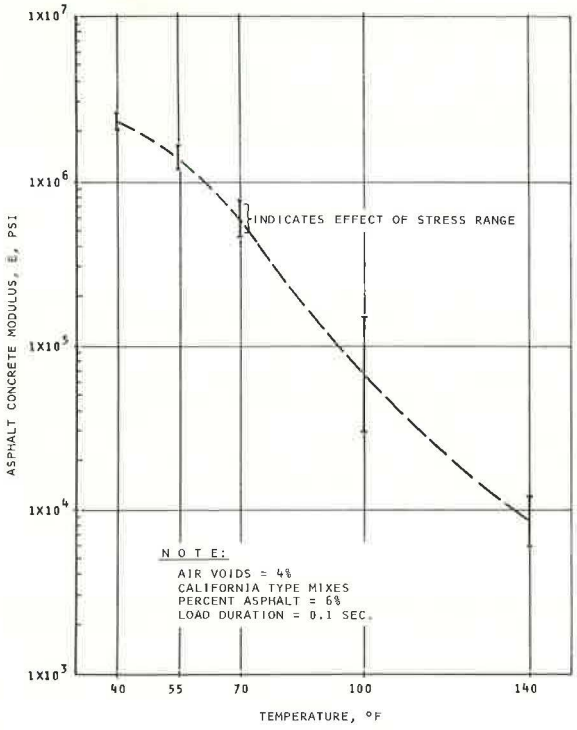

sis. These structural sections are representative of a pavement constructed on a subgrade with an average modulus of 5,000 psi. An average value for Poisson's ratio of 0.4 was selected as representative of most subgrades.

ASPHALT CONCRETE FAILURE CHARACTERISTICS

The fatigue failure characteristics of the asphalt concrete used in this analysis were those developed by Monismith et al. (5). These failure criteria were determined from laboratory repeated flexure tests on asphalt concrete beams and a regression fit of the data. The results are presented in the form of maximum initial tensile bending strain compared with repetitions to failure as shown in Figure 4. The fatigue life (number of repetitions to failure) was determined from this figure for each particular strain and asphalt concrete stiffness (temperature). The general form of the fatigue criteria is $N_f = K_1 (1/\epsilon)^{K_2}$, where N_f is the fatigue life, K_1 and K_2 are constants that depend on asphalt concrete modulus, and ϵ is the maximum tensile strain in the asphalt concrete.

LOADING CONDITION

One loading condition was used for the entire sensitivity analysis. It was recognized that the load magnitudes applied to a pavement are distributed in some random fashion. Normally, the effect on fatigue life prediction of varying load magnitudes is considered through Miner's hypothesis of a linear summation of damage due to each load magnitude. For the purposes of this sensitivity analysis, it was sufficient to examine one typical loading condition.

The loading condition analyzed was a single 9,000-lb wheel load with a tire pressure of 70 psi. The load area was assumed to be circular, which resulted in a load radius of 6.40 in.

FACTORS INFLUENCING FAILURE PREDICTION

The following factors were considered significant in their influence on the prediction of fatigue failure in an asphalt concrete pavement: environment, construction effects, material characterization, and failure characteristics. It was necessary to translate the effects of these factors into actual inputs of the fatigue performance subsystem.

Variable inputs to the fatigue failure subsystem used for this sensitivity analysis were material properties and geometry. Therefore, within the context of the model, the influence of the preceding factors on the prediction of failure could only be analyzed through their effect on material properties and the structural section geometry inputs. These factors were subdivided into a number of specific parameters; e.g., environment was broken down into temperature and moisture. It was then necessary to establish the relations between material properties and the various parameters.

With these relations between material properties and parameters affecting fatigue performance, it was possible to examine the influence of variations in each parameter on the prediction of pavement failure. This information could then be used to examine the relative importance of the uncertainty (range of variation) associated with each parameter on the prediction of fatigue performance.

RANGE OF PARAMETERS AND RELATION TO INPUTS

Environment

The environment was assumed to affect only the material properties and not the geometry of the pavement material. The environment can be described by temperature and moisture parameters.

Temperature—Temperature was assumed to affect only the asphalt concrete properties. Temperature exerts a major influence on both the asphalt concrete modulus and fatigue characteristics. Therefore, two levels of the temperature parameter were considered in the analysis, a macrolevel and a microlevel.

Four macrolevels were considered: 40, 60, 80, and 100 F, which were representative of climates ranging from cold to hot. Within each macrotemperature level,

microtemperature variations of ±1, ±3, and ±6 F were considered. The microlevels represent the uncertainty in the predicted temperature environment used for design and the actual temperature environment experienced by the pavement within each type of climate. The microtemperature uncertainties selected were small variations because most recently developed rational pavement design procedures consider the temperature environment in sufficient detail that the actual temperature environment will be well represented.

The temperature uncertainty was related to the modulus using Figure 3. Its effects on both the strain value predicted from the structural analysis model and the fatigue characteristics were considered.

Moisture—The moisture environment of a pavement system can vary throughout the year and was assumed to affect only the modulus of the untreated base course and subgrade. Relations between modulus and moisture content vary with the specific materials. Therefore, it was decided that selection of a representative effect would be more appropriate. A range of modulus variation of ±25 percent from the average value was selected as representative of seasonal moisture variation effects for the base course and the subgrade.

Construction

Construction effects were selected to be representative of the differences that can be expected between design values and the actual as-built values because of the limits of construction control. Construction was considered to affect both the geometry of the pavement system and the material properties.

Thickness of Asphalt Concrete—The construction effect on geometry was considered only for the thickness of the asphalt concrete. Although it was recognized that the thicknesses of other layers will also be affected, these effects on the performance of the pavement are small in comparison. Thickness variations of ±¼ in. and ±½ in. from the average design values for the asphalt concrete were considered in the analysis. Construction effects on material properties were considered through variations expected for air void content of the asphalt concrete, placement water content, and density of the base course and subgrade.

Air Voids—Variations in air void content affect both the modulus and the fatigue characteristics (at a given modulus and strain level) of asphalt concrete. The effect of air void variations on modulus has been established (5, 9). It has been shown that, at a given temperature, the logarithm of modulus decreases linearly with increase in air voids. The effect of air void content on the fatigue life at a given modulus and strain level has been established (5): A linear decrease in the logarithm of fatigue life occurs with increase in air voids. The slopes of these relations were used to consider the effects of air void variations of ±1, ±2, and ±3 from the average (design) value.

Water Content and Density—The limits of construction control also induce variation from the design value of the water content and density of the base course and subgrade at the time of placement. The effect of water content and density variation on the moduli values is dependent on the specific materials used. Therefore, a representative range of variation of ±25 percent from the average value for both the base course and the subgrade modulus was selected.

MATERIAL CHARACTERIZATION

All materials considered in this analysis were characterized by linear-isotropic elasticity. The two constitutive constants utilized were modulus and Poisson's ratio. Uncertainty in these material "constants" arises because of deviations from ideal behavior and possible experimental errors.

Asphalt Concrete

The range of moduli values indicated by the vertical bars shown in Figure 3 at each temperature tested indicates the magnitude of uncertainty associated with a range of stress states representative of those expected for in-service conditions. Moduli varia-

tions of ±10, ±20, and ±40 percent from the average value at each temperature were considered. A ±0.1 variation in Poisson's ratio was analyzed.

Untreated Base Course

The preliminary layered non-linear-elastic analysis used to establish an average linear-elastic modulus for the base course was also used to select a representative range of variation of modulus. These results indicated that variations of -20, -40, -60, +25, +50, and +100 percent from the average modulus were representative of possible uncertainties associated with an average linear-elastic base course modulus. A variation of ±0.1 from the average Poisson's ratio was also considered.

Subgrade

The modulus of a particular subgrade varies with stress state and number of load repetitions. Subgrade modulus variations of -20, -40, -60, +25, +50, and +100 percent from the average value were considered. A ±0.1 variation of Poisson's ratio was also considered.

Asphalt Concrete Failure Characteristics

The fatigue failure characteristics for each asphalt concrete stiffness shown in Figure 4 are best-fit regression lines. The scatter of experimental results about each regression line can be measured by the standard error of estimate. Uncertainty in the fatigue criteria themselves was considered using a representative standard error magnitude of 0.2 (5) and ±1 and ±2 standard errors from the average regression fits.

The parameters considered in the sensitivity analysis, range of variations about their average value, and system inputs affected are given in Table 1. Temperature and air voids were not direct system inputs but were related to the system inputs utilizing previously mentioned relations. The range of uncertainty of each parameter given in Table 1 was investigated for each of the three structural sections and four macrotemperature levels.

PROCEDURE FOR CONDUCT OF ANALYSIS

The procedure for conducting the analysis was to first predict the fatigue life for each structural section and macrotemperature level using the average values for all system inputs. These fatigue lives are considered to be the average fatigue life for each condition. Once the average fatigue life values had been established, the influence of variations (uncertainty) in the system inputs caused by variations in the parameters given in Table 1 was considered. Each level of uncertainty in each parameter was considered independently. Therefore, each fatigue life was determined by changing one parameter from its average value while holding all others at their average value. This defined a new fatigue life prediction caused by a change in each parameter. The change in fatigue life from the average value could then be expressed as a percentage of the average fatigue life. These percentage changes were utilized to evaluate the sensitivity of fatigue life to uncertainty levels in each parameter.

Figure 5 shows the percentage of decrease in fatigue life from the average fatigue life as a function of the range of variation of each parameter for section 2 at 60 F. Only parameter variations causing decreases in fatigue life are presented here because prevention of premature failures is normally the objective of a pavement design or construction specification. Similar plots were made for each structural section and macrotemperature level.

RELATIVE SENSITIVITY OF FAILURE TO PARAMETER VARIATIONS

The relative sensitivity of fatigue life prediction to parameter variations is obtained by selecting and comparing the effect of compatible uncertainty (variation) levels of each parameter. The technique used to establish compatible uncertainty levels for each parameter was to select each parameter variation such that each had approximately the same likelihood of occurring.

Figure 4. Fatigue failure criteria (5).

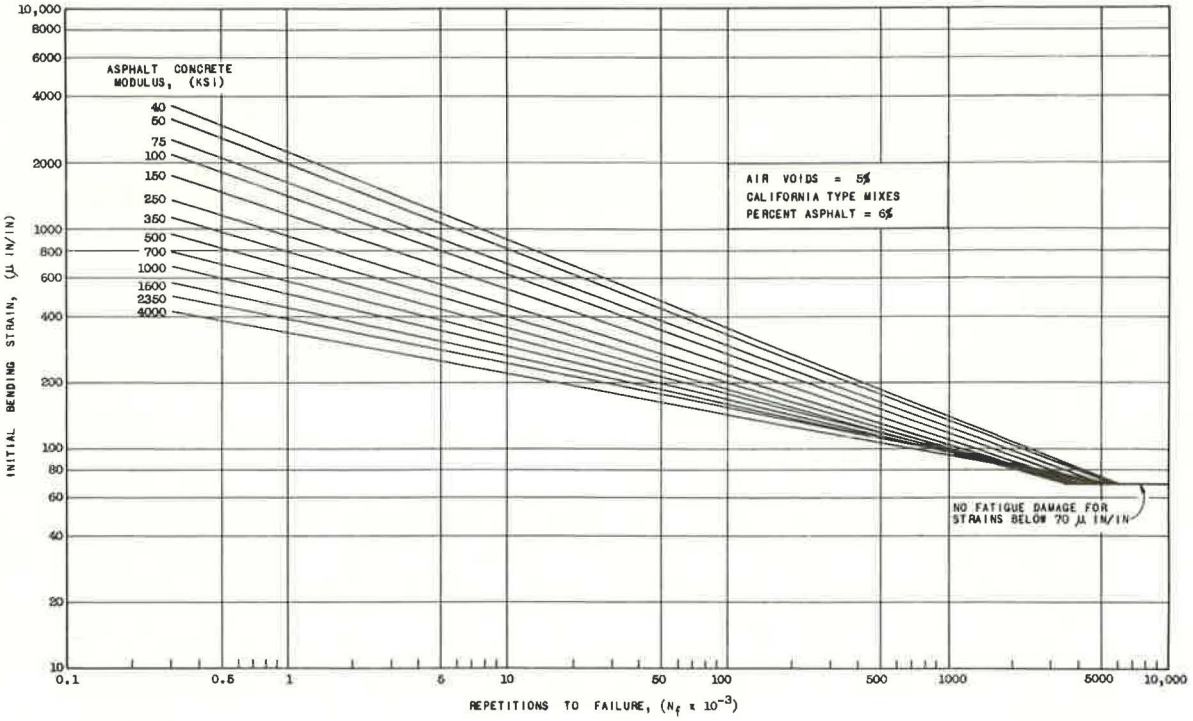

Table 1. Study parameters.

Parameter	Range of Variation About Average Value	System Input Affected
Temperature (T)	±1, ±3, ±6 F	Modulus of asphalt concrete and fatigue criteria
Air voids (AV)	±1, ±2, ±3 percent	Modulus of asphalt concrete and fatigue criteria
Thickness of asphalt concrete[a] (t_{AC})	±¼, ±½ in.	Thickness of asphalt concrete
Fatigue criteria[a] (N_f)	±0.2, ±0.4 (standard error)	Fatigue criteria
Modulus[a]		
Asphalt concrete (E_{AC})	±10, ±20, ±40 percent	Modulus of asphalt concrete and fatigue criteria
Base course (E_{BC})	-20, -40, -60, +25, +50, +100 percent	Modulus of base course
Subgrade (E_{SG})	-20, -40, -60, +25, +50, +100 percent	Modulus of subgrade
Poisson's ratio[a]		
Asphalt concrete (ν_{AC})	±0.1	Poisson's ratio of asphalt concrete
Base course (ν_{BC})	±0.1	Poisson's ratio of base course
Subgrade (ν_{SC})	±0.1	Poisson's ratio of subgrade

[a]These represent system inputs.

The level of each compatible parameter variation was selected such that the probability that variations would be less than the selected level or of opposite sign was 0.7 to 0.8. This selection was based on experimental results and published statistical properties of each parameter when possible (6, 10, 11, 12).

Table 2 gives relative sensitivity results for section 2 at each macrotemperature level. The compatible (equal likelihood) uncertainty levels selected for each parameter are indicated in parentheses. Similar tables for sections 1 and 3 using the same compatible uncertainty levels were used to construct plots of the relative sensitivity results shown in Figures 6, 7, and 8.

Relative sensitivity results for section 1 at 40 and 60 F and section 2 at 40 F were not meaningful because the fatigue criteria utilized predict no fatigue damage for strains below 70 μin./in. Results for section 3 at 80 F and 100 F were not possible because the tensile strains exceed the defined range of the fatigue criteria.

Relative sensitivity results for both -25 and -50 percent variations, in untreated base course and subgrade moduli, are shown for each section because little information was available to separate the influence of deviations from ideal material behavior and variation of in-place properties (i.e., water content and density). The -25 percent results are thought to be representative of the influence of modulus uncertainty due to either cause, and the -50 percent results are representative of the combined influence of modulus uncertainty due to both in-place field variations and nonideal material behavior.

INTERPRETATION OF RESULTS

The relative sensitivity results were derived for constitutive material characterization errors representative of those utilizing isotropic linear-elastic theory. However, the temperature dependence of asphalt concrete modulus was recognized and considered. Therefore, the uncertainties induced in fatigue life because of variations in the elastic parameters considered here reflect characterization uncertainties caused by anisotropy or nonlinearities and experimental error or both rather than the differences in viscoelastic or "pseudo" elastic characterizations.

The relative sensitivity analysis was conducted for several macrotemperature levels for each structural section and represents climates ranging from cold to hot. The variation of temperature about some average value influences the interpretation of the relative sensitivity results because a Miner's hypothesis for cumulative fatigue damage is normally used when more than one temperature level is considered.

The fatigue life at a particular strain level increases with temperature increase. However, because the asphalt concrete modulus decreases with increase in temperature, the maximum tensile strain in the asphalt concrete increases. The net result of a temperature increase for the pavement sections analyzed is that the effect of the higher strain level dominates and results in a smaller fatigue life. This is according to the criteria developed by Monismith and his associates. It is recognized that there are other fatigue criteria that would not give this result. Because the volume of traffic is normally considered uniformly distributed throughout the year and Miner's cumulative damage hypothesis is used, the majority of the fatigue damage occurs during the warmer months of the year. Therefore, the relative sensitivity of fatigue life to variable uncertainty at the higher macrotemperature levels is more significant than at lower macrotemperature levels for mixed temperature environments.

Note that uncertainty in fatigue life induced by uncertainty of in situ air voids, asphalt concrete thickness, and fatigue criteria definition can be considered independent of the constitutive parameter uncertainties because of the manner in which each was considered. The uncertainty induced by these three parameters would exist even if each material were perfectly characterized by linear-isotropic elasticity. Therefore, the combined uncertainty due to these three parameters can be used as a measure of the relative significance of constitutive parameter uncertainty.

The relative sensitivity results shown in Figures 6, 7, and 8 provide a quantitative measure of the relative importance of uncertainty induced by nonideal behavior and experimental errors in materials characterization on fatigue life prediction. Further-

Figure 5. Sensitivity of fatigue life to parameter variations for section 2.

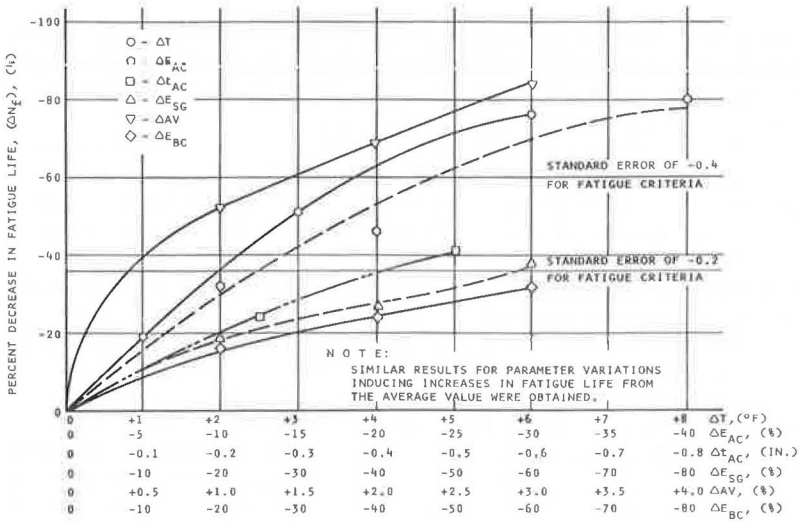

Table 2. Relative sensitivity analysis of section 2.

Parameter	T = 40 F[a] ($\bar{\epsilon}$ = 50 μin./in., $\bar{N}_f$ = > 5 × 10^6)		T = 60 F ($\bar{\epsilon}$ = 105 μin./in., $\bar{N}_f$ = 740 × 10^3)		T = 80 F ($\bar{\epsilon}$ = 300 μin./in., $\bar{N}_f$ = 36 × 10^3)		T = 100 F ($\bar{\epsilon}$ = 635 μin./in., $\bar{N}_f$ = 14 × 10^3)	
	$\frac{\Delta N_f}{\bar{N}_f}$ (percent)	Percentage of Total	$\frac{\Delta N_f}{\bar{N}_f}$ (percent)	Percentage of Total	$\frac{\Delta N_f}{\bar{N}_f}$ (percent)	Percentage of Total	$\frac{\Delta N_f}{\bar{N}_f}$ (percent)	Percentage of Total
ΔE_{AC}[b] (varies)	0	0	30	12	22	13	7	4
ΔT (+1 F)	0	0	19	8	8	4	14	8
Δt_{AC} (-0.25 in.)	0	0	24	10	11	6	14	8
ΔN_f (-1 standard error)	0	0	36	14	36	21	36	21
ΔE_{SG} (-25 percent)	0	0	21	8	10	6	9	5
ΔE_{BC} (-25 percent)	0	0	18	7	17	10	27	16
ΔAV (+2 percent)	0	0	69	27	47	27	43	25
$\Delta \nu_{AC}$ (-0.1)	0	0	16	6	14	8	4	2
$\Delta \nu_{BC}$ (+0.1)	0	0	11	4	6	3	11	7
$\Delta \nu_{SG}$ (+0.1)	0	0	11	4	4	2	4	2
Total	0	0	255	100	175	100	169	100

Note: $\Delta E_{BC} = \Delta E_{SG}$ = -25 percent.

[a]No fatigue damage for strains below 70 μin./in.

[b]ΔE_{AC} = -2 percent at T = 40 F, ΔE_{AC} = -10 percent at 60 F, ΔE_{AC} = -20 percent at 80 F, ΔE_{AC} = -35 percent at T = 100 F.

Figure 6. Relative sensitivity of fatigue life to parameter variations for section 1.

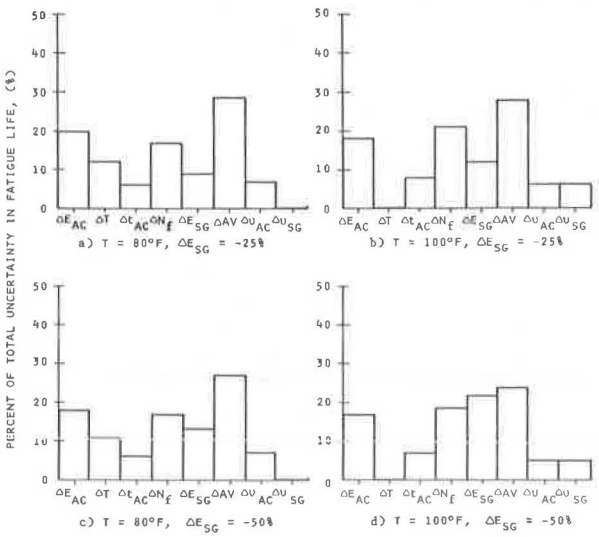

Figure 7. Relative sensitivity of fatigue life to parameter variations for section 2.

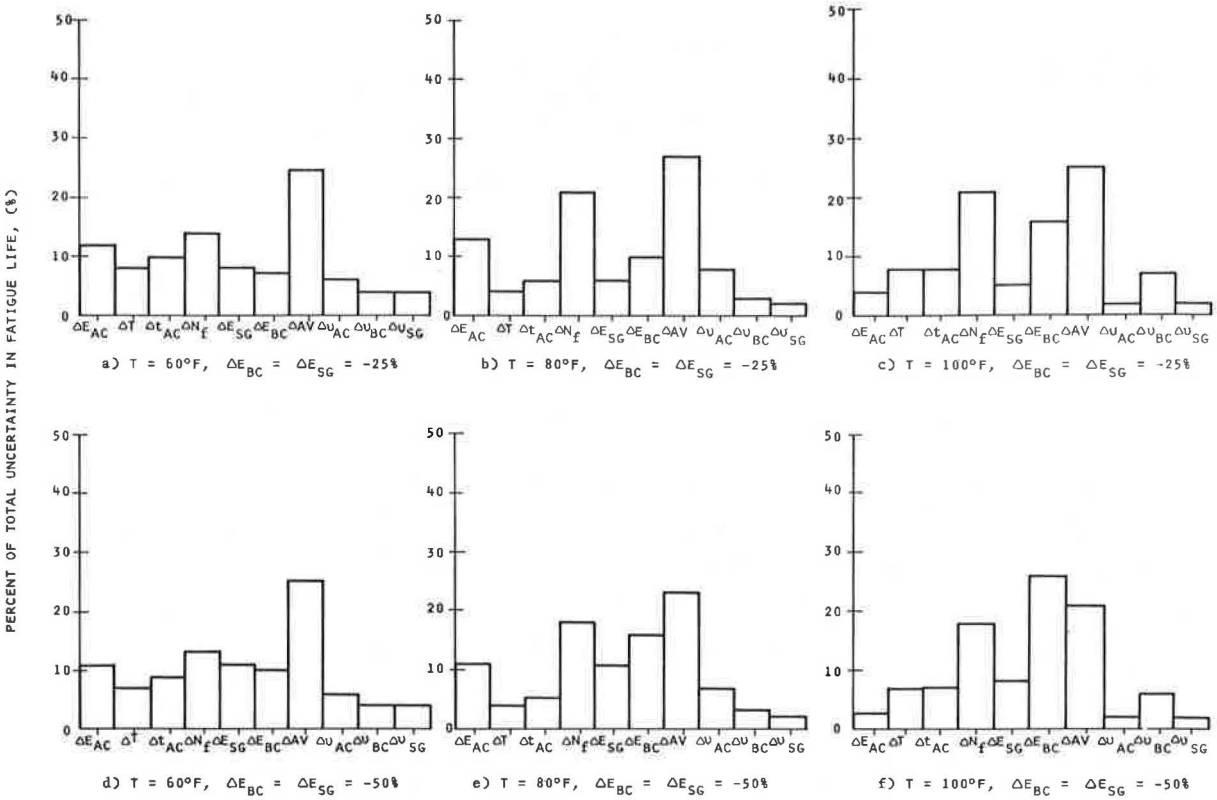

Figure 8. Relative sensitivity of fatigue life to parameter variations for section 3.

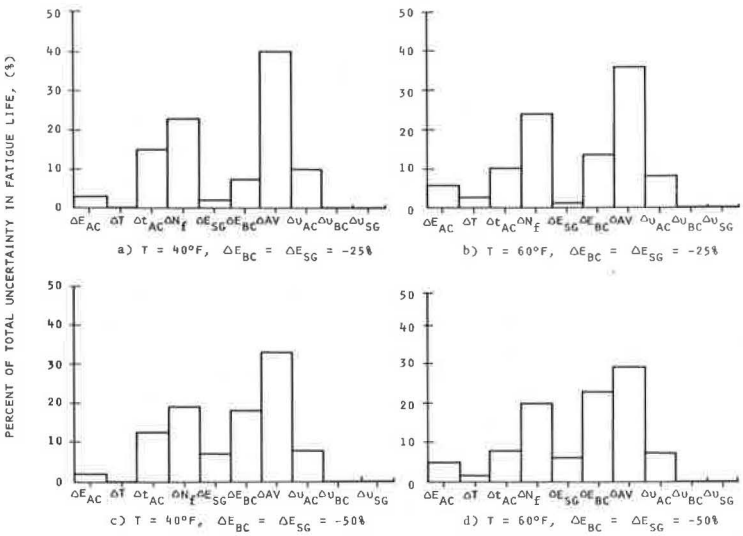

more, the relative sensitivity results can be utilized to select the areas of pavement research that could prove most beneficial in improving our ability to reduce fatigue failure of pavements. Better control or definition of parameters that induce large uncertainties in fatigue life would result in substantial reductions in highway maintenance costs.

With one exception, variation in the air void content of the asphalt concrete was the single most important parameter inducing uncertainty in the fatigue life of a pavement. It should be recognized that influence of air voids was examined through its effect on both the modulus and fatigue characteristics of the asphalt concrete. This dual influence emphasizes the need for better construction control techniques of asphalt concrete air void content.

The results also indicate that, generally, the second most important parameter variation inducing uncertainty in the fatigue life is that associated with the definition of the fatigue criteria themselves. Although much effort has been spent in developing the currently available fatigue criteria, it appears further work could greatly improve the ability to predict and, therefore, control the fatigue failure of flexible pavements.

The variability in the thickness of asphalt concrete surfacing due to construction practices has a relatively minor influence on the total uncertainty of fatigue life for pavement sections similar to sections 1 and 2. However, for pavements with thin asphalt concrete surfaces (section 3) the control of thickness is more critical.

The temperature parameter variation utilized for the relative sensitivity analysis was selected, based on accurate consideration of the temperature environment currently used in the more recently developed pavement design and analysis methods. Therefore, the variation more closely represents the uncertainty in predicting the average daily temperature rather than the uncertainty in predicting average yearly temperature. The effect of temperature variation was relatively minor for all cases. Methods that consider the temperature regime by an average yearly temperature would induce a much larger uncertainty in fatigue life because of the temperature parameter variation. Overall, the temperature regime itself has more influence on the fatigue life than any parameter considered in this analysis. This fact is not directly evident from the relative sensitivity analysis because the influence of the temperature regime was considered using several macrotemperature levels. In fact, the two levels (micro and macro) of the temperature parameter utilized in this analysis were motivated by this very fact.

The influence of water content and density variations in the base course and subgrade is revealed by comparison of the upper and lower (-25 percent and -50 percent) modular variation relative sensitivity results shown in Figures 6, 7, and 8. Examination of these results reveals that the importance of water content and density variations increases as temperature increases for each structural section. This occurs because the base course and subgrade contribute more to the total strength of the structural section as the temperature increases and the asphalt concrete contribution decreases. Thus, induced base course and subgrade modular variations at higher temperatures become more significant. It appears that measurable improvements in fatigue life could be gained from control and consideration of water content and density variations in the base course and subgrade for pavements in hot climates.

The effect of variations in the asphalt concrete modulus parameter induced by deviations from ideal isotropic linear-elastic behavior and experimental errors is more important for full-depth sections (section 1) than for thin-surfaced sections (section 3). (The uncertainty induced in fatigue life is of major significance for section 1, but of almost no significance for section 3. The effect on fatigue life for section 2 is intermediate, except at 100 F where it is of no practical significance.) Generally, the effect of asphalt concrete modular variations decreases with increase in temperature even though the percentage of variation in modulus used for the relative sensitivity analysis (characterization variations) increased with temperature (Table 2).

The influence of variation of the base course modulus parameter induced by isotropic linear-elastic characterization errors (-25 percent variation) was of similar magnitude to that associated with asphalt concrete modulus for the lower temperatures for section 2 and of greater significance at both temperatures for section 3.

The effect of variation in the subgrade modulus parameter induced by isotropic linear-elastic characterization errors (-25 percent variation) was generally of minor significance. The effect was of most importance for the full-depth section (section 1) and was of practically no significance for section 3.

The influence of variations in the Poisson's ratio parameter for each material was only of minor significance for all structural sections. In some cases, Poisson's ratio variations showed no measurable effect on fatigue life uncertainty.

It should be recognized that all the sensitivity results were based on only the fatigue mode of pavement distress. Although this is a logical initial step for determining the relative significance of adequate constitutive characterizations for each material type, the sensitivity results may be quite different for other modes of pavement distress. A pavement must be designed for all modes of pavement distress to ensure that it provides adequate performance. For example, this sensitivity analysis has shown that the single most important parameter uncertainty contributing to the total uncertainty in fatigue life was control of air voids in the field. The air void content uncertainty above a specified level can be reduced by increasing the asphalt content of the mix or by increasing the density. However, this may result in instability of the mix, unacceptable plastic deformations, and hazardous skid resistance conditions due to flushing of the asphalt. Therefore, all modes of pavement distress need to be considered for a complete definition of an adequate characterization of each material.

CONCLUSIONS

The results of the relative sensitivity analysis indicate the following conclusions concerning the improvement of prediction and control of flexible pavement fatigue life:

1. The predominant parameter variation causing uncertainty in fatigue life is that associated with construction control of air voids in the asphalt concrete.
2. A more accurate definition of the fatigue failure criteria for asphalt concrete would be more beneficial than improvement of the constitutive material characterization beyond isotropic linear elasticity.
3. The uncertainty associated with characterization of pavement materials by isotropic linear elasticity can contribute significant uncertainty to the prediction of fatigue life. However, this induced uncertainty in fatigue life is of less significance than that induced by field control of air voids or fatigue criteria definition. Improved characterization of asphalt concrete would be most beneficial for full-depth and thick asphalt concrete surface pavements. More accurate characterization of untreated granular base course material would also be advantageous, especially for pavements located in hot climates. An isotropic linear-elastic characterization of subgrades is adequate if the characterization is performed under stress levels representative of in-service subgrades.
4. Consideration of variations in water content and densities of in situ base course and subgrade materials would be beneficial for pavements located in hot climates.
5. Within the existing techniques for considering temperature in the analysis, the ability to predict the temperature is sufficiently accurate.
6. Thickness control of the asphalt concrete layer during construction is currently sufficiently accurate.

It should be recognized that the adequacy of a material characterization is a dynamic phenomenon. As our ability to describe and control the effects of other parameters influencing the fatigue life of flexible pavements improves, currently adequate characterizations may become inadequate.

ACKNOWLEDGMENTS

This research is part of a current study to develop procedures for characterization of pavement materials under the sponsorship of the U. S. Department of Transportation, Federal Highway Administration. The opinions, findings, and conclusions expressed in this publication are those of the authors and not necessarily those of the sponsors of this project.

REFERENCES

1. Finn, F. N. Observations of Distress in Full-Scale Pavements. HRB Spec. Rept. 126, 1970, pp. 86-90.
2. Deacon, J. A. Fatigue of Asphalt Concrete. Univ. of California, Berkeley, PhD thesis, 1965.
3. Monismith, C. L. Asphalt Mixture Behavior in Repeated Flexure. Univ. of California, Berkeley, Rept. TE 66-6, 1966.
4. Monismith, C. L., Epps, J., and Kasianchuk, D. Asphalt Mixture Behavior in Repeated Flexure. Univ. of California, Berkeley, Rept. TE 68-8, 1968.
5. Monismith, C. L., Epps, J., Kasianchuk, D., and McLean, D. Asphalt Mixture Behavior in Repeated Flexure. Univ. of California, Berkeley, Rept. TE 70-5, 1970.
6. Nair, K., and Chang, C. Y. Translating AASHO Road Test Findings: Basic Properties of Pavement Components—Materials Characterization. Materials Research and Development, 1970.
7. Nair, K., Smith, W., and Chang, C. Y. Characterization of Asphalt Concrete and Cement-Treated Granular Base Course. Materials Research and Development, 1972.
8. Hicks, R. G. Factors Influencing the Resilient Properties of Granular Materials. Univ. of California, Berkeley, PhD thesis, 1970.
9. Shook, J. F., and Kallas, B. F. Factors Influencing Dynamic Modulus of Asphalt Concrete. Proc. AAPT, Vol. 38, 1969, pp. 140-178.
10. The AASHO Road Test: Report 2—Materials and Construction. HRB Spec. Rept. 61B, 1962.
11. Sherman, G. B. In Situ Materials Variability. HRB Spec. Rept. 126, 1970, pp. 180-188.
12. Quality Assurance in Highway Construction. Bureau of Public Roads, Research and Development Rept., 1970.

THE PRINCIPLE OF SUPERPOSITION IN PAVEMENT ANALYSIS

R. G. Ahlvin, Y. T. Chou, and R. L. Hutchinson,
U.S. Army Engineer Waterways Experiment Station, Vicksburg

The principle of superposition was used in analysis of instrumentation data obtained in test sections constructed at the Waterways Experiment Station. Included were homogeneous sand and clayey silt test sections under plate loads and the multiple-wheel heavy gear load flexible pavement test sections under single- and multiple-wheel loads. It is found that the principle of superposition is approximately valid, indicating linear theory is not unreasonable in application to pavement analysis, although laboratory tests have definitely proved pavement materials behave nonlinearly under loads. The authors cannot answer the problem; the central purpose of this paper is to stimulate discussions by other researchers that will aid in pavement analysis.

IN dealing with the stress and deformation of continuous media caused by loads in mechanics problems, it is frequently convenient to consider the loads to be composed of two or more systems of loads and to assume that each system produces stresses and deformations independently, as though it were the only system of loads acting on the body. The actual effect is then considered to be the resultant of the effects of the two systems of loads. The method of obtaining the actual effect as a resultant effect, by adding or combining independent partial effects, is called the method of superposition. The method is applicable only if a linear relation exists between the loads and the effect they produce (1).

The method of superposition has been used very frequently by engineers. The method used is based on the assumption that the small displacements in the deformation do not affect substantially the action of the external forces; otherwise the justification of superposition principle fails. This method of superposition provides the backbone for the mathematical theory of linear elasticity. Because the stress-strain relation is linear, the deformation is a linear function of the load, regardless of the order in which the loads are applied; also the material constants are the same for compression and for tension and are invariant relative to the state of the stress.

Although the principle of superposition possesses overwhelming advantage in its simplicity of application, it is the principle itself that so drastically limits the application of the theory to the field of pavement design. Laboratory tests indicate that pavement materials generally do not exhibit linear stress-strain behavior and that the elastic moduli of such materials vary with the state of the stresses (except perhaps under very small stresses and strains). In this study, the principle of superposition was used in the analysis of instrument-measured data from homogeneous sand and clayey silt test sections under plate loads (2, 3) and from the multiple-wheel heavy gear load (MWHGL) flexible pavement test sections under single- and multiple-wheel loads (4). The results and measured values are presented and followed by discussions.

SUPERPOSITION OF MEASURED STRESSES AND DEFLECTION

In spite of nonlinearity of the soil, the principle of superposition was found to be reasonable in homogeneous test sections (2, 3) where stresses and deflections were

Publication of this paper sponsored by Committee on Theory of Pavement Design.

measured at different locations under single and dual plates of various sizes and load intensities. The plotted points shown in Figure 1 represent deflections in the sand test section measured beneath dual plates, which were 1,000 in.^{2} in size and were spaced 4.5 ft center to center. Curves were developed by superposing ordinates from smooth curves drawn through points representing deflections measured beneath single-plate loads. Figure 2 shows relations for vertical stresses developed in the same manner as shown in Figure 1. It is seen that the principle of superposition is more valid for stress than for displacement.

Figures 3 and 4 show data from the clayey silt test sections and are similar to Figures 1 and 2 respectively. The dual plates were 500 in.^{2} in size and were spaced 3.0 ft center to center Measurements of single-plate loads smaller than 500 in. were not available (2). For the purpose of this study, measurements at the outside region of dual-plate loads spaced at 7.5 ft center to center were considered to be the same as measurements of single-plate loads. The readings so obtained are slightly greater than actual single-plate loads would be, but the differences are believed to be negligibly small. The plots strongly indicate that the principle of superposition is more valid in clay than in sand.

Results shown in Figures 1 through 4 are for homogeneous soil masses. The principle of superposition was also applied to instrumentation data obtained in test item 3 of the MWHGL test section (4). The item consisted of a 3-in. asphaltic concrete surface, a 6-in. graded crushed-stone base, a 24-in. gravelly sand subbase, and a 4-CBR heavy clay subgrade soil. WES pressure cells (3, p. 19), LVDT, and other instruments were embedded in the pavement at different depths up to 12 ft. Figures 5 and 6 show the results of deflection measurements at various depths for loading by one twin-tandem component of a Boeing 747 wheel assembly (120 kip) and a C-5A 12-wheel gear assembly (360 kip) respectively. The gear configurations are shown in Figure 7. The plots in Figures 5 and 6 strongly indicate that the principle of superposition is reasonably valid for flexible pavements except at depths near the surface. It appears that large stress intensities involved near the surface have stressed the material into its nonlinear range, whereas materials below the surface are still within or near their linear ranges. It should be noted that the analysis presented in this paper is based on heavy aircraft loads and relatively thin pavement; the principle of superposition should be more valid for light highway loads.

IMPLICATION OF THE PRINCIPLE OF SUPERPOSITION

In the application of linear theory of elasticity to compute the maximum stresses and displacements in a pavement structure under multiple-wheel loads, the computations are carried out for each individual load, and the results are linearly summed up for all loads. The principle of superposition is used in the Corps of Engineers flexible pavement method of design to estimate the equivalent single-wheel load (ESWL), which is defined as the load on a single tire of an assembly that produces the same vertical deflection of the supporting medium as that particular multiple-wheel assembly. The computations are usually carried out by constructing the deflection-offset curve under a single-wheel load and then summing the ordinates at the proper offsets, which gives the deflection due to the multiple-wheel load.

For dual wheels, it has been found that the use of the superposition principle gives results that are within the acceptable limit of error. For multiple-wheel heavy gear loads, however, such as Boeing 747 and C-5A, the computed ESWL becomes so large that the current criterion is too conservative (4). The error is not directly caused by the use of superposition principle but by many other inadequate assumptions of the linear theory of elasticity. This can best be explained by the MWHGL test results (4).

Figure 8 shows measured and computed deflection basins at the 12-ft depth of item 3 of the MWHGL test section. The deflections were induced by a single-wheel load (30 kip) and by the C-5A 12-wheel gear assembly (360 kip). The computed deflections are plotted in percentage of the maximum values. In both cases, the basin shape is quite different between computed and measured values. However, when the superposition principle is used on the measured single-wheel deflection basin (instead of the

Figure 1. Superposition of deflections measured in sand test sections.

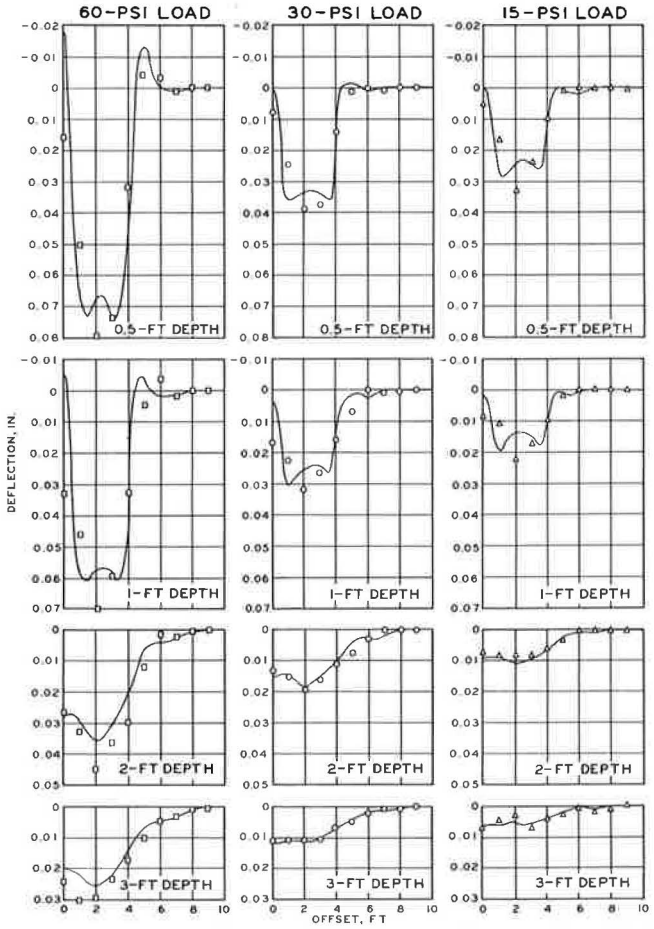

Figure 2. Superposition of stresses measured in sand test sections.

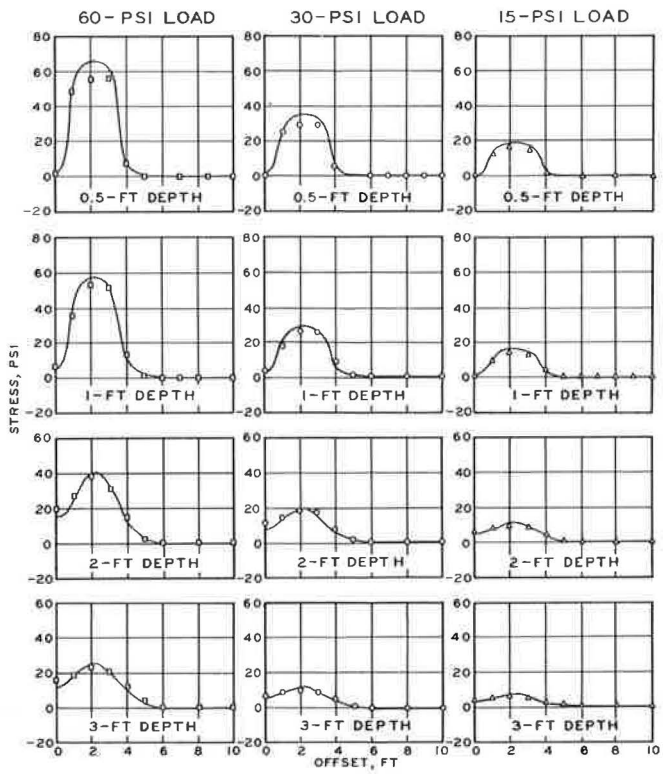

Figure 3. Superposition of deflections measured in clayey silt test sections.

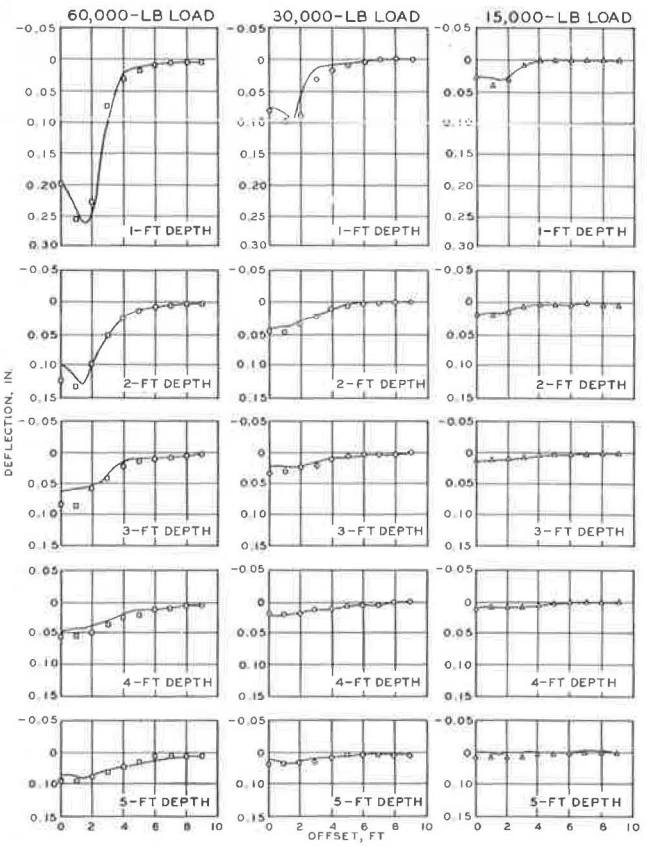

Figure 4. Superposition of stresses measured in clayey silt test sections.

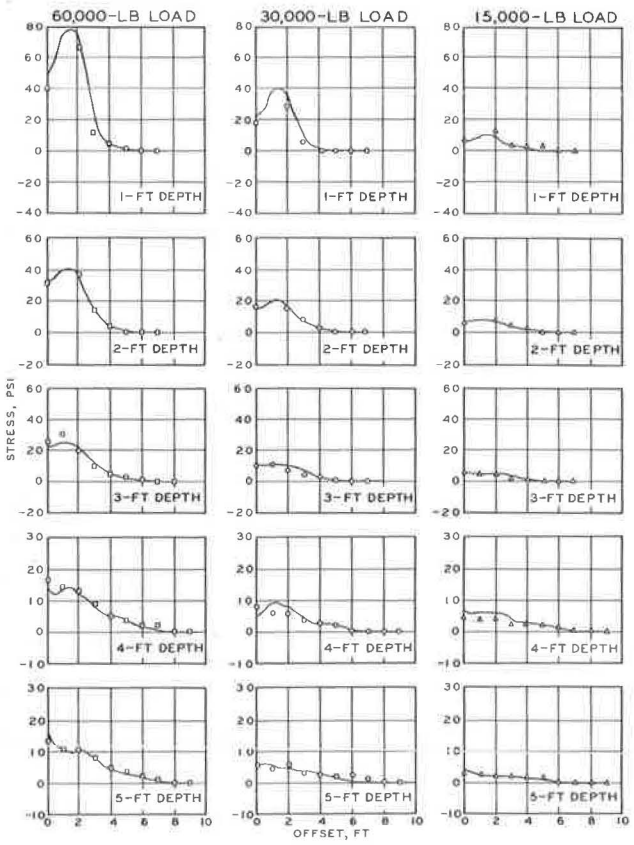

Figure 5. Superposition of deflections measured under loading by twin-tandems component, Boeing 747 assembly.

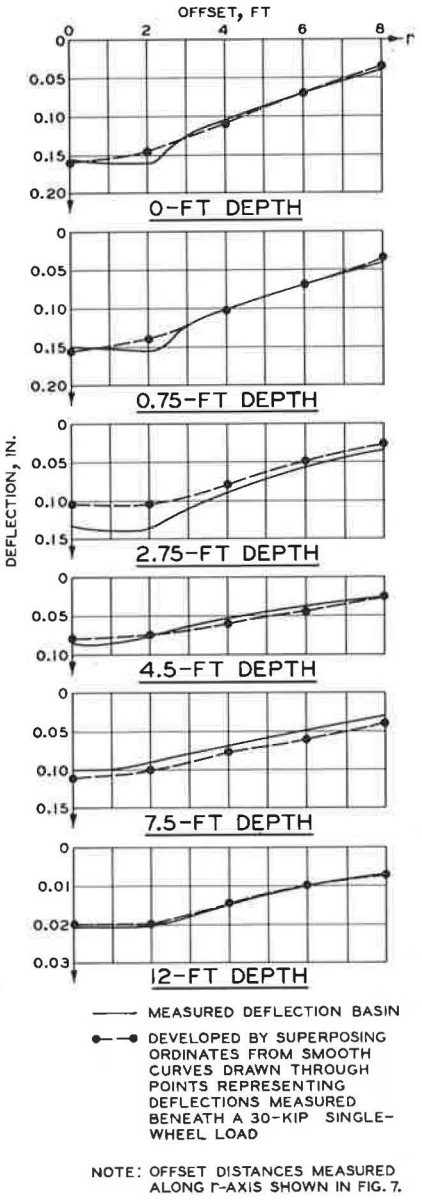

Figure 6. Superposition of deflections measured under loading by a 12-wheel gear, C-5A assembly.

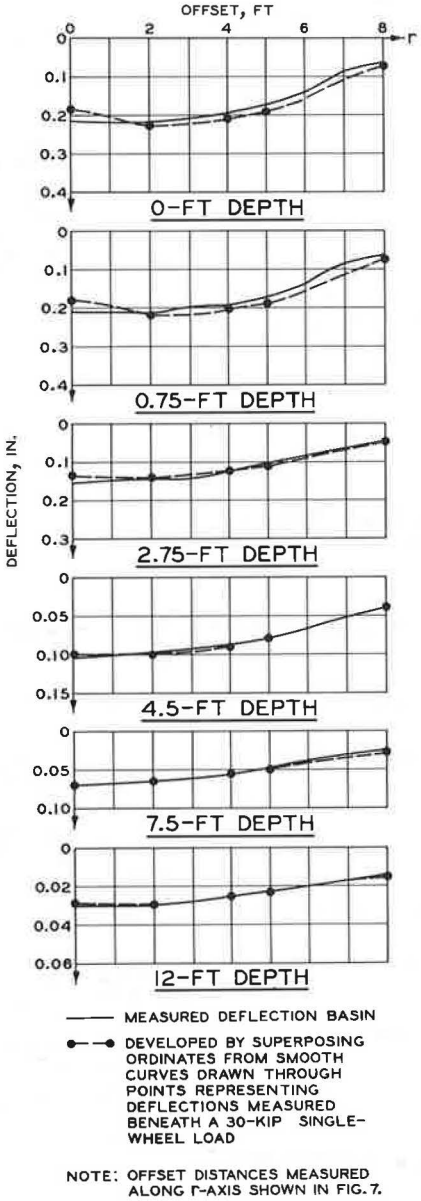

Figure 7. Gear configurations of C-5A and Boeing 747 test assemblies.

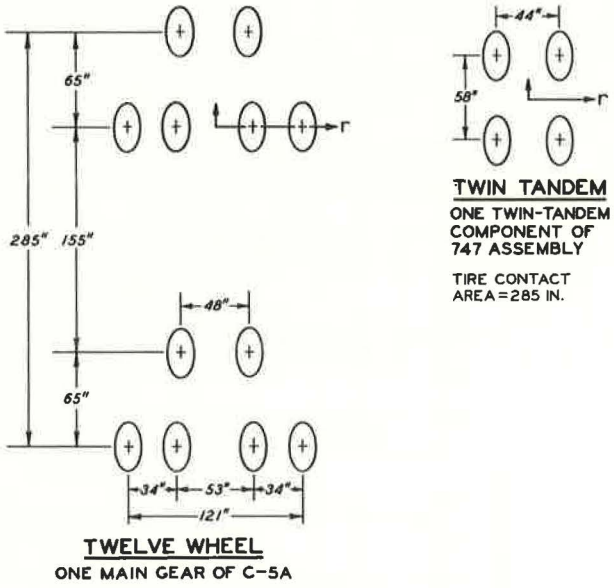

Figure 8. Theoretical and measured deflection basins.

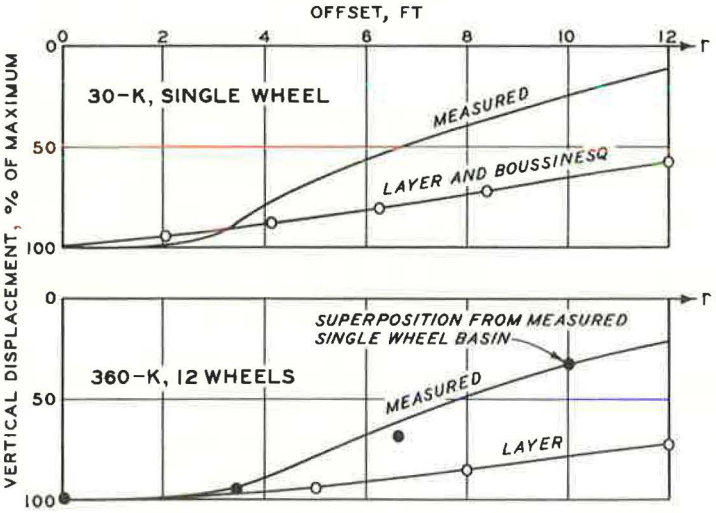

theoretical one) to obtain that of the 12-wheel basin, the resulting basin value is astonishingly close to the measured one of the 12-wheel basin. These are shown by the dots along the measured 12-wheel basin. Similar relations were also found for deflections measured at other depths. Test results shown in Figure 8 strongly verified the remark made in a previous paragraph regarding the source of error in the ESWL derived for multiple-wheel heavy gear loads.

As discussed earlier, the principle of superposition provides the backbone of the linear matematical theory of elasticity. The question promptly arises as to why the superposition principle is approximately valid for pavement problems but the linear theory of elasticity is not.

Elasticity implies that the material resumes its initial form completely after removal of loads and that the stress path is independent. Linearity further assumes the validity of the principle of superposition; i.e., the strain is linearly proportional to the stress, and the tension and compression properties are identical. For instance, when a triaxial sample is subjected to an axial compressive stress of 30 psi, if the material is linear, the sample would behave identically when the load is replaced by an axial compressive stress of 60 psi and an axial tensile stress of 30 psi. Certainly the assumption of linear elasticity is not true for soils unless the stresses and strains are very small.

Under pure shear, a linear isotropic material should suffer no volume change because the contraction in one direction is compensated for by an expansion of equal magnitude in the perpendicular direction. Consequently, the change in volume is the effect of hydrostatic forces, and the change in shape is the effect of shear forces. Because any state of stresses can be resolved into a mean normal stress and a pure shear, an ideally linear material, in which the principle of superposition is valid, must satisfy the following requirements: The change in volume resulting from the mean normal stress must be independent of the pure shear, and the change in shape resulting from the pure shear must be independent of the mean normal stress. Consequently, a stress tensor can be separated into two independent parts, one of which is the hydrostatic forces and the other is shear forces. The shear forces govern distortion, and the hydrostatic forces control dilatation.

Laboratory tests have definitely shown that the stress-strain relations for pavement materials are not linear because the shear strain depends not only on the shear stress but also on the mean normal stress, and the volume change depends on the mean normal stress as well as the shear stress. The dependence of shear strain on the mean normal stress naturally leads to the conclusion that material properties are different for tension and for compression.

The analysis presented in Figures 1 through 8 demonstrates that the principle of superposition as applied to pavement design is approximately valid. The stresses and deflections under multiple-wheel loads can be obtained from the correct stress and deflection basins of single-wheel load by the use of superposition principle. The implication is that the stresses and strains in the pavement, except near the surface, are so small that materials are stressed within or near their linear ranges; hence, linear analysis may not be the most critical factor in the disagreement between measurements and predictions. Evidently, there is a strong contradiction between prototype field measurements and laboratory findings in material behaviors. The writers cannot answer this problem; the central purpose of this paper is to stimulate discussions by other researchers that will aid in pavement analysis. It is also our intent to propose that, because the superposition principle has been proved valid (at least experimentally), efforts should be concentrated for refining technology in the nonlinear finite-element analysis method under single-wheel loads and that second priority should be given to efforts for developing a computer program for multiple-wheel loads, at least at the present time. This recommendation is made mainly because of the excessive computer time involved in multiple-wheel load analysis.

REFERENCES

1. Seely, F. B., and Smith, J. O. Advanced Mechanics of Materials. John Wiley and Sons, 1965.
2. Investigations of Pressures and Deflections for Flexible Pavements: Report 1—Homogeneous Clayey-Silt Test Section. U.S. Army Engineer Waterways Experiment Station, Vicksburg, Miss., Tech. Memo. 3-323, March 1951.
3. Investigations of Pressures and Deflections for Flexible Pavements: Report 4—Homogeneous Sand Test Section. U.S. Army Engineer Waterways Experiment Station, Vicksburg, Miss., Tech. Memo. 3-323, Dec. 1954.
4. Ahlvin, R. G., et al. Multiple-Wheel Heavy Gear Load Pavement Tests. U.S. Army Engineer Waterways Experiment Station, Vicksburg, Miss., Tech. Rept. S-71-17, Vols. 1-4, Nov. 1971.

DISCUSSION

Mihai Rafiroiu, University of Michigan

The authors of this paper deal with a fundamental problem concerning the structural design of pavements.

Their results are very important because they demonstrate experimentally that, despite the nonlinear behavior of the highway construction materials, under current loading highway pavements behave almost like linear-elastic solids.

It must be emphasized again that the real problem we deal with is the highway itself and not the theories and that experience can be the origin of knowledge. It also follows that every theoretical development should be verified experimentally. It is very difficult to do this because of the variance in properties of materials we use and the variance of the thickness of the layers. But, despite these difficulties, there is a method that can be used to eliminate any lack of fit between theory and practice.

Let us define the standard deviation of the characteristics of the materials by σ_j^m and the standard deviation of the thicknesses by σ_j^t. Let us also define the factors that are used in the design formula by P and a particular factor by P_i.

The particular factor P_i can be calculated in relation to the others (P_i^c):

$$P_i^c = f(P) \tag{1}$$

or it can be measured (P_i^m).

The function f in Eq. 1 may be either theoretical or empirical. Either one is useful, provided the computed results agree with the measured values.

Let us now define the control factor of the parameter P_i by X_i,

$$X_i = \frac{P_i^m}{P_i^c} \tag{2}$$

The perfect situation would be when, having P_i^c's as the abscissa and P_i^m's as the ordinate, one would get for X_i's a straight line (Fig. 9).

Unfortunately, this situation never occurs. If it were to take place, it could be represented from a statistical point of view (Fig. 10).

Generally, one gets more or less normal distribution values (Fig. 11).

The fact that the mode M is not at $X_i = 1$ indicates that the theoretical model is not perfect.

The quality of the model can be appreciated by the obliquity of the distribution of X_i. If one knows the standard deviation of the distribution in X_i (σ_{xi}), one can define the obliquity (O_i) as being

$$O_i = \frac{M - 1}{\sigma_{xi}} \tag{3}$$

Figure 9. Perfect correlation between measured and calculated values.

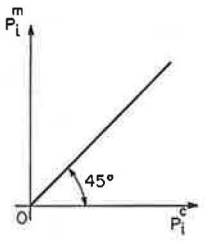

Figure 10. Perfect statistical correlation.

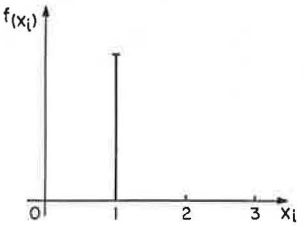

Figure 11. Normal distribution with obliquity.

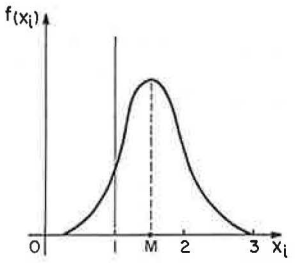

Figure 12. Two normal distributions with different standard deviations.

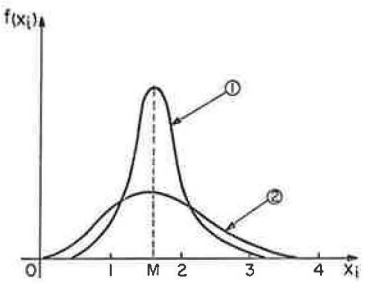

An obliquity rating scale has been proposed by the author as follows:

Obliquity	Rating
0 to 0.3	Perfect
0.3 to 0.8	Excellent
0.8 to 0.15	Very good
0.15 to 0.32	Good
0.32 to 0.50	Acceptable
More than 0.50	Not acceptable

But the distribution of X_i can be a sharp or a flat one (Fig. 12). Which is better?

To answer this question, let us consider that, starting from the design formula, one can develop a variance model that predicts a theoretical standard deviation of X_i ($\sigma^{o}_{x_i}$). Let us now consider that the actual standard deviation of k_i is $\sigma^{m}_{x_i}$.

One can state that the design formula is good if

$$\frac{\sigma^{m}_{x_i}}{\sigma^{o}_{x_i}} \approx 1 \qquad (4)$$

The author considers that a design formula is good if, and only if, the obliquity is low and the relation given in Eq. 4 is observed for each factor P_i that occurs in the design method.

If the principle of superposition really works, even for flexible pavements, the way for elastic methods is open indeed. However, all of the preceding considerations will have to be accounted for to get a consistent and sensitive method of design.

PAVEMENT SLABS RESTING ON ELASTIC FOUNDATION

Surendra K. Saxena, Port Authority of New York and New Jersey

The development of a rational method of analysis of any system must include the selection and analysis of a model for realistic input parameters. Based on this idea, a simple method has been developed for solution of often encountered problems of engineering practice involving slabs resting on subgrade. The slab is represented by a physical model, which is helpful in visualizing the problem and forming a solution. Regarding subgrade, most of the available analyses assume it to be a Winkler model, a physical model of a heavy liquid, or a bed of springs. In this paper the soil is treated as an elastic solid. With these two models for slab and subgrade, a computer method based on matrix analysis has been developed. From the solution of reactive subgrade pressures, the deflections are then subsequently used to compute stresses and bending moments. Two exemplary problems, one with a corner load and one with a center load, have been included. Comparison of the latter with the Winkler model is illustrated.

•MOST pavement analyses are based on the assumption that the deflection of the slab at any point is proportional to the reaction pressure at that point and does not depend on the pressure at any other point of foundation. This assumption, originating from Winkler (1), corresponds to the physical model of a heavy liquid or bed of springs.

The physical properties of the soils, however, are much more complicated than indicated by such a simple relation assumed by Winkler. From the known fact that soils can propagate waves, it is obvious that they can behave closer to elastic solids than to beds of springs. Wieghart (2) was the first to investigate the analogous beam problem under the general assumption that the deflection at any point depends on the subgrade reactions along a certain length 2L of the subgrade:

$$y(x) = \text{const.} \int_{-L}^{+L} g(\xi)k(|x - \xi|)d\xi \qquad (1)$$

where

y = deflection of a beam,
g = subgrade reaction,
k = a kernel function depending on type of subgrade.

Several investigators (3-8) developed solutions for different kernels, k, mostly through the use of Fourier integrals. However, no kernel function of space coordinates could reproduce the exact actual behavior of the subgrade. With the knowledge of soil behavior, the investigators have, of late, tried to include a function of time in the relation between deflection and reaction pressure. Ideally, such a model will be a nearly true representative of soil subgrade; its application has been very limited because of the rigorous mathematics involved.

Publication of this paper sponsored by Committee on Theory of Pavement Design.

In the particular case of a thin slab of infinite extent, exact solutions have been provided by Hogg (9) and Holl (10) by using elastic solid subgrade. Burmister (11), treating both the slab and the subgrade as elastic isotropic solids, has proceeded from the three-dimensional general equations of elasticity to find the solutions for a two- or three-layered solid. His work, however, deals with slabs of infinite extent only. Circular slabs of limited dimensions have been dealt with by Habel (12), who used difference methods. Other specific cases of slabs of finite dimensions have been investigated by De Beer (13), Grasshoff (14), Schultze (15), Kany (16), and Krasmanovic (17). A summary of extensive Russian studies along similar lines has been completed by Vlassov and Leont'ev (18).

Because of the rigor of mathematics used, few of the preceding works have been adopted by practicing engineers as regular tools in analysis. Limited solutions suitable for practical use aimed at load distributions over only circular loading surfaces have been developed (19, 20) where the influence values for a load on the interior of a slab have been calculated according to Hogg (elastic solid subgrade), but the edge loads have been computed according to Westergaard (Winkler subgrade). This work was subsequently extended by Pickett, Badaruddin, and Ganguli (21) to include the case of semi-infinite slab.

In the present paper, based on thin-plate theory, a physical model of the slab has been adopted. The model can handle homogeneous as well as orthotropic slabs of variable thickness. The subgrade is represented by an elastic, isotropic, homogeneous solid of infinite extent with a modulus of elasticity E_s and Poisson's ratio ν_s.

PHYSICAL MODEL OF THE SLAB

The finite-element model of the slab in this study was developed after Newmark by Hudson and Matlock (22). Figure 1 shows a typical nodal point. The axial deformability and Poisson's effects of slab elements are represented by elastic blocks. The torsional stiffness of the elements is represented by torsion bars and is always active in the system. It should be noted that the slab so formed may be of orthotropic behavior in any single element. There may be also arbitrary differences in individual stiffnesses of different elements. The free-body diagram of a nodal point giving all internal forces of the system is shown in Figure 2.

In the Hudson-Matlock model, the reaction of the subgrade was represented by a spring, giving it Winkler qualities. In the present study, the subgrade is treated as an isotropic elastic solid, and the reaction of the subgrade is represented by a force under the nodal point. This reactive force under node affects the whole continuum (elastic solid) and consequently influences all the forces and displacements of the continuum. The real difficulty experienced in the use of this subgrade is to account for all these influences. With the help of computers, it has been accomplished by superposition, by using Boussinesq's solution and Maxwell's reciprocal relation.

FORMULATION OF EQUATIONS

The equation of vertical equilibrium of a nodal point can be written as

$$-Q_{i,j} + S_{i,j} = V^x_{i,j} + V^y_{i,j} - V^x_{i+1,j} - V^y_{i,j+1} \qquad (2)$$

The shearing forces V in this expression can be evaluated in terms of bending and twisting moments that, in turn, can be expressed by their finite difference equivalents in terms of deflections of adjacent points.

After all transformations, Eq. 2 appears as a linear equation containing an unknown deflection of 13 nodal points clustered in a rhomboidal array around the considered nodal point i, j. It can be represented in matrix form as

$$[K_p]\{W\} = -\{Q\} + \{P\} \qquad (3)$$

Figure 1. Typical joint i with j taken from finite-element slab model (22).

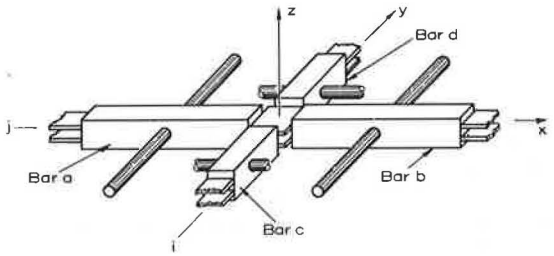

Figure 2. Free body of slab mesh point.

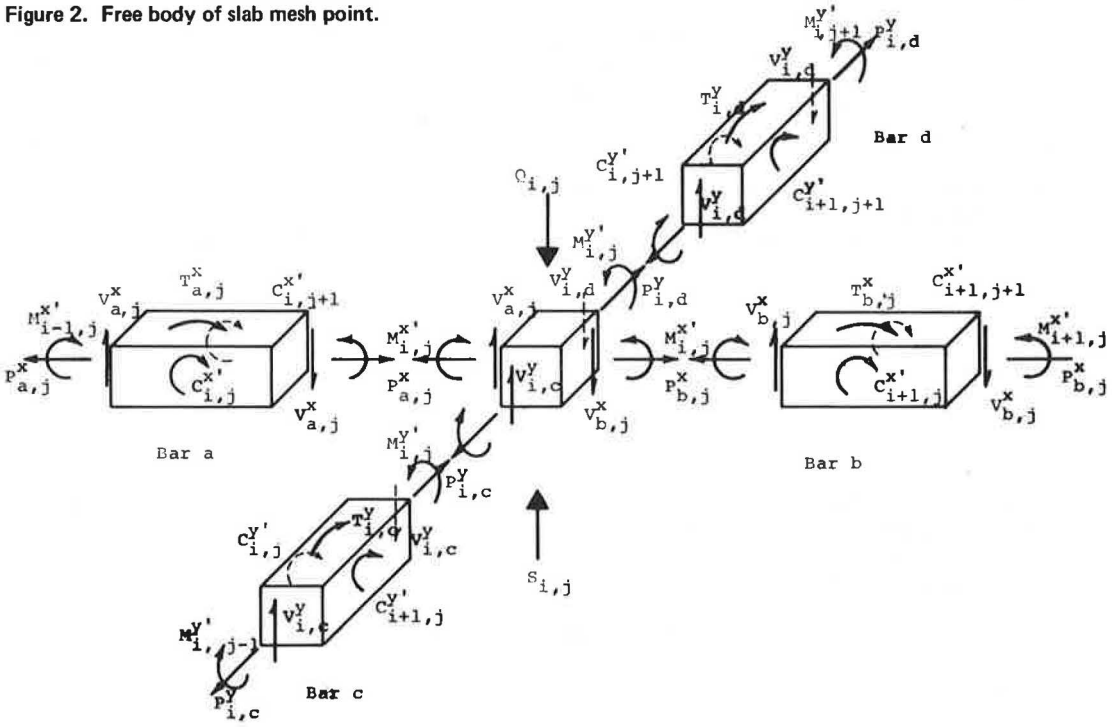

where

$[K_p]$ is termed as stiffness matrix of slab,
$\{W\}$ is deflection matrix,
$\{Q\}$ is load matrix, and
$\{P\}$ is reaction matrix.

Because we are using the finite-difference equations for moments, the stiffness matrix so obtained utilized one fictitious station beyond the real boundary of the slab. At those points, the terms in the load and reaction matrices are zero; i.e., the right-hand side of Eq. 3 is equal to zero. If the equations at these points were written, it would be immediately clear that they represent the so-called Kirchoff's conditions of the bending moments, being zero at edges. Figure 3 shows the forms of the K_p, W, Q, and P matrices.

The matrix $[K_p]$ and W can be rearranged as follows:

$$\begin{bmatrix} K_p^1 & K_p^2 \\ \hline K_p^3 & K_p^4 \end{bmatrix} \begin{Bmatrix} W_e \\ \hline W_i \end{Bmatrix} = \begin{Bmatrix} 0 \\ \hline -Q \end{Bmatrix} + \begin{Bmatrix} 0 \\ \hline P \end{Bmatrix} \tag{4}$$

where

$\{W_e\}$ represents deflections of all points external to real slab boundary, i.e., the fictitious points used; and
$\{W_i\}$ represents all internal points, i.e., points within real slab boundary.

Equation 4 can then easily be split into two as follows:

$$[K_p^1]\{W_e\} + [K_p^2]\{W_i\} = 0 \tag{5}$$

and

$$[K_p^3]\{W_e\} + [K_p^4]\{W_i\} = -\{Q\} + \{P\} \tag{6}$$

Equation 5 can furnish W_e in terms of W_i so as to satisfy the bending moments at boundaries to be zero. It may, however, be noted that the deflections W_e are not real because the slab does not exist there. They are used only to satisfy the boundary conditions in terms of finite differences. Consequently, from Eq. 5

$$\{W_e\} = -[K_p^1]^{-1}[K_p^2]\{W_i\} \tag{7}$$

Substituting this value of W_e in Eq. 6

$$-[K_p^3][K_p^{12}]\{W_i\} + [K_p^4]\{W_i\} = -\{Q\} + \{P\} \tag{8}$$

where

$$[K_p^{12}] = [K_p^1]^{-1}[K_p^2] \tag{9}$$

Naming

$$[BK_p] = [K_p^3][K_p^{12}] \tag{10}$$

one gets

$$\left[[K_p^4] - [BK_p]\right]\{W_i\} = -\{Q\} + \{P\} \tag{11}$$

Finally, calling

$$[AK_p^4] = [K_p^4] - [BK_p]$$

the simplified form of the equation becomes

$$[AK_p^4]\{W_1\} = -\{Q\} + \{P\} \tag{12}$$

This equation utilizes only the points within the real boundary of the slab and also serves to satisfy the boundary conditions.

FLEXIBILITY MATRIX OF SUBGRADE

It can be noted in Eq. 12 that matrix $[AK_p^4]$ is known and $\{Q\}$ is known, but the terms of matrices $\{W_1\}$ and $\{P\}$ are both unknown. Consequently the necessity of expressing the relation between $\{W_1\}$ and $\{P\}$ becomes obvious.

For an elastic isotropic solid, the deflection due to unit vertical and horizontal point loads has been given by Boussinesq and Cerruti. According to them the deflection at any point B due to a point load A is given as

$$W_{BA} = \frac{P}{\pi d_s} \frac{(1 - \nu_s^2)}{E_s} \tag{13}$$

where

P = load at point A, and
d_s = radial distance between points A and B.

Other terms have been previously explained. From Eq. 13, the deflection at the center of a uniformly loaded rectangular area (a × b) can be obtained by integration (Fig. 4):

$$W_1 = 2 \int_0^{x=a/2} \int_0^{y=b/2} \frac{P}{ab} \frac{(1 - \nu_s^2)}{\pi E_s} \frac{dx\,dy}{\sqrt{x^2 + y^2}} = \frac{P}{b} \frac{(1 - \nu_s^2)}{\pi E_s} I_w \tag{14}$$

where I_w for the case a = b equals 3.525. The value of I_w for cases commonly found are a/b = 2, I_w = 2.406; a/b = 3, I_w = 1.867; a/b = 4, I_w = 1.543; and a/b = 5, I_w = 1.322.

For any point outside the loaded area, one can do similar integration, but very good approximation can be achieved only by using Eq. 13 (by taking P as total load over the rectangle and d_s as center to center distance). Zienkiewicz (24) compared some exact results with that from Eq. 13 and found that, even for x = a, the error is only some 4 percent and decreases rapidly with increase of x.

Hence, using any set of grid points, in the case when the subgrade is of infinite depth, the deflections can be written as

$$W = -\frac{(1 - \nu_s^2)}{\pi E_s b} [f_f]\{P\} \tag{15}$$

where $[f_f]$ is the flexibility matrix of the foundation and can be obtained by Eq. 13 for points off the loaded area and by Eq. 14 for points under the loaded area.

COUPLING THE STIFFNESS MATRIX OF SLAB AND FLEXIBILITY MATRIX OF SUBGRADE

The column matrix W discussed previously is formed by the deflections of the interior points of any real slab and is thus analogous to the column matrix W_1 of Eq. 12. Substituting therefore the value of W from Eq. 15 into Eq. 12, one gets

$$[AK_p^4][AF_f]\{P\} = -\{Q\} + \{P\} \tag{16}$$

where

$$[AF_f] = -\frac{(1 - \nu_s^2)}{\pi E_s a}[f_f] \tag{17}$$

or

$$\left[[AK_p^4][AF_f] - I\right] \times \{P\} = -\{Q\}$$

where I is an identity matrix or

$$\{P\} = \left[[AK_p^4][AF_f] - I\right]^{-1} \{-Q\} \tag{18}$$

Having known $\{P\}$, we can find the deflections from Eq. 15. By using this approach, it is not necessary to invert the matrix $[AF_f]$. In all, two inversions are involved in the whole process, one being the inversion of matrix $[K_p^1]$ that will invariably be a small matrix and the other being inversion of a large matrix (size equal to number of increments in x-direction multiplied by number of increments in y-direction), $\left[[AK_f^4][AF_f] - I\right]$.

PROBLEM EXAMPLES

For illustration, two problems have been selected. The first case is a square slab with corner load, and the second one is with a center load.

Square Slab With Corner Load

The problem has been analyzed for different values of a nondimensional flexibility number

$$\alpha = \frac{E_s b a^3}{EI}$$

where

b = breadth of slab,
a = length of slab,
I = moment of inertia per unit width of slab,
E = modulus of slab, and
E_s = modulus of subgrade.

A larger value of α indicates a more flexible slab and vice versa.

Figure 5 shows a square slab in plan with many lines, each identified by a flexibility number. The two edges 1-2 and 1-4, and each one of these lines, represent the area of contact of the slab with subgrade, when the point of application of load is point 1.

Westergaard's corner formula has been investigated by many workers. According to it, the numerically greatest value of bending moment per unit widths is given by

$$M = -\frac{Q}{2}\left\{1 - \left(\frac{a_1}{1_0}\right)^{0.6}\right\} \tag{19}$$

where

$a_1 = r\sqrt{2}$, and
r = the diameter of area on which the load is acting.

This bending moment M occurs approximately at a distance

$$x_1 = 2\sqrt{a_1}\, 1_0 \tag{20}$$

from the load $\left[1_0 = \text{radius of relative stiffness} = \sqrt[4]{\frac{Et^5}{12(1 - \nu)k}}\right]$

Figure 3. Form of K, W, Q, and P matrices.

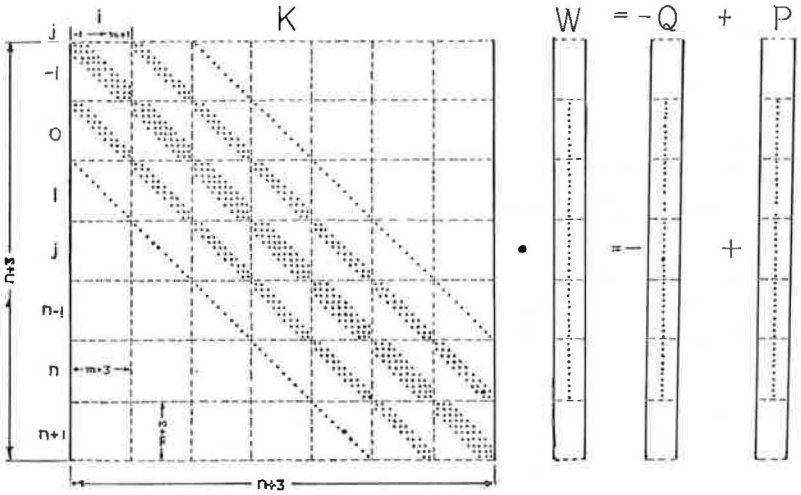

Figure 4. Deflection due to a uniformly loaded slab on isotropic solid subgrade.

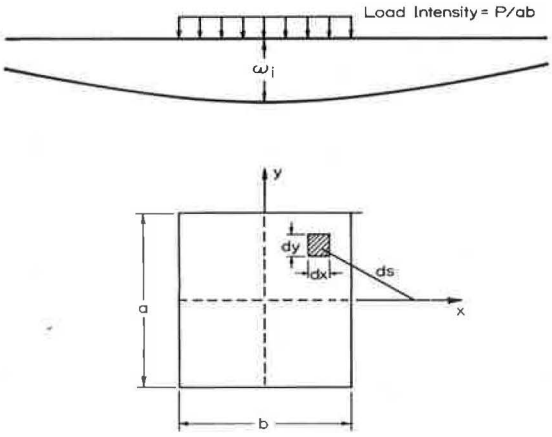

Figure 5. Lines of separation of contact with subgrade.

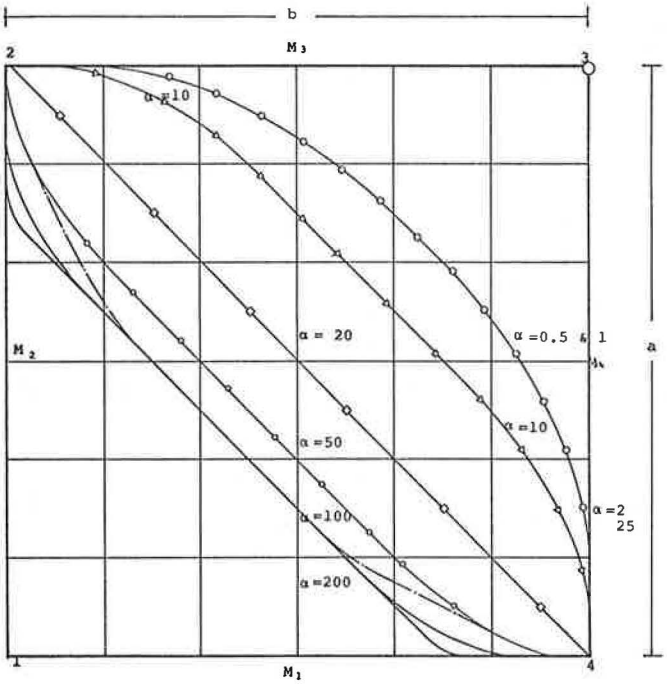

In cases where r = 0, a_1 will automatically become zero. The maximum moment becomes equal to $-\frac{Q}{2}$ and, according to formula, should occur under the load. This result that, regardless of the stiffness of slab and modulus of subgrade, the maximum bending moment will always be $-\frac{Q}{2}$ does not seem correct.

Investigations were therefore done for a point load applied at a corner of slabs of different rigidities. Figures 5 through 12 show the results of investigations. From Figure 7, it appears that the maximum moment along the diagonal changes in magnitude as well as location with the α-value. The peak moment is nearer to the point of application of load in case of flexible slabs and is farther for rigid slabs. The magnitude also increases with rigidity. Table 1 gives the results of investigations. The maximum bending moments due to Westergaard's considering the load as point load have been computed. Also computed are the bending moments, when the load is considered to be uniformly spread over a circle of radius r such that

$$\pi r^2 = (h_x/4) \times (h_y/4)$$

It was also revealed that, if the value of α is plotted on log scale against the distance of peak points from the point of load application, the points fall on a straight line. Figure 9 shows such a plot. From the figure one can get the relation

$$d_1 = d \left\{0.083 + 0.0765 \left(\log \frac{330}{\alpha}\right)\right\} \qquad (21)$$

where

d = diagonal of square slab, and
d_1 = distance of maximum moment point from corner where load is applied.

It was also found that if α is plotted on log scale against magnitude of maximum bending moments, the points fall on one straight line. Figure 10 is a plot of this type and gives the following relation

$$M_{max} = Q \left(0.21 + 0.0215 \log \frac{420}{\alpha}\right) \qquad (22)$$

It may be pointed out that, for values of α less than 2, the preceding relations do not hold, though they will not be far off.

For a slab with a corner load, this is a significant relation that relates the moments to the relative flexibility number and has been derived for the first time.

Square Slab With Center Load

This example compares the results obtained from an elastic solid model with that of a Winkler model. This comparison was part of a model test (performed under controlled conditions) to study the effect on stresses due to load alone (25).

An aluminum slab 2 ft sq and ½ in. thick was used. The ratio between thickness and length in this test was 1:48, whereas in actual pavements it ranges from 1:40 to 1:80. The modulus of elasticity of aluminum used is 10.5×10^6 psi, and its Poisson's ratio is 0.33. The loads were applied through a 4-ton hydraulic jack, in equal increments. The maximum load was well below the ultimate load that could cause yield in slab. A yellow silty clay with a maximum dry density of 111 lb/ft^3 at optimum moisture content of 16 percent was used as soil model.

Loads were recorded by a calibrated proving ring, and strain gauges were used to read strains at various slab locations. For deflection measurements, dial gauges were utilized. Figure 13 shows the setup, and Figure 14 shows the plan of slab with position of dial and strain gauges.

Figure 6. Pressure distributions along edge of square slab loaded at corner.

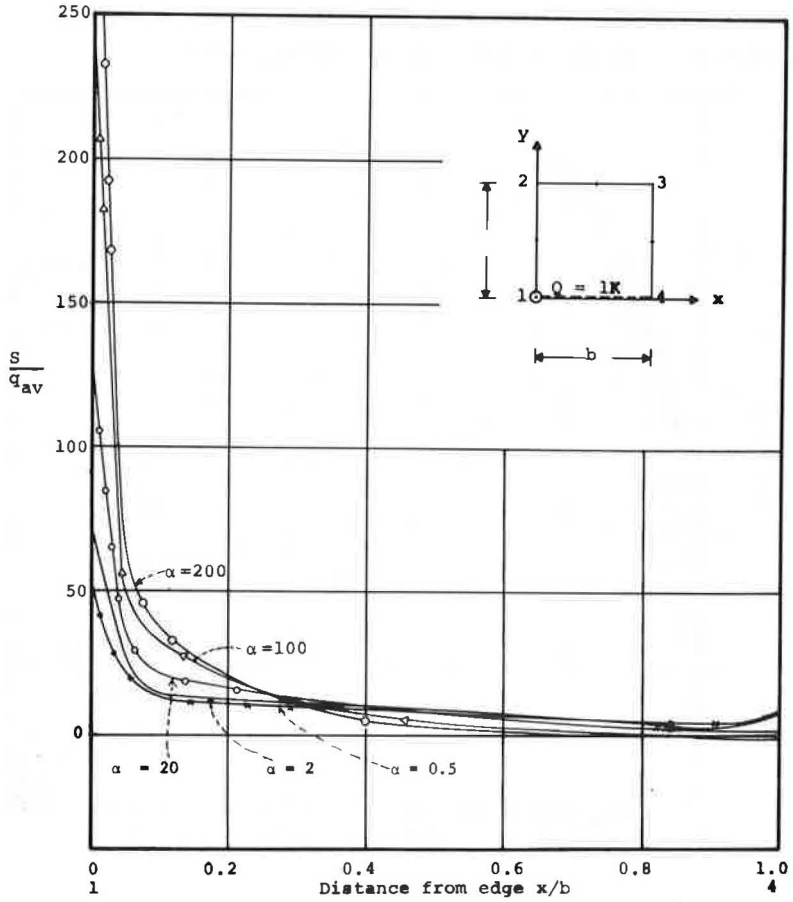

Figure 7. Bending moment along diagonal of square slab loaded at corner.

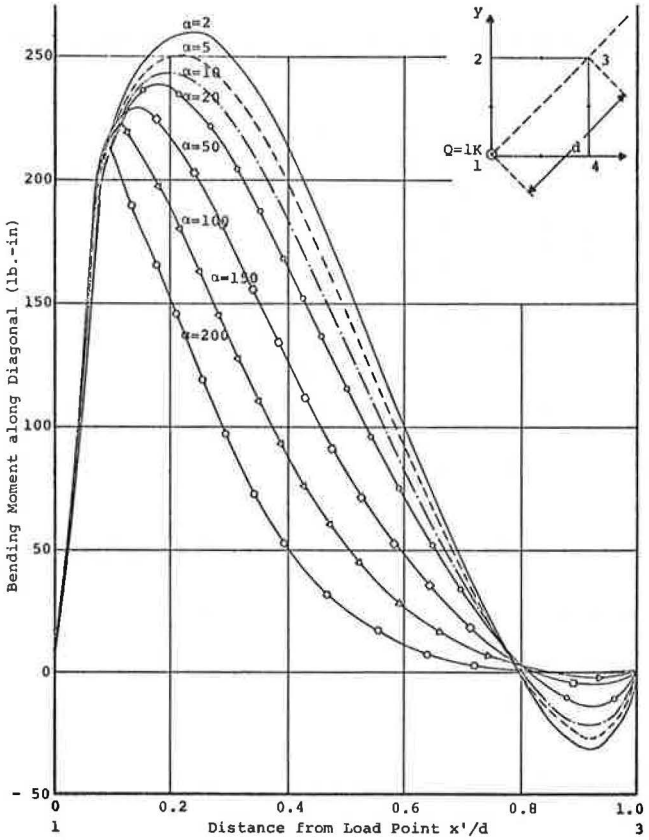

Figure 8. Bending moment along edge of slab loaded at corner.

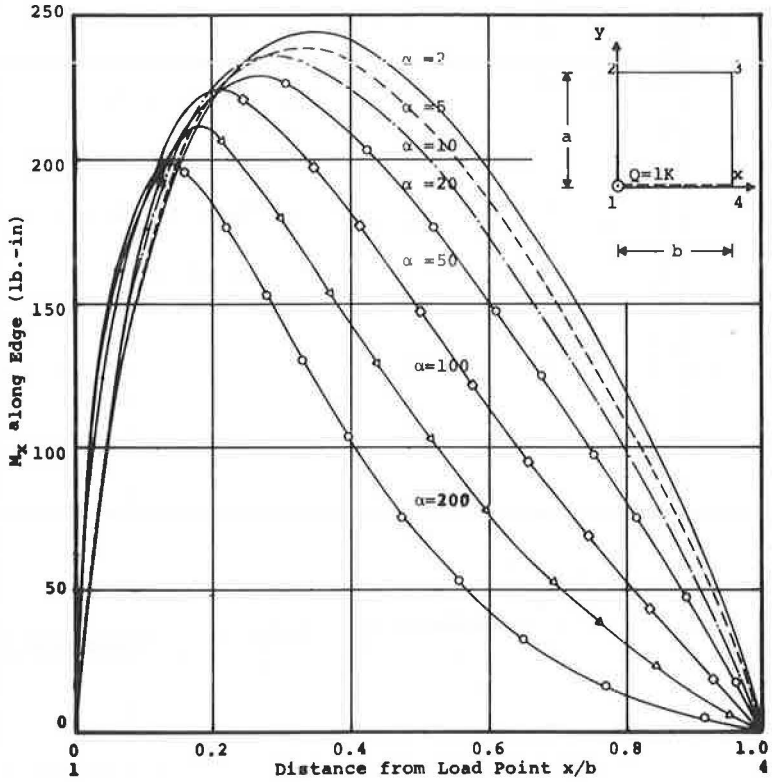

Figure 9. Relation of location point of maximum stress and flexibility number for corner load.

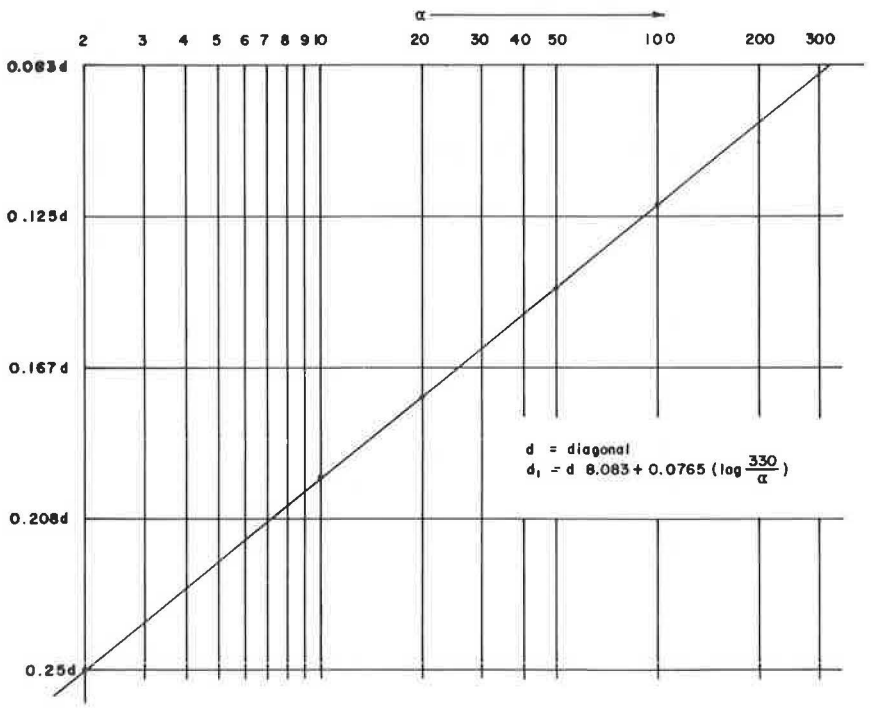

Figure 10. Relation of maximum bending moment and flexibility number for corner load.

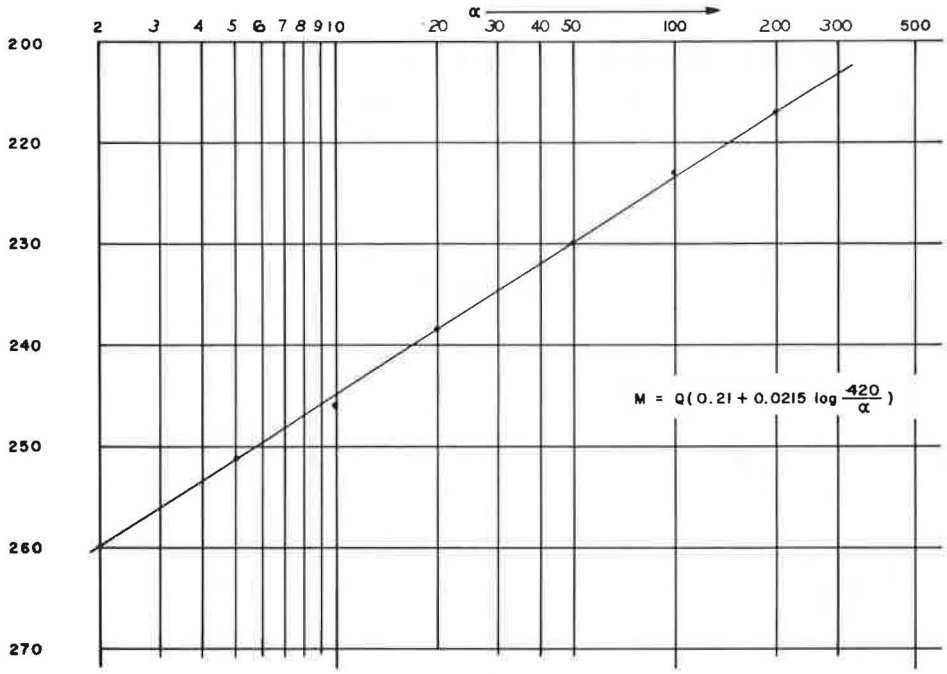

Figure 11. Deflection along edge of square slab loaded at corner.

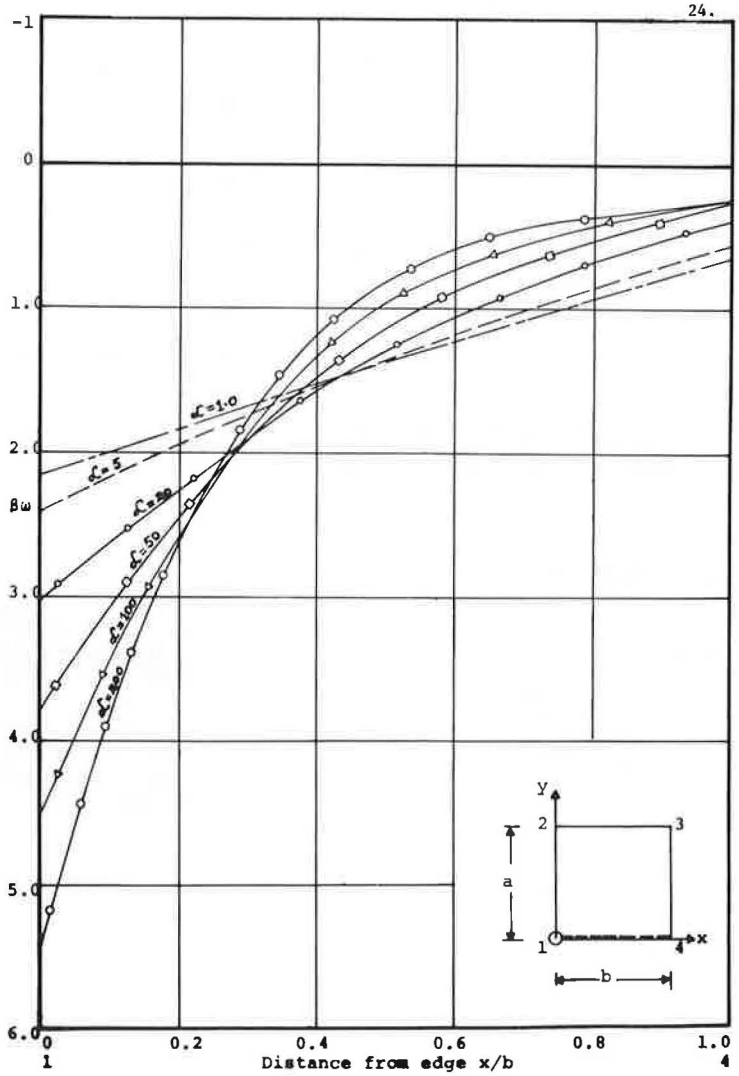

Figure 12. Deflection along diagonal of square slab loaded at corner.

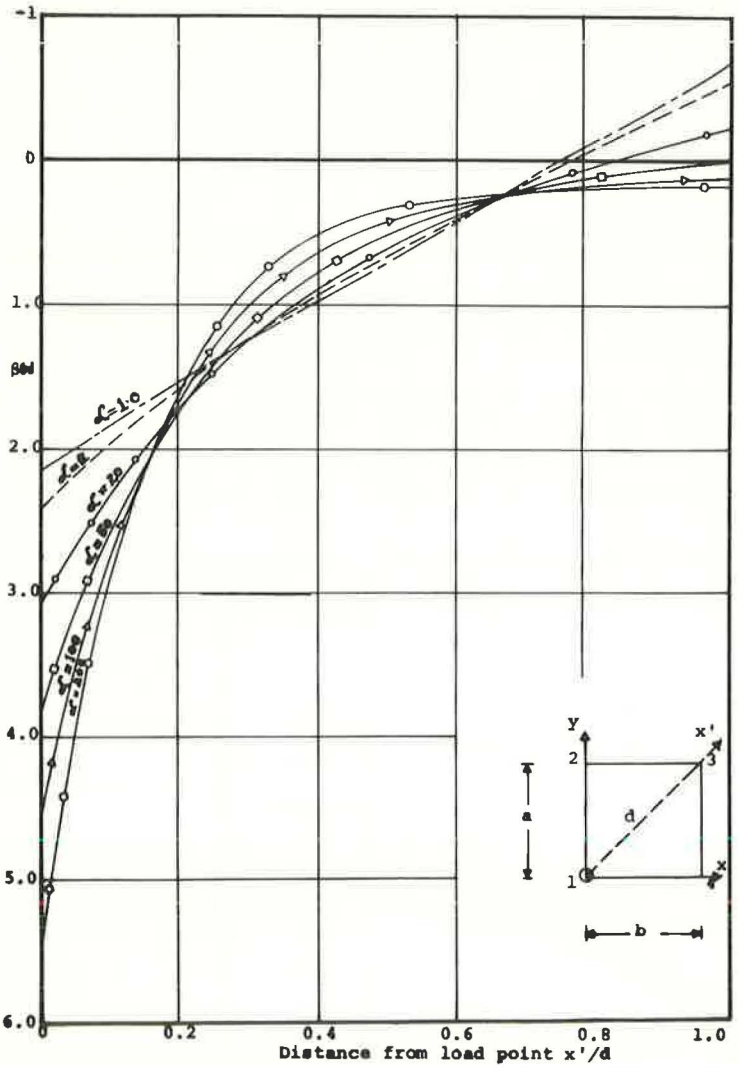

Table 1. Maximum moments in square slab with corner load.

Flexibility Number	Maximum Moments, Westergaard (lb-in.)		Maximum Moments, Elastic Solid Subgrade (lb-in.)
	With Point Load	With Load Spread on $\left(\frac{h_x}{4} \times \frac{h_y}{4}\right)$	
2	500	444	260
5	500	433	251
10	500	423	246
20	500	411	239
50	500	394	230
100	500	378	222
200	500	360	212

Figure 13. Test equipment.

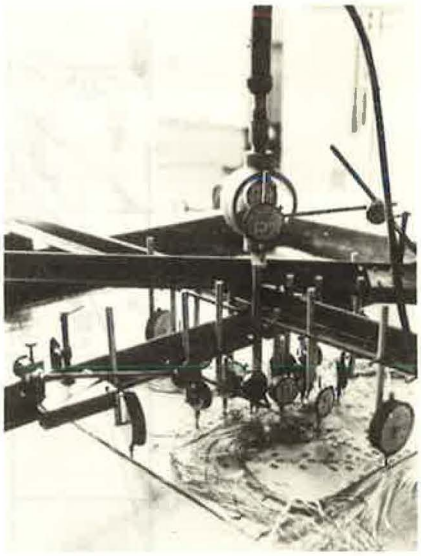

The modulus value of the soil was computed from the measured deflection bowl by the following formula developed by Losberg (26):

$$E_s = [\theta t E^{1/3} (1 - \nu_s^2)]^{3/4}$$

where

t = the thickness of slab,
E = modulus of elasticity of slab, and
θ = slope of load versus depression volume curve.

The value of E_s obtained was 1,550 psi.

Figure 15 shows the deflections. The results show that the values of deflection computed from Westergaard's formula and those from discrete-element model using Winkler subgrade are comparable. These values differ from the elastic solid subgrade though the patterns are very nearly the same. The deflection computed from the discrete-element model using elastic solid subgrade shows remarkable agreement with observed deflections.

From Figure 16, one can see that the observed stresses and those computed by using both Winkler subgrade and elastic solid subgrade are very nearly the same except at maximum point. The difference between observed stresses and those computed by elastic solid theory is about 8 percent. The difference between the observed stresses and those computed using Winkler subgrade is 21 percent. The stresses were computed by Westergaard's formula as well, and the difference between the observed and Westergaard's is about 40 percent. The stresses according to Westergaard's formula are for an infinite slab and a Poisson's ratio of 0.15, whereas the value used in other computations was 0.33. The k-value used in Westergaard's formula was computed from the following:

$$k = \frac{1}{t} (E_s/E^{1/3}) [E_s/(1 - \nu_s^2)]$$

The relevant results are maximum center load, 3,953 lb; maximum observed stress, 20,750 psi; maximum theoretical stress (Westergaard), 31,625 psi; maximum theoretical stress (Winkler), 25,110 psi; maximum theoretical stress (elastic solid), 22,400 psi; maximum observed deflection, 0.180 in.; maximum theoretical deflection (Winkler), 0.123 in.; and maximum theoretical deflection (elastic solid), 0.1825 in.

CONCLUSIONS AND RECOMMENDATIONS

A simple method for solutions of often encountered problems of engineering practice, involving slabs resting on an elastic solid subgrade, has been developed. The slab model utilized is a discrete model developed by Hudson and Matlock (22). The discrete model allows the use of two-dimensional structural elements to represent a thin slab, and the behavior of the elements of assembly of different structural elements forming the slab can be described by algebraic equations. The model is not equivalent to the exact one, but can be made as accurate as desired.

Two illustrative examples have been presented. For the case of square slab with corner load, it is found that the location and the magnitude of peak moments change with the rigidity of slab. Simple expressions for predicting the location as well as magnitude of maximum moments are furnished.

In the second problem, an experimental investigation has been compared with various theoretical soil models. It was found that results from Westergaard's formula agree closely with that of Winkler model and that the elastic solid model simulated the actual behavior better.

When the subgrade is not an elastic half-space but is made up of layers of different materials with different moduli of elasticity and Poisson's ratios, the case becomes more complicated. The deflection of a slab of finite dimensions, resting on elastic layers, has not yet been solved. Steinbrenner (27) has worked an approximate solution

Figure 14. Plan of slab with position of gauges.

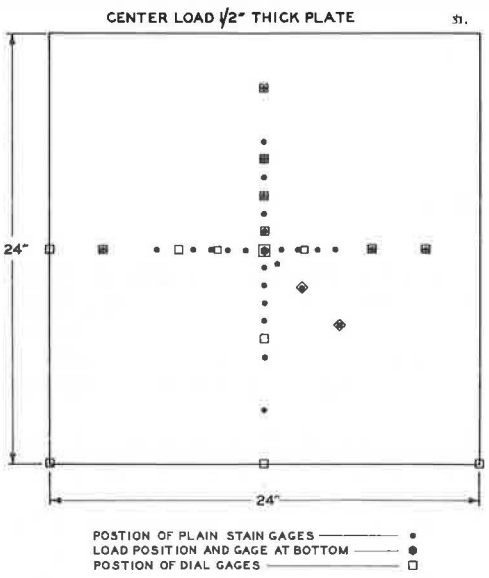

Figure 15. Stress along centerline of ½-in. thick slab.

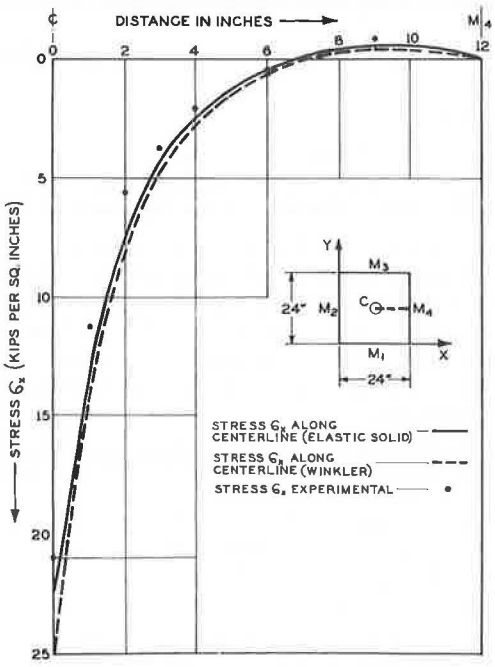

Figure 16. Deflection profile of ½-in. thick slab.

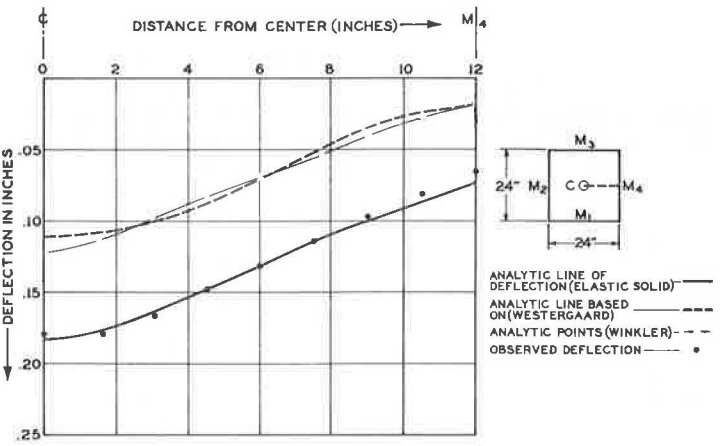

that, according to Terzaghi, is accurate enough for practical purposes. Extension of the work to account for three layers of soil has been completed by Saxena (25).

ACKNOWLEDGMENTS

The valuable guidance and help in this analytical work from A. S. Vesic of Duke University is gratefully acknowledged.

The assistance of Margo Downey, who typed the manuscript, is appreciated.

The encouragement of the Port Authority of New York and New Jersey by providing facilities is deeply appreciated.

REFERENCES

1. Winkler, E. Die Lehre von der Elastizitat und Festigkeit. Prague, 1867, p. 182.
2. Wieghart. Ueber den Balken auf nachgiebiger Unterlage. ZAMN, Vol. 2, 1922, pp. 165-184.
3. Prager, W. Zur Theorie elastisch gelagerter Construktionen. ZAMN, Vol. 7, 1927, pp. 354-360.
4. Nemenyi, P. Tragwerke auf elastisch nachgiebiger Unterlage. ZAMN, Vol. 2, 1931, pp. 224-231.
5. Marguerre, K. Ueber den Traeger auf elastischer Unterlage. ZAMN, Vol. 17, 1937, pp. 224-231.
6. Biot, M. A. Bending of an Infinite Beam on an Elastic Foundation. Trans. ASME, Vol. 59, PPA1-A7, 1937.
7. Reissner, E. On the Theory of Beams Resting on a Yielding Foundation. Proc. National Academy of Sciences, Vol. 23, 1937, pp. 328-333.
8. Volterra, E. Sul Problema Generale della trave poggiata su suolo elastico. Rend. Acad. Nazionale die Lincei, Vol. 2, Series 8, 1947, pp. 307-311, 418-421.
9. Hogg, A. H. A. Equilibrium of a Thin Slab on Elastic Foundations of Finite Depths. Phil. Magazine, Vol. 35, 1944, pp. 265-276.
10. Holl, D. L. Thin Plates on Elastic Foundations. Proc. 5th Internat. Congress on Applied Mechanics, Cambridge, Mass., 1938.
11. Burmister, D. M. The General Theory of Stresses and Displacements in Layered Systems. Jour. Applied Physics, Vol. 16, Feb., March, May 1945.
12. Habel, A. Die auf dem elastisch-isotropen Halbraumn aufruhende zentral symmetrisch belastete elastische Kreisplatte. Bauing, Vol. 18, 1937.
13. De Beer, E. E., Lousberg, E., and Van Beveren, P. Le Calcul de poutres et plaques appuyées sur le sol. Annales des travaux publics de Belgique, No. 2-3, 1956.
14. Grasshoff, H. Die Berechnung einachsig Ausgesteifter Grundungsplatten. Bautechnik, Vol. 32, p. 396. (See also Influence of Flexural Rigidity of Superstructure on Distribution of Contact Pressure and Bending Moments of an Elastic Combined Footing. Proc. 4th Internat. Conf. on Soil Mechanics and Foundation Engineering, London, Vol. 1, pp. 300-356.)
15. Schultze, E. Distribution of Stress Beneath a Rigid Foundation. Proc. 5th Internat. Conf. on Soil Mechanics and Foundation Engineering, 1961, pp. 807-813.
16. Kany, M. Berechnung von Flachengrundungen. Verlag and Ernst und Sohn, Berlin.
17. Krasmanovic, D. Influence de la continuité et de la rigidité sur le calcul des constructions et des poutres continues de foundations. Annales des Travaux Publics de Belgique, Vol. 108, 1955, p. 61.
18. Vlasov and Leont'ev. Beams, Plates and Shells on Elastic Foundation. Israel Program for Scientific Translation, Jerusalem, 1966. (In Russian.)
19. Pickett, G., and Ray, G. K. Influence Charts for Concrete Pavement. Trans. ASCE, Paper 2425, Vol. 116, 1951, p. 49.
20. Pickett, G., Raville, M. E., Jones, W. C., and McCormick, F. J. Deflections, Moments and Reactive Pressure for Concrete Pavements. Kansas State College, Manhattan, Bull. 65, Oct. 15, 1951.

21. Pickett, G., Badaruddin, S., and Ganguli, S. C. Semi-Infinite Pavement Slab Supported by an Elastic Solid Subgrade. First Congress on Theoretical and Applied Mechanics, Kharagpur, India, 1955, pp. 52-60.
22. Hudson, W. R., and Matlock, H. Analysis of Discontinuous or Isotropic Pavement Slabs Subjected to Combined Loads. Center for Highway Research, Univ. of Texas at Austin, Aug. 1965.
23. Todhunter, I., and Pearson, K. A History of the Theory of Elasticity. Cambridge Univ. Press, 1893.
24. Zienkiewicz, O. C., and Cheng, Y. K. Plates and Tanks on Elastic Foundations: An Application of Finite Element Method. Internat. Jour. of Solid Structures, Vol. 1, 1965, pp. 451-461.
25. Saxena, S. K. Foundation Mats and Pavement Slabs Resting on an Elastic Foundation: Analyzed Through a Physical Model. Duke Univ., Durham, PhD dissertation, 1971.
26. Losberg, A. Structurally Reinforced Concrete Pavement. Chalmers Tekniska Hogskolas Handingar, Goteberg, dissertation, 1960.
27. Steinbrenner, W. C. Tafelen zur Setzungsberechnung. Die Strasse, Vol. 1, 1951, pp. 121-124.

PAVEMENT FEEDBACK DATA SYSTEM

Oren G. Strom, Air Force Weapons Laboratory, Kirtland Air Force Base; and
W. R. Hudson and Frank Yu, University of Texas at Austin

This paper is a case study of the systems development phase of a pavement feedback data system for the state of Texas. The pavement feedback data system is intended to complement the flexible pavement design system currently being implemented in 10 districts of the Texas Highway Department. There is a need to collect, store, and analyze carefully selected performance data from full-scale, in-service pavements to guide the design of new and reconstructed pavements. A search for an appropriate generalized data management system in terms of hardware restrictions, cost, record file management, and general adaptability was conducted. In addition, a record control key or common base of reference was studied. File definition and data structures are presented in conceptual form. The recent acquisition of a specific proprietary data handling package, MARK IV, by the Texas Highway Department resulted in the recommendation of strategies to be adopted for pavement feedback data system implementation.

•THE complex character of highway pavements, ever-increasing traffic volumes, and variability of climatic conditions have made it imperative that service life data be collected and analyzed to guide the design of new and reconstructed pavements. The development of a system to collect, store, and analyze carefully selected performance feedback data from full-scale, in-service pavements has been proposed to overcome inherent deficiencies of the mechanistic and road-test research techniques.

The most efficient method of storing and retrieving the vast quantities of data involved in such a system uses an electronic computer as a data bank. The Center for Highway Research of the University of Texas at Austin, the Texas Transportation Institute of Texas A&M University, and the Texas Highway Department, in cooperation with the Federal Highway Administration, have recently completed a systems study of a pavement feedback data system (PFDS). Figure 1 shows the components and scope of PFDS. Details of the study are reported elsewhere (2).

SELECTION OF DATA

The danger of "data pollution," a term connoting an undesirably high level of data accumulation that is not assimilated in a meaningful way, has been recognized (3).

With this in mind, the project team began a program that was discriminatory and highly selective in the choice of parameters or variables for use in PFDS. The Wisconsin Department of Transportation had done considerable work with a technical data system called highway network data and information system (HNDI) (4). In discussions with Wisconsin personnel, it was learned that the selection of data parameters must be accomplished with the system users in mind; in fact, it is probable that the ultimate users should actually take part in the selection process. If the users are initially bypassed, the consequences can be omission of desirable data parameters, duplication of data, and reluctance of the users to use the system.

It was concluded that, beyond the initial framework, all developmental work on PFDS should be oriented toward the engineer users.

Publication of this paper sponsored by Committee on Theory of Pavement Design.

Consideration of the flexible pavement design system (FPS) appeared to be the optimum starting point. This computer-based design method was implemented on a pilot basis in 10 of the 25 Texas Highway Department districts, and initial response of the personnel involved was favorable. The decision was made, therefore, to construct a data system that included only the variables needed for FPS input, thus reducing the scope of the proposed data system to less than one-fifth of the first estimate. This also satisfied the other prerequisites that were considered important; i.e., it reduced the number of data parameters to the absolute minimum, offered the users complete knowledge of the data system contents, and did not generate any new data collection requirements. Although not the ultimate answer, this system did represent a baseline, a valid and known point of departure. A typical list of input to FPS is shown in Figure 2.

DATA SOURCES

A study of the Texas Highway Department data records revealed that a number of FPS input variables were already a part of one or more Planning Survey Division data files. Three files of particular value were traffic, road life, and road inventory. The traffic file was found to be essentially complete with no immediate changes required. The road life file contained valuable historical data on the structural character of the pavements, and the road inventory contained valuable data for the management functions.

Another valuable data source was the National Weather Service magnetic-tape records of temperature, wind, and precipitation for some 1,000 stations in Texas. The temperature data are particularly important in the FPS environmental submodel. It is anticipated that other climatic factors will become increasingly important when more is learned about the swelling clay phenomenon in Texas, a significant consideration of pavement design.

Although the scope of the data collection plan was vastly reduced, there remained the task of checking and revising the data sampling plans already in existence and developing new plans and procedures for the data introduced by FPS. It was obvious that this phase of PFDS was a "field endeavor," and again the importance of the user in the development process was emphasized.

As a result of this investigation, the first phase of PFDS implementation was defined. The Texas Highway Department districts involved in this phase are now examining their data collection and sampling plans.

SOFTWARE ACQUISITION

In the automation of any data system, two important decisions to be made are the choice of hardware and the acquisition of software through purchase of a proprietary package or development of a "custom" package to suit specific needs. Usually the latter decision is influenced to a major degree by the hardware configuration. The Texas Highway Department currently has two IBM 370/155 units in operation, and, therefore, the choice of software is governed by this equipment.

A search of the literature revealed that a variety of generalized data management systems had been under development for nearly two decades. The generalized systems are claimed to be applicable to nearly any situation, easy to use, relatively easy to apply, flexible for changing situations, and efficient from a computer equipment standpoint. Most software vendors will "install" their system on the buyer's equipment, thus theoretically eliminating any programming effort on the buyer's part.

The software choice for PFDS was comparatively difficult. An evaluation was made of 21 specific packages, and all but five were dismissed from consideration because of incompatibility with IBM hardware or the resident operating system, or because the package was no longer maintained. Detailed specifications for PFDS were developed and grouped into three categories: mandatory, desirable, and optional. Each of the five remaining packages was checked against the specifications, and no generalized system, as then defined, met all of the mandatory specifications without considerable implementing programming effort. Incidentally, MARK IV was rejected from consideration for PFDS, only because of costs.

Figure 1. Components and scope of a pavement feedback data system.

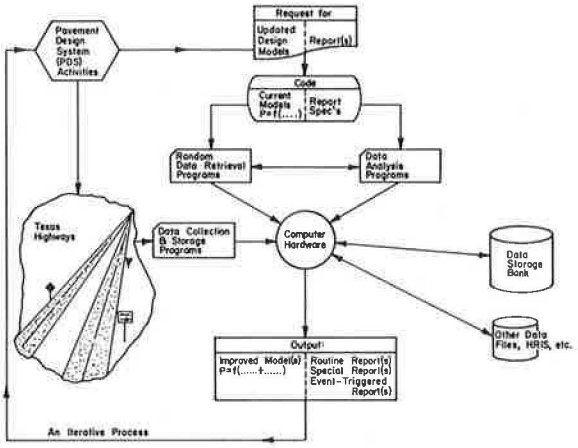

Figure 2. Typical FPS input data listing.

TEXAS HIGHWAY DEPARTMENT
FPS - 11
FLEXIBLE PAVEMENT DESIGN

PROB	DIST.	COUNTY	CONT.	SECT.	HIGHWAY	DATE	IPE	PAGE
18	14	TRAVIS	3136	01	LP 1 MOPAC	12/28/71	238	1

****

BASIC DESIGN CRITERIA
****

LENGTH OF THE ANALYSIS PERIOD (YEARS)	20.0
MINIMUM TIME TO FIRST OVERLAY (YEARS)	4.0
MINIMUM TIME BETWEEN OVERLAYS (YEARS)	6.0
MINIMUM SERVICEABILITY INDEX P2	3.0
DESIGN CONFIDENCE LEVEL	E
INTEREST RATE OR TIME VALUE OF MONEY (PERCENT)	7.0

PROGRAM CONTROLS AND CONSTRAINTS
****

NUMBER OF SUMMARY OUTPUT PAGES DESIRED (8 DESIGNS/PAGE)	3
MAX FUNDS AVAILABLE PER SQ.YD. FOR INITIAL DESIGN (DOLLARS)	8.00
MAXIMUM ALLOWED THICKNESS OF INITIAL CONSTRUCTION (INCHES)	36.0
ACCUMULATED MAX DEPTH OF ALL OVERLAYS (INCHES) (EXCLUDING LEVEL-UP)	6.0

TRAFFIC DATA
****

ADT AT BEGINNING OF ANALYSIS PERIOD (VEHICLES/DAY)	39330.
ADT AT END OF TWENTY YEARS (VEHICLES/DAY)	64752.
ONE-DIRECTION 20.-YEAR ACCUMULATED NO. OF EQUIVALENT 18-KSA	6894000.
AVERAGE APPROACH SPEED TO THE OVERLAY ZONE(MPH)	50.0
AVERAGE SPEED THROUGH OVERLAY ZONE (OVERLAY DIRECTION) (MPH)	20.0
AVERAGE SPEED THROUGH OVERLAY ZONE (NON-OVERLAY DIRECTION) (MPH)	50.0
PROPORTION OF ADT ARRIVING EACH HOUR OF CONSTRUCTION (PERCENT)	5.5
PERCENT TRUCKS IN ADT	8.0

ENVIRONMENT AND SUBGRADE
****

DISTRICT TEMPERATURE CONSTANT	21.0
SWELLING PROBABILITY	0.85
POTENTIAL VERTICAL RISE (INCHES)	5.00
SWELLING RATE CONSTANT	0.08
SUBGRADE STIFFNESS COEFFICIENT	0.26

CONSTRUCTION AND MAINTENANCE DATA
****

SERVICEABILITY INDEX OF THE INITIAL STRUCTURE	4.0
SERVICEABILITY INDEX P1 AFTER AN OVERLAY	3.9
MINIMUM OVERLAY THICKNESS (INCHES)	0.8
OVERLAY CONSTRUCTION TIME (HOURS/DAY)	7.0
ASPHALTIC CONCRETE COMPACTED DENSITY (TONS/C.Y.)	1.26
ASPHALTIC CONCRETE PRODUCTION RATE (TONS/HOUR)	75.0
WIDTH OF EACH LANE (FEET)	12.0
FIRST YEAR COST OF ROUTINE MAINTENANCE (DOLLARS/LANE-MILE)	100.00
INCREMENTAL INCREASE IN MAINT. COST PER YEAR (DOLLARS/LANE-MILE)	10.00

DETOUR DESIGN FOR OVERLAYS
****

TRAFFIC MODEL USED DURING OVERLAYING	3
TOTAL NUMBER OF LANES OF THE FACILITY	6
NUMBER OF OPEN LANES IN RESTRICTED ZONE (OVERLAY DIRECTION)	1
NUMBER OF OPEN LANES IN RESTRICTED ZONE (NON-OVERLAY DIRECTION)	3
DISTANCE TRAFFIC IS SLOWED (OVERLAY DIRECTION) (MILES)	1.00
DISTANCE TRAFFIC IS SLOWED (NON-OVERLAY DIRECTION) (MILES)	0.0
DETOUR DISTANCE AROUND THE OVERLAY ZONE (MILES)	0.0

PAVING MATERIALS INFORMATION
****

LAYER	MATERIALS CODE	NAME	COST PER CY	STR. COEFF.	MIN. DEPTH	MAX. DEPTH	SALVAGE, PCT.
1	A	LT. WT. ACP	21.42	0.96	1.00	1.00	10.00
2	B	ACP	15.48	0.96	1.50	1.50	10.00
3	C	BLACK BASE	13.93	0.96	2.50	10.00	30.00
4	D	CRUSHED STONE	4.40	0.60	10.00	18.00	80.00
5	E	LIME TREATED SUBG	2.40	0.40	6.00	6.00	100.00

Meanwhile, the Automation Division of the Texas Highway Department was searching for a package that would serve general departmental functions, particularly in personnel and fiscal accounting, and standard MARK IV/260 (5) was selected. From a departmental standpoint, the cost ($40,000) was minimal.

This action was a turning point for the PFDS research group. A standard file processing environment was created for the Texas Highway Department, and the basic package could be enhanced with extra-cost optional features (6) that would make it suitable for the technically oriented PFDS.

The PFDS research group then turned to file definitions in the MARK IV environment. Six basic files are envisioned: structural, layer character and thickness (Fig. 3); environment, swelling clay and temperature; performance, serviceability index; costs, initial construction, overlay, etc.; traffic, traffic counts and equivalent wheel loads; and constraints, program controls and judgment factors.

Each file except constraints was subdivided into a prime and a trailer file. The prime file contains fixed length records of all design data, and the trailer file includes variable length records of the as-built and subsequent data values taken during the life of the pavement. The prime and trailer files can be processed individually or simultaneously to yield any desired combination of time-dependent data.

RECORD CONTROL KEY

In a computerized highway network data system, a method is needed to uniquely identify data with a particular segment or point of roadway. The resulting device is called a "record control key." If several data files are used to describe different highway system characteristics, it is important that the same record control key be used as the common base of reference for all files to allow combined file processing and data analysis or correlation of data.

The proposed key is a concatenation of the following items:

1. District—inclusion of the district (there are 25 in the Texas Highway Department) justified from efficient retrieval and administrative points of view;
2. Control—a length of roadway 50 to 100 miles long with well-fixed geographic termini;
3. Section—a subunit or length of "control," typically 10 to 15 miles long, with well-defined geographic termini;
4. Job number—a sequentially assigned number within the control section used to identify special maintenance or construction work or both to be performed on a given segment of roadway at a given time (the job number may cover all or any fractional part of a control section, and jobs extending over more than one control section are assigned a separate job number within each control section);
5. Roadway—a travel way designation (its inclusion is necessary to distinguish between service roads and Interstate main lanes where both roadways carry the same control section designation); and
6. Lane—self-explanatory.

Figure 4 shows the record control key components.

The PFDS key looks cumbersome, but it is a result of several considerations. Most Texas Highway Department data files, automated or otherwise, are referenced by the district, control, section, and job number, and review of all known common bases of references (7) indicated that the best method is a function of installation and maintenance costs, educational effort required, and flexibility of the system.

CUSTOM-WRITTEN ANALYSIS PROGRAMS

Data analysis with MARK IV is limited, but the operations possible are easily invoked by terse entries on the standard form. The following data manipulations are available:

1. Sorting values in sequence, ascending or descending; and
2. Providing summaries of total value of items, cumulative value of items, count

Figure 3. Structural prime file.

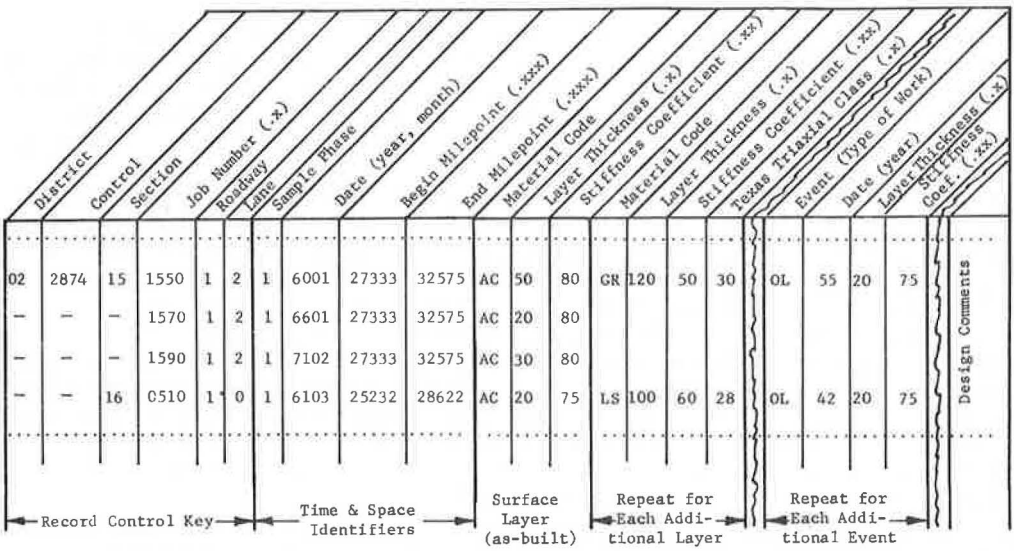

Notes: (1) Each row equals one record.

(2) In programming, a count field will be inserted before each repeated series of fields, i.e., before subsurface layers and events.

Figure 4. Record control key components.

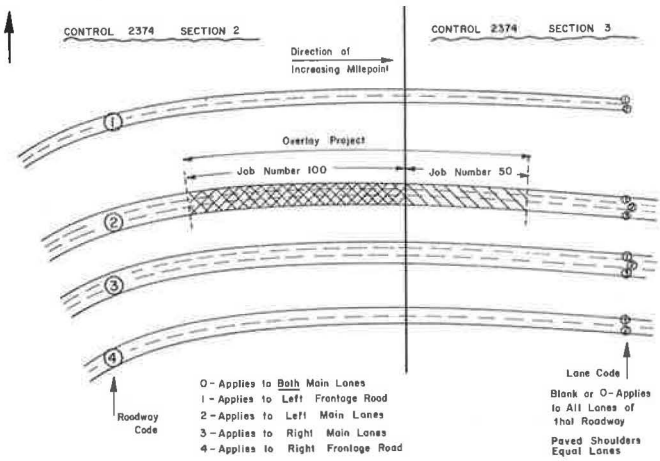

number of items, select maximum value, select minimum value, and compute average value.

A typical PFDS input coding and output using MARK IV is shown in Figure 5.

Some mathematical analyses necessary for PFDS are not possible or practical with MARK IV, but it is possible to access the MARK IV files with a custom-written analysis routine or module and perform the desired computations. The analysis module can be written in a high-level language with index sequential accessibility (8) such as PL/1.

Some rather elaborate analysis routines for use as management tools can easily be envisioned. Event-triggered reports, for example, would be useful. One such report could be a serviceability-loss prediction that is automatically triggered when the design life performance curve projects to a service life of less than a specified percentage of the design life. The computation would be automatically invoked each time a serviceability, traffic, or surface curvature index value is input to PFDS. This is shown in Figure 6, where the as-built serviceability index was well below the design value of 4.2. When the as-built value of 3.9 is input to PFDS, the performance curve projection is computed by the analysis module and intersects the minimum serviceability index level just before the 17th year of service. Thus, the pavement engineer would know to expect a higher cost of maintenance or would plan an earlier overlay to prevent accelerated damage due to dynamic loads.

A good deal of imperfection in the existing models may make such analyses as these somewhat premature. A better feeling for the distribution of data values may be needed, and it is therefore suggested that the initial analysis routines be limited to the following:

1. A program to recreate the FPS-11 design inputs in the conventional order (Fig. 2). This will involve extracting the design values from each of the PFDS prime files and combining them with the constraints file to permit a complete reevaluation of the design decision at a later date and allow direct comparison of design estimates with actual performance.
2. A routine containing the following performance model (9):

$$N = \frac{Q\alpha}{KS^2}$$

where

N = number of 18-kip single axles,
$Q = \sqrt{5 - P} - \sqrt{5 - P_1}$,
P_1 = initial serviceability index,
P = present serviceability index,
α = district temperature constant,
S = surface curvature index, and
K = regression coefficient.

3. A routine with the swelling clay model (10):

$$P = P_1 - f(\alpha_1, \alpha_2, C_1, C_2, C_3, t)$$

where

P = present serviceability index,
P_1 = initial serviceability index,
$\alpha_1 = 0.335$,
$\alpha_2 = 0.17$,
C_1 = swell probability,
C_2 = potential vertical rise,
C_3 = swell rate constant, and
t = time, in years.

Figure 5. Typical PFDS input coding and output.

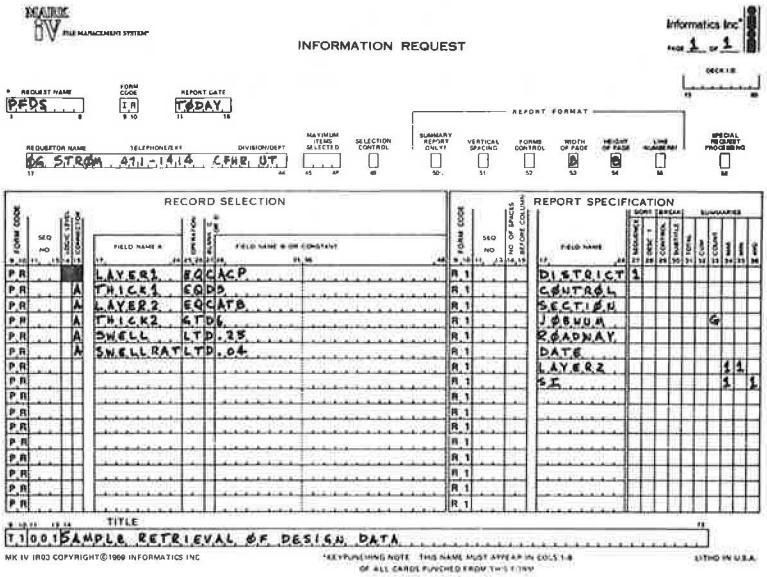

05/01/72 SAMPLE RETRIEVAL OF DESIGN DATA PAGE 2

DISTRICT	CONTROL	SECTION	JOB NO	ROADWAY	LANE	DATE CONSTR	LAYER THICK	SI LOSS/YR
2	314	3	3	0	0	68/10	8	.21
5	297	5	7	0	0	62/06	8	.22
6	1140	3	6	0	0	67/12	10	.17
9	258	8	10	0	0	68/08	10	.15
12	338	3	7	0	0	69/10	7	.25
14	573	2	5	0	0	66/02	12	.10
17	212	2	7	0	0	67/04	8	.19
19	520	4	9	0	0	70/06	7	.22
22	37	8	4	0	0	70/05	14	.05
GRAND COUNT			9					
MAX.							14	.25
MIN.							7	
AVG.								.173

Figure 6. An event-triggered report of serviceability life of pavement.

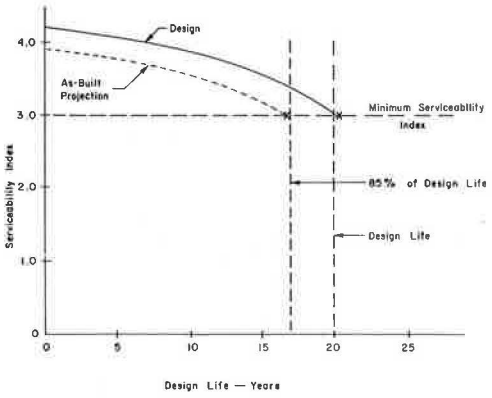

4. Routines accessing the stiffness coefficient and profile analysis computer programs explained elsewhere (11). Care must be taken to ensure that the data names in PFDS and these analysis programs agree. If PFDS is loaded on the MARK IV system, the two analysis programs must be revised slightly to reconcile terminology.
5. A statistical program to compute mean, variance, standard deviation, and coefficient of variation.

CONCLUSIONS

The function of PFDS is to provide the engineer-users with useful information. It was designed to meet the needs of the three classes of users: department headquarters personnel, district engineers, and researchers. As pointed out previously, the essential variables were selected with the users in mind, and the first phase of PFDS implementation calls for an immediate review of the variables to be sure that they are the right ones. Development of the record control key, also, was heavily influenced by the needs of the potential users. A determined effort was made to employ a system requiring as little new coding as possible. An analysis module was not a specific development in the initial version of PFDS, but one must be designed to interact with the basic MARK IV file handling modules and provide each of the three classes of users with the desired information summaries.

Two suggestions to potential highway information system developers are in order. First, a dedicated effort should be made to identify and use data already being collected and stored by the department. This may appear easy, but the data may be available in deceptive form or they may not be trusted by some other branch of the department. However, both of these potential problems can be overcome by close examination of the data and a process of validation. Second, little effort should be spent on writing custom software for the data processing because existing generalized software is readily available for a cost much less than for custom building it. Furthermore, generalized data management systems permit changes in the data base with little programming effort. It is reasonable to expect that the software available in the marketplace will improve rapidly now that competition has been established by some creditable system performers.

A working PFDS is considered mandatory for improving techniques in pavement design. Systematic data collection from in-service pavements will take time to yield results, but the potential is exceptionally promising.

ACKNOWLEDGMENTS

This investigation was conducted at the Center for Highway Research, University of Texas at Austin. The authors wish to thank the sponsors, the Texas Highway Department, and the Federal Highway Administration, U.S. Department of Transportation.

The contents of this report reflect the views of the authors, who are responsible for the facts and the accuracy of the data presented here. The contents do not necessarily reflect the official views or policies of the Federal Highway Administration. This report does not constitute a standard, specification, or regulation.

REFERENCES

1. Hudson, W. R., McCullough, B. F., Scrivner, F. H., and Brown, J. L. A Systems Approach Applied to Pavement Design and Research. Texas Highway Department; Center for Highway Research, Univ. of Texas at Austin; and Texas Transportation Institute, Texas A&M Univ., Res. Rept. 123-1, March 1970.
2. Strom, O. G., Hudson, W. R., and Brown, J. L. A Pavement Feedback Data System. Texas Highway Department; Center for Highway Research, Univ. of Texas at Austin; and Texas Transportation Institute, Texas A&M Univ., Res. Rept. 123-12, May 1972.
3. Structural Design of Asphalt Concrete Pavement Systems. HRB Spec. Rept. 126, 1971.
4. Development of Wisconsin's Integrated Operation System. Highway Research Record 326, 1970.

5. MARK IV File Management System Product Line. Informatics, Inc., Document Sp-71-860-200.
6. MARK IV File Management System Overviews of MARK IV Special Features. Informatics, Inc., Document SP-71-850-45A.
7. Blessing, W. E. Coordinated Data System for Highway Planning. Highway Planning Tech. Rept. 7, May 1968.
8. Data File Handbook. IBM Corporation, GC20-1638-2, Third Ed., Sept. 1969.
9. Scrivner, F. H., Moore, W. M., McFarland, W. F., and Carey, G. R. A Systems Approach to the Flexible Pavement Design Problem. Texas Transportation Institute, Texas A&M Univ., Res. Rept. 32-11, 1968.
10. Lytton, R. L. Prediction of Pavement Roughness Using Expansive Clay Theory. Texas Transportation Institute, unpublished, June 1971.
11. Flexible Pavement Designer's Manual, Part I. Texas Highway Department, March 1970.

SPONSORSHIP OF THIS RECORD

GROUP 2—DESIGN AND CONSTRUCTION OF TRANSPORTATION FACILITIES
John L. Beaton, California Division of Highways, chairman

PAVEMENT DESIGN SECTION
George B. Sherman, California Division of Highways, acting chairman

Committee on Rigid Pavement Design
B. F. McCullough, University of Texas at Austin, chairman
Henry Aaron, Kenneth J. Boedecker, Jr., Philip P. Brown, W. Herman Carter, Bert E. Colley, Donald K. Emery, Jr., Phillip L. Melville, Lionel T. Murray, L. Frank Pace, R. G. Packard, Thomas J. Pasko, Jr., Frank H. Scrivner, M. D. Shelby, Don L. Spellman, W. T. Spencer, T. C. Paul Teng, William Van Breemen

Committee on Flexible Pavement Design
Stuart Williams, Federal Highway Administration, chairman
J. A. Bishop, Robert A. Crawford, James M. Desmond, W. B. Drake, Charles R. Foster, John M. Griffith, Frank B. Hennion, John W. Hewett, William S. Housel, R. V. LeClerc, R. E. Livingston, Alfred W. Maner, Chester McDowell, Carl L. Monismith, William M. Moore, Frank P. Nichols, Jr., Donald R. Schwartz, George B. Sherman, Eugene L. Skok, Jr., Richard Lonnie Stewart, B. A. Vallerga, Anwar E. Z. Wissa

Committee on Theory of Pavement Design
W. Ronald Hudson, University of Texas at Austin, chairman
Richard G. Ahlvin, Ernest J. Barenberg, Richard D. Barksdale, Santiago Corro Caballero, Ralph C. G. Haas, Eugene Y. Huang, William J. Kenis, Fred Moavenzadeh, Carl L. Monismith, Thomas D. Moreland, R. G. Packard, W. H. Perloff, Dale E. Peterson, Robert L. Schiffman, G. Y. Sebastyan, James F. Shook, Roberto Sosa Garrido, Aleksandar S. Vesic, E. B. Wilkins, Loren M. Womack, Nai C. Yang

Lawrence F. Spaine, Highway Research Board staff

Sponsorship is indicated by a footnote on the first page of each report. The organizational units and the chairmen and members are as of December 31, 1972.